Protein-Protein and Protein-Small-Molecule Inhibitor Interactions in the Measles Virus Replication Complex

Von der Fakultät Energie-, Verfahrens- und Biotechnik der Universität Stuttgart zur Erlangung der Würde eines Doktors der Naturwissenschaften (Dr. rer. nat.) genehmigte Abhandlung

Vorgelegt von

Stefanie Anja Krumm

aus Mühlacker

Hauptberichter:	Prof. Dr. Dieter Wolf
1. Mitberichter:	Prof. Dr. Peter Scheurich
2. Mitberichter:	Prof. Dr. Richard Plemper

Tag der mündlichen Prüfung: 11. Dezember 2013

Institut für Biochemie der Universität Stuttgart

2013

All experimental work towards this thesis was carried out under the guidance of Dr. Richard K Plemper in Dr. Plemper's laboratories in the Department of Pediatrics at Emory University School of Medicine and the Center for Inflammation, Immunity & Infection at Georgia State University in Atlanta, GA, USA. The work was supported, in part, by Public Health Service grants AI071002 and AI083402 from the NIH/NIAID to R.K.P.

I hereby certify that I performed this work independently without additional help or materials other than stated.

Hiermit erkläre ich, dass ich die vorliegende Arbeit selbständig verfasst habe und keine anderen als die angegebenen Quellen und Hilfsmittel benutzt habe.

Stefanie Krumm

Vaihingen, den 14.10.2013

Table of Content

Abbreviations

ADEM	acute disseminated encephalomyelitis
ATP	adenosine 5’-triphosphate
CDV	canine distemper virus
CNS	central nervous system
CR	conserved regions
C-terminal	carboxy-terminal
DC	dendritic cells
DC-SIGN	dendritic cell-specific ICAM-3 grabbing non-integrin
CDK	cyclin-dependent kinase
DENV	dengue virus
DHODH	dihydroorotate dehydrogenase
DNA	desoxyribonucleic acid
DRACO	double-stranded RNA activated caspase oligomerizer
ds	double stranded
EM	electron microscopy
F	fusion protein
FDA	Food and Drug Administration
H	hemagglutinin protein
h1/h2	hypervariable region 1/2
HAART	highly active anti-retroviral therapy
HCV	hepatitis C virus
HeV	Hendra virus
HIV	human immunodeficiency virus
HTS	high-throughput screening
IFN	interferon
Ig	immune globulin
IND	investigational new drug
IRES	internal ribosome entry site
L	polymerase
LD	lethal dose
M	matrix protein
MAPK	mitogen-activated protein kinase

MEK	MAPK kinase
MeV	measles virus
MIBE	measles inclusion body encephalitis
MMR	measles-mumps-rubella vaccine
MOA	mechanism of activity
MoRE	helical molecular recognition element
mRNA	messenger ribonucleic acid
MuV	mumps virus
N	nucleoprotein
NiV	Nipah virus
NMR	nuclear magnetic resonance
NNSV	non-segmented negative strand RNA virus
N-terminal	amino-terminal
ORF	open reading frame
P	phosphoprotein
PBMC	peripheral blood mononuclear cell
PCT	carboxy-terminal part of P
PNT	animo-terminal part of P
RdRp	RNA-dependent-RNA-polymerase
RNA	ribonucleic acid
RNP	ribonucleoprotein complex
RSV	respiratory syncytial virus
SLAM	signaling lymphocyte activation molecule
SSPE	subacute sclerosing panencephalitis
UV CD	ultraviolet circular dichroism
VSV	vesicular stomatitis virus
XD	X domain of P

Abstract

The disease measles is caused by the highly contagious measles virus (MeV). MeV belongs to the paramyxovirus family together with respiratory syncytial virus, human parainfluenza viruses and metapneumovirus. Paramyxoviruses are responsible for major pediatric morbidity and mortality. Despite the availability of an effective MeV vaccine, measles case numbers increased alarmingly in the past few years especially in Europe. The return of endemic measles in the European population can directly be linked to the decrease in acceptance/use of the measles-mumps-rubella (MMR) vaccine. The Measles Initiative has set a goal to eliminate measles by 2015. The MMR vaccine, although highly efficacious, has not been sufficient to meet previous goals set by the Initiative. The addition of an effective antiviral to quickly treat sporadic outbreaks and the surrounding communities would greatly aid in the measles eradication efforts.

Fundamental understanding of the viral replication mechanism at the molecular level will be critical for the successful development of antivirals. Therefore the following dissertation examined the protein-protein interactions in the measles virus polymerase complex to understand the events taking place at the molecular level. Additionally, it engaged in protein-small-molecule interactions to identify small-molecule inhibitors of viral replication and their targets.

The first part of the thesis focused on molecular interactions in the viral replication complex. The viral replication complex is an attractive target for antiviral therapy since it possesses unique features and is expressed and functions in a subcellular compartment distinct from host cell polymerases. The polymerase complex consists of the phosphoprotein (P) and the polymerase (L) protein. The P-L complex only interacts with nucleoprotein (N) encapsidated RNA (RNP) for transcription and replication. MeV N contains a core domain involved in RNA encapsidation and a 125-residue carboxy (C)-terminal tail (Ntail) considered to mediate P-L binding to RNP for polymerization. Ntail of MeV is largely unstructured, but a terminal microdomain is implicated in P binding. C-terminal tail truncated N mutant proteins progressively eliminating this microdomain and upstream tail sections demonstrated that the interaction of the Ntail microdomain with a C-terminal domain in P is not required for polymerase recruitment and initial binding of L to its template. Additional

investigations showed that disrupting the domain organization by insertion of an epitope tag in the Ntail did not affect polymerase activity, but rather affected particle assembly. Cell free virions contained reduced levels of envelope proteins which did not affect cell-to-cell fusion kinetics. However, the N-mutant virus was observed to have a kinetic delay of viral mRNA and genome production.

Studies to identify and characterize small-molecule antiviral compounds and their targets were conducted in the second part of this thesis. Non-nucleoside small-molecules are suitable antiviral therapeutics. There are two main approaches in identifying antivirals. First, compounds that target the virus, for example the RNA replication machinery, can be assayed for. Alternatively, compounds that target a host factor that the virus requires can also be a viable strategy. Cellular factors may also be necessary for the entire family of viruses and therefore compounds aiming for host factors may be more likely to be broadly active inhibitors.

A potent pathogen-directed small-molecule compound class had been identified in a high-throughput screen. Hit-to-lead chemistry yielded a highly potent and water soluble compound ERDRP-0519. It targets the L subunit of the morbillivirus polymerase complex directly, since resistance-mediating mutations were exclusively located in the L protein. Unparalleled efficacy of this orally available small-molecule inhibitor was demonstrated and pioneered a path towards an effective morbillivirus therapy that can support measles eradication efforts.

Therapeutic targeting of host cell factors required for virus replication rather than of pathogen components opens new perspectives to counteract virus infections. JMN3-003 is a potent broadly active inhibitor of viral RdRp activity with a host factor mediated profile. It inhibited a wide range of different viral targets. Its antiviral activity was host cell species dependent and induced a temporary cell cycle arrest. While the compound inhibited viral mRNA and genome production, it left host cell mRNA and protein production unaffected.

Taken together, this PhD studies changed the prevailing paradigm in polymerase recruitment and provided strong proof of concept for the potential of the development of pathogen- and host-directed antiviral therapy. These studies demonstrated how basic molecular research of protein-protein interactions critical for virus replication can complement a translational approach to identify, characterize, and improve novel antiviral candidates.

Zusammenfassung

Die Masern, eine hochansteckende Erkrankung, werden durch den Masernvirus verursacht. Der Masernvirus gehört zusammen mit dem Respiratory Syncytial Virus, dem Metapneumovirus und den humanen Parainfluenzaviren zur Familie der Paramyxoviren. Paramyxoviren sind hauptverantwortlich für Morbidität und Mortalität bei Kindern. Obwohl ein wirksamer Impfstoff verfügbar ist, hat sich die Anzahl der Masernerkrankungen in den letzten Jahren besonders in Europa drastisch erhöht.

Die Rückkehr endemischer Masernausbrüche in der europäischen Bevölkerung kann direkt auf eine geringere Akzeptanz/Anwendung der Masern-Mumps-Röteln-Impfung (MMR) zurückgeführt werden. Die „Measles Initiative“ hat sich die Masernausrottung bis 2015 zum Ziel gesetzt. Trotz der hochwirksamen MMR-Impfung konnten die bisher gesetzten Fristen der Initiative nicht erreicht werden. Eine Maßnahme zur Unterstützung der Masernausrottung wäre die Verwendung wirkungsvoller antiviraler Therapeutika, um größere Ausbrüche zu kontrollieren und einzudämmen.

Für die erfolgreiche Entwicklung von antiviralen Medikamenten ist es von fundamentaler Bedeutung, den genauen Replikationsmechanismus des Virus auf molekularer Ebene zu verstehen. Daher beschäftigte sich die nachfolgende Dissertation zum einen mit Protein-Protein-Wechselwirkungen im viralen Polymerasekomplex, um die Ereignisse während einer viralen Infektion genau zu verstehen und zum anderen mit Protein-Wirkstoff-Wechselwirkungen, um kleine Moleküle, die die virale Replikation verhindern, zu identifizieren und deren Zielproteine zu finden.

Der erste Teil der Dissertation konzentrierte sich auf die molekularen Interaktionen im viralen Replikationskomplex. Dieser ist ein attraktives Ziel für eine antivirale Therapie, da er einzigartige Eigenschaften besitzt und in einem subzellulären Kompartiment getrennt von Polymerasen der Wirtszelle exprimiert wird. Er besteht aus dem Phosphoprotein (P) und der Polymerase (L). Der P-L Komplex erkennt die virale RNA für Transkription und Replikation nur, wenn sie von dem Nukleoprotein (N) umschlossen ist und als Ribonukleoproteinkomplex (RNP) vorliegt. Das N Protein besteht aus einer aminoterminalen Domäne, die mit der RNA assoziiert (Ncore) und einer carboxyterminalen Domäne (Ntail), die für die Bindung von P und L an die RNP verantwortlich ist. Die Ntail Domäne ist weitgehend unstrukturiert, aber eine

Mikrodomäne im Ntail ist an der Bindung zu P beteiligt. Es wurden N Mutanten hergestellt, die schrittweise diese Mikrodomäne und Sequenzen davor nicht mehr exprimierten. Mit ihnen konnte gezeigt werden, dass die Wechselwirkungen von der Mikrodomäne im Ntail mit einer carboxyterminalen Domäne in P nicht benötigt werden, um die Polymerase zu rekrutieren und an die RNP zu binden. Weitere Untersuchungen zeigten, dass eine Störung des Domänenaufbaus im Ntail durch Einfügung eines HA-Tags nicht die Polymeraseaktivität beeinflusst. Es wurde jedoch die Assemblierung der viralen Proteine im späteren viralen Lebenszyklus gestört. Zellfreie virale Partikel hatten weniger Membranproteine in der Hülle integriert, aber dies hatte keinerlei Auswirkungen auf die Zell-zu-Zell-Fusionskinetik. Vielmehr war die Produktionskinetik von viraler mRNA und Genom beim mutierten Virus zeitlich verzögert.

Im zweiten Teil der Dissertation wurden antivirale kleinmolekulare Wirkstoffe, die die virale Replikation verhindern, durch Protein-Wirkstoff-Wechselwirkungen identifiziert und charakterisiert. Nicht-Nukleosid kleine Moleküle sind als Wirkstoff für eine antivirale Therapie gut geeignet. Es gibt zwei Hauptverfahren um antivirale Moleküle zu identifizieren. Zum einen kann man nach Wirkstoffen suchen, die den Erreger, z.B. die virale Replikationsmaschinerie, direkt inhibieren. Eine alternative Strategie zielt darauf Wirkstoffe zu finden, die wichtige Faktoren für den Virus in der Wirtszelle blockieren. Diese Zellfaktoren können auch von anderen Mitgliedern der gleichen Virusfamilie beansprucht werden und so können Wirkstoffe, die einen dieser Faktoren blockieren, ein breites Spektrum verschiedener Viren hemmen.

Eine Molekülklasse, die sich direkt gegen den Erreger richtet, wurde in einem High-Throughput-Experiment identifiziert. Durch eine Hit-to-Lead-Optimierung wurde der hochwirksame und wasserlösliche kleinmolekulare Wirkstoff ERDRP-0519 entwickelt. Dieser inhibierte direkt die Morbillivirus Polymerase, da resistenzvermittelnde Mutationen ausschließlich im L Protein entdeckt wurden. Zum allerersten Mal konnte die antivirale Effektivität eines oral verabreichbaren Wirkstoffs in einem Kleintiermodell gezeigt werden. Dieses bahnbrechende Ergebnis hat somit den Grundstein für die Entwicklung einer effektiven Morbillivirus Therapie gelegt und kann die Masernausrottung erheblich unterstützen.

Eine zweite Molekülklasse griff in der Wirtszelle einen Faktor an, der für die virale Replikation von Bedeutung ist und blockierte dadurch ein breites Spektrum von

Viren. JMN3-003 ist ein potenter Wirkstoff, der die virale Replikation hemmte, indem er einen dafür notwendigen Wirtszellfaktor inhibierte. Er unterband die Replikation vieler verschiedener positiv und negativ RNA-Viren sowie DNA-Viren, wobei seine antivirale Aktivität abhängig von der Spezies der Wirtszelle war. Außerdem bewirkte JMN3-003 einen temporären Stillstand des Zellzyklus. Während er die virale mRNA- und Genom-Produktion hemmte, ließ er die mRNA- und Protein-Produktion der Wirtszelle unberührt.

Diese Dissertation hat das vorherrschende Model zur Rekrutierung der viralen MeV Polymerase modifiziert und einen guten Beweis dafür geliefert, dass Wirkstoffe, die sich direkt gegen den Erreger richten bzw. die Faktoren der Wirtszelle als Zielgruppe haben, sich für eine antivirale Therapie eignen. Sie hat gezeigt, in welcher Weise grundlegende molekulare Untersuchungen der Protein-Protein-Wechselwirkungen und Methoden zur Identifizierung, Charakterisierung und Verbesserung neuer therapeutischer Wirkstoffe ineinandergreifen und sich ergänzen können.

1 Overview

1.1 Measles Virus

Measles virus (MeV), a major human pathogen, is one of the most infectious viruses known and cause of the corresponding disease measles. Belonging to the order of *Mononegavirales,* MeV is a non-segmented negative strand RNA virus (NNSV). This group comprises four major families which include human and animal pathogens: *Bornaviridae* (Borna disease virus), *Filoviridae* (Ebola virus, Marburg virus), *Paramyxoviridae* (MeV, canine distemper virus (CDV), respiratory syncytial virus (RSV), mumps virus (MuV), Hendra- and Nipahviruses (HeV and NiV)) and *Rhabdoviridae* (rabies virus, vesicular stomatitis virus (VSV)). Measles virus is furthermore classified in the genus *Morbillivirus* within the *Paramyxovirinae* subfamily.

The MeV non-segmented genome encodes for 6 structural proteins - the nucleoprotein (N), the phosphoprotein (P), the matrix protein (M), the fusion protein (F), the hemagglutinin protein (H) and the RNA-dependent-RNA large polymerase (RdRp) protein (L) - as well as 2 nonstructural proteins, the C and V proteins. They are encoded in the P open reading frame (ORF) and expressed by alternative translation initiation or RNA editing, respectively (figure 1).

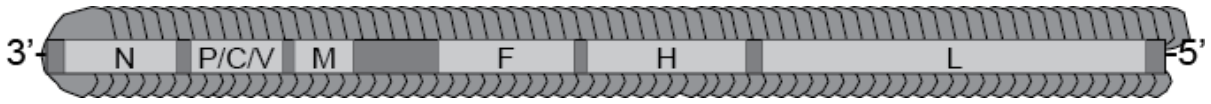

Figure 1: Schematic of the nucleocapsid and genome organization of MeV

The nonstructural proteins interfere with the innate host immune response by inhibiting the interferon signaling. The lipid bilayer envelope derived from the host cell contains the viral transmembrane glycoproteins, the H attachment protein and the F protein. The M protein is associated with the inner surface of the envelope and regulates MeV RNA synthesis and particle assembly by interacting with N as well as the internal tails of H and F (Iwasaki et al., 2009; Pohl et al., 2007). As a common feature shared by all NNSV, the viral RNA is encapsidated by multiple copies of the

nucleoprotein N and forms a helical N:RNA structure, called the ribonucleoprotein complex (RNP) or nucleocapsid. Only the N:RNA is recognized by the viral polymerase complex and used as a template for transcription and replication, which are mediated by the L protein in association with its co-factor, the P protein. However, all enzymatic activity required for transcription and replication is concentrated within the L protein.

1.2 Measles Virus Pathogenesis and Prevalence

As one of the most contagious pathogens, MeV has an extremely high basic reproductive number R_0 of 11-18. The R_0 value indicates the average number of secondary cases directly infected by one infectious individual during the entire infectious cycle in a totally susceptible population (Plans-Rubió, 2012). MeV spreads via droplets and infects resident dendritic cells (DC) and alveolar macrophages in the lung epithelial. There are three known receptors used by MeV for attachment and cell entry. The first identified receptor is the membrane cofactor CD 46, an ubiquitously expressed receptor on all nucleated cells. Only the vaccine or laboratory adapted MeV strains, but not the wild type MeV strains, can use CD 46 for attachment and entry (Dorig et al., 1993; Naniche et al., 1993). The signaling lymphocyte activation molecule (SLAM) or CD150 expressed on activated T and B cells, macrophages and mature DCs is used as a receptor by all MeV stains (Tatsuo et al., 2000). The recently identified third receptor used by all MeV strains, Nectin-4/PVRL4, is located in the basolateral side of the airway epithelium (Muhlebach et al., 2011; Noyce et al., 2011). Other attachment receptors have been identified such as dendritic cell-specific ICAM-3 grabbing non-integrin (DC-SIGN) and Neurokinin-1. However, interaction of H with those receptors does not result in fusion with the host membrane. Attachment of H to DCs and alveolar macrophages via DC-SIGN induces delocalization of intracellular SLAM to the cell surface (Avota et al., 2011; Ferreira et al., 2010; Lemon et al., 2011).

Infected DCs and macrophages transport the virus to the draining lymph nodes where they infect T and B cells via the SLAM receptor causing the first viremia. Receptor specificity renders the virus largely lymphotropic. From there, the virus

spreads through lymphoid organs and tissues such as spleen or thymus as well as the liver, skin, tonsils and respiratory mucosal surfaces causing the second viremia (de Swart et al., 2007). Within the respiratory tract, MeV spreads through virus infected immune cells to the basolateral side of the airway epithelium via the Nectin-4/PVRL4 receptor resulting in virus shedding (Ludlow et al., 2013b). Ludlow et al. recently demonstrated in a macaque animal study that tonsillar and adenoidal epithelium was disrupted by virus infected and uninfected inflammatory immune cell infiltration. This caused a large number of MeV infected cells or cell debris being spilled into the respiratory tract. This damage can cause coughing and sneezing and consequently lead to the expulsion of both cell-associated and cell free virus for host-to-host transmission (Ludlow et al., 2013a). Immune cells essentially deliver MeV exactly where it can shed most effectively, which may contribute to the exceptionally high attack rates of the virus.

Symptoms such as fever, conjunctivitis, cough, coryza and Koplik's spots in the mouth begin only about 10-12 days post infection. The typical maculopapular rash follows about 1-2 days later. The rash is caused by infiltration of leukocytes and monocytes into sites of virus replication in the skin (Polack et al., 1999). By the time symptoms occur, virus has already shed and the immune system has started to clear the virus. Exposure to either wild type or attenuated MeV in form of the trivalent vaccine measles-mumps-rubella (MMR) delivers a lifetime protection mediated by antibodies delivered from memory B cells (Bouche et al., 2002; Hilleman, 2001). However, continued natural boosting is required to maintain high level protection since antibodies induced by MMR vaccine wane over time. This is especially the case when the occurrences of measles, mumps, and rubella incidences decrease and natural diseases cannot boost the acquired antibody levels (Davidkin et al., 2008).

Measles virus infection causes temporary immunosuppression. While mechanistically not fully understood yet, many contributing factors were identified: for instance, lymphopenia, decreased IL-12 and increased IL-10 production that skews a Th1 response to a prolonged Th2 response, and T cell non-responsiveness due to virus induced immaturity of infected DC cells (Coughlin et al., 2013; Fugier-Vivier et al., 1997; Karp et al., 1996; Schneider-Schaulies and Schneider-Schaulies, 2009; Servet-Delprat et al., 2000).

This effect allows secondary acute viral, bacterial or parasitic infections to arise, e.g. pneumonia or otitis media that are often the cause of death in fatal cases (Beckford et al., 1985). In 2011, there were about 158,000 measles related death cases reported (WHO-media-center, 2013). The case fatality rate of measles itself is about 1:5000 in developed countries (Public-Health-England, 2013). Additional complications and disorders after virus clearance such as acute disseminated encephalomyelitis (ADEM), an autoimmune demyelination of neurons in the brain, can occur within 2 weeks after the onset of rash, and the progressive measles inclusion body encephalitis (MIBE) can arise up to 6 months post viral clearance or even later (Freeman et al., 2004; Freeman et al., 1967; Schneider-Schaulies et al., 1999). Measles infected patients furthermore are susceptible to develop subacute sclerosing panencephalitis (SSPE) several years after the primary infection. SSPE is a fatal disease of the central nervous system (CNS) caused by demyelination and develops due to persistence of the virus in neuronal cells of the brain (Freeman et al., 1967; Garg, 2008). Symptoms are generic and include seizures, cognitive impairment, ataxia, irritability, forgetfulness or paralysis that get progressively worse. On a molecular level, MeV mutates predominantly in the M protein by A-to-G hypermutation destroying the M protein-coding frame as well as in the cytoplasmic tails of H and F rendering the virus cell-associated and causing persistent infection (Oldstone et al., 2005). As of today, it is unclear how MeV infects neurons within the CNS (Delpeut et al., 2012). Neurokinin-1 has been suggested to mediate trans-synaptic spread of MeV in primary neurons (Makhortova et al., 2007). Initially, a non-cytolytic clearance is implemented to maintain integrity and functionality of neurons. Since neurons cannot be replaced, massive death of infected cells is devastating. Clearance of virus from neurons requires infiltration of B and T cells into the CNS to provide antiviral antibodies, CD8+ T cell and interferon (IFN)-γ (Griffin, 2011). MeV specific antibodies circulating in the CNS alone fail to clear the virus. However, they may prime the infected neurons to an antiviral state by binding MeV proteins expressed on the cell surface and changing cell signaling. IFN-β and -γ control viral RNA production by activating the JAK/STAT pathway and induce an antiviral state within the cell (Burdeinick-Kerr et al., 2009). What exactly reactivates the virus is unknown; Hsp 72 and Peroxiredoxin have been suggested to be involved in that process (Carsillo et al., 2006; Watanabe et al., 2011). Rapid replication in the CNS

causes neuronal damage by either the virus infection or the immune response to the infection resulting in demyelination (Honda T, 2013). Concerns had been raised that the available MMR vaccine itself can cause SSPE, but the opposite has been demonstrated. Vaccination prevented more cases of SSPE than actually estimated (Bellini et al., 2005).

Furthermore, a fraudulent report that the MMR vaccine may be related to the development of autism in 1998 caused many parents to decide against the vaccination (Wakefield et al., 1998). Even though the report has been formally proven flawed (DeStefano and Chen, 2001; Taylor et al., 1999), public fear remained and vaccination numbers decreased.

A herd immunity of 95% is required to prevent endemic outbreaks (Berger, 1999; Gay, 2004), but the global coverage in 2011 was only at 84% (WHO-media center, 2013). WHO recommends two doses of measles vaccine - the first dose should be administered to children with 9-15 months of age and the booster should be given between 2-5 years of age. It has been estimated that about 20 million children worldwide did not receive the first vaccination dose in 2011 and more than half of those live in the Democratic Republic of the Congo (0.8 million), Ethiopia (1 million), India (6.7 million), Nigeria (1.7 million) and Pakistan (0.9 million) (WHO-media-center, 2013). A population of about 300.000 unvaccinated individuals is sufficient to maintain measles virus circulation.

1.3 Objectives of this Study

To quickly control large measles outbreaks, protect susceptible individuals and the surrounding communities and close the immunity gap to support global measles virus eradication, the addition of an effective antiviral therapeutic would be of great aid.

For the successful development of novel therapeutic and prophylactic strategies, it is instrumental to understand the fundamental principles of the viral replication mechanism at a molecular level. In the case of therapeutics development, this knowledge can be applied to the design of screening campaigns, to predict potential hit structures, to identify druggable domains within a viral protein complex, or to find completely new targets.

During my PhD work I focused on the viral replication complex. Especially the polymerase L is an attractive druggable target since it is a unique complex that is expressed and functional in a subcellular compartment distinct from host cell polymerases. I approached this problem from two different angles. Firstly, I studied the protein-protein interactions in the RdRp complex, the mechanistic role of the proposed interactions between N and P as well as N and P/L in RdRp loading, and identified the basic molecular requirements for the assembly of functional RdRp replicase and transcriptase with emphasis on the N protein as introduced and discussed in Chapters 1.4 and 1.5, respectively. Secondly, I evaluated protein-small-molecule interactions by characterizing and analyzing two different small-molecule inhibitor classes - one targets the virus directly, the other uses a novel antiviral therapy approach that targets host factors required for the pathogen life cycle. The need for antiviral therapy is introduced in Chapter 1.6. Both small-molecule inhibitor classes aimed to inhibit viral replication via two distinct mechanisms and are topic in Chapter 1.7. The development of a novel screen to identify new broadly active small-molecule inhibitors is part of this chapter as well.

1.4 Measles Virus Replication

Viral replication takes place in the host cell cytoplasm immediately after entry and release of the genome into the cell. A 3’ noncoding leader region and a 5’ noncoding trailer region flank the coding part of the non-segmented genome. Those sequences of 107 and 109 nucleotides length, respectively, contain the viral polymerase promoter as well as information for gene start/end. Intergenic junctions that contain gene start/end information also separate each of the individual genes. Since the MeV genome is of negative polarity, the viral RdRp first needs to transcribe it into positive polarity mRNA, which is capped and polyadenylated by L.

For both transcription and replication, the viral polymerase complex exclusively initiates polymerization at the 3’ end of the N encapsidated RNA (Emerson, 1982). It copies and releases the first nucleotides, continues at the first gene start signal for N mRNA production at position 55 and polymerizes along the template. At the same time, the polymerase adds a 5’ cap to the nascent mRNA, then pauses at the

intergenic junctions for polyadenylation and re-initiation of the next gene mRNA. During that process the polymerase must not disconnect from the template, since no target sites for internal reentry exist in the paramyxovirus genome. The likelihood of premature detachment increases with template length, resulting in lower mRNA levels of downstream genes, which creates a transcription gradient. During replication, transcription still continues, but many polymerase complexes switch their activity mode to ignore the intergenic junctions and produce a complete plus polarity copy of the genome called antigenome which is concurrently encapsidated by N. The polymerase initiates antigenome production from the leader region. To produce new minus polarity encapsidated genomes the polymerase replicates the antigenome and, in this case, uses the trailer region as its promoter.

Sequence alignment of different NNSV family members identified six conserved regions (CR) within the L protein (Poch et al., 1990) and several catalytic centers have been localized in those CRs (figure 2).

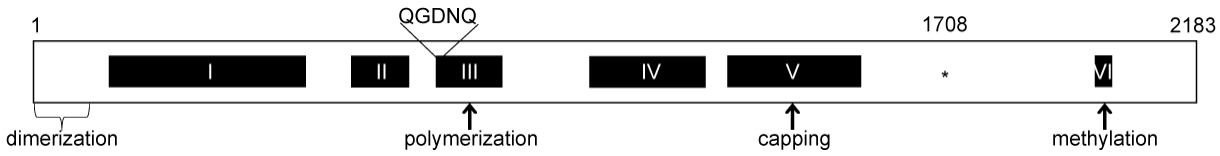

Figure 2: Schematic of MeV polymerase L highlighting CR domains in black and catalytic activities and dimerization region, asterisk (*) marks location of position 1708 (not drawn to scale)

Domain III harbors the polymerization site with the QGDNQ motif (Malur et al., 2002), while the capping domain is located in the CR V (Li et al., 2008). It has been shown for VSV that this virus uses a different method than mammalian cells to cap its mRNA. It links GDP to a 5′-monophosphorylated viral mRNA with the RNA-GDP polyribonucleotidyltransferase activity in CR V (Ogino and Banerjee, 2007). Domain VI has methyltransferase activity that is needed to methylate the mRNA cap (Ferron et al., 2002). L is predicted to form a dimer and the dimerization domain is located at the amino (N)-terminus (Cevik et al., 2004).

Multiple catalytic activities all located in one polypeptide suggest a domain organization in which individual catalytic centers fold independently and are connected by flexible linker regions. Sequence alignment of morbillivirus L has suggested a three-domain organization linked by 2 hypervariable regions (h1 and

h2). It has been demonstrated for MeV L that an insertion of a complete GFP ORF at position 1708 in h2 is well tolerated, both in transient activity assays and in the context of infectious virus (Duprex et al., 2002). This suggested that the methyltransferase activity in CR VI is located in an independent folding domain. In fact, our laboratory identified a second potential interdomain section at position 615 by insertion of a 10 amino acid linker tag (Publication 6, figure 1). Further investigations demonstrated that the MeV polymerase can be physically split at position 1708, and bioactivity can be reconstituted through co-expression of both fragments in the presence of additional oligomerization tags (Publication 6, figure 2). This finding also extended to other members (RSV and NiV) of the paramyxovirus family (Publication 6, figure 4). Equivalently split fragments of NiV, RSV, and MeV L oligomerized with comparable efficiency in all homo- and heterotypic combinations, but only the homotypic pairs were able to transcomplement (Publication 6, figure 5) **(see Appendix - Publication 6: Dochow M, Krumm SA, Crowe JE Jr, Moore ML, Plemper RK, "Independent structural domains in paramyxovirus polymerase protein", J Biol Chem., 2012 Feb 24)**. This study demonstrated that the *Paramyxoviridae* polymerase doesn't need to be synthesized as a single polypeptide and individual domains fold correct independently and adopt a proper tertiary conformation to reconstitute bioactivity. Using electron microscopy (EM) analysis of the VSV polymerase, it has been demonstrated that VSV L is indeed organized into discernible domains. Rahmeh et al. demonstrated that two physically split L fragments resolved into distinguished structural domain elements. They also tested in an *in vitro* RNA synthesis assay whether the two fragments could complement one another functionally. However, in this assay, the two L fragments were not able to reconstitute and synthesize RNA (Rahmeh et al., 2010).

Single stranded RNA viruses have developed different ways to initiate polymerization. Generally, there are two principally different mechanisms: *de novo* and primer-dependent initiation. The *de novo* synthesis has been demonstrated for closely related viruses to MeV such as VSV and RSV. The polymerase is preloaded with the first two nucleotides in case of VSV or the third in case of RSV and uses those to initiate polymerization (Morin et al., 2012; Noton et al., 2010). The same has been shown for dengue virus (DENV): the DENV polymerase contains an ATP binding site and uses this for *de novo* initiation (Selisko et al., 2012).

Other viruses developed a primer-dependent initiation mechanism, using either oligonucleotide or protein primers. The 5' end of the +RNA of picornaviruses is coupled with a viral protein VPg that provides the hydroxyl group for the formation of a phosphodiester bond with the first nucleotide (Ferrer-Orta et al., 2009; Paul et al., 1998). Influenza uses a cap snatching mechanism (Plotch et al., 1981). The virus encodes an endonuclease, which is located within the polymerase protein PA and creates short capped primers by cleaving cellular mRNAs (Dias et al., 2009). The viral polymerase uses the cleavage products for initiation of transcription only; for replication it uses a *de novo* mechanism (Deng et al., 2006). The 3' end of viral RNA can also back loop and anneal with itself to serve as a primer, as shown for hepatitis C virus (HCV) (Behrens et al., 1996; Luo et al., 2000). Human immunodeficiency virus (HIV) uses tRNA(Lys3) that is incorporated into the virion during assembly to prime reverse transcription of RNA into DNA (Marquet et al., 1995).

Immediately after entry, all NNS viruses start mRNA production. Later during infection, the viruses replicate their genomes. The mechanism inducing the switch between transcription and replication is not fully understood. For example, the VSV polymerase interacts with different parts of the promoter region during transcription or replication (Whelan and Wertz, 1999). The RSV polymerase can initiate polymerization at either +1 or +3 position (Tremaglio et al., 2013). When it initiates at +3, it transcribes the first 25 nucleotides where it reaches a "checkpoint", aborts polymerization and reinitiates at the gene start sequence for mRNA production. For replication, the polymerase initiates as well at position +3, but adds nucleotides 1 and 2 in a non-templated fashion (Noton et al., 2010). If the RNA is encapsidated before the polymerase reaches the checkpoint, replication commences; if not, the polymerase aborts and continues mRNA production (Tremaglio et al., 2013). For successful transcription and replication, NNSV rely heavily on host cellular factors. Their relative small genomes do not encode for transcription and translation factors itself. For instance, the leader region of MeV polymerase interacts with different host proteins, which could assist in regulation of transcription and replication (Leopardi et al., 1993). It has also been shown by purification of two distinct VSV polymerase complexes, that the transcriptase and the replicase are associated with different factors (Qanungo et al., 2003). For example, purified VSV transcriptase only associates with elongation factor -1 or Hsp 60 (Das et al., 1998). In case of influenza

virus replication regulation, it has been suggested that increasing nonstructural NS2/NEP protein levels downregulate transcription and support replication by assisting the production of virus-derived small viral RNAs (Robb et al., 2009). These small RNAs align predominantly to the 5′ end of each of the eight segments of the viral genome (Perez et al., 2010). Similarly, MeV M protein inhibits replication to facilitate particle assembly (Iwasaki et al., 2009).

Generally, all NNSV polymerases recognize only encapsidated RNA as template. VSV L alone can transcribe naked RNA *in vitro*, but RNA synthesis is very inefficient. P is needed to enhance initiation and processivity, but for full processivity N encapsidated RNA is required (Morin et al., 2012).

The MeV polymerase cofactor P, the phosphoprotein, is a 507 amino acid long tetramer. P is comprised of a disordered amino (N)-terminal part (PNT, amino acid 1-230) containing a N binding site and a carboxy (C)-terminal part (PCT, amino acid 231-507). Within PCT resides the tetramerization domain (P multimerization domain, PMD) as well as the X domain (XD) located at the very C-terminus (amino acid 459-507). The X domain folds into an antiparallel triple helix and interacts with a distinct domain in the N protein. P proteins of paramyxoviruses can not only tether L onto its template, they furthermore alter polymerase structure as shown for VSV in single particle EM studies (Rahmeh et al., 2010). In a follow-up study, Rahmeh et al. showed, that VSV PNT is sufficient to induce the conformational changes (Rahmeh et al., 2012). MeV P additionally modifies polymerase activity based on its phosphorylation status (Sugai et al., 2012). This status is affected by N-P association. Phosphorylation of sites in P usually covered by binding to N downregulates transcription activity and therefore regulates viral gene expression for efficient viral growth.

The 525 amino acid long MeV nucleoprotein is the most abundant viral protein and forms a homo-oligomer that encapsidates the viral RNA to form a helical rod-shaped nucleocapsid. N is comprised of two domains; the globular N-terminal 400 amino acid Ncore is responsible for RNA binding and contains the oligomerization domain. The intrinsically disordered flexible C-terminal 125 amino acids comprise the Ntail (figure 3). Within the tail there are three highly conserved regions called box 1 (amino acid 400-420), box 2 (amino acid 489-506), which also contains an α-helical molecular recognition element (MoRE, amino acid 488–499), and box 3 (amino acid 517-525).

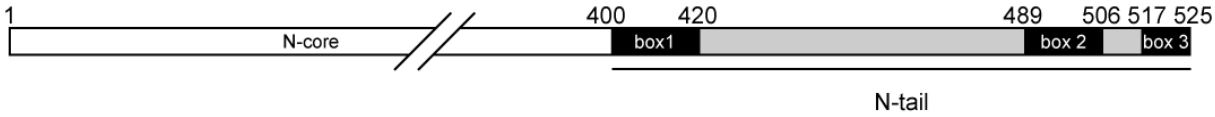

Figure 3: Schematic of the MeV nucleoprotein organization. The Ncore is colored in white, the Ntail is highlighted in grey, and locations of the 3 conserved boxes are colored in black

Box 1 was suggested to interact with a yet undefined receptor (Laine et al., 2003; Laine et al., 2005). Boxes 2 and 3 associate with Hsp 70 (Couturier et al., 2010), and the MeV M protein also binds to box 3. This interaction can be abolished by deletion of the three C-terminal amino acids of the N protein (Iwasaki et al., 2009). Box 2 represents the PCT-interacting domain. This interaction has been specifically mapped to the MoRE domain within box 2 in N.

MoRE domains are short order-prone regions within an intrinsically disordered domain that undergoes induced folding by binding to its partner. The driving force is burying the hydrophobic residues of MoRE into the hydrophobic cleft of the triple helical X domain of P. Direct high affinity binding of N-MoRE to P-XD has been demonstrated via structural studies using far-ultraviolet circular dichroism (UV CD), heteronuclear nuclear magnetic resonance (NMR) and surface plasmon resonance studies or site-directed spin labeling electron paramagnetic resonance spectroscopy. Those measurements were preformed with purified proteins encoding only the Ntail or parts of it and the purified P-XD (Longhi, 2012). N binds also the translation initiation factor eIF3-p40; this interaction is suggested to be involved in MeV induced host translation suppression (Sato et al., 2007). N activity is also regulated by phosphorylation (Hagiwara et al., 2008). In contrast to P phosphorylation, phosphorylation of N increases L activity.

For several NNSV, the N crystal structures were solved. They share overall the same structural elements (figure 4). N adopts a bi-lobal fold into amino-terminal and carboxyl-terminal globules creating a positively charged RNA binding groove in the center to coordinate and shield the RNA (Ruigrok and Crepin, 2010). The differences between various N proteins are how many nucleotides per N are embraced (e.g. MeV=6 nucleotides, RSV=7 nucleotides) and the RNA orientation. For RSV, the RNA faces to the outside of the helical turn, while in the case of rabies virus the RNA faces to the inside.

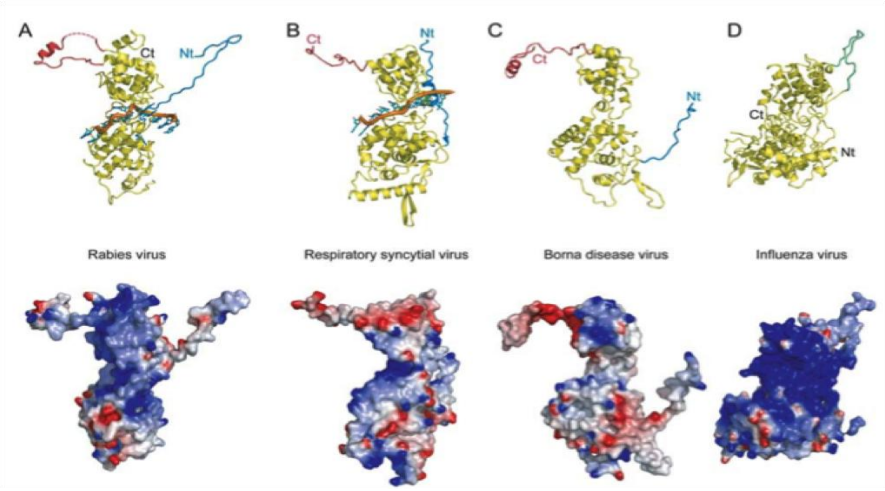

Figure 4: Crystal structure of different NNSV nucleoproteins (from Ruigrok and Crépin, Viruses 2012)

To gain some insight into MeV RNP structure, the RSV N crystal structure was docked into the EM density map of MeV RNP (Tawar et al., 2009). Using this model, and additional small angle scattering, nuclear magnetic resonance spectroscopy and EM analysis, the beginning of Ntail was placed in the inside of the N-RNA helical ring (Jensen et al., 2011). The Ntail is thought to protrude through the interstitial space between successive turns, leaving about 50 amino acids located inside the RNP and 75 amino acids freely exposed on the surface (figure 5). This *in situ* analysis furthermore provided evidence that the MoRE domain interacts transiently with Ncore. Removal of the Ntail allows direct contact between consecutive turns and rigidifies the helical structure (Desfosses et al., 2011; Schoehn et al., 2004), which is in good agreement with the RSV-based MeV N-RNA model.

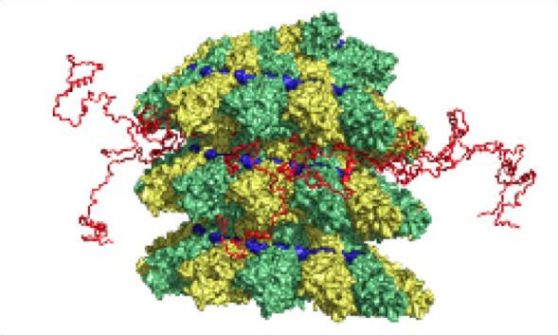

Figure 5: Model of RSV 3-D coordinates docked into the EM density map of MeV RNP and proposed location of the Ntail (in red) (from Jensen et al., PNAS 2011)

1.5 Protein-Protein Interactions in the Replication Complex

There are two different N-P interactions described. The first one is the interaction of N assembled in RNP with P-XD via the surface exposed Ntail-MoRE domain, which is believed to be the only point of contact that allows binding of RdRp to its template. The second one is a soluble complex of free, unassembled N with P called the N^o-P complex that involves the interaction between Ncore and PNT. This complex serves two purposes: 1) it guides N to newly synthesized genomic RNA and 2) P functions as a chaperon to prevent N from nonspecifically binding cellular RNA.

Different models are discussed in the field of how the polymerase is recruited to its template and progresses along the RNA, and what interactions are formed between the key players. One common factor, however, is the P protein functioning as the mediator between L and N-RNA.

The cartwheeling model represents the prevailing paradigm for MeV RdRp polymerization (Curran, 1998; Kolakofsky et al., 2004). In this model, RdRp recruitment to its template is driven through interaction of the Ntail-MoRE domain in the box 2 and the X domain in P. This association alone is believed to be crucial and strictly required for recruiting and binding of L to the template. Consecutive dynamic release and reformation of the N-MoRE-P-XD interaction allows P to cartwheel L along the nucleocapsid. Box 3 in the Ntail has been shown to stabilize the MoRE-XD complex (Yegambaram and Kingston, 2010). The N-MoRE-P-XD complex has been crystallized and is depicted in figure 6 (Kingston et al., 2004).

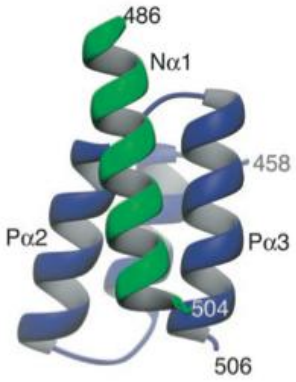

Figure 6: Co-crystal of $Ntail_{468-505}$ (red) with triple helical $P\text{-}XD_{457-507}$ (blue) (from Kingston et al., PNAS 2004)

The proposed model for the *Rabdoviridae* is the jumping model. The main difference to the cartwheeling model is that the dimeric P remains continuously associated with Ntail via its C-terminal domain while L jumps between bound P proteins (Ribeiro Ede et al., 2009).

Both models rely exclusively on the tight interaction with the C-terminal domain in N and PCT only. For MeV and Sendai virus, PCT does not interact with Ncore, at least not biochemically appreciable.

The first part of this thesis addressed the central question on how the MeV polymerase is precisely loaded onto its template with emphasis on the requirements for initial recruitment. C-terminal tail truncated N progressively eliminating the MoRE domain and upstream tail sections were engineered. This exercise confirmed previous reports that RNPs lacking the C-terminal 43 amino acids (N-Δ_C43) harboring the MoRE domain cannot serve as template for the viral RdRp. Removal of all tail residues predicted to be surface exposed restored RNP bioactivity (Publication 3, figure 1). That bioactive N protein mutant lacks the C-terminal 86 amino acids (N-Δ_C86). This experiment further suggested a regulatory role of the exposed central Ntail section present in the bioinactive N-Δ_C43 construct but absent in the bioactive N-Δ_C86 variant. Randomizing its sequence and length confirmed negative regulatory effect of predicted to be surface exposed tail residues without the MoRE domain independently of length/sequence (Publication 3, figure 3). A recombinant MeV virus harboring the bioactive truncated N-Δ_C86 version was recovered, but was unable to sustain viral replication (Publication 3, figure 4). Generation of a replication competent virus encoding the N-Δ_C86 protein in addition to standard N protein assisted in confirmation of integrity of the genome termini (Publication 3, figure 5, table 1) and demonstrated that presence of N-Δ_C86 in nucleocapsids affects the stability of P binding to RNPs (Publication 3, figure 6). Deletion of the N-MoRE binding domain in P abrogated polymerase recruitment to standard nucleocapsids, but polymerase activity was partially restored when Ntail truncated RNPs serve as template (Publication 3, figure 7). This study redefined a fundamental aspect of the cartwheeling model: the N-MoRE interaction with P-XD is not required to recruit or position the polymerase complex on the RNP template. It is rather necessary to organize free moving Ntails to facilitate access to the RNA and to stabilize the complex during its movement along the template (**see Appendix - Publication 3:**

Krumm SA, Takeda M and Plemper RK, "The Measles Virus Nucleocapsid Protein Tail Domain is Dispensable for Viral Polymerase Recruitment and Activity", J. Biol. Chem., 2013 Oct 11). These results suggested furthermore an as of now unappreciated direct interaction of either PNT or even L with Ncore in the nucleocapsid formation. Independent confirmation for the conclusions comes from the recent demonstration that the N-terminal region of related mumps virus P can also bind to N assembled in RNP (Cox et al., 2013).

A parallel study focused on the functional domain organization of the N protein. *In situ* analysis of N structure used bioinformatics to predict unstructured domains in the protein: one in a central part of Ncore as well as all of the Ntail. Testing the accuracy of the predictions, the domain organization was probed by systematic linker insertion and bioactivity was measured in a minireplicon assay. A hinge region in the Ncore as well as most of the tail domain tolerated linker insertions (Manuscript 1, figure 1). Follow-up with larger tag insertions (HA epitope tag or tetracysteine tag) showed that a region in N upstream of the MoRE domain predicted to be located within the interstitial space of consecutive turns had the highest bioactivity (Manuscript 1, figure 1 and 2). The position was at N-E436. Recovery of recombinant virus harboring an HA epitope tag or a tetracysteine tag at E436 was successful. However, the recombinant virus harboring the tetracysteine tag mutated the second cysteine pair to two arginines reducing the tag's overall structure (Manuscript 1, figure 2). Therefore only the recMeV N-E436HA tagged virus was used for further investigations. Supernatant virus composition surprisingly showed reduced amounts of viral envelope glycoproteins packaged into the mutant virion even though viral mRNA levels in virus infected cells were unchanged. Reduced amounts of envelope proteins in the particle left cell-to-cell fusion kinetics unaffected (Manuscript 1, figure 3). In a multi-step growth curve the recombinant mutant virus showed a 24-hour initial delay in replication, followed by wild type-like proliferation. Using peak titers of this growth curve to start a new one reproduced this growth profile excluding viral adaptation during the lag phase (Manuscript 1, figure 4). Analyzing kinetics of N mRNA and genome production revealed a 6-hour delay in mRNA production and hence delayed genome amplification for the mutant virus. This led to delayed progeny particle production and release (Manuscript 1, figure 5) (**see Appendix - Manuscript 1: Krumm SA, Sohn M, Kazarian T, Messner M, Rostad K, and Plemper RK, "Tag**

insertion in the Measles Virus Nucleoprotein Tail Contributes to Packaging of Viral Polymerase Components and Leaves Polymerase Activity Unaffected", in preparation). This project showed that tag insertion in the Ntail leaves polymerase activity unaffected and highlights a regulatory role of the domain organization in the Ntail region which affects particle assembly.

With these two studies, the prevailing paradigm in polymerase recruitment and Ntail functionality was changed. Polymerase loading onto the template proceeds independently of the N-MoRE/P-XD interaction. Both studies demonstrated that the Ntail has a regulatory role, potentially involving interaction with host factors, in addition to stabilizing the advancing polymerase.

1.6 Need for Antiviral Therapy

Overall, the number of deaths caused by measles infections globally decreased 71% from 542,000 to 158,000 between 2000 and 2011. At the same time, new measles cases dropped 58% from 853,500 incidences in 2000 to 355,000 incidences in 2011 (WHO-media-center, 2013). However, despite all efforts and measurements by the CDC, WHO and the in 2001 founded Measles Initiative (led by the American Red Cross, the United Nations Foundation, the CDC, UNICEF and WHO) to increase vaccination coverage, the number of measles incidences increased alarmingly in 2011 especially in European and African countries such as France, Spain, Italy, Romania, Ethiopia, Zambia and Sudan, but also in Indonesia and the Philippines (WHO-media-center, 2013). Since MeV lacks an animal reservoir nor does transmission involve arthropod vectors, eradication should in principle be possible (Rima and Duprex, 2011). However, the WHO has postponed the timing of the goal of global control several times. Surprisingly, highly developed countries such as Germany and the UK are largely responsible for missed control targets.

The measles incidence numbers in Germany have increased over the last few years. Case numbers in 2000-2007 were low. However, there were about 915 cases in 2008, 571 cases in 2009 and 780 cases reported in 2010 (Mankertz et al., 2011). In 2011 the incidence number increased to over 1600. In 2012 the number reduced to 166 cases (European Centre for Disease Prevention and Control, 2010-2012). In the

first six months of 2013 (as of June 17, 2013) already about 905 cases were reported (Robert-Koch-Institut, 2013). Most incidences occurred in Bavaria (388 cases) and Berlin (356 cases). The relatively low case numbers in 2012 may therefore not indicate a trend improvement for this area. Vaccination rate of children under the age of 2 in Berlin and especially in the south of Germany is very low at only about 70%-80% (Schulz M, 2013). It was recently discussed to introduce a mandatory immunization against measles. Mandatory immunization in Germany was lastly applied for poxvirus immunization, which led to the successful eradication of this virus (Klein et al., 2012). In the UK, the vaccination rate is back up to 92.8% after it fell in 1995 to 79.9%. However, areas of low coverage within a high population density such as London with only 87% immunized individuals still exist. Not surprisingly, recent outbreaks mainly affected children in the age between 10 and 18, who missed vaccination in the late 1990s (Wise, 2013).

As of today, there is no highly efficacious measles virus therapeutic available for treatment of acute disease. Ribavirin, a guanosine analogue, is approved for the treatment of some paramyxovirus infections after the onset of clinical symptoms (Chakrabarti et al., 2001) but has limited efficacy against measles (Barnard, 2004). It reduces, however, respiratory distress (Stogner et al., 1993) and may have some effect when given intraventricularly in combination with IFN-α for the treatment of SSPE (Hara et al., 2003; Hosoya et al., 2004). Apart from supportive care (e.g. acetaminophen), administration of a measles virus specific immune serum globulin (Ig) was applied for temporary protection of children (less than 1 year old) and the immunocompromised (Public-Health-Foundation, 2008). These antibodies can prevent measles disease or reduce symptoms when given within six days post exposure (Black and Yannet, 1960). However, this kind of treatment is quite expensive. Ig administration requires sterile materials, trained personnel, uninterrupted cold storage and is therefore generally not practicable for treatment of an entire population during large outbreaks (Plemper and Snyder, 2009). Administration of high doses of vitamin A could reduce risk of mortality in children under the age of two (Huiming et al., 2005).

Not only for controlling measles virus outbreaks, but also for treatment of acute respiratory infections caused by MeV related viruses such as RSV or influenza viruses, antiviral therapy would be beneficial. For RSV, there is no vaccine available.

Severe RSV infections can only be treated with oxygen, moist (humidified) air and fluids given intravenously. High-risk infants receive the expensive treatment with the humanized RSV monoclonal antibody palivizumab (Fernandez et al., 2010). Currently, infections with influenza viruses are treated with neuramidase inhibitors (oseltamivir phosphate (Tamiflu) and zanamivir (Relenza)).

To control large outbreaks of measles, treat infected patients and protect unvaccinated or immunosuppressed individuals an effective therapeutic for post-exposure prophylaxis would be highly desirable. This therapy could not only be used to reduce severity of symptoms associated with measles, but also prevent spread within larger unvaccinated communities such as day care centers or schools. Given the long prodromal phase of MeV infection, a reasonably large time window for antiviral treatment is available. After diagnosis of the first index case, administration of the drug for post-exposure prophylaxis to persons who were in close contact and/or are known/suspected to be submissive to infection (because they did not receive the first or second vaccination and hence are very likely infected), could either suppress or reduce severity of the disease and therefore minimize spread. Given the fact that symptoms arise when viral titers peak, individuals starting treatment before clinical signs manifest are likely to remain subclinical. Therapeutic treatment of the index case may improve disease management, and potentially protect from secondary infection (Pal, 2011; Stogner et al., 1993). These antivirals may also be used for treatment of SSPE patients. Unfortunately, SSPE is rarely diagnosed at an early phase, since generic symptoms require highly trained pediatricians to reach the diagnosis and test for MeV early. Destroyed neurons will not regenerate. Therefore, treatment decisions may be ethically challenging in individual cases. This difficult judgment should be made with consultation of other experts and the final decision nonetheless needs to be made by the immediate family.

Antivirals include small-molecule allosteric and competitive inhibitors, antisense molecules, peptidic inhibitors, natural extracts or even larger proteins. For instance, DRACO (Double-stranded RNA (dsRNA) Activated Caspase Oligomerizer) utilizes a chimeric protein expressed in bacteria with a dsRNA detection domain and an apoptosis induction domains directly linked. It is designed to selectively and rapidly kill virus-infected cells while not harming uninfected cells (Rider et al., 2011).

Non-nucleoside small-molecule compound antivirals are very suitable antiviral therapeutics. They can be produced highly cost effectively in large scale, have a long shelf life at ambient temperature and can be administered orally.

There are different approaches to design antiviral small-molecule drugs. On the one hand they can block the virus by targeting virus encoded enzymes such as the RdRp in case of paramyxoviruses, reverse transcriptase or integrase in case of HIV, the neuraminidase needed for release of budding particles of influenza viruses, or the internal ribosome entry site (IRES) of HCV (Zhou et al., 2013). On the other hand many related pathogens share cellular pathways required for completion of their life cycle. Targeting an essential host factor in such a pathway allows moving towards a broad pathogen target range with one therapeutic only. Potential candidates are host proteases or kinases needed to regulate signaling of host or viral protein activity. Another example is the drug-mediated induction of an antiviral state, for instance through mitogen-activated protein kinase (MAPK) signaling or the phosphorylation-mediated JAK/STAT pathway, respectively (Ma-Lauer et al., 2012). Additional targets provide ribosomes, spliceosomes and chaperones needed for successful replication (Chase et al., 2008; Shaw, 2011).

Antiviral compounds can be discovered through either automated high-throughput screening (HTS) of chemical libraries with conditions designed to inhibit viral factor/s or to identify host factors involved in viral life cycle, or by knowledge-driven direct identification of individual targets (Debnath et al., 1999; Deng et al., 2006; Mao et al., 2008; Prussia et al., 2011; Santhakumar et al., 2010; White et al., 2007; Yoon et al., 2008). Furthermore, systems-wide screens utilizing RNA interference to identify host factors blocking the virus replication were used for different viruses such as influenza viruses (Hao et al., 2008; Karlas et al., 2010; Konig et al., 2010; Shapira et al., 2009), HIV-1 (Konig et al., 2008; Zhou et al., 2008), HCV (Li et al., 2009), Tai et al., 2009), DENV (Sessions et al., 2009) and West Nile virus (Krishnan et al., 2008). Also applied were yeast-two-hybrid approaches e.g. for Epstein-Bar virus, HCV or HIV-1 (Calderwood et al., 2007; Das and Kalpana, 2009; de Chassey et al., 2008). This acquired knowledge can also be used to repurpose or reposition Food and Drug Administration (FDA) approved commercially available drugs. For instance Gleevec (Imatinib mesylate), an Abl tyrosine kinase inhibitor used to treat cancer blocks poxviruses (Goldman and Druker, 2001; Reeves et al., 2005). Another example is

U0126, a MAPK kinase (MEK) inhibitor that inhibits influenza viruses by blocking the Raf/MEK/ERK cascade (Ludwig, 2009; Pleschka et al., 2001). This method accelerates drug discovery at a low financial risk (Ashburn and Thor, 2004). Cruz et al. tested this approach by utilizing a kinase inhibitor library with known binding sites to identify DENV inhibitors (Cruz et al., 2013). An alternative, but also more challenging way of finding druggable targets is identifying protein-protein interfaces of multi-protein complexes that mediate cell regulation that can be modulated by small-molecule inhibitors (Arkin and Wells, 2004; Wells and McClendon, 2007). Examples are the identification of p53:MDM2/X used for anticancer drug discovery and the transcription factor complex MAML-1:Notch interaction; both involve helices at their interaction site (Bernal et al., 2010; Moellering et al., 2009). However, binding pockets are often not well defined and the interface needs to be reasonably small and accessible for small-molecule inhibitors to be able to block or alter this usually strong interaction.

1.7 Protein-Small-Molecule Interactions

The second part of this thesis concentrated on protein-small-molecule interactions to identify or narrow down the target of small-molecule inhibitor candidates. Small-molecules can impede different steps during the viral life cycle such as entry, uncoating, transcription and replication, assembly or budding, and potentially can become a drug to treat measles in infected patients, prevent spread to neighboring permissive communities and protect the immunosuppressed.
This PhD work explored antivirals representing either inhibition strategy - virus specific and host-directed small-molecule inhibitors - and analyzed and characterized the mechanism of activity (MOA) of lead compounds.

1.7.1 Pathogen-directed Antivirals

The first project contributed to the development of an antiviral directly targeting a viral factor. Clinical examples for this approach are the in Chapter 1.6 mentioned FDA-

approved influenza virus neuraminidase blockers, but also HIV nucleoside reverse transcriptase inhibitors such as zidovudine or didanosine and HIV protease inhibitors such as saquinavir or ritonavir (De Clercq, 2012). Herpes simplex virus (HSV) is blocked by nucleoside analogues acyclovir or valacyclovir.

Investigations during my undergraduate studies characterized a MeV-specific RdRp inhibitor (Yoon et al., 2009). This compound class was identified by our laboratory in a high throughput screen (White et al., 2007) and hit-to-lead chemistry yielded AS-136A as the most potent analog (Sun et al., 2008). AS-136A targets the L subunit of the viral polymerase complex directly, since resistance-mediating mutations were exclusively located in this protein.

While very potent, aqueous solubility of AS-136A was poor. In a collaborative study involving medicinal chemistry, pharmacology and molecular virology, the more water soluble analog ERDRP-0519 with almost identical antiviral activity (EC_{50} = 60nM; Publication 5, figure 1 and 2, table 1 and 3) and good oral availability in SD rats was developed (Publication 5, figure 3, table 4). In a minireplicon assay ERDRP-0519 inhibited viral replication with identical potency as AS-136A (Publication 5, figure 4) (**see Appendix - Publication 5: Ndungu JM, Krumm SA, Yan D, Arrendale RF, Reddy GP, Evers T, Howard R, Natchus MG, Saindane MT, Liotta DC, Plemper RK, Snyder JP, Sun A, "Non-nucleoside inhibitors of the measles virus RNA-dependent RNA polymerase: synthesis, structure-activity relationships, and pharmacokinetics", J Med Chem., 2012 May 10**). Figure 7 shows the structures of the initial screening hit 16677 (1), the more potent analog AS-136A (2) and the water soluble analog ERDRP-0519 (2o).

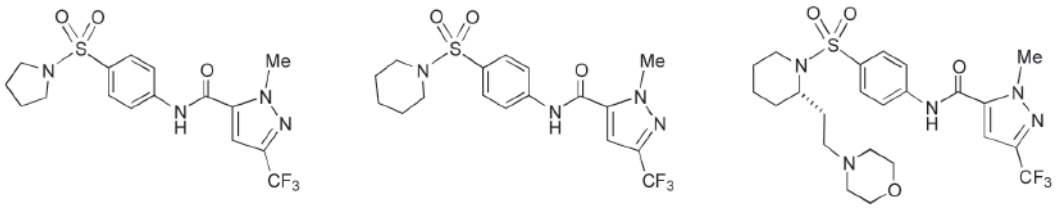

Figure 7: Structure of hit and lead compounds: (1) initial hit candidate 16677, (2) more potent hit-to-lead analog AS-136A and (2o) water soluble analog ERDRP-0519 (from Ndungu et al., J Med Chem 2012)

In a follow-up study efficacy of ERDRP-0519 *in vivo* was assessed. Since there is no suitable animal model for MeV infections available, the lethal CDV-ferret model was chosen as a surrogate assay. Like MeV a member of the *Morbillivirus* genus, the CDV disease profile in ferrets resembles that of MeV in humans. The virus also causes primary and secondary viremia, and clinical symptoms such as fewer and rash. However, progression of CDV disease is more severe, leading to approximately 30% mortality in dogs and 100% mortality in ferrets after intranasal infection with 10^5 infectious particles (LD_{50} 10^4). The compound ERDRP-0519 potently inhibits CDV at 500 nM *in vitro* and has good oral availability in ferrets (Publication 2, figure 1). CDV was adapted to grow in presence of the compound and escape mutations mapped to locations in the polymerase equivalent to those obtained in MeV during adaptation to AS-136A (Publication 2, figure 2). This finding supports conserved compound docking pose and MOA in different morbillivirus targets. Ferrets were infected intranasally with a lethal CDV dose and treated either prophylactically 24 hours pre infection or therapeutically 3 days post infection. Prophylactic treatment of ferrets significantly prolonged survival, reduced viral load and delayed lymphopenia (Publication 2, figure 3). Post-exposure therapeutic treatment at onset of viremia resulted in complete survival of the animals. They showed low-grade viral loads, remained subclinical and recovered from infection, while control animals succumbed to the disease (Publication 2, figure 3). Importantly, all recovered ferrets developed a robust immune response and were fully protected against re-challenge with a lethal CDV dose. Drug-resistant recombinant CDVs were generated and in a challenge exercise to assess virulence *in vivo* found to be attenuated and transmission-impaired compared to the genetic parent (Publication 2, figure 4) **(see Appendix – Publication 2: Krumm SA, Yan D, Hovingh ES, Evers TJ, Enkirch T, Reddy GP, Sun A, Saindane MT, Arrendale RF, Painter G, Liotta DC, Natchus MG, von Messling V and Plemper RK., "An orally available, small-molecule polymerase inhibitor shows efficacy against a lethal morbillivirus infection in a large animal model.", Sci Transl Med., 2014 Apr 16)**. Proven efficacy against CDV provides confidence for the development of an Investigational New Drug (IND) filing package and clinical testing as an anti-measles therapeutic. Alternatively, the drug may be used as a veterinary therapeutic to treat morbillivirus infection of domestic animals and livestock. These findings demonstrate unparalleled efficacy of this orally

available small-molecule inhibitor and pioneer a path towards an effective morbillivirus therapy that can support measles eradication efforts to close herd immunity gaps due to vaccine refusal.

One of the major challenges of pathogen-directed strategy is the rapid emergence of resistance or pre-existing resistance to individual drugs. In the case of RNA viruses, this problem is aggravated by the high mutation rate caused by the lack of polymerase proofreading function. To counteract the problem, several drugs with distinct targets are used in combination therapies as in the case of HAART for the treatment of HIV infections (Fischl, 1999; Shafer and Vuitton, 1999). Those drugs have distinct resistance profiles and heighten the barrier for viral escape. Nonetheless, this approach falls short of addressing the problem conceptually, and multi-therapy failures present an ongoing clinical challenge.

1.7.2 Host-directed Antivirals

An independent project therefore explored the hypothesis that targeting host factors required for the pathogen life cycle will reduce the frequency of viral escape. While clinically yet untested, host-directed antiviral therapy may become a game-changer, since it has high potential to advance beyond the current one-drug one-bug paradigm of antiviral therapeutics. The strategy reduces the risk of viral resistance, since mutations in the viral genome do not replace the absence or reduced activity of the host factor. In addition, several related viral pathogens depend on the same or overlapping host cell pathways, preparing the ground for developing much-needed broad-spectrum therapeutics. However, host-directed antivirals have an inherently higher potential for undesirable drug-induced side effects. This may be alleviated in the case of myxovirus therapy, since the viruses are predominantly associated with acute disease, allowing short treatment times and hence limited host exposure to the drug. Most desirable would be a compound targeting factors that are essential for completion of the pathogen life cycle but are dispensable at least for the time of treatment. There are several promising examples of host-directed antivirals such as the compound DAS 181, a sialidase fusion protein removing the influenza virus receptor α(2,3)- and α(2,6)-linked sialic acid from the cell surface (Belser et al., 2007;

Malakhov et al., 2006), currently in Phase II clinical trial for the treatment of influenza infections (Moss et al., 2012). Kim et al. identified a HMG-CoA reductase inhibitor blocking HCV (Kim et al., 2007), while Hoffmann et al. found that a sodium channel opener or protein kinase C inhibitor hindered influenza virus replication (Hoffmann et al., 2008). An example for treatment of chronical viral infection is Maraviroc, a 2007 FDA approved CCR5 co-receptor antagonist for the treatment of HIV infections (Dorr et al., 2005). Other host-directed therapeutics under development for the treatment of chronic viral infections such as HSV-1 or HIV-1 involved host cyclin-dependent kinase (CDK) inhibitors (Koon et al., 2005; Salerno et al., 2007). A yet experimental broadly active small-molecule called FGI-106 is active *in vitro* and *in vivo* against HIV, HCV and hemorrhagic fever pathogens such as Ebola virus, Rift Valley virus or DENV (Aman et al., 2009; Warren et al., 2010). The target is still unknown, but given its broad inhibition profile, the compound is considered to address a host cell factor.

Our laboratory developed novel drug screening protocols specifically designed to identify host-directed hits (Yan et al., 2013). One screen identified the small-molecule compound 22407448 that displayed good antiviral activity against MeV and in a counterscreen exhibited a broad range antiviral effect against CDV, human parainfluenza virus 3 and MeV (Yoon et al., 2008). Hit-to-lead chemistry identified a more potent and non-toxic analog named JMN3-003 (Publication 7, table 1)

(**see Appendix - Publication 7: Sun A, Ndungu JM, Krumm SA, Yoon JJ, Thepchatri P, Natchus MG, Plemper RK, Snyder JP, "Host-directed Inhibitors of Myxoviruses: Synthesis and in vitro Biochemical Evaluation", ACS Med Chem Lett., 2011 August 23**).

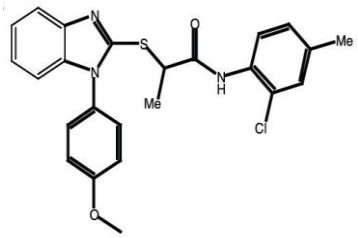

Figure 8: Structure of lead candidate JMN3-003 (from Krumm et al., PLoS ONE 2011)

My graduate studies evaluated and characterized the inhibition profile of JMN3-003. The compound inhibited not only MeV with an inhibitory concentration in the low nanomolar range, but was equally potent against a broad range of other viruses such

as influenza viruses of different strain origin and paramyxovirus strains like RSV and MuV as well as some positive polarity RNA and DNA viruses (Publication 8, figure 1, table 1). Its antiviral activity was host cell species dependent, which indicates a host-directed MOA (Publication 8, table 2), and extended to primary human PBMCs (Publication 8, figure 2). Even though JMN3-003 showed a cytostatic effect, causing a temporary cell cycle arrest in G_1/S phase, it did not affect host mRNA production and protein biosynthesis (Publication 8, figure 4 and 5). Time of addition, real time assessment of viral mRNA and genome production, and reporter based minireplicon assays demonstrated that JMN3-003 inhibits viral replication (Publication 8, figure 6 and 7). Also, viral adaptation events failed to induce resistance to the compound, while resistance to a conventional, pathogen-directed inhibitor was readily induced (Publication 8, figure 8) (**see Appendix - Publication 8: Krumm SA, Ndungu JM, Yoon J-J, Dochow M, Sun A, Natchus MG, Snyder JP, Plemper RK, "Host-Directed Small-Molecule Inhibitors of Myxovirus RNA-dependent RNA-polymerases", PLoS ONE, 2011 May 16**). This study provides strong proof of concept for the potential of the development of host-directed antiviral therapy.

Since the release of this study, two other groups have reported structurally similar broadly active small-molecule inhibitors (Hoffmann et al., 2011; Wang et al., 2011). Both identified dihydroorotate dehydrogenase (DHODH) as potential target. This is an enzyme converting dihydroorotate to orotate during the fourth step in the pyrimidine *de-novo* biosynthesis pathway located in the mitochondria. Hoffmann et al. reverted the inhibition of viral replication by supplementing orotate, the product of DHODH, while Wang et al. identified the enzyme through a chemo proteomics approach and showed direct binding of the compound to the purified enzyme.

In recent work, our laboratory has developed a groundbreaking novel approach to identify broad-spectrum antivirals while simultaneously probing for pathogen-specific hits. The approach is based on the hypothesis that the anticipated broad target spectrum of host-directed antivirals itself can be employed for hit identification, and simultaneously monitors inhibition of two distinct myxoviruses using a dual luciferase readout in a single-well setting. This approach is highly time and resource effective, rendering the screening method more cost-effective than conventional HTS campaigns. MeV from the paramyxovirus family and Influenza A virus from the orthomyxovirus family were chosen. These two are related, but distinct viruses and

co-replicated unimpaired of each other at almost identical rates (Publication 4, figure 1). The protocol was validated for up to a 384-well plate format (Publication 4, figure 2 and 3, table 1), and a proof-of-concept screen of a 10,000-entry library identified a new chemical class of broadly active myxovirus inhibitors (Publication 4, figure 4 and 5) that triggered the host cell ISG signaling pathway and primed the innate cellular antiviral response (Publication 4, figure 6) (**see Appendix - Publication 4: Yan D, Krumm SA, Sun A, Steinhauer DA, Luo M, Moore ML, Plemper RK, "Dual Myxovirus Screen Identifies a Small-Molecule Agonist of the Host Antiviral Response", J Virol., 2013 Aug 7**). This screening method is easily transferable to non-myxovirus pathogen-target pairs, provided that their replication kinetics are comparable and they can co-replicate unrestrictedly in a single well setting.

All three small-molecule inhibitor screens performed resulted in the identification of at least one potent hit candidate. These hit classes have a very distinct inhibition profile and therefore unique clinical advantages, rendering them promising for morbillivirus and/or broad-spectrum myxovirus therapy. Also, this thesis provided proof for the concept that targeting host factors has high potential for antiviral drug therapy.

2 Concluding Remarks

Despite major global efforts, measles virus remains a serious threat to children and the immunocompromised. In order to search for inhibitors of viral replication, it is crucial to understand the events taking place at the molecular level during viral infection. Based on the findings regarding polymerase loading and the fact that the virus harboring the N-Δ_C86 mutation does not sustain replication, compounds targeting the Ntail or P-XD region or the N-MoRE-P-XD interface could likely result in robust inhibition of viral replication. They could possibly pass the screening cutoff for potential candidates rendering N and P and the N/P interface a druggable target.

For better understanding on how the polymerase interacts with the nucleocapsid template for transcription and replication, a well-established model of MeV transcription and replication was challenged. The findings change the paradigm of RdRp loading and demonstrate that the interaction of N-MoRE with P-XD is not required for loading and activity of the polymerase. It is rather needed for stabilization of the proceeding RdRp complex along the template and organization of the central tail region to allow docking of the polymerase. Furthermore, altering the Ntail organization with tag insertions did not affect polymerase activity *per se*. It still remains unknown, however, how precisely the polymerase gains access to the N-encapsidated RNA. The relatively slow polymerization speed of about 3 nucleotides per second argues for an active displacement of N. If L or P serve as the mediator for this step needs to be determined. Mechanistic research in the NNSV polymerase field would greatly benefit from a high-resolution structure of the L protein. This is not only required to fully understand the process and mechanism of L activity, but would also illuminate the role of P as mediator for replication and P interaction sites with L.

The development and target identification of pathogen- or host-directed small-molecule compounds have not only the advantage of virus inhibition; confirmed small-molecule hits can also be used as molecular probes aiding crystallization of the protein target. In case of the MeV polymerase, this can be beneficial in two ways. Firstly, since the polymerase of NNSV is too large for full-length protein purification and crystallization, it needs to be truncated and substructures solved individually. In this setting, unimpaired compound binding can serve as a probe to identify a folding-competent minimal protein subunit. The molecular analysis of the domain

organization of L currently contributes to guide the design of appropriate truncations. Secondly, the compound can be used to initiate crystallization, resulting in a co-crystal of the target-compound complex. Solving the docking pose or pharmacophore of the compound will provide insight into the binding pocket and positioning of the compound side chains. This information may also be valuable for tailoring the compound to related pathogen polymerases, since structural similarity is anticipated based on sequence comparisons, or drive structure-based rational drug design campaigns. In the case of the compounds AS-136A or ERDRP-0519, the overlapping MeV and CDV resistance profiles obtained render such an approach promising for the morbillivirus inhibitor class.

Innovative screens such as the recently reported campaign have high potential to deliver the set of next generation antivirals that will be required to combat existing, emerging, and reemerging viral pathogens. The availability and fast production of large libraries that are accessible to the private and academia drug-seeking community, and the implementation of improved robotic equipment in both settings will accelerate the speed of discovery and increase the chances for successful development of novel clinical entities.

In the case of compound ERDRP-0519, screen and hit-to-lead development identified an orally bioavailable, highly active clinical candidate. An *in vivo* post-exposure therapeutic study with ferrets demonstrated that animals remained symptom free after a lethal dose of CDV, and also mounted a neutralizing antibody response and therefore are protected against re-infection. Same could be achieved with the vaccine, but the application of the compound is mostly for people who do not want to vaccinate. Also, to control large outbreaks the compound would be cheaper, easier to administer and to distribute, since no cold chain needs to be maintained.

This dissertation demonstrates how basic molecular research of protein-protein interactions critical for virus replication can be interphased with a translational approach to identify, characterize, and improve novel therapeutic candidates.

3 References

Aman, M.J., et al., 2009. Development of a broad-spectrum antiviral with activity against Ebola virus. Antiviral Res. 83**,** 245-51.

Arkin, M.R., Wells, J.A., 2004. Small-molecule inhibitors of protein-protein interactions: progressing towards the dream. Nat Rev Drug Discov. 3**,** 301-17.

Ashburn, T.T., Thor, K.B., 2004. Drug repositioning: identifying and developing new uses for existing drugs. Nat Rev Drug Discov. 3**,** 673-83.

Avota, E., Gulbins, E., Schneider-Schaulies, S., 2011. DC-SIGN mediated sphingomyelinase-activation and ceramide generation is essential for enhancement of viral uptake in dendritic cells. PLoS Pathog. 7**,** e1001290.

Barnard, D.L., 2004. Inhibitors of measles virus. Antivir Chem Chemother. 15**,** 111-9.

Beckford, A.P., Kaschula, R.O., Stephen, C., 1985. Factors associated with fatal cases of measles. A retrospective autopsy study. S Afr Med J. 68**,** 858-63.

Behrens, S.E., Tomei, L., De Francesco, R., 1996. Identification and properties of the RNA-dependent RNA polymerase of hepatitis C virus. EMBO J. 15**,** 12-22.

Bellini, W.J., et al., 2005. Subacute sclerosing panencephalitis: more cases of this fatal disease are prevented by measles immunization than was previously recognized. J Infect Dis. 192**,** 1686-93.

Belser, J.A., et al., 2007. DAS181, a novel sialidase fusion protein, protects mice from lethal avian influenza H5N1 virus infection. J Infect Dis. 196**,** 1493-9.

Berger, A., 1999. How does herd immunity work? BMJ. 319**,** 1466-7.

Bernal, F., et al., 2010. A stapled p53 helix overcomes HDMX-mediated suppression of p53. Cancer Cell. 18**,** 411-22.

Black, F.L., Yannet, H., 1960. Inapparent measles after gamma globulin administration. JAMA. 173**,** 1183-8.

Bouche, F.B., Ertl, O.T., Muller, C.P., 2002. Neutralizing B cell response in measles. Viral Immunol. 15**,** 451-71.

Burdeinick-Kerr, R., Govindarajan, D., Griffin, D.E., 2009. Noncytolytic clearance of sindbis virus infection from neurons by gamma interferon is dependent on Jak/STAT signaling. J Virol. 83**,** 3429-35.

Calderwood, M.A., et al., 2007. Epstein-Barr virus and virus human protein interaction maps. Proc Natl Acad Sci U S A. 104**,** 7606-11.

Carsillo, T., et al., 2006. hsp72, a host determinant of measles virus neurovirulence. J Virol. 80**,** 11031-9.

Cevik, B., et al., 2004. The phosphoprotein (P) and L binding sites reside in the N-terminus of the L subunit of the measles virus RNA polymerase. Virology. 327**,** 297-306.

Chakrabarti, S., et al., 2001. Pre-emptive oral ribavirin therapy of paramyxovirus infections after haematopoietic stem cell transplantation: a pilot study. Bone Marrow Transplant. 28**,** 759-63.

Chase, G., et al., 2008. Hsp90 inhibitors reduce influenza virus replication in cell culture. Virology. 377**,** 431-9.

Coughlin, M.M., Bellini, W.J., Rota, P.A., 2013. Contribution of dendritic cells to measles virus induced immunosuppression. Rev Med Virol. 23**,** 126-38.

Couturier, M., et al., 2010. High affinity binding between Hsp70 and the C-terminal domain of the measles virus nucleoprotein requires an Hsp40 co-chaperone. J Mol Recognit. 23**,** 301-15.

Cox, R., et al., 2013. Structural and functional characterization of the mumps virus phosphoprotein. J Virol. 87**,** 7558-68.

Cruz, D.J., et al., 2013. High content screening of a kinase-focused library reveals compounds broadly-active against dengue viruses. PLoS Negl Trop Dis. 7**,** e2073.

Curran, J., 1998. A role for the Sendai virus P protein trimer in RNA synthesis. J Virol. 72**,** 4274-80.

Das, S., Kalpana, G.V., 2009. Reverse two-hybrid screening to analyze protein-protein interaction of HIV-1 viral and cellular proteins. Methods Mol Biol. 485**,** 271-93.

Das, T., et al., 1998. RNA polymerase of vesicular stomatitis virus specifically associates with translation elongation factor-1 alphabetagamma for its activity. Proc Natl Acad Sci U S A. 95**,** 1449-54.

Davidkin, I., et al., 2008. Persistence of measles, mumps, and rubella antibodies in an MMR-vaccinated cohort: a 20-year follow-up. J Infect Dis. 197**,** 950-6.

de Chassey, B., et al., 2008. Hepatitis C virus infection protein network. Mol Syst Biol. 4**,** 230.

De Clercq, E., 2012. Human viral diseases: what is next for antiviral drug discovery? Curr Opin Virol. 2**,** 572-9.

de Swart, R.L., et al., 2007. Predominant infection of CD150+ lymphocytes and dendritic cells during measles virus infection of macaques. PLoS Pathog. 3**,** e178.

Debnath, A.K., Radigan, L., Jiang, S., 1999. Structure-based identification of small molecule antiviral compounds targeted to the gp41 core structure of the human immunodeficiency virus type 1. J Med Chem. 42**,** 3203-9.

Delpeut, S., et al., 2012. Host factors and measles virus replication. Curr Opin Virol. 2**,** 773-83.

Deng, T., Vreede, F.T., Brownlee, G.G., 2006. Different de novo initiation strategies are used by influenza virus RNA polymerase on its cRNA and viral RNA promoters during viral RNA replication. J Virol. 80**,** 2337-48.

Desfosses, A., et al., 2011. Nucleoprotein-RNA orientation in the measles virus nucleocapsid by three-dimensional electron microscopy. J Virol. 85**,** 1391-5.

DeStefano, F., Chen, R.T., 2001. Autism and measles-mumps-rubella vaccination: controversy laid to rest? CNS Drugs. 15**,** 831-7.

Dias, A., et al., 2009. The cap-snatching endonuclease of influenza virus polymerase resides in the PA subunit. Nature. 458**,** 914-8.

Dorig, R.E., et al., 1993. The human CD46 molecule is a receptor for measles virus (Edmonston strain). Cell. 75**,** 295-305.

Dorr, P., et al., 2005. Maraviroc (UK-427,857), a potent, orally bioavailable, and selective small-molecule inhibitor of chemokine receptor CCR5 with broad-spectrum anti-human immunodeficiency virus type 1 activity. Antimicrob Agents Chemother. 49**,** 4721-32.

Duprex, W.P., Collins, F.M., Rima, B.K., 2002. Modulating the function of the measles virus RNA-dependent RNA polymerase by insertion of green fluorescent protein into the open reading frame. J Virol. 76**,** 7322-8.

Emerson, S.U., 1982. Reconstitution studies detect a single polymerase entry site on the vesicular stomatitis virus genome. Cell. 31**,** 635-42.

European Centre for Disease Prevention and Control, E., 2010-2012. Number of measles cases.

http://www.ecdc.europa.eu/en/healthtopics/measles/epidemiological_data/Pages/Number-of-measles-cases-2010.aspx.; 9/10/2013, 2:05pm

Fernandez, P., et al., 2010. A phase 2, randomized, double-blind safety and pharmacokinetic assessment of respiratory syncytial virus (RSV) prophylaxis with motavizumab and palivizumab administered in the same season. BMC Pediatr. 10**,** 38.

Ferreira, C.S., et al., 2010. Measles virus infection of alveolar macrophages and dendritic cells precedes spread to lymphatic organs in transgenic mice expressing human signaling lymphocytic activation molecule (SLAM, CD150). J Virol. 84**,** 3033-42.

Ferrer-Orta, C., et al., 2009. Structural insights into replication initiation and elongation processes by the FMDV RNA-dependent RNA polymerase. Curr Opin Struct Biol. 19**,** 752-8.

Ferron, F., et al., 2002. Viral RNA-polymerases -- a predicted 2'-O-ribose methyltransferase domain shared by all Mononegavirales. Trends Biochem Sci. 27**,** 222-4.

Fischl, M.A., 1999. Antiretroviral therapy in 1999 for antiretroviral-naive individuals with HIV infection. AIDS. 13 Suppl 1**,** S49-59.

Freeman, A.F., et al., 2004. A new complication of stem cell transplantation: measles inclusion body encephalitis. Pediatrics. 114**,** e657-60.

Freeman, J.M., et al., 1967. Additional evidence of the relation between subacute inclusion-body encephalitis and measles virus. Lancet. 2**,** 129-31.

Fugier-Vivier, I., et al., 1997. Measles virus suppresses cell-mediated immunity by interfering with the survival and functions of dendritic and T cells. J Exp Med. 186**,** 813-23.

Garg, R.K., 2008. Subacute sclerosing panencephalitis. J Neurol. 255**,** 1861-71.

Gay, N.J., 2004. The theory of measles elimination: implications for the design of elimination strategies. J Infect Dis. 189 Suppl 1**,** S27-35.

Goldman, J.M., Druker, B.J., 2001. Chronic myeloid leukemia: current treatment options. Blood. 98**,** 2039-42.

Griffin, D.E., 2011. Viral encephalomyelitis. PLoS Pathog. 7**,** e1002004.

Hagiwara, K., et al., 2008. Phosphorylation of measles virus nucleoprotein upregulates the transcriptional activity of minigenomic RNA. Proteomics. 8**,** 1871-9.

Hao, L., et al., 2008. Drosophila RNAi screen identifies host genes important for influenza virus replication. Nature. 454**,** 890-3.

Hara, S., et al., 2003. Combination therapy with intraventricular interferon-alpha and ribavirin for subacute sclerosing panencephalitis and monitoring measles virus RNA by quantitative PCR assay. Brain Dev. 25**,** 367-9.

Hilleman, M.R., 2001. Current overview of the pathogenesis and prophylaxis of measles with focus on practical implications. Vaccine. 20**,** 651-65.

Hoffmann, H.H., Palese, P., Shaw, M.L., 2008. Modulation of influenza virus replication by alteration of sodium ion transport and protein kinase C activity. Antiviral Res. 80**,** 124-34.

Hoffmann, H.H., et al., 2011. Broad-spectrum antiviral that interferes with de novo pyrimidine biosynthesis. Proc Natl Acad Sci U S A. 108**,** 5777-82.

Honda T, Y.M., Sato H and Kai C, 2013. Pathogenesis of Encephalitis Caused by Persistent Measles Virus Infection. Encephalitis. ISBN 978-953-51-0925-9.

Hosoya, M., et al., 2004. Pharmacokinetics and effects of ribavirin following intraventricular administration for treatment of subacute sclerosing panencephalitis. Antimicrob Agents Chemother. 48**,** 4631-5.

Huiming, Y., Chaomin, W., Meng, M., 2005. Vitamin A for treating measles in children. Cochrane Database Syst Rev. CD001479.

Iwasaki, M., et al., 2009. The matrix protein of measles virus regulates viral RNA synthesis and assembly by interacting with the nucleocapsid protein. J Virol. 83**,** 10374-83.

Jensen, M.R., et al., 2011. Intrinsic disorder in measles virus nucleocapsids. Proc Natl Acad Sci U S A. 108**,** 9839-44.

Karlas, A., et al., 2010. Genome-wide RNAi screen identifies human host factors crucial for influenza virus replication. Nature. 463**,** 818-22.

Karp, C.L., et al., 1996. Mechanism of suppression of cell-mediated immunity by measles virus. Science. 273**,** 228-31.

Kim, S.S., et al., 2007. A cell-based, high-throughput screen for small molecule regulators of hepatitis C virus replication. Gastroenterology. 132**,** 311-20.

Kingston, R.L., et al., 2004. Structural basis for the attachment of a paramyxoviral polymerase to its template. Proc Natl Acad Sci U S A. 101**,** 8301-6.

Klein, S., Schoneberg, I., Krause, G., 2012. [The historical development of immunization in Germany. From compulsory smallpox vaccination to a National Action Plan on Immunization]. Bundesgesundheitsblatt Gesundheitsforschung Gesundheitsschutz. 55**,** 1512-23.

Kolakofsky, D., et al., 2004. Viral DNA polymerase scanning and the gymnastics of Sendai virus RNA synthesis. Virology. 318**,** 463-73.

Konig, R., et al., 2008. Global analysis of host-pathogen interactions that regulate early-stage HIV-1 replication. Cell. 135**,** 49-60.

Konig, R., et al., 2010. Human host factors required for influenza virus replication. Nature. 463**,** 813-7.

Koon, H.B., et al., 2005. Imatinib-induced regression of AIDS-related Kaposi's sarcoma. J Clin Oncol. 23**,** 982-9.

Krishnan, M.N., et al., 2008. RNA interference screen for human genes associated with West Nile virus infection. Nature. 455**,** 242-5.

Laine, D., et al., 2003. Measles virus (MV) nucleoprotein binds to a novel cell surface receptor distinct from FcgammaRII via its C-terminal domain: role in MV-induced immunosuppression. J Virol. 77**,** 11332-46.

Laine, D., et al., 2005. Measles virus nucleoprotein induces cell-proliferation arrest and apoptosis through NTAIL-NR and NCORE-FcgammaRIIB1 interactions, respectively. J Gen Virol. 86**,** 1771-84.

Lemon, K., et al., 2011. Early target cells of measles virus after aerosol infection of non-human primates. PLoS Pathog. 7**,** e1001263.

Leopardi, R., et al., 1993. Cell proteins bind to sites within the 3' noncoding region and the positive-strand leader sequence of measles virus RNA. J Virol. 67**,** 785-90.

Li, J., et al., 2008. A conserved motif in region v of the large polymerase proteins of nonsegmented negative-sense RNA viruses that is essential for mRNA capping. J Virol. 82**,** 775-84.

Li, Q., et al., 2009. A genome-wide genetic screen for host factors required for hepatitis C virus propagation. Proc Natl Acad Sci U S A. 106**,** 16410-5.

Longhi, S., 2012. The measles virus N(TAIL)-XD complex: an illustrative example of fuzziness. Adv Exp Med Biol. 725**,** 126-41.

Ludlow, M., et al., 2013a. Infection of lymphoid tissues in the macaque upper respiratory tract contributes to the emergence of transmissible measles virus. J Gen Virol. 94**,** 1933-44.

Ludlow, M., et al., 2013b. Measles virus infection of epithelial cells in the macaque upper respiratory tract is mediated by subepithelial immune cells. J Virol. 87**,** 4033-42.

Ludwig, S., 2009. Targeting cell signalling pathways to fight the flu: towards a paradigm change in anti-influenza therapy. J Antimicrob Chemother. 64**,** 1-4.

Luo, G., et al., 2000. De novo initiation of RNA synthesis by the RNA-dependent RNA polymerase (NS5B) of hepatitis C virus. J Virol. 74**,** 851-63.

Ma-Lauer, Y., et al., 2012. Virus-host interactomes--antiviral drug discovery. Curr Opin Virol. 2**,** 614-21.

Makhortova, N.R., et al., 2007. Neurokinin-1 enables measles virus trans-synaptic spread in neurons. Virology. 362**,** 235-44.

Malakhov, M.P., et al., 2006. Sialidase fusion protein as a novel broad-spectrum inhibitor of influenza virus infection. Antimicrob Agents Chemother. 50**,** 1470-9.

Malur, A.G., et al., 2002. Analysis of the mutations in the active site of the RNA-dependent RNA polymerase of human parainfluenza virus type 3 (HPIV3). Gene Expr. 10**,** 93-100.

Mankertz, A., et al., 2011. Spread of measles virus D4-Hamburg, Europe, 2008-2011. Emerg Infect Dis. 17**,** 1396-401.

Mao, H., et al., 2008. Inhibition of human parainfluenza virus type 3 infection by novel small molecules. Antiviral Res. 77**,** 83-94.

Marquet, R., et al., 1995. tRNAs as primer of reverse transcriptases. Biochimie. 77**,** 113-24.

Moellering, R.E., et al., 2009. Direct inhibition of the NOTCH transcription factor complex. Nature. 462**,** 182-8.

Morin, B., Rahmeh, A.A., Whelan, S.P., 2012. Mechanism of RNA synthesis initiation by the vesicular stomatitis virus polymerase. EMBO J. 31**,** 1320-9.

Moss, R.B., et al., 2012. A phase II study of DAS181, a novel host directed antiviral for the treatment of influenza infection. J Infect Dis. 206**,** 1844-51.

Muhlebach, M.D., et al., 2011. Adherens junction protein nectin-4 is the epithelial receptor for measles virus. Nature. 480**,** 530-3.

Naniche, D., et al., 1993. Human membrane cofactor protein (CD46) acts as a cellular receptor for measles virus. J Virol. 67**,** 6025-32.

Noton, S.L., et al., 2010. Evidence that the polymerase of respiratory syncytial virus initiates RNA replication in a nontemplated fashion. Proc Natl Acad Sci U S A. 107**,** 10226-31.

Noyce, R.S., et al., 2011. Tumor cell marker PVRL4 (nectin 4) is an epithelial cell receptor for measles virus. PLoS Pathog. 7**,** e1002240.

Ogino, T., Banerjee, A.K., 2007. Unconventional mechanism of mRNA capping by the RNA-dependent RNA polymerase of vesicular stomatitis virus. Mol Cell. 25**,** 85-97.

Oldstone, M.B., et al., 2005. A role for dual viral hits in causation of subacute sclerosing panencephalitis. J Exp Med. 202**,** 1185-90.

Pal, G., 2011. Effects of ribavirin on measles. J Indian Med Assoc. 109**,** 666-7.

Paul, A.V., et al., 1998. Protein-primed RNA synthesis by purified poliovirus RNA polymerase. Nature. 393**,** 280-4.

Perez, J.T., et al., 2010. Influenza A virus-generated small RNAs regulate the switch from transcription to replication. Proc Natl Acad Sci U S A. 107**,** 11525-30.

Plans-Rubió, P., 2012. Is the basic reproductive number (R0) for measles viruses observed in recent outbreaks lower than in the pre-vaccination era? Eurosurveillance 17.

Plemper, R.K., Snyder, J.P., 2009. Measles control--can measles virus inhibitors make a difference? Curr Opin Investig Drugs. 10**,** 811-20.

Pleschka, S., et al., 2001. Influenza virus propagation is impaired by inhibition of the Raf/MEK/ERK signalling cascade. Nat Cell Biol. 3**,** 301-5.

Plotch, S.J., et al., 1981. A unique cap(m7GpppXm)-dependent influenza virion endonuclease cleaves capped RNAs to generate the primers that initiate viral RNA transcription. Cell. 23**,** 847-58.

Poch, O., et al., 1990. Sequence comparison of five polymerases (L proteins) of unsegmented negative-strand RNA viruses: theoretical assignment of functional domains. J Gen Virol. 71 (Pt 5), 1153-62.

Pohl, C., et al., 2007. Measles virus M and F proteins associate with detergent-resistant membrane fractions and promote formation of virus-like particles. J Gen Virol. 88, 1243-50.

Polack, F.P., et al., 1999. Production of atypical measles in rhesus macaques: evidence for disease mediated by immune complex formation and eosinophils in the presence of fusion-inhibiting antibody. Nat Med. 5, 629-34.

Prussia, A., et al., 2011. Systematic Approaches towards the Development of Host-Directed Antiviral Therapeutics. Int J Mol Sci. 12, 4027-52.

Public-Health-England, 2013. Measles - The Disease. Green Book Chapter 21.

Public-Health-Foundation, 2008. Epidemiology and Prevention of Vaccine-Preventable Diseases. Public Health Foundation, Washington, DC, USA. 11th.

Rahmeh, A.A., et al., 2010. Molecular architecture of the vesicular stomatitis virus RNA polymerase. Proc Natl Acad Sci U S A. 107, 20075-80.

Rahmeh, A.A., et al., 2012. Critical phosphoprotein elements that regulate polymerase architecture and function in vesicular stomatitis virus. Proc Natl Acad Sci U S A. 109, 14628-33.

Reeves, P.M., et al., 2005. Disabling poxvirus pathogenesis by inhibition of Abl-family tyrosine kinases. Nat Med. 11, 731-9.

Ribeiro Ede, A., Jr., et al., 2009. Binding of rabies virus polymerase cofactor to recombinant circular nucleoprotein-RNA complexes. J Mol Biol. 394, 558-75.

Rider, T.H., et al., 2011. Broad-spectrum antiviral therapeutics. PLoS One. 6, e22572.

Rima, B.K., Duprex, W.P., 2011. New concepts in measles virus replication: getting in and out in vivo and modulating the host cell environment. Virus Res. 162, 47-62.

Robb, N.C., et al., 2009. NS2/NEP protein regulates transcription and replication of the influenza virus RNA genome. J Gen Virol. 90, 1398-407.

Robert-Koch-Institut, 2013. http://www.rki.de/DE/Content/Infekt/EpidBull/Archiv/2013/Ausgaben/25_13.pdf?__blob=publicationFile.; 9/10/2013, 2:15pm

Ruigrok, R.W., Crepin, T., 2010. Nucleoproteins of negative strand RNA viruses; RNA binding, oligomerisation and binding to polymerase co-factor. Viruses. 2**,** 27-32.

Salerno, D., et al., 2007. Direct inhibition of CDK9 blocks HIV-1 replication without preventing T-cell activation in primary human peripheral blood lymphocytes. Gene. 405**,** 65-78.

Santhakumar, D., et al., 2010. Combined agonist-antagonist genome-wide functional screening identifies broadly active antiviral microRNAs. Proc Natl Acad Sci U S A. 107**,** 13830-5.

Sato, H., et al., 2007. Measles virus N protein inhibits host translation by binding to eIF3-p40. J Virol. 81**,** 11569-76.

Schneider-Schaulies, J., et al., 1999. Measles virus in the CNS: the role of viral and host factors for the establishment and maintenance of a persistent infection. J Neurovirol. 5**,** 613-22.

Schneider-Schaulies, S., Schneider-Schaulies, J., 2009. Measles virus-induced immunosuppression. Curr Top Microbiol Immunol. 330**,** 243-69.

Schoehn, G., et al., 2004. The 12 A structure of trypsin-treated measles virus N-RNA. J Mol Biol. 339**,** 301-12.

Schulz M, M.S., 2013. Masernimpfung bei Kindern bis zu einem Alter von zwei Jahren. Versorgungsatlas, http://www.versorgungsatlas.de/themen/alle-analysen-nach-datum-sortiert/?tab=1&uid=43.; 9/11/2013, 10:34am

Selisko, B., et al., 2012. Molecular basis for nucleotide conservation at the ends of the dengue virus genome. PLoS Pathog. 8**,** e1002912.

Servet-Delprat, C., et al., 2000. Measles virus induces abnormal differentiation of CD40 ligand-activated human dendritic cells. J Immunol. 164**,** 1753-60.

Sessions, O.M., et al., 2009. Discovery of insect and human dengue virus host factors. Nature. 458**,** 1047-50.

Shafer, R.W., Vuitton, D.A., 1999. Highly active antiretroviral therapy (HAART) for the treatment of infection with human immunodeficiency virus type 1. Biomed Pharmacother. 53**,** 73-86.

Shapira, S.D., et al., 2009. A physical and regulatory map of host-influenza interactions reveals pathways in H1N1 infection. Cell. 139**,** 1255-67.

Shaw, M.L., 2011. The host interactome of influenza virus presents new potential targets for antiviral drugs. Rev Med Virol. 21**,** 358-69.

Stogner, S.W., et al., 1993. Ribavirin and intravenous immune globulin therapy for measles pneumonia in HIV infection. South Med J. 86**,** 1415-8.

Sugai, A., et al., 2012. Phosphorylation of measles virus phosphoprotein at S86 and/or S151 downregulates viral transcriptional activity. FEBS Lett. 586**,** 3900-7.

Sun, A., et al., 2008. Potent non-nucleoside inhibitors of the measles virus RNA-dependent RNA polymerase complex. J Med Chem. 51**,** 3731-41.

Tatsuo, H., et al., 2000. SLAM (CDw150) is a cellular receptor for measles virus. Nature. 406**,** 893-7.

Tawar, R.G., et al., 2009. Crystal structure of a nucleocapsid-like nucleoprotein-RNA complex of respiratory syncytial virus. Science. 326**,** 1279-83.

Taylor, B., et al., 1999. Autism and measles, mumps, and rubella vaccine: no epidemiological evidence for a causal association. Lancet. 353**,** 2026-9.

Tremaglio, C.Z., et al., 2013. Respiratory syncytial virus polymerase can initiate transcription from position 3 of the leader promoter. J Virol. 87**,** 3196-207.

Wakefield, A.J., et al., 1998. Ileal-lymphoid-nodular hyperplasia, non-specific colitis, and pervasive developmental disorder in children. Lancet. 351**,** 637-41.

Wang, Q.Y., et al., 2011. Inhibition of dengue virus through suppression of host pyrimidine biosynthesis. J Virol. 85**,** 6548-56.

Warren, T.K., et al., 2010. Antiviral activity of a small-molecule inhibitor of filovirus infection. Antimicrob Agents Chemother. 54**,** 2152-9.

Watanabe, A., et al., 2011. Peroxiredoxin 1 is required for efficient transcription and replication of measles virus. J Virol. 85**,** 2247-53.

Wells, J.A., McClendon, C.L., 2007. Reaching for high-hanging fruit in drug discovery at protein-protein interfaces. Nature. 450**,** 1001-9.

Whelan, S.P., Wertz, G.W., 1999. Regulation of RNA synthesis by the genomic termini of vesicular stomatitis virus: identification of distinct sequences essential for transcription but not replication. J Virol. 73**,** 297-306.

White, L.K., et al., 2007. Nonnucleoside inhibitor of measles virus RNA-dependent RNA polymerase complex activity. Antimicrob Agents Chemother. 51**,** 2293-303.

WHO-media-center, 2013. WHO: Measles deaths decline,but elimination progress stalls in some regions. http://www.who.int/mediacentre/news/notes/2013/measles_20130117/en/.; 9/11/2013, 5:50 pm

Wise, J., 2013. Largest group of children affected by measles outbreak in Wales is 10-18 year olds. BMJ. 346**,** f2545.

Yan, D., et al., 2013. Dual Myxovirus Screen Identifies a Small-Molecule Agonist of the Host Antiviral Response. J Virol.

Yegambaram, K., Kingston, R.L., 2010. The feet of the measles virus polymerase bind the viral nucleocapsid protein at a single site. Protein Sci. 19**,** 893-9.

Yoon, J.J., et al., 2008. High-throughput screening-based identification of paramyxovirus inhibitors. J Biomol Screen. 13**,** 591-608.

Yoon, J.J., et al., 2009. Target analysis of the experimental measles therapeutic AS-136A. Antimicrob Agents Chemother. 53**,** 3860-70.

Zhou, H., et al., 2008. Genome-scale RNAi screen for host factors required for HIV replication. Cell Host Microbe. 4**,** 495-504.

Zhou, S., et al., 2013. Screening for inhibitors of the hepatitis C virus internal ribosome entry site RNA. Bioorg Med Chem.

4 Acknowledgments

First of all, I would like to thank my mentor Professor Richard Plemper at Georgia State University. I am very grateful that he gave me the opportunity to work in the exciting field of measles virus replication and antiviral development. His continuous and endless support, guidance advice, patience, motivation, discussions and encouragement helped me to advance my PhD studies, my scientific thinking and become the scientist I am today. He supported and backed-up all different kinds of new methods and never hesitated to establish new techniques or collaborations. Thank you so much for that.

I am very thankful to Professor Dieter Wolf at the University of Stuttgart for giving me the opportunity to go abroad to perform all experimental studies at the Richard Plemper laboratory. Without his support, this study and experience would not have been possible.

A special thanks to all members of the Plemper lab for their help and contribution to my projects and a great working atmosphere.
I am especially thankful to Melinda and Dan for great team-work, good suggestions and helpful discussion for my projects as well as support in conducting experiments. I learned so much from both of them. Thank you also for introducing me to smores and lots of different Chinese dishes.

I am grateful to a number of students with whom I worked with at Emory University and at Georgia State University. Thanks to Tanja, Melanie, Max, Moritz, Isabel, and Andrea for friendship, support and fun in the lab. I am thankful to Tamara, Leah, Alexandria, Erica and Adam for their technical support in the lab. I worked only a few weeks with Sukanya, Hari, Vidhi and Neha, but it was a great experience to have them around and work with them.

I would like to thank Abel for his encouragement, discussions about my project, his patience and tolerance. He encouraged and supported me at every step. I am especially thankful for his understanding and his love.

A very special thanks goes out to my parents, Sylvia and Dieter, my brother Thorsten and my sister Leonie. Even though we were miles apart, their support and encouragement was endless. They were wonderful and stood by me in every situation. I am greatly thankful for their help, efforts, advices, motivation and guidance that they have always given me.

Last but not least, this thesis would not have been possible without the help and contribution of many people. I thank everyone that I forgot to mention here.

5 Curriculum Vitae

Personal Details:

Name	Stefanie Anja Krumm, Diplom-Biologin (technically oriented, t. o.)
Date of Birth	October 01, 1983
Nationality	German

Academic Education:

Since Jan 2010	PhD student at the University of Stuttgart, Germany Mentor: Prof. Richard Plemper, Ph.D., Georgia State University, Center for Inflammation, Immunity & Infection, Atlanta, GA, USA Graduate advisor: Dieter Wolf, Ph.D., Professor, Department of Biochemistry, University of Stuttgart
Oct 30, 2009	Diploma thesis at the Department of Pediatrics, Emory University, Atlanta, USA and Department of Biochemistry, University of Stuttgart
Oct 2009	Pre-Diploma thesis at the Institute of Biology, Department of Animal Physiology, University of Stuttgart
Oct 2003 - Oct 2009	Study of Technical Biology at University of Stuttgart
July 2003	Abitur at the Stromberg Gymnasium, Vaihingen

Publications:

Stefanie A Krumm[#], Dan Yan[#], Elise S Hovingh, Taylor J Evers, Theresa Enkirch, G. Prabhakar Reddy, Aiming Sun, Manohar T Saindane, Richard F Arrendale, George Painter, Dennis C Liotta, Michael G Natchus, Veronika von Messling and Richard K Plemper

“An orally available, small-molecule polymerase inhibitor shows efficacy against a lethal morbillivirus infection in a large animal model.” SCIENCE TRANSLATIONAL MEDICINE, April 2014, [#] *equal contribution*

Stefanie A Krumm, Makoto Takeda and Richard K Plemper

“The Measles Virus Nucleocapsid Protein Tail Domain is Dispensable for Viral Polymerase Recruitment and Activity”, THE JOURNAL OF BIOLOGICAL CHEMISTRY, October 2013

Dan Yan, **Stefanie A Krumm**, Aiming Sun, David A Steinhauer, Mingh Luo, Martin L Moore and Richard K Plemper
"Dual Myxovirus Screen Identifies a Small-Molecule Agonist of the Host Antiviral Response", JOURNAL OF VIROLOGY, August 2013

J. Maina Ndungu, **Stefanie A Krumm**, Dan Yan, Richard F Arrendale, G. Prabhakar Reddy, Taylor Evers, Randy B Howard, Michael G Natchus, Manohar T Saindane, Dennis C Liotta, Richard K Plemper, James Patrick Snyder and Aiming Sun
"Non-nucleoside Inhibitors of the Measles Virus RNA-dependent RNA Polymerase: Synthesis, Structure-Activity Relationships and Pharmacokinetics", JOURNAL OF MEDICINAL CHEMISTRY, May 2012

Melanie Dochow, **Stefanie A Krumm**, James E Crowe Jr, Martin L Moore and Richard K Plemper
"Independent Structural Domains in the Paramyxovirus Polymerase Protein", THE JOURNAL OF BIOLOGICAL CHEMISTRY, February 2012

Aiming Sun, J. Maina Ndungu, **Stefanie A Krumm**, Jeong-Joong Yoon, Pahk Thepchatri, Michael G Natchus, Richard K Plemper and James P Snyder
"Host-Directed Inhibitors of Myxoviruses: Synthesis and in Vitro Biochemical Evaluation", ACS MEDICINAL CHEMISTRY LETTERS, August 2011

Stefanie A Krumm, J. Maina Ndungu, Jeong-Joong Yoon, Melanie Dochow, Aiming Sun, Michael G Natchus, James P Snyder and Richard K Plemper
"Potent Host-Directed Small-Molecule Inhibitors of Myxovirus RNA-dependent RNA-polymerases", PLoS ONE, 6 (5): e20069, May 2011

Jeong-Joong Yoon†, **Stefanie A Krumm†**, J. Maina Ndungu, Vanessa Hoffman, Bettina Bankamp, Paul A Rota, Aiming Sun, James P Snyder and Richard K Plemper
"Target Analysis of the Experimental Measles Therapeutic AS-136A", ANTIMICROBIAL AGENTS AND CHEMOTHERAPY, September 2009, † *equal contribution*

6 Appendix: Publications and Manuscripts

Summary of attached publications/manuscripts listed in chronological order:

1. **Stefanie A Krumm**, Maximilian Sohn, Tamara Kazarian, Moritz Messner, Kristina Rostad and Richard K Plemper
   "Tag insertion in the Measles Virus Nucleoprotein Tail Contributes to Packaging of Viral Polymerase Components and Leaves Polymerase Activity Unaffected"
   In preparation

2. **Stefanie A Krumm**[#], Dan Yan[#], Elise S Hovingh, Taylor J Evers, Theresa Enkirch, G. Prabhakar Reddy, Aiming Sun, Manohar T Saindane, Richard F Arrendale, George Painter, Dennis C Liotta, Michael G Natchus, Veronika von Messling and Richard K Plemper
   "An orally available, small-molecule polymerase inhibitor shows efficacy against a lethal morbillivirus infection in a large animal model."
   SCIENCE TRANSLATIONAL MEDICINE, April 2014
   [#]These authors contributed equally

3. **Stefanie A Krumm**, Makoto Takeda and Richard K Plemper
   "The Measles Virus Nucleocapsid Protein Tail Domain is Dispensable for Viral Polymerase Recruitment and Activity"
   THE JOURNAL OF BIOLOGICAL CHEMISTRY, October 2013

4. Dan Yan, **Stefanie A Krumm**, Aiming Sun, David A Steinhauer, Mingh Luo, Martin L Moore and Richard K Plemper
   "Dual Myxovirus Screen Identifies a Small-Molecule Agonist of the Host Antiviral Response"
   JOURNAL OF VIROLOGY, August 2013

5. J. Maina Ndungu, **Stefanie A Krumm**, Dan Yan, Richard F Arrendale, G. Prabhakar Reddy, Taylor Evers, Randy B Howard, Michael G Natchus, Manohar T Saindane, Dennis C Liotta, Richard K Plemper, James P Snyder, and Aiming Sun
   "Non-nucleoside Inhibitors of the Measles Virus RNA-dependent RNA Polymerase: Synthesis, Structure-Activity Relationships and Pharmacokinetics"
   JOURNAL OF MEDICINAL CHEMISTRY May 2012

6. Melanie Dochow, **Stefanie A. Krumm**, James E Crowe Jr, Martin L Moore and Richard K Plemper
   "Independent Structural Domains in the Paramyxovirus Polymerase Protein"
   THE JOURNAL OF BIOLOGICAL CHEMISTRY, February 2012

7. Aiming Sun, J. Maina Ndungu, **Stefanie A Krumm**, Jeong-Joong Yoon, Pahk Thepchatri, Michael G Natchus, Richard K Plemper, and James P Snyder
   "Host-Directed Inhibitors of Myxoviruses: Synthesis and in Vitro Biochemical Evaluation"
   ACS MEDICINAL CHEMISTRY LETTERS, August 2011

8. **Stefanie A Krumm**, J. Maina Ndungu, Jeong-Joong Yoon, Melanie Dochow, Aiming Sun, Michael G Natchus, James P Snyder and Richard K Plemper
   "Potent Host-Directed Small-Molecule Inhibitors of Myxovirus RNA-dependent RNA-polymerases"
   PLoS ONE, 6 (5): e20069, May 2011

Manuscript 1

Stefanie A Krumm, Maximilian Sohn, Tamara Kazarian, Moritz Messner, Kristina Rostad and Richard K Plemper

“Tag insertion in the Measles Virus Nucleoprotein Tail Contributes to Packaging of Viral Polymerase Components and Leaves Polymerase Activity Unaffected”

In preparation

Tag insertion in the Measles Virus Nucleoprotein Tail Contributes to Packaging of Viral Polymerase Components and Leaves Polymerase Activity Unaffected

Stefanie A Krumm[1], Maximilian Sohn[1], Tamara Kazarian[1], Moritz Messner[1], Kristina Rostad[1] and Richard K Plemper[1,2,*]

[1] Center for Inflammation, Immunity & Infection, Georgia State University, Atlanta, GA 30303

[2] Department of Pediatrics, Emory University School of Medicine, Atlanta, GA 30322

Running title: Changing Ntail domain organization leaves Polymerase activity leaves unaffected

* corresponding author: Petit Science Center/Ste 712
100 Piedmont Av
Center for Inflammation, Immunity & Infection
Georgia State University
Atlanta, GA 30303
Phone: 404-413-3579
E-mail: rplemper@gsu.edu

Abstract

The paramyxovirus polymerase complex consists of the phosphoprotein (P) and the poylmerasen (L) proteins that interact with nucleocapsid (N) protein-encapsidated RNP for replication and transcription. N contains a core domain involved in RNA encapsidation and a 125-residue C-terminal Ntail considered to mediate P-L binding to RNP for polymerization. Ntail of measles virus (MeV) is largely unstructured, but a terminal microdomain is implicated in P binding. To better understand the organization of MeV N and the role of Ntail sections upstream of this microdomain in polymerase activity and particle assembly, we subjected the protein to linker insertion mutagenesis and monitored N bioactivity in minireplicon assays. A central section of Ncore and all sites tested in Ntail tolerated linker insertion. However, only Ntail accepted insertion of larger epitope tags upstream of the interaction microdomain in minireplicon assays and, after recovery of the corresponding recombinant MeV, the context of viral infection. This recombinant mutant virus showed reduced glycoprotein levels embedded in the envelope and increased P and matrix protein (M) levels. Mutant virus maintained wild type like fusion kinetics. However, it showed a 24-hour initial delay in replication, followed by wild type-like proliferation. Reinfection with progeny virus reproduced this growth profile, excluding viral adaptation during the lag phase. Monitoring the amplification kinetic of viral mRNA and genome after infection revealed a threshold-effect: delayed onset of primary transcription and replication, followed by wild type-like late-state polymerization. Our study identifies folding domains in the MeV Ncore and Ntail. Modifying the Ntail section has little effect on polymerase bioactivity, but a proper spatial organization of the tail is critical for efficient packaging of viral components into particles.

Introduction

Measles virus (MeV) among other human and animal pathogens such as respiratory syncytial virus (RSV), Nipah and Hendra viruses or canine distemper virus (CDV), belongs to the *Paramyxoviridae* family. Together myxoviruses are the major cause for human morbidity and mortality due to viral respiratory illness globally (42). Being part of the order *Mononegavirales,* measles virus' key feature is the nonsegmented negative strand RNA genome packaged in an enveloped pleomorphic particle. The RNA is encapsidated by multiple copies of the nucleoprotein (N) to form the helical N-RNA complex called RNP. Only the encapsidated RNA is the template used by the viral polymerase for transcription and replication (27). The newly synthesized viral genome is encapsidated by N concurrently with its synthesis. The viral transcription and replication machinery is composed of the polymerase (L) and its cofactor, the phosphoprotein (P) as well as several host factors (27). The polymerase is thought to contain all major enzymatic activities required for mRNA synthesis and genome production such as capping, polyadenylation, methylation and nucleotide polymerization (29, 35, 36). The P protein, for which the tetramerization domain (PMT) has been solved recently (10), is comprised of a N-terminal part (PNT amino acid1-230) and a C-terminal part (PCT amino acid 231-507). The N protein is composed of a conserved core domain (Ncore, amino acid 1-400) which contains the N self-assembly domain and RNA binding function as well as the interaction site with PNT in the N^0-P complex and an intrinsically disordered tail domain (Ntail, amino acid 401-525) which is exposed at the surface of the viral nucleocapsid (9). Ncore furthermore determines the spatial organization of the helical RNP complex, whereas the presence or absence of the Ntail alters overall RNP structure (11). Complete removal of the Ntail by trypsin digestion decreases RNP diameter and pitch and increases its rigidity. Based on sequence alignment, the Ntail is comprised of 3 conserved boxes namely box 1 (amino acid 400-420), box 2 (amino acid 489–506) and box 3 (amino acid 517-525) as well as an α-helical molecular recognition element (α-MoRE, amino acid 488–499) located within box 2 (12). The Ntail interacts with a domain in P (XD, a triple α -helical domain) located at the very C-terminus in the PCT part of P (amino acid -507) via its MoRE domain. There are two models described on how the N-MoRE-P-XD complex formation occurs (33). The fly casting model describes induced folding of the MoRE domain to an α-helical configuration upon interaction with XD whereas the conformer selection model proposes a partially

preformed helical complexity of the MoRE domain. Both result in a tight bond between the MoRE and the XD domain. This interaction is proposed to be critical for replication and transcription. The sequence upstream of MoRE domain stays unstructured and nothing is known about this section's function and organization (33). The unknown receptor NR interacting with box1 can still bind when the MoRE domain is bound to XD. Additionally, Ntail has been shown to interact with the matrix protein (M) (21) facilitating assembly of viral particles while inhibiting transcription and replication as well as cellular factors such as Hsp72 and IRF3 (6, 9).

To gain some insight into MeV RNP structure, the RSV N-RNA crystal structure was docked into the EM density map of MeV RNP. Using this model, and additional small angle scattering, nuclear magnetic resonance spectroscopy and EM analyses, the beginning of Ntail was placed in the inside of the N-RNA helical ring (22). The Ntail is thought to protrude through the interstitial space between successive turns, leaving about 50 amino acids located inside the RNP and 75 amino acids freely exposed on the surface. This *in situ* analysis furthermore provided evidence that the MoRE domain interacts transiently with Ncore. Consequently, removal of the Ntail allows direct contact between consecutive turns and rigidifies the helical structure and this furthermore validates the RSV-based MeV N-RNA model.

Several predictors have been utilized to examine the domain organization of N *in silico*. Extensive studies have demonstrated that the Ntail is largely unstructured and the N protein was categorized as an intrinsically disordered protein (premolten globules) ((46) and reviewed in (33)). That work focused predominantly on the MoRE domain in box 2 as well as box 3 in the Ntail and their binding affinities and induced folding upon binding of P-XD (34). Other available data centered around protein-protein or protein-RNA interactions rather than on bioactivity of the N protein to support RdRp function and the Ntail section upstream of the MoRE domain (1, 3, 19, 24, 25, 34). Therefore, no comprehensive *in vitro* bioactivity data are available that systematically investigate the complete domain and microdomain architecture including the Ncore.

For the first time, we subjected the complete MeV nucleoprotein N to an *in vitro* biochemical functional study to probe its domain organization as predicted by the disordered regions estimates *in silico* and assess bioactivity in a minireplicon assay as well as in the viral context. Guided by this screen, we confirmed the accuracy of disordered region predictions by demonstrating that tag insertions in the N protein at

locations predicted to be disordered are tolerated and the proteins are bioactive. We also emphasized the necessity to combine several algorithms for highest precision. Furthermore, successful recovery of a recombinant measles virus harboring a larger tag in a microdomain in the Ntail region upstream of the MoRE domain demonstrated that addition of the tag did not affect polymerase activity. It rather affected proper particle assembly which consequently delayed onset of primary transcription and hence replication.

Material and Methods

Cell Culture, viruses and transfection

African green monkey kidney epithelial (CCK-81;ATCC) cells stably expressing human signaling lymphocytic activation molecule (SLAM) (Vero/hSLAM, (37)) and baby hamster kidney (C-13; ATCC) cells stably expressing T7 polymerase (BSR-T7/5, (5)) were maintained in Dulbecco's modified Eagle's medium supplemented with 10% fetal bovine serum at 37°C and 5% CO_2. Every fifth passage, both cell lines were incubated in the presence of G-418 (100 µg/ml). In this study, recombinant MeV-Edmonston (recMeV) and the modified N-436HA variant (recMeV N-436HA) were used. For virus stock preparation, Vero-hSLAM cells were infected at a multiplicity of infection (MOI) of 0.001, incubated at 37°C and cell associated virus was released through two consecutive freeze/thaw cycles. Viral titers were determined by 50 % tissue culture infectious dose ($TCID_{50}$) as described (15). Cells were transfected using Lipofectamine 2000 (Invitrogen) according to manufactures instructions. Calcium phosphate precipitation (Promega) was used for transfection for virus recovery.

Minireplicon luciferase reporter assay

BSR-T7/5 cells ($4x10^5$ in a 12 well plate format) were transfected with plasmids encoding for Edm-L (1.1µg), Edm-P (0.27µg), Edm-N and Edm-N mutant variants (0.42µg) and the MeV luciferase replicon reporter (1.2µg). Otherwise identically transfected control cells received vector DNA in place of the N expression plasmid (mock). Cells were lysed 40 hours post transfection in Glo lysis buffer (Promega) and luciferase activities in cleared lysates were determined using Bright-Glo luciferase substrate (Promega) in a top count reader (Perkin Elmer) or a Synergy H1 microplate reader (BioTek). Mock values were subtracted from values obtained of various N mutants and normalized for those obtained in the presence of standard N.

Molecular biology

For N domain screening, four amino acid (GDAS) linker insertion constructs were cloned with appropriate primers introducing a silent NsiI restriction site according to QuikChange protocol (Stratagene). Constructs were sequence confirmed as well as presence of the NsiI restriction site was confirmed. For detection purposes, those constructs were tagged with a HA tag (SGGGYPYDVPDYA) at the C-terminus of N through PCR amplification using appropriate primer and religation using a silent NdeI restriction site in the tag sequence.

Same strategy was applied to introduce the HA tag flanked by a short linker sequence (SGGGYPYDVPDYAGGGS) at various positions in the N protein as well as the tetracysteine tag (SGGGFLNCCPGCCMEPGGGS), using the NdeI silent restriction site or a SmaI restriction site, respectively, for relegation of the amplified product.

Plasmids containing cDNA full length copies of MeV Edm were modified by replacing the N open reading frame (ORF) with an N-E436HA or the L ORF with L-Flag ORF. All newly generated constructs were sequence confirmed.

Antibodies, SDS-PAGE and immunoblotting

BSR-T7/5 cells were transfected in a 12-well plate format (4x105 per well) with 2 µg of N-encoding plasmid DNA and 40 hours post transfection cells were washed once with phosphate buffered saline (PBS) and lysed in RIPA buffer (1% sodium deoxycholate, 1% NP-40, 150 mM NaCl, 50 mM Tris-Cl, pH 7.2, 10 mM EDTA, 50 mM NaF, 0.05% SDS, protease inhibitors [Roche], 1 mM phenylmethylsulfonyl fluoride). Cleared lysates (20.000xg, 10 min, 4°C) were mixed with 5 x urea protein loading buffer (200 mM Tris, pH 6.8; 8 M urea; 5% sodium dodecyl sulfate (SDS); 0.1 mM EDTA; 0.03% bromphenol blue; 1.5% dithiothreitol). Samples were denatured for 30 min at 50°C, fractionated on 8 % SDS-PAGE gels, blotted on polyvinylidene difluoride (PVDF) membranes (Millipore) and subjected to enhanced chemiluminescence detection (Pierce) using specific antibodies directed against MeV-N (83KKKII, Millipore), MeV-P (9H4, Abcam), MeV-M (MAB8910, Millipore), MeV-F, MeV-H, GAPDH (6C5, Ambion) or HA (16B12, Abcam) as specified.Immunoblots were developed using a ChemiDoc digital imaging system (Bio-Rad). The Image Lab package (Bio-Rad) was used for densitometry.

Virus recovery

Recombinant MeV was recovered in BSR-T7/5 cells by transfecting 5 µg of the cDNA copy of the modified genome and ICB-N (0.8 µg), ICB- P (0.6 µg) and ICB-L (0.55 µg) by calcium phosphate precipitation. Cells were overlaid 48 hrs post transfection onto Vero/hSLAM cells and emerging infectious particles were passaged twice in Vero/hSLAM cells. Integrity of newly rescued virus was confirmed by extracting total RNA from virus infected cells (RNeasy mini kit, Quiagen) and cDNA was created using random hexamer primers and Superscript III reverse transcriptase (Invitrogen). Modified genome regions were amplified using appropriate primers and sequenced.

Fusion content mixing assay

Vero/hSLAM effector cells were transfected with plasmids encoding (Dsp1–7) dual split-protein component (26) and Vero/hSLAM target cells received plasmid DNA encoding the Dsp8–11 subunit. Both populations were combined 24 hours post transfection and reseeded in a solid wall 96-well plate in CO_2 independent media supplemented with 15% FBS (GIBCO). The EnduRen (Promega) life cell substrate was added six hours later and incubated for 60 min at 37°C. Cells were then infected with recMeV and recMeV N-E436HA with a MOI of 25 and the virus was spin inoculated for 1600 rpm, 40 min, 4°C. Reconstitution of renilla luciferase as a marker for cell content-mixing was recorded in a Synergy H1 (BioTek) multi-function microplate reader continuously at 37°C for 14 hours. The results of individual experiments were normalized for the peak value of the recMeV dataset, followed by averaging of the normalized values. The averages of relative recMeV values do not reach 100% at any time, since peak values are not reached at exactly identical time points in individual experiments.

Multi step growth curve

Prior to infection for the multi step growth curve, viral stocks were diluted to about $1x10^4$ $TCID_{50}$/ml and titers were reconfirmed by $TCID_{50}$ titration. Vero/hSLAM cells ($1x10^5$ per well in a 12 well format) were infected with the different MeV variants at a MOI of 0.01 $TCID_{50}$/well for 1 hr and the inoculum was replaced by DMEM with 7.5% FBS. Every 12 hours cell-associated virus was harvested. Virus was released by two consecutive freeze and thaw cycles and titer was determined by $TCID_{50}$ titration method.

Virus adaptation

To induce better growth, Vero-hSLAM cells were infected with recMeV N-E436-4xcys of 0.1 TCID50/ml and incubated. When extensive viral CPE was detected, cell-associated viral particles were released, diluted 10-fold and used for infection of fresh cell monolayers. Adaptation was terminated when viral growth was readily detectable.

Viral mRNA quantification

To determine mRNA ratios of cell associated virus, Vero/hSLAM cells were infected with a MOI of 0.02 of the recMeV and 0.05 for the recMeV N-E436HA. When maximal cytopathic effect was observed, total RNA was isolated with the RNeasy Mini kit (Quiagen) according to manufacture instructions. Next, cDNA was created using oligo dT primer and Superscript RT III (Invitrogen). The mRNA was quantified

using primer annealing in the N-, P-, M-, H- and GAPDH-ORFs and iTaq SybrGreen Supermix with Rox (Biorad) in an Ambion 7500 Fast thermal cycler.

One step growth curve assessment of viral titers, mRNA and genome amplification

This assay was performed as previously described (38). To quantify cell associated viral titers, mRNA and genome amplification in a one step growth curve, Vero/hSlam cells were infected with a MOI of 0.2 and spin inoculated (3000 rpm, 30 min, 4 °C). For viral titers assessment, cell associated virus was harvested every two hours and determined with TCID50 method. For mRNA and genome amplification, total RNA was harvested hourly. To quantify mRNA copy numbers, oligo dT cDNA was synthesized; for genome copy numbers a specific primer located in the leader (gtaaggatagttcaatcaatg) was used. qPCR was performed in a 7500 Fast real-time PCR system (Applied Biosystems) using Fast 1xstep Mix (Applied Biosystems) omitting the RT step and specific primer pair 3 (20). To quantify copy numbers a standard curve was created using the pTM1-Edm N plasmid linearized with BamHI as template.

Cell free virus purification

Two 15 cm dishes were infected with revMeV (moi 0.02) and recMeV N-E436HA (moi 0.05) and supernatant was harvested when max CPE was observed. Supernatant was cleared at 1.500xg for 20 min at 4°C, PEG precipitated (10% PEG, 2% NaCl) at10.000xg, 90 min, 4°C, separated through a 20%/60% sucrose cushion (SW 41, 30.000 rpm, 90 min 4°C) and pelleted (SW41, 30.000 rpm, 20 min, 4°C). Pellet was resuspended immediately in protein loading buffer. Samples were fractionated through SDS-PAGE as described and normalized for equal amount of N protein. The Image Lab package (Bio-Rad) was used for densitometry.

***In silico* analysis of MeV N domain organization**

Identification of linker domain organization was performed as described previously (13). Briefly, MeDor (30) was used to predict disordered domains in MeV-Edm N using the IUPred (14), GlobPlot2 (32), DisEMBL (31), FoldIndex (39), SPITZ (47) and RONN (50) algorithms. Furthermore, MeV-Edm N was submitted to PONDRFIT (49) and Disopred (48) for disorder predictions. To quantitatively assess the consensus of all algorithms, average values of GlobPlot2, FoldIndex and DomCut were transformed to positive integers and positive output scores of all algorithms were normalized for identical hit cut-off values. All averaged were then transformed to a 0-

10 scale and plotted as a function of MeV N residues. MeV N secondary structure prediction was based on the StrBioLib library of the Pred2ary program (8), embedded in the MeDor package. For DomCut (45) based identification of disordered regions in MeV N, paramyxovirus N protein sequences were aligned using the ClustalW2 (28) and MUSCLE (17) algorithm. Results of three different settings were compared and relative DomCut propensity scores then averaged separately based on the different sequence alignments.: A) different MeV genotypes (MeV-Edm (genotype A), MeV-Gambia (genotype B2), MeV-Toulon (genotype C2), MeV-Amsterdam (genotype G2), MeV-Illinois (genotype D3), MeV-Alaska (genotype H2); B) different morbilliviruses (MeV-Edm, MeVGambia B2, MeV-Toulon, MeV-Alaska, MeV Amsterdam, RPV-KabeteO, canine distemper virus (CDV) Onderstepoort, CDV 5804, peste des petits ruminants virus Turkey 2000, dolphin morbillivirus and C) members of all paramyxovirus genera (MeV-Edm, CDV 5804, NIV, HPIV type 1 C35, HPIV type 3 LZ22, HPIV type 2, HPIV type 4 SKPIV4, NDV-ISG0210 (Genbank JF340367), Tupaia paramyxovirus , RSV A2, human metapneumovirus Sabana). For references regarding viral isolated see reference (13).

Results

Bioinformatics analysis to predict unstructured and disordered regions in the N protein suggested a flexible linker region in Ncore. The hinge region is expected to be located between amino acids 131-146 (2, 18). To increase accuracy of the prediction, we combined a panel of different algorithms to identify intrinsically disordered sections within the N protein. We started by applying the DomCut algorithm to three groups of viruses. Firstly, we generated average propensity scores for the N protein sequence of a variety of MeV genotypes. In the same way, we then compared in the second group different members of the *Morbillivirus* genus and the third group examined members of each genus of the *Paramyxovirinae* and *Pneumovirinae* all belonging to the *Paramyxoviridae* family. DomCut scores were in a second step cross-referenced quantitatively with the MeDor (MEtaserver of DisOrder), PONDR-FIT meta-predictor, and DRIP-PRED predictors of unstructured sections and the results were graphically plotted as a function of MeV N in figure 1A. In total we applied nine algorithms and a secondary structure prediction embedded in the StrBioLib library of the Pred2ary program. Top panels shows each used algorithm and predicted unstructured regions are color-coded. The last panel is a color-representation of the average values of all used predictors. This analysis is in agreement with the published one and highlighted three candidate domains, one at the N-terminus (around amino acids 10-30), one in a central Ncore section (around amino acids 110-145) and the last one in the complete Ntail starting at amino acid 401.

Four amino acid insertion analysis of the nucleoprotein

To perform a structural analysis and probe accuracy of secondary structure predictions of the nucleoprotein biochemically, 42 constructs were engineered with a four amino acid linker (GDAS) inserted approximately every 10 to 20 amino acids throughout the complete N protein. The precise insertion positions were chosen with consideration of structure predictions. The standard N protein and all four amino acid tagged constructs were HA tagged at their C-terminus for detection purposes only. Immunoblot analysis demonstrated that all constructs were expressed albeit at different steady state levels presumably due to misfoldings caused by the four amino acid tag (figure 1B). To assess impact of the tag insertion on N protein functionality, all constructs were tested in the minireplicon reporter assay using firefly luciferase activity for quantification of bioactivity relative to a C-terminally HA tagged only

variant. This C-terminally HA tagged construct itself had a 30% decrease in bioactivity when compared to the unmodified N (data not shown). Analysis of bioactivity of the 42 constructs showed that insertion of GDAS was only tolerated at nine different positions. Tag insertion at positions M1, F131, H133 and S138 in the Ncore and positions N427, E436, E446, A459 and T469 in the Ntail returned high levels of activity between 70 to 130% compared to C-terminally HA tagged standard (figure 1C, black line). Overlay of activity data with the average scores of nine different predictions revealed agreement of high level of bioactivity and high score number of predicted unstructured regions and confirms flexible linker in the region from amino acid 131 to 145 (figure 1C, grey line).

To further evaluate the structural domain organization, a larger and structurally more prominent HA tag (SGGGYPYDVPDYAGGGS) was inserted at the four most active sites, two in the Ncore and two in the Ntail domain, identified in the four amino acid insertion screen. Figure 1D shows that all constructs were expressed at levels comparable to unmodified MeV N protein. Bioactivity was determined in the minireplicon assay in comparison to otherwise unchanged N protein. Placing the HA tag in the hinge region at position F131 substantially reduced bioactivity to about ~7% of standard N protein while the tag at position S138 resulted in about ~40% activity. Tag insertion at position E436 in the Ntail turned out to be the most active N protein with only 10% reduction in bioactivity, while insertion at position T469 reduced bioactivity to about 70% compared to unmodified N protein (figure 1E). This screen identified microdomains, one in the Ncore and several in the Ntail. However, one microdomain around residue 436 in the Ntail returned high levels of bioactivity.

Effects of larger structure tag insertions in the Ntail

To further evaluate flexibility of the hinge region and the most active region in the Ntail, a structurally dominant tetracysteine tag (4xcys, SGGGFLNCCPGCCMEP GGGS) was inserted at both termini (M1 and D525) and at positions F131, S138, N427 and E436 in the N protein. Variants with the tag at positions F131 and S138 showed reduced expression levels while all other constructs are standard N-like expressed (figure 2A). Bioactivity was tested in the minireplicon assay. Only the variants with the 4xcys tag in the Ntail at positions N427 and E436 showed about 20% and 40% activity, respectively, when compared with the standard N protein (figure 2B). The other four constructs with the 4xcys tag added either at the termini or in the Ncore returned only very low bioactivity (about 4% for F131 4xcys and 5% for

C-terminally tagged D525 4xcys) or lacked detectable bioactivity (>1% for N-terminally tagged M1 4xcys and S138 4xcys). This outcome highlights the same bioactivity tendencies as those determined with the HA tagged constructs.

We next assessed the impact of the 4xcys tag at position E436 in the viral context and recovered a recombinant virus harboring the E436-4xcys tag in N protein. The recombinant virus displayed poor growth in infected cells as determined by reduced and slow lateral spread through the cell monolayer. Sequencing of the modified part in N protein at day 15 post rescue after the RT-PCR confirmed tag integrity and therefore we continued to passage the virus to test if better growth can be induced by allowing the virus to adapt. Adaptation was monitored by speed and spread of cytopathic effect (CPE) development. After eleven more re-infections of new host cells the adapted virus displayed faster growth and spread through the cell monolayer than the rescued version three days post infection at same multiplicity of infection (MOI) as shown in the microphotographs in figure 2C. To confirm integrity of the 4xcys tag, the modified region in the N protein of the adapted virus was sequence analyzed again at day 45 post rescue and two point mutations in the tag were identified replacing the second pair of two cysteines with two arginines which destroys the tag integrity (figure 2D). The first amino acid in the tag, a phenylalanine, was changed to the amino acid leucine in half the viral genomes. This result underlines that a tag at this position in the Ntail is tolerated, but also demonstrates preference for a sequence with low structural elements.

To test if increased or decreased flexibility of sequences flanking the tag is of importance for tolerance of the tag regarding bioactivity of the construct, different spacer lengths (0=no spacer, 2=SGGGSGGG) were introduced at position F131 in the core, and also at positions E436, K441 and T469 in the tail and compared to the original linker length (SGGG) in a minireplicon assay. When comparing the expression levels in whole cell lysates the proteins with a 4xcys tag at position F131 again had the lowest steady state expression level while all other variants were standard N-like expressed independently of the linker length (S1A). No improved bioactivity was detectable in the minireplicon luciferase activity assay when the linker length was varied (S1B).

HA tag insertion in Ntail is viable in the context of viral particles but affects particle assembly

Since the HA epitope tag was the largest accepted tag located in Ntail domain at position E43 with highest (standard N-like) bioactivity in the minireplicon assay, we continued to assess the impact of the HA tag in the context of viral particles. The N-E436HA mutation was inserted into the nucleoprotein ORF in a cDNA copy of recMeV and the virus was recovered successfully. To compare viral protein composition, cell free virions were purified through a discontinuous sucrose gradient centrifugation and concentrated by pelleting the purified virions. The protein composition was analyzed by western blotting with antibodies specific for MeV proteins. We adjusted for equal N protein signal intensities and showed that the mutant virus has more P and M and less H and F proteins than the unmodified recombinant virus as depicted qualitatively in figure 3A and quantitatively in figure 3B. To evaluate if this changes in viral protein production reflects changes in mRNA steady state levels, we quantified $\Delta\Delta$Ct values from mRNA of virus infected cells with similar CPE (figure 3C). There are no significant changes in P, M or H mRNA levels when adjusted for equal N mRNA levels. Since it was surprising to see a reduced level of envelope proteins in the mutant virions, we assessed impact of this phenotype on fusion in a cell-to-cell fusion kinetic assay that measures content mixing in almost real time (4). This assay measures reconstitution of individually expressed chimeric eGFP-Luciferase protein halves upon membrane fusion mediated by the virus. Although the recMeV N-E436HA virus had reduced amounts of H and F in the envelope, the assay revealed that the mutant virus induces fusion much faster than the unmodified virus. The recMeV N-E436HA virus reached also much higher peak values earlier than the standard recMeV (figure 3D). Taken together, these data suggest that the tag insertion in the Ntail affects particle assembly only.

recMeV N-E436HA shows delayed onset of growth kinetics

To further evaluate effect of the tag in the N protein and the consequences of more M and P proteins in the virion on viral growth kinetics, we subjected the mutant virus to a multi-step growth curve comparison with standard recMeV (figure 4A). Cell associated virus was harvested every 12 hours and titers determined by $TCID_{50}$. Standard recMeV reached peak titers at 48 hours post infection (pI) while onset of production of progeny particles of the mutant virus was delayed for 24 hrs, followed by standard recMeV like growth. The recMeV N-E436HA virus reached one log lower peak titer at 60 hours pI. To exclude the possibility that the mutant virus genetically

changed during the 24 hours lag phase, the samples at each peak titer (48 hrs for recMeV and 60 hrs for revMeV-NE436HA) were diluted, new titers determined and used as inoculum for a second (reinfected) growth curve performed under the same conditions as the previous one (figure 4B). Both viruses revealed the same growth kinetics as in the first comparison, the mutant virus reached its one magnitude lower peak titers even later at 84 hours. But the 24 hours delayed onset followed by wild type-like growth in the log phase phenotype was identical. Identical pattern in signal intensity increase could be detected when same samples were probed for the P protein in western blot as depicted in figure 4C. The P protein signal intensifies later during the time course for the mutant virus as viral titers increase. This indicates that polymerase activity *per se* is not affected by the tagged N protein. However, onset of replication is delayed.

Delayed transcription and replication in mutant virus

To investigate if this delayed progeny particle production phenotype was due to altered transcription or replication speed, we next quantified mRNA and genome levels during infection to compare RNA amplification kinetics. Both viruses were spin inoculated for a one step growth curve at a MOI of 0.2 and cell associated virus harvested every 2 hours. In parallel, total RNA was isolated hourly. Titer of inoculum was determined to confirm that the experiment started with same amount of infectious particles (figure 5A). Titer of cell-associated virus was determined and the one step growth curve revealed the identical phenotype as the multi step growth curve (figure 5B). Titers for recMeV were first detectable at 12 hours pI and reached a plateau at 24 hours pI. The mutant virus showed same delay in onset of progeny particle formation as in a multi step growth curve and it reached similar titers as the wild type about 10 hours later and grew finally to almost the same peak titer as recMeV at about 33 hrs pI. To assess mRNA and genome production during the time course, total RNA was harvested hourly until 14 hrs pI, continued after 24 hrs and followed until 30 hours pI. cDNA was created using either oligo dT primer for mRNA or a leader specific primer for genomic RNA amplification. To quantify relative copy numbers, a quantitative real time PCR (qPCR) with a N standard curve using a Taqman probe was performed. The recMeV virus on the one hand displayed linear amplification until 6 hours pI and continued with a logarithmic increase of N mRNA copies until it reached its plateau about 25 hours pI. This is consistent with the viral plateau/peak titers at around 24 - 25 hours pI. Genomic amplification was delayed

until 6 hours pI. After that initial lag phase genome copy numbers started to increase linearly for 2 hours and at 10 hours pI logarithmic amplification launched. Beginning of linear amplification of the genome goes hand in hand with onset of logarithmic mRNA production. Consequently, the first progeny virus particles were detectable 11 hours pI. The mutant recMeV N-E436HA on the other hand showed delayed onset of mRNA production until 6 hours pI. Linear amplification of mRNA copies commenced between 6 to 10 hours pI and only then it continued with logarithmic increase in N mRNA copy numbers. Examination of genome copy numbers revealed a delay in production until 10 hours post infection, followed by linear increase for 2 hours (same as WT) and only after 14 hours logarithmic production of genomes started. As a result, first progeny viral particles were detected 24 hours post infection. Both viruses showed identical curves, even almost identical copy numbers; the only difference the four hours delayed onset of the transcription/replication process for the recMeV N-E436HA. Essentially when recMeV started its logarithmic phase, the mutant virus began its linear phase. This experiment confirmed that RdRp activity is not inhibited by the HA tagged N protein but delayed progeny particle formation is due to delayed onset of transcription.

Discussion

The measles virus nucleoprotein N belongs to the family of intrinsically disordered proteins. Secondary structure predictors can be utilized to predict domain organization for this category of proteins. There are several predictors with different algorithms available. They compare the primary amino acid sequence for composition, low secondary structure content, low sequence complexity and high sequence variability. It has been shown that for most accurate predictions, several predictors need to be combined and analyzed (2, 18). This fact has been demonstrated for the MeV polymerase L. *In silico* predictions suggested and *in vitro* bioactivity data confirmed a three domain organization of L (13, 16). Our investigations evaluated the domain organization of MeV nucleoprotein and we confirmed the hinge region at amino acids 131-145 in the N core in a bioactivity assay. This supports the overall bi-lobal folding in two globules of the MeV Ncore as determined by crystallization of other viruses of the order *Mononegavirales* (40). The complete Ntail is structurally disordered and we identified microdomains that tolerated larger structurally dominant tag insertions such as a HA epitope and a tetracysteine tag. The residue in the N protein that tolerated a tag insertion best was at E436 in the Ntail. The RSV-based model of MeV RNP places the beginning of the Ntail inside the helical RNP and the first 50 amino acids from the Ntail (amino acid 401-450) inside the interstitial space. This model posits the residue E436 inside the RNP turns. The 4xcys virus that replaced the two consecutive cysteines with arginines in the tag reducing its structure is the best indication for high selective pressure to keep structure at a minimum in this area in the tail, while additional increase in tail length can be tolerated. For bioactivity, the HA epitope tag seemed to be the best compromise regarding its structure. Examination of viral protein composition of recovered recombinant virus revealed reduced levels of the envelope proteins H and F but increased P and M protein concentrations. That reduction of surface glycoproteins in the viral envelope did not affect fusion kinetics as measured by cell-to-cell fusion content mixing. This fusion kinetic assay measures fusion of virus membrane with host membranes and host cell content mixing; it does not assess viral content release. Genomic RNA quantification at time point 0 in the one step growth curve revealed that there is about three fold more genomic RNA copies for the recMeV N-E436 than for recMeV in the inoculum. To achieve same infectivity

more input viral particles were required. This reduced infectivity could be due to defective interfering (DI) particles even though the virus stock was prepared at low MOI to avoid DI particle production. Detected DI genomes in the qPCR must have internal deletions since trailer copyback DI would not have been detected in this qPCR since primer for first strand synthesis annealed in the leader region. It has been shown that paramyxovirus DI particles contain more trailer copyback than internal deletion DIs (23). Hence, actual number of DI particles can be much higher. This affects the cell-to-cell fusion assay majorly, since DI particles have functional envelope proteins that mediate fusion. For this kind of assay it would be beneficial to adjust for same amounts of envelope proteins rather than for same infectious particles. Taken that fact into account, it can be concluded that fusion of the mutant virus is not affected when compared to the untagged recMeV.

The Longhi group has demonstrated that introducing single point mutations in box 2 in the Ntail abolished P-XD induced alpha-helical folding and reduces the binding affinity of N-MoRE to P-XD drastically (41). The group was able to recover viable recombinant virus, which showed only slight changes in transcription elongation speed. Interestingly, the Longhi group also observed and concluded that MeV L activity, but not infectivity, tolerates modifications in the Ntail. In the study at hand, all domains required to stabilize the polymerase complex onto the template are still present and the MoRE domain in box 2 as well as box 3 are still functional.

Reduced level of H and F in the envelope and more P and M did, however, affect mRNA amplification and as a consequence thereof genome production and infectious particle formation and release. In this present study, changes in RNP structure that would alter P and/or L interactions with N in RNP formation or the N^0-P interaction are unlikely to occur since transcription and replication is only delayed, but once it started, it is wild-type like.. The high levels of P and M proteins could be a contributing factor. Abundance of P could inhibit RdRp activity. P protein phosphorylation has been shown to downregulate transcription. Strong P phosphorylation sites are usually covered by association with N and are therefore protected (43). Lots of free P have those phosphorylation sites exposed and therefore are likely to be phosphorylated and consequently inhibit transcription. M itself is a negative regulator of MeV transcription (21, 44). By binding to box 3 in Ntail, M promotes virus assembly and particle release (7). The amounts of M in the particle could inhibit primary transcription initially until it e.g. dissociates or diffuses in the

cytosol. It furthermore could be the contributing factor later in the viral life cycle for misbalance in particle assembly since M also interacts with the cytoplasmic tails of H and F. Epitope tag addition in the Ntail could affect N-M interactions and therefore alter M functionality.

There are four speculative explanations and events that could account for that phenotype induced by the HA epitope tag in the Ntail. I) Even though the initial fusion event was unaffected, release of viral RNP from the particle could be either delayed or hindered and hence this step in the viral life cycle is slower and not all N encapsidated genomes might be released into the cytosol successfully. II) The addition of the epitope tag itself could affect interactions with other viral proteins and /or host cell factors. This interaction could be required for RdRp to efficiently use all RNP as templates. Based on delayed mRNA amplification, it can be assumed that this interaction involves most likely factors that are needed predominantly for transcription or that are required for release of the RNP and transportation to its destination for replication. III) Fusion and particle content release are wild-type like. The tag insertion in the Ntail provokes that sequence sections usually buried within the RNP in between the turns are exposed on the RNP surface. This effect might alter structure or flexibility in sections that are in close proximity to E436 and also have consequences on interactions with other factors. IV) The addition of the HA or the 4xcys tag could furthermore change the distance of MoRE/box3 domain with regard to Ncore. That also could affect factors that are required for transcription and/or assembly. With regard to viral players, P and M are the most likely ones.

In conclusion, this study demonstrated that integrity of Ntail domain organization is required for efficient packaging of viral proteins into the particle. It does not affect RdRp activity *per se*. It modifies interaction of viral of host factors that are not required for polymerase activity and fidelity but rather for assembling the viral components into particles. As a consequence, reinfection of new cells with modified virions affects initiation of transcription.

Acknowledgements

This work was supported, in part, by Public Health Service grants AI071002 and AI057157 from the NIH/NIAID (to R.K.P.).

References

1. **Bernard, C., S. Gely, J. M. Bourhis, X. Morelli, S. Longhi, and H. Darbon.** 2009. Interaction between the C-terminal domains of N and P proteins of measles virus investigated by NMR. FEBS letters **583:**1084-1089.
2. **Bourhis, J. M., B. Canard, and S. Longhi.** 2007. Predicting protein disorder and induced folding: from theoretical principles to practical applications. Current protein & peptide science **8:**135-149.
3. **Bourhis, J. M., K. Johansson, V. Receveur-Brechot, C. J. Oldfield, K. A. Dunker, B. Canard, and S. Longhi.** 2004. The C-terminal domain of measles virus nucleoprotein belongs to the class of intrinsically disordered proteins that fold upon binding to their physiological partner. Virus research **99:**157-167.
4. **Brindley, M. A., M. Takeda, P. Plattet, and R. K. Plemper.** 2012. Triggering the measles virus membrane fusion machinery. Proceedings of the National Academy of Sciences of the United States of America **109:**E3018-3027.
5. **Buchholz, U. J., S. Finke, and K. K. Conzelmann.** 1999. Generation of bovine respiratory syncytial virus (BRSV) from cDNA: BRSV NS2 is not essential for virus replication in tissue culture, and the human RSV leader region acts as a functional BRSV genome promoter. Journal of virology **73:**251-259.
6. **Carsillo, T., Z. Traylor, C. Choi, S. Niewiesk, and M. Oglesbee.** 2006. hsp72, a host determinant of measles virus neurovirulence. Journal of virology **80:**11031-11039.
7. **Cathomen, T., B. Mrkic, D. Spehner, R. Drillien, R. Naef, J. Pavlovic, A. Aguzzi, M. A. Billeter, and R. Cattaneo.** 1998. A matrix-less measles virus is infectious and elicits extensive cell fusion: consequences for propagation in the brain. The EMBO journal **17:**3899-3908.
8. **Chandonia, J. M.** 2007. StrBioLib: a Java library for development of custom computational structural biology applications. Bioinformatics **23:**2018-2020.
9. **Colombo, M., J. M. Bourhis, C. Chamontin, C. Soriano, S. Villet, S. Costanzo, M. Couturier, V. Belle, A. Fournel, H. Darbon, D. Gerlier, and S. Longhi.** 2009. The interaction between the measles virus nucleoprotein and the Interferon Regulator Factor 3 relies on a specific cellular environment. Virology journal **6:**59.

10. **Communie, G., T. Crepin, D. Maurin, M. R. Jensen, M. Blackledge, and R. W. Ruigrok.** 2013. Structure of the tetramerization domain of measles virus phosphoprotein. Journal of virology **87:**7166-7169.
11. **Desfosses, A., G. Goret, L. Farias Estrozi, R. W. Ruigrok, and I. Gutsche.** 2011. Nucleoprotein-RNA orientation in the measles virus nucleocapsid by three-dimensional electron microscopy. Journal of virology **85:**1391-1395.
12. **Diallo, A., T. Barrett, M. Barbron, G. Meyer, and P. C. Lefevre.** 1994. Cloning of the nucleocapsid protein gene of peste-des-petits-ruminants virus: relationship to other morbilliviruses. The Journal of general virology **75 (Pt 1):**233-237.
13. **Dochow, M., S. A. Krumm, J. E. Crowe, Jr., M. L. Moore, and R. K. Plemper.** 2012. Independent structural domains in paramyxovirus polymerase protein. The Journal of biological chemistry **287:**6878-6891.
14. **Dosztanyi, Z., V. Csizmok, P. Tompa, and I. Simon.** 2005. The pairwise energy content estimated from amino acid composition discriminates between folded and intrinsically unstructured proteins. Journal of molecular biology **347:**827-839.
15. **Doyle, J., A. Prussia, L. K. White, A. Sun, D. C. Liotta, J. P. Snyder, R. W. Compans, and R. K. Plemper.** 2006. Two domains that control prefusion stability and transport competence of the measles virus fusion protein. Journal of virology **80:**1524-1536.
16. **Duprex, W. P., F. M. Collins, and B. K. Rima.** 2002. Modulating the function of the measles virus RNA-dependent RNA polymerase by insertion of green fluorescent protein into the open reading frame. Journal of virology **76:**7322-7328.
17. **Edgar, R. C.** 2004. MUSCLE: multiple sequence alignment with high accuracy and high throughput. Nucleic acids research **32:**1792-1797.
18. **Ferron, F., S. Longhi, B. Canard, and D. Karlin.** 2006. A practical overview of protein disorder prediction methods. Proteins **65:**1-14.
19. **Gely, S., D. F. Lowry, C. Bernard, M. R. Jensen, M. Blackledge, S. Costanzo, J. M. Bourhis, H. Darbon, G. Daughdrill, and S. Longhi.** 2010. Solution structure of the C-terminal X domain of the measles virus phosphoprotein and interaction with the intrinsically disordered C-terminal

domain of the nucleoprotein. Journal of molecular recognition : JMR **23:**435-447.

20. **Hummel, K. B., L. Lowe, W. J. Bellini, and P. A. Rota.** 2006. Development of quantitative gene-specific real-time RT-PCR assays for the detection of measles virus in clinical specimens. Journal of virological methods **132:**166-173.
21. **Iwasaki, M., M. Takeda, Y. Shirogane, Y. Nakatsu, T. Nakamura, and Y. Yanagi.** 2009. The matrix protein of measles virus regulates viral RNA synthesis and assembly by interacting with the nucleocapsid protein. Journal of virology **83:**10374-10383.
22. **Jensen, M. R., G. Communie, E. A. Ribeiro, Jr., N. Martinez, A. Desfosses, L. Salmon, L. Mollica, F. Gabel, M. Jamin, S. Longhi, R. W. Ruigrok, and M. Blackledge.** 2011. Intrinsic disorder in measles virus nucleocapsids. Proceedings of the National Academy of Sciences of the United States of America **108:**9839-9844.
23. **Killip, M. J., D. F. Young, D. Gatherer, C. S. Ross, J. A. Short, A. J. Davison, S. Goodbourn, and R. E. Randall.** 2013. Deep sequencing analysis of defective genomes of parainfluenza virus 5 and their role in interferon induction. Journal of virology **87:**4798-4807.
24. **Kingston, R. L., D. J. Hamel, L. S. Gay, F. W. Dahlquist, and B. W. Matthews.** 2004. Structural basis for the attachment of a paramyxoviral polymerase to its template. Proceedings of the National Academy of Sciences of the United States of America **101:**8301-8306.
25. **Kolakofsky, D., P. Le Mercier, F. Iseni, and D. Garcin.** 2004. Viral DNA polymerase scanning and the gymnastics of Sendai virus RNA synthesis. Virology **318:**463-473.
26. **Kondo, N., K. Miyauchi, and Z. Matsuda.** 2011. Monitoring viral-mediated membrane fusion using fluorescent reporter methods. Current protocols in cell biology / editorial board, Juan S. Bonifacino ... [et al.] **Chapter 26:**Unit 26 29.
27. **Lamb RA, P. G.** 2007. Paramyxoviridae: The viruses and their replication. Knipe DM, Howley PM, eds. Fields Virology, Philadelphia: Wolters Kluwer/Lippincott Williams & Wilkins. **5:**1449–1496.
28. **Larkin, M. A., G. Blackshields, N. P. Brown, R. Chenna, P. A. McGettigan, H. McWilliam, F. Valentin, I. M. Wallace, A. Wilm, R. Lopez, J. D.**

Thompson, T. J. Gibson, and D. G. Higgins. 2007. Clustal W and Clustal X version 2.0. Bioinformatics **23:**2947-2948.

29. **Li, J., A. Rahmeh, M. Morelli, and S. P. Whelan.** 2008. A conserved motif in region v of the large polymerase proteins of nonsegmented negative-sense RNA viruses that is essential for mRNA capping. Journal of virology **82:**775-784.
30. **Lieutaud, P., B. Canard, and S. Longhi.** 2008. MeDor: a metaserver for predicting protein disorder. BMC genomics **9 Suppl 2:**S25.
31. **Linding, R., L. J. Jensen, F. Diella, P. Bork, T. J. Gibson, and R. B. Russell.** 2003. Protein disorder prediction: implications for structural proteomics. Structure **11:**1453-1459.
32. **Linding, R., R. B. Russell, V. Neduva, and T. J. Gibson.** 2003. GlobPlot: Exploring protein sequences for globularity and disorder. Nucleic acids research **31:**3701-3708.
33. **Longhi, S.** 2012. The measles virus N(TAIL)-XD complex: an illustrative example of fuzziness. Advances in experimental medicine and biology **725:**126-141.
34. **Longhi, S., V. Receveur-Brechot, D. Karlin, K. Johansson, H. Darbon, D. Bhella, R. Yeo, S. Finet, and B. Canard.** 2003. The C-terminal domain of the measles virus nucleoprotein is intrinsically disordered and folds upon binding to the C-terminal moiety of the phosphoprotein. The Journal of biological chemistry **278:**18638-18648.
35. **Malur, A. G., N. K. Gupta, P. De Bishnu, and A. K. Banerjee.** 2002. Analysis of the mutations in the active site of the RNA-dependent RNA polymerase of human parainfluenza virus type 3 (HPIV3). Gene expression **10:**93-100.
36. **Ogino, T., and A. K. Banerjee.** 2007. Unconventional mechanism of mRNA capping by the RNA-dependent RNA polymerase of vesicular stomatitis virus. Molecular cell **25:**85-97.
37. **Ono, N., H. Tatsuo, Y. Hidaka, T. Aoki, H. Minagawa, and Y. Yanagi.** 2001. Measles viruses on throat swabs from measles patients use signaling lymphocytic activation molecule (CDw150) but not CD46 as a cellular receptor. Journal of virology **75:**4399-4401.
38. **Plumet, S., W. P. Duprex, and D. Gerlier.** 2005. Dynamics of viral RNA synthesis during measles virus infection. Journal of virology **79:**6900-6908.

39. **Prilusky, J., C. E. Felder, T. Zeev-Ben-Mordehai, E. H. Rydberg, O. Man, J. S. Beckmann, I. Silman, and J. L. Sussman.** 2005. FoldIndex: a simple tool to predict whether a given protein sequence is intrinsically unfolded. Bioinformatics **21:**3435-3438.
40. **Ruigrok, R. W., and T. Crepin.** 2010. Nucleoproteins of negative strand RNA viruses; RNA binding, oligomerisation and binding to polymerase co-factor. Viruses **2:**27-32.
41. **Shu, Y., J. Habchi, S. Costanzo, A. Padilla, J. Brunel, D. Gerlier, M. Oglesbee, and S. Longhi.** 2012. Plasticity in structural and functional interactions between the phosphoprotein and nucleoprotein of measles virus. The Journal of biological chemistry **287:**11951-11967.
42. **Stiver, G.** 2003. The treatment of influenza with antiviral drugs. CMAJ : Canadian Medical Association journal = journal de l'Association medicale canadienne **168:**49-56.
43. **Sugai, A., H. Sato, M. Yoneda, and C. Kai.** 2012. Phosphorylation of measles virus phosphoprotein at S86 and/or S151 downregulates viral transcriptional activity. FEBS letters **586:**3900-3907.
44. **Suryanarayana, K., K. Baczko, V. ter Meulen, and R. R. Wagner.** 1994. Transcription inhibition and other properties of matrix proteins expressed by M genes cloned from measles viruses and diseased human brain tissue. Journal of virology **68:**1532-1543.
45. **Suyama, M., and O. Ohara.** 2003. DomCut: prediction of inter-domain linker regions in amino acid sequences. Bioinformatics **19:**673-674.
46. **Uversky, V. N.** 2002. Natively unfolded proteins: a point where biology waits for physics. Protein science : a publication of the Protein Society **11:**739-756.
47. **Vullo, A., O. Bortolami, G. Pollastri, and S. C. Tosatto.** 2006. Spritz: a server for the prediction of intrinsically disordered regions in protein sequences using kernel machines. Nucleic acids research **34:**W164-168.
48. **Ward, J. J., L. J. McGuffin, K. Bryson, B. F. Buxton, and D. T. Jones.** 2004. The DISOPRED server for the prediction of protein disorder. Bioinformatics **20:**2138-2139.
49. **Xue, B., R. L. Dunbrack, R. W. Williams, A. K. Dunker, and V. N. Uversky.** 2010. PONDR-FIT: a meta-predictor of intrinsically disordered amino acids. Biochimica et biophysica acta **1804:**996-1010.

50. **Yang, Z. R., R. Thomson, P. McNeil, and R. M. Esnouf.** 2005. RONN: the bio-basis function neural network technique applied to the detection of natively disordered regions in proteins. Bioinformatics **21:**3369-3376.

Figure legends

Figure 1: Probing MeV N folding domains through four amino acid linker and HA epitope tag insertion analysis A) Shown is a graphic representation of the disorder propensity scores of nine individual algorithms. To identify candidate disordered domains in MeV L, the MeDor (encompassing RONN, DisEMBL REM465, IUPRED, GLOBPLOT2, and FoldIndex) meta-analysis tool, SPRITZ, PONDR-FIT, DRIP-PRED, and DomCut algorithms were used. Also used were secondary structure predictions (SSP), based on the Pred2ary program embedded in MeDor, and graphed were postulated α-helical areas in red or β-sheet regions in blue. B) Depicted is a representative immunoblots (IB) of whole cell lysates (WCL) of cells transfected with N-encoding plasmids or vector DNA (mock). Blots were probed with specific antibodies for the HA tag, and reprobed with antibodies directed against cellular GAPDH. C) Relative luciferase reporter activity (RLU) in cells expressing the minireplicon construct, L, P, and the specified N variant are blotted as a function of MeV N (black line). Values were normalized for those obtained in the presence of N-D525HA tagged variant and represent averages of four independent experiments ± SD for the active constructs and two independent experiments ± SD for the inactive ones. The grey line represents a graphic illustration of average disorder propensity scores as a function of MeV N. D) Whole cell lysates (WCL) of BSR-T7/5 cells transfected with N-encoding plasmids as indicated were gel-fractionated followed by immunoblotting (IB) and probed with specific antibodies directed against the HA epitope tag. Cellular GAPDH was analyzed on the same blot. E) Minireplicon reporter assay to determine bioactivity of HA tagged N variants is graphed. Values are relative to the minireplicon system containing standard N, and represent averages of at least four experiments ± SD.

Figure 2: Addition of a tetracystein tag in the N protein in the viral context A) Representative immunoblot (IB) of cells expressing full-length MeV N variants with tetracysteine (4xcys) tag at the indicated positions was probed with an antibody specific for the N protein and same blot was reprobed for cellular GAPDH. B) Relative luciferase reporter activity (RLU) in cells expressing the minireplicon construct, L, P, and the specified 4xcys tagged N variant were normalized for those obtained in the presence of standard N and represent averages of at least four independent experiments ± SD. C) Microphotographs of cell monolayers infected with recovered recMeV N-E436-4xcys and the adapted recMeV N-E436-4xcys at a MOI of

0.01 were taken 3 days post infection. Representative fields of view are shown at a magnification of 200x. D) Sequence analysis of recMeV N-E436-4xcys input DNA (day 0), at the time of recovery (day 15) and after 45 days of continued eleven more passagings.

Figure 3: Cell free particle composition and fusion kinetics A) Representative immunoblots (IB) and B) graphic representation of quantification of viral proteins relative to N of purified cell free particles were densitometrically adjusted for ± 10% equal amounts of nucleocapsid material by N signal intensity and subjected to SDS-PAGE fractionation. The same blots were probed with specific antibodies for either N, M, P, F or H proteins and the relative amounts of each material was determined. B) Numbers of viral protein quantification relative represent ratios normalized to MeV N and are averages of densitometric quantifications of two independent experiments ± value range. C) Depicted is the quantification of viral mRNA levels in virus infected cells. qPCR analysis of relative N, M, P, and H mRNA levels represent averages of three independent experiments, each quantified in duplicates, ± SD. D) Quantitative cell-to-cell fusion kinetic in real time measures content mixing. Effector cells expressing one DSP subunit were mixed 1:1 with target cells expressing the complementary DSP component 24 hours post transfection. Mixed cell population was spin inoculated with recMeV and revMeV N-E436HA 6 hours later. Relative luciferase units (RLU) were measured continuously for 14 hours. Results were normalized for peak values observed with recMeV and represent averages of at least eight independent experiments ± SEM.

Figure 4: recMeV N-E436HA displayed initial growth delay A) Shown is the multi-step growth curve of recMeV and recMeV N-E436HA in Vero/hSLAM cells infected at a MOI of 0.01. Cell associated virus was harvested every 12 hours and titers determined by $TCID_{50}$. Viral titer values represent averages of three independent experiments ± SD. B) Viral peak titers of growth curve in A) (48 hours for recMeV and 60 hours for recMeV N-E436HA) were diluted, titers determined and used as inoculum for reinfected growth curve. Viral titer values represent averages of three independent experiments ± SD.C) Representative immunoblots (IB) show P protein levels in fractionated viral growth curve samples on SDS-PAGE. Blots were probed with a P specific antibody.

Figure 5: Delayed mRNA and genomic amplification in a one step growth curve A) Viral titers for recMeV and recMeV N-E436HA of the inoculum used for the one step

growth curve were determined by $TCID_{50}$ method. Titers represent averages of three independent experiments ± SD. B) One step growth curve of recMeV and recMeV N-E436HA in Vero/hSLAM cells infected by spin inoculation at an MOI of 0.2 is shown. Every two hours cell associated virus was harvested and titers determined by $TCID_{50}$. Titers represent averages of three independent experiments ± SD. C) mRNA and genomic RNA quantification of recMeV and recMeV-E436HA during one step growth curve. Total RNA was isolated hourly up until 14 hours pI and continued at 24 to 30 hours pI. Oligo dT cDNA was created. N mRNA and genomic RNA copy numbers were quantified by Taqman qRT-PCR using a N RNA standard curve. Values represent averages of at least three independent replicates ± SD. D) Enlarged picture of mRNA and genomic quantification of the first 20 hours pI.

Supplemental figure S1: Varying linker length does not improve bioactivity A) Shown is a representative immunoblot (IB) of N proteins harboring the 4xcys tag with different linker length as indicated of whole cell lysates (WCL) of BSR-T7/5 cells transfected with the different N expression plasmids that were gel fractionated and immunostained using specific antibodies directed against N or cellular GAPDH. B) Minireplicon reporter assay to determine bioactivity of 4xcys tagged N variants with different linker length (0=no linker, 2=SGGGSGGG, unmarked=SGGG). Values represent averages of at least four experiments ± SD.

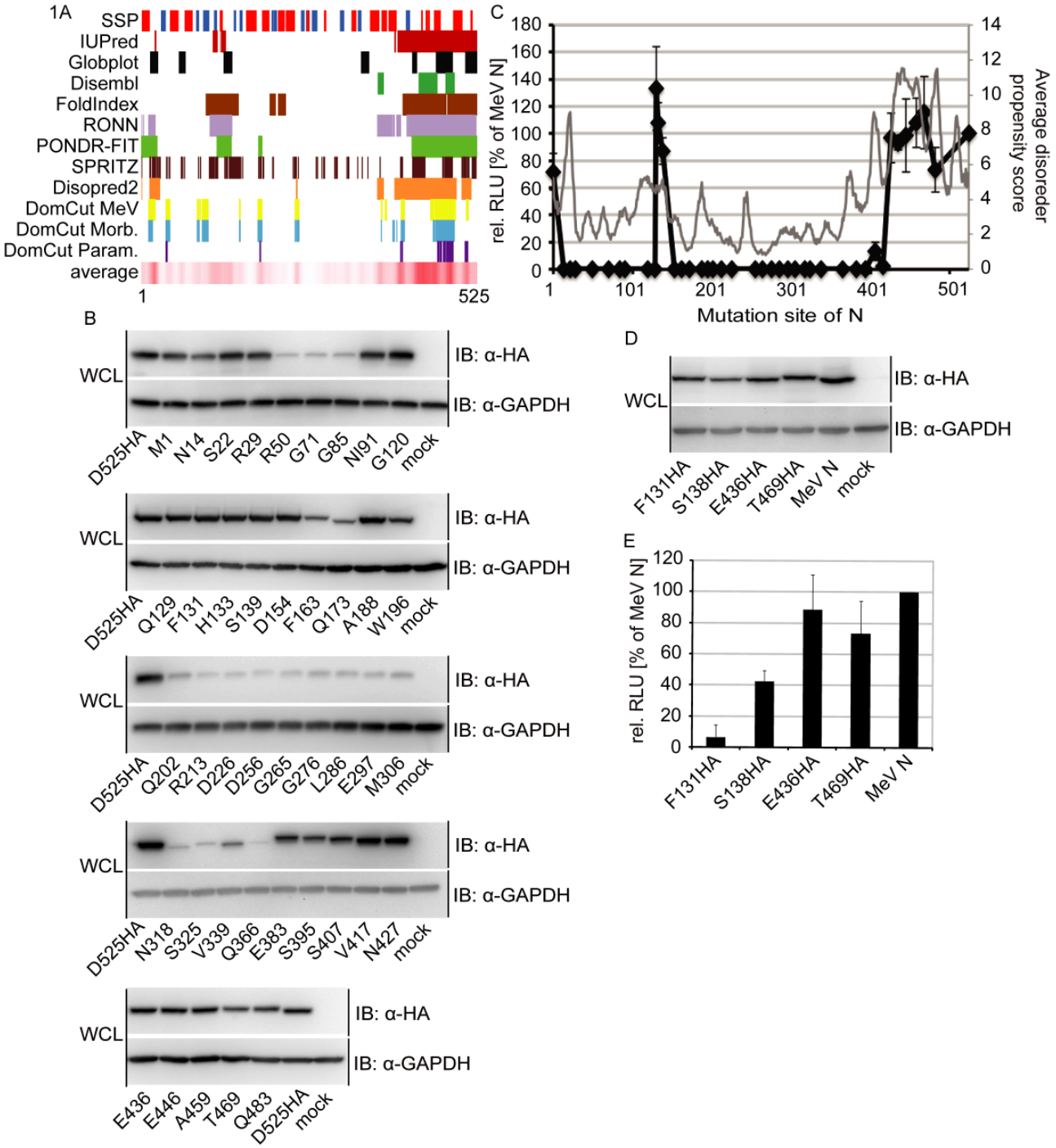
1A
SSP
IUPred
Globplot
Disembl
FoldIndex
RONN
PONDR-FIT
SPRITZ
Disopred2
DomCut MeV
DomCut Morb.
DomCut Param.
average
1
525
C
rel. RLU [% of MeV N]
Average disoreder propensity score
Mutation site of N
B
WCL
IB: α-HA
IB: α-GAPDH
D525HA
M1
N14
S22
R29
R50
G71
G85
NI91
G120
mock
Q129
F131
H133
S139
D154
F163
Q173
A188
W196
Q202
R213
D226
D256
G265
G276
L286
E297
M306
N318
S325
V339
Q366
E383
S395
S407
V417
N427
E436
E446
A459
T469
Q483
D
F131HA
S138HA
E436HA
T469HA
MeV N
E

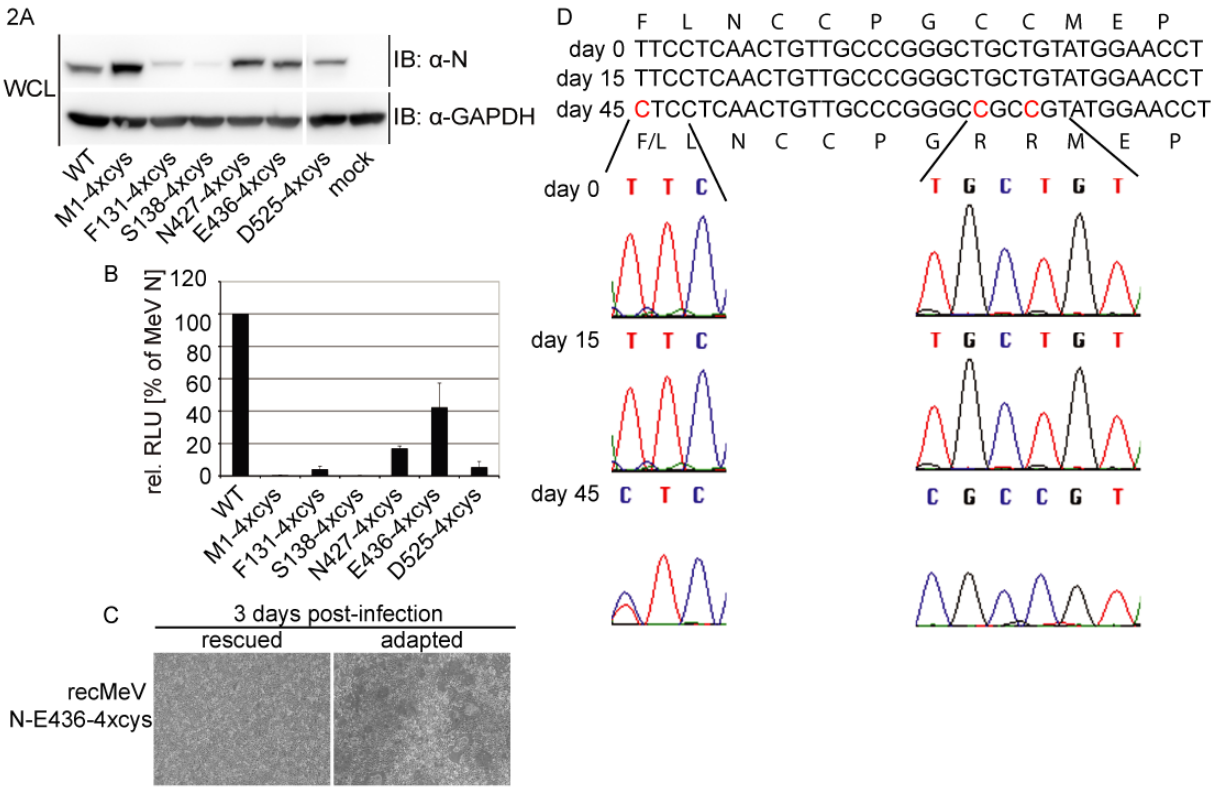
2A
WCL
IB: α-N
IB: α-GAPDH
WT
M1-4xcys
F131-4xcys
S138-4xcys
N427-4xcys
E436-4xcys
D525-4xcys
mock
B
rel. RLU [% of MeV N]
120
100
80
60
40
20
0
C
3 days post-infection
rescued
adapted
recMeV
N-E436-4xcys
D
F L N C C P G C C M E P
day 0 TTCCTCAACTGTTGCCCGGGCTGCTGTATGGAACCT
day 15 TTCCTCAACTGTTGCCCGGGCTGCTGTATGGAACCT
day 45 CTCCTCAACTGTTGCCCGGGCCGCCGTATGGAACCT
F/L L N C C P G R R M E P
day 0
day 15
day 45

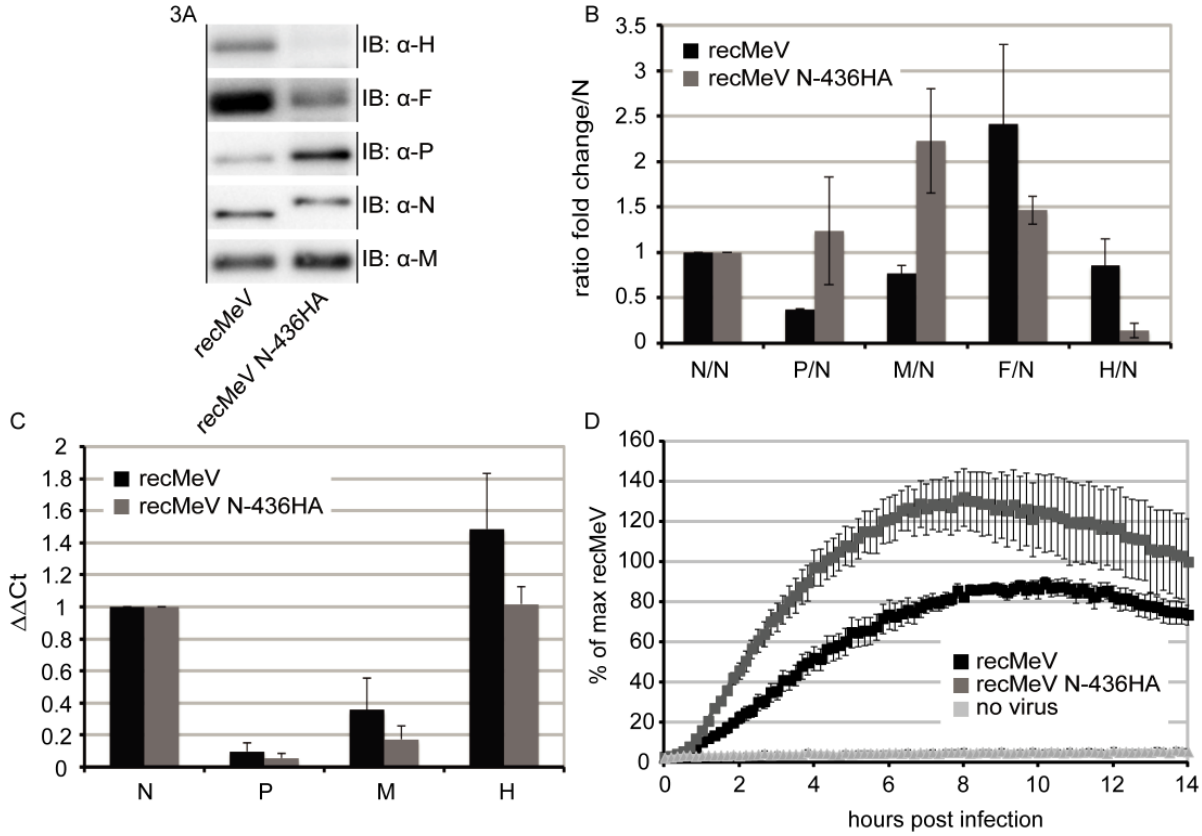
3A
IB: α-H
IB: α-F
IB: α-P
IB: α-N
IB: α-M
recMeV
recMeV N-436HA
B
recMeV
recMeV N-436HA
ratio fold change/N
N/N
P/N
M/N
F/N
H/N
C
recMeV
recMeV N-436HA
ΔΔCt
N
P
M
H
D
recMeV
recMeV N-436HA
no virus
% of max recMeV
hours post infection

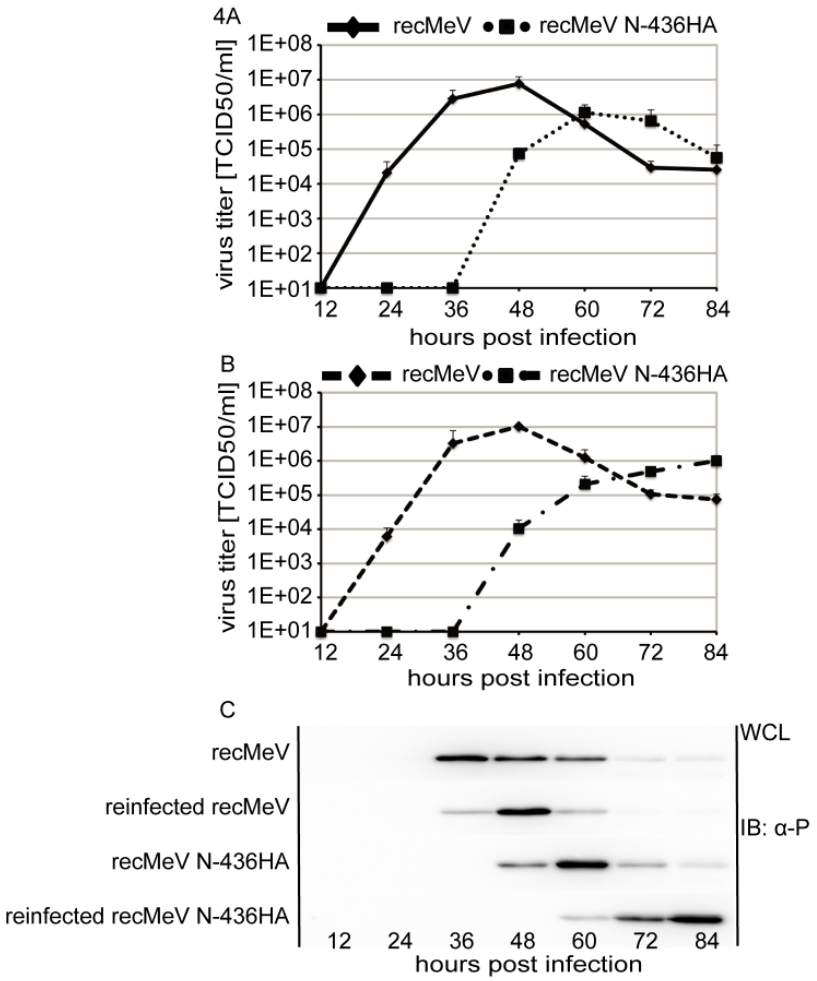
4A
recMeV
recMeV N-436HA
virus titer [TCID50/ml]
1E+08
1E+07
1E+06
1E+05
1E+04
1E+03
1E+02
1E+01
12
24
36
48
60
72
84
hours post infection
B
recMeV
recMeV N-436HA
virus titer [TCID50/ml]
hours post infection
C
recMeV
reinfected recMeV
recMeV N-436HA
reinfected recMeV N-436HA
WCL
IB: α-P
hours post infection

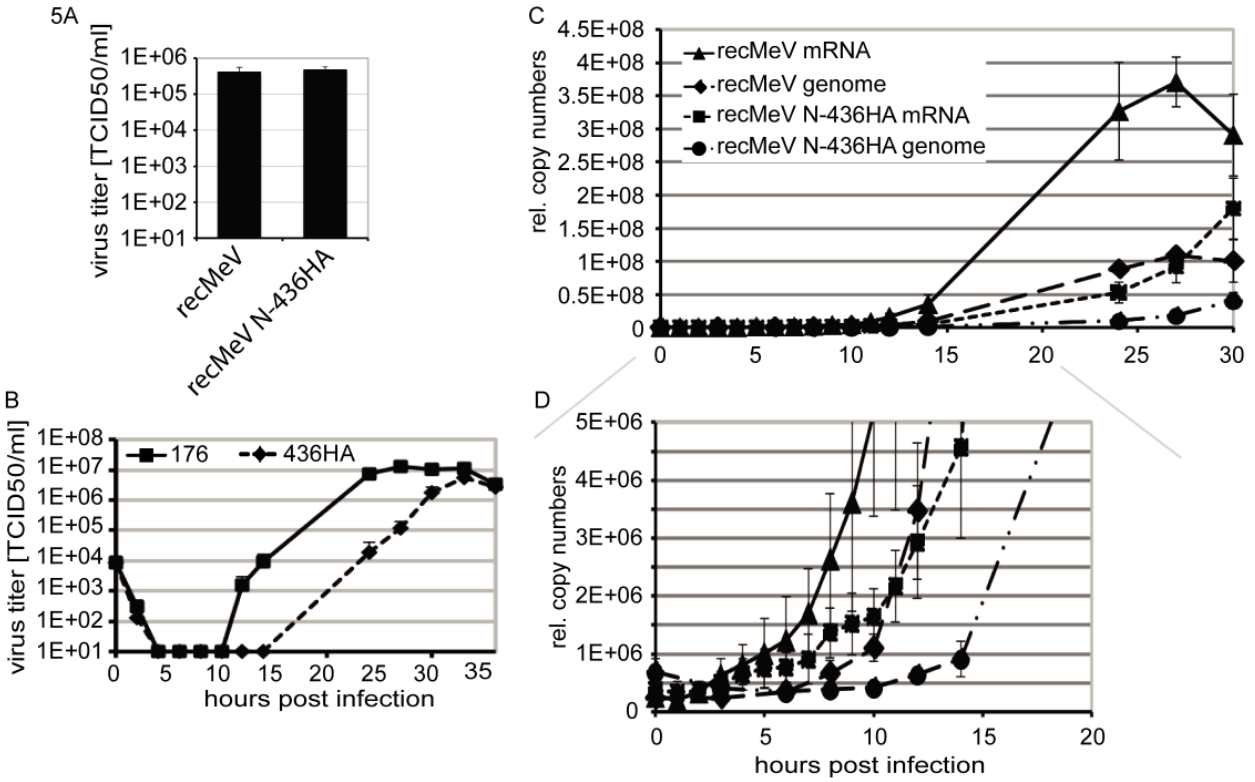
5A
virus titer [TCID50/ml]
1E+06
1E+05
1E+04
1E+03
1E+02
1E+01
recMeV
recMeV N-436HA
C
rel. copy numbers
4.5E+08
4E+08
3.5E+08
3E+08
2.5E+08
2E+08
1.5E+08
1E+08
0.5E+08
0
recMeV mRNA
recMeV genome
recMeV N-436HA mRNA
recMeV N-436HA genome
0 5 10 15 20 25 30
B
virus titer [TCID50/ml]
1E+08
1E+07
1E+06
1E+05
1E+04
1E+03
1E+02
1E+01
176
436HA
0 5 10 15 20 25 30 35
hours post infection
D
rel. copy numbers
5E+06
4E+06
3E+06
2E+06
1E+06
0
0 5 10 15 20
hours post infection

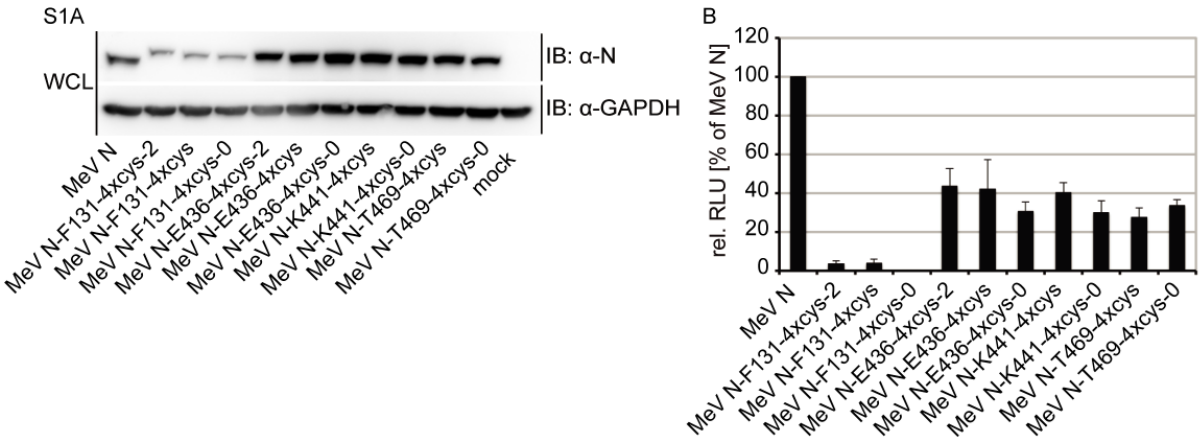
S1A
WCL
IB: α-N
IB: α-GAPDH
MeV N
MeV N-F131-4xcys-2
MeV N-F131-4xcys
MeV N-F131-4xcys-0
MeV N-E436-4xcys-2
MeV N-E436-4xcys
MeV N-E436-4xcys-0
MeV N-K441-4xcys
MeV N-K441-4xcys-0
MeV N-T469-4xcys
MeV N-T469-4xcys-0
mock
B
rel. RLU [% of MeV N]
120
100
80
60
40
20
0
MeV N
MeV N-F131-4xcys-2
MeV N-F131-4xcys
MeV N-F131-4xcys-0
MeV N-E436-4xcys-2
MeV N-E436-4xcys
MeV N-E436-4xcys-0
MeV N-K441-4xcys
MeV N-K441-4xcys-0
MeV N-T469-4xcys
MeV N-T469-4xcys-0

Publication 2

Stefanie A Krumm#, Dan Yan#, Elise S Hovingh, Taylor J Evers, Theresa Enkirch, G. Prabhakar Reddy, Aiming Sun, Manohar T Saindane, Richard F Arrendale, George Painter, Dennis C Liotta, Michael G Natchus, Veronika von Messling and Richard K Plemper

“An orally available, small-molecule polymerase inhibitor shows efficacy against a lethal morbillivirus infection in a large animal model.”

SCIENCE TRANSLATIONAL MEDICINE, April 2014

# These authors contributed equally

Sci Transl Med accepted manuscript (“Orally Available Small-Molecule Polymerase Inhibitor Cures a Lethal Morbillivirus Infection”) and published in PubMed Central by copyright permission of American Association for the Advancement of Science

Orally Available Small-Molecule Polymerase Inhibitor Cures a Lethal Morbillivirus Infection

Stefanie A Krumm[1]†, Dan Yan[1]†, Elise S Hovingh[2], Taylor J Evers[3], Theresa Enkirch[2,4], G. Prabhakar Reddy[3], Aiming Sun[3], Manohar T Saindane[3], Richard F Arrendale[3], George Painter[3,5], Dennis C Liotta[6], Michael G Natchus[3], Veronika von Messling[2,4] and Richard K Plemper[1,7,] *

Affiliations:

[1]Institute for Biomedical Sciences, Georgia State University, Atlanta, GA 30303

[2]Veterinary Medicine Division, Paul-Ehrlich-Institut, Federal Institute for Vaccines and Biomedicines, 63225 Langen, Germany

[3]Emory Institute for Drug Development, Emory University, Atlanta, GA 30322

[4]Emerging Infectious Disease Program, Duke-NUS Graduate Medical School, 169857 Singapore

[5]Drug Innovation Ventures at Emory, Atlanta, GA 30309

[6]Department of Chemistry, Emory University, Atlanta, GA 30322

[7]Department of Pediatrics, Emory University, Atlanta, GA 30322

†These authors contributed equally to this work

*To whom correspondence should be addressed: Richard K Plemper, rplemper@gsu.edu

One Sentence Summary: This study demonstrates unprecedented oral efficacy of a newly developed pan-morbillivirus inhibitor, outlining a tangible approach to solve currently experienced obstacles associated with the eradication of measles virus, a member of the morbillivirus genus, by synergizing vaccination with an effective therapeutic.

Abstract: Measles virus (MeV) is a highly infectious morbillivirus responsible for major human morbidity and mortality in the non-vaccinated. The related, zoonotic canine distemper virus (CDV) induces morbillivirus disease in ferrets with 100% lethality. We report an orally available, shelf-stable pan-morbillivirus inhibitor that targets the viral polymerase. Prophylactic oral treatment of ferrets infected intranasally with a lethal CDV dose reduced viremia and prolonged survival. Equally infected ferrets receiving post-infection treatment at the onset of viremia showed low-grade viral loads, remained asymptomatic and recovered from infection, while control animals succumbed to the disease. Recovered animals also mounted a robust immune response and were protected against re-challenge with a lethal CDV dose. Drug-resistant viral recombinants were generated and found attenuated and transmission impaired compared to the genetic parent. These findings pioneer a path towards an effective morbillivirus therapy that aids measles eradication by synergizing vaccine and therapeutics to close herd immunity gaps due to vaccine refusal.

Introduction

Among respiratory viruses of the *Paramyxoviridae* family, members of the morbillivirus genus such as measles virus (MeV) and canine distemper virus (CDV) are recognized for their exceptionally high attack rates, initial host invasion through lymphatic cells and organs, obligatory development of cell-associated viremia, and an extended period of immunosuppression following the primary infection (*1-4*). Inherently lymphotropic, morbilliviruses spread rapidly from lymphatic organs to epithelial cells and can cause neurologic complications (*5, 6*). Despite their overlapping disease profile, the severity and outcome of infection differ widely between individual members of the genus; for instance, the case fatality rate of MeV is approximately 1:1,000 in developed countries (*5*), whereas CDV is lethal in up to 50% of cases in dogs and 100% in ferrets (*7*), positioning the CDV/ferret system among the most lethal acute viral infections known.

Due to very efficient viral spread, a herd immunity of approximately 95% is required to prevent sporadic MeV outbreaks (*8*) and measles typically reemerges first when vaccination coverage in a population drops (*9*). Globally, major progress towards measles control was made in the 2000-2007 period, resulting in a 71%-reduction in measles mortality. However, estimated annual deaths have since plateaued at around 150,000 (*10, 11*). Compared to 2009, the European region reported an approximately four-fold increase to over 30,000 measles cases in 2011 (*12*), and high 2013 viral activity in Germany, for instance, suggests that comparably low case numbers in 2012 may not stand for a general trend reversal for that region (*13*). Causative are public reservations surrounding the MMR vaccine (*14*), which were aggravated by a fraudulent link to autism (*15*) and persist despite major educational efforts (*16*). Paradoxically, measles control suffers from its own success, since disease awareness increasingly fades from public

memory as prevalence declines (*17, 18*). As a consequence, public risk perception changes, which leads to increasing vaccine refusal and creates a major challenge to viral eradication (*19*). This eroding public acceptance of continued vaccination may also trigger a future decline in immunity in regions with currently high coverage such as North America (*20*). While global eradication through vaccination alone is considered feasible (*8, 21*), a drawn-out endgame for MeV elimination will test public resolve, challenge regional control targets, and could jeopardize the ultimate success of the program (*19*).

Synergizing an effective therapeutic with vaccination may cut through this endgame conundrum by overcoming vaccine refusal and shortening the timeline to complete viral control. Since the disease is mostly immune-mediated (*1, 9*), drug intervention should reasonably concentrate on the extended latent/prodromal and early symptomatic stages of infection through post-exposure prophylaxis. Immunologically-naïve contacts of confirmed index cases are identifiable in the developed world, but post-exposure vaccination is largely ineffective (*22*). Predominantly prophylactic application dictates the desired drug profile: the article must be orally efficacious, ideally shelf-stable at ambient temperature, amenable to cost-effective production, and possess outstanding safety and resistance profiles. Small-molecule therapeutics are best suited to fulfill these requirements (*23*).

We have identified and characterized an allosteric small-molecule inhibitor class of the MeV RNA-dependent RNA-polymerase (RdRp) complex (*24, 25*). Hit-to-lead chemistry has produced analogs with nanomolar potency against a panel of MeV targets and compelling safety profile (*26*). These analogs meet key features of the desired drug product, but the identification of a clinical candidate has been hampered by the lack of a small-animal model that accurately

reproduces symptoms of human MeV infection, since only primates develop a measles-like disease (*27*).

Pioneering the therapeutic intervention of morbillivirus infection, we implemented in this study the CDV/ferret system (*28*) as a surrogate assay to monitor treatment of morbillivirus infection in a natural host. Having examined ferret pharmacokinetics of a selected lead compound and its mechanism of activity against pathogenic CDV, we determined oral efficacy in ferrets intranasally infected with a lethal dose of CDV. Viral adaptation and transfer of escape mutations into a recombinant pathogenic CDV strain revealed the consequences of resistance for viral fitness and pathogenesis *in vitro* and *in vivo*.

Results

Building on a series of MeV inhibitors (*25*), synthetic scaffold development in preparation for this study was predominantly directed at improving oral absorption of the article to meet the desired drug properties, primarily by increasing aqueous solubility. The resulting lead ERDRP-0519 (fig. 1A) showed an excellent 39% oral availability in the rat model, high bidirectional membrane permeability (*26*), and was suitable for synthesis scale-up (fig. S1).

Identification of an orally available pan-morbillivirus inhibitor

Activity testing of ERDRP-0519 against a panel of MeV isolates representing clades currently endemic worldwide demonstrated continued nanomolar antiviral potency of the compound after optimization (fig. 1B and C). This favorable efficacy profile coincided with low cytotoxicity in established human and animal cell lines and primary human PBMCs (table S1), resulting in selectivity indices (SI) >200 against all MeV targets analyzed. The indication spectrum of the compound extended to pathogenic CDV strains, recombinant CDV-5804PeH (*4,*

29) and the neuroadapted Snyder Hill isolate (*30*), albeit with potency reduced approximately 2-fold (fig. 1C). To explore suitability of the ferret host for efficacy testing, we determined PK parameters after single-dose oral administration (fig. 1D and table S2). Peak plasma concentrations exceeded 1,500 ng/ml (corresponding to approximately 3.5 μM) and reached thus about 5-times the *in vitro* EC_{50} concentration of CDV-5804PeH. Serum protein binding of ERDRP-0519 was <95%, and shelf-stability at ambient temperature exceeded one year without loss of activity (fig. S2), making ERDRP-0519 a promising candidate for morbillivirus therapy.

ERDRP-0519 targets the morbillivirus polymerase complex

Compounds of the ERDRP-0519 class block activity of the MeV RdRp complex (*24*). To determine whether this mechanism of activity extends to CDV polymerase, we compared the compound in subinfection replicon reporter assays established for MeV (*31*), CDV, and a distant member of the paramyxovirus family, respiratory syncytial virus (RSV) (*32*). Both morbillivirus-derived polymerase complexes were potently inhibited by ERDRP-0519, while the RSV replicon was not blocked, confirming morbillivirus-specific, dose-dependent inhibition of RdRp activity (fig. 2A).

Adaptation of MeV to growth in the presence of this compound class has identified several hot-spots of resistance in the viral L protein, the catalytically active subunit of the polymerase complex. Most prominently, we found that several escape mutants framed a GDNQ motif in L that is considered the active center for phosphodiester bond formation (*33*). To address whether inhibition of MeV and CDV RdRp complexes by ERDRP-0519 is based on comparable docking poses, we generated escape variants of CDV strains Snyder Hill and 5804P (fig. S3). Candidate mutations identified in nine discrete adaptation campaigns were rebuilt individually in the CDV replicon system, followed by inhibition testing (fig. S4). This procedure highlighted eight

substitutions affecting six discrete positions in CDV L that improved bioactivity in the presence of the inhibitor compared to unmodified CDV L (fig. 2B).

For each resistance site identified, we transferred one substitution into a cDNA copy of the CDV-5804P genome (*4, 29*) and recovered the corresponding CDVs. All recombinants contained an additional eGFP open reading frame, which does not impair pathogenicity of the virus in ferrets (*4*). Dose-response curves (fig. 2C) revealed robust resistance of CDV-5804PeH-L_{T751I} and L_{T776A} (EC_{90} concentrations increased >20-fold), intermediate resistance of CDV-5804PeH-L_{H589Y}, L_{H816L}, and L_{G835R} (EC_{90} concentrations increased approximately 8-fold), and moderate resistance of CDV-5804PeH-L_{N398D} (approximately 2-fold increase in EC_{90} concentration). We noted high consistency in the location of escape sites between CDV and MeV. Escape mutations mapped to the amino-terminal half of the L protein and resistance sites 589 and 776, the latter bordering the GDNQ motif, were identical in both pathogens (fig. 2B).

Oral efficacy against a lethal morbillivirus infection

Having established mechanistic reproducibility between different morbillivirus targets, we employed the CDV/ferret system to assess efficacy of anti-morbillivirus therapy in a natural host. We administered ERDRP-0519 orally at 50 mg/kg body mass b.i.d., following either a prophylactic or post-exposure therapeutic (PET) study protocol. For the former, dosing was initiated 24 hours pre-infection, while the latter commenced at the onset of viremia, three days post-infection, and was continued for 14 days (fig. 3A). Control group received vehicle only, following the prophylactic protocol, since comparison tests confirmed that the vehicle dosing regimen has no effect on disease progression and viremia titers (fig. S5).

All animals were infected intranasally with 1×10^5 $TCID_{50}$ units of CDV-5804PeH, which corresponds to approximately 10 LD_{50} (*29*). Vehicle-treated ferrets developed viremia three days

post-infection, showed first clinical signs of morbillivirus disease such as rash and fever at day seven, and succumbed to the disease after approximately 12-15 days (*4, 29*). Prophylactic treatment significantly prolonged animal survival, reduced viral load and delayed lymphopenia (fig. 3B-D).

Remarkably, PET dosing resulted in complete survival of infected animals (fig. 3B). All ferrets showed an approximately 99% reduction in virus load and experienced only mild, transient lymphocyte depletion (fig. 3C and D). Consistent with the results of our single-dose PK studies in rats and ferrets, plasma analysis revealed robust, micromolar steady-state levels of the drug (fig. 3E). PBMC responsiveness was only transiently impaired in the PET group, intermediately reduced in the prophylactically treated animals, but essentially abrogated in the vehicle-treated controls (fig. 3F).

Quantification of type I interferon and Mx1 (ISG representative) induction levels in PBMCs isolated from animals of each treatment group revealed robust stimulation of the host interferon response in the PET dosing group at day 7 post-infection, when virus replication was impaired by the compound (figure 3G). By contrast, animals of the vehicle control group lacked a comparable innate response, consistent with host immune suppression by the viral V protein (*34*). Efficient suppression of virus replication at all times in prophylactically treated animals was reflected by low interferon induction levels.

Lasting immunoprotection against morbillivirus infection is antibody-mediated (*9*). Importantly, ferrets in the PET group remained subclinical (fig. S6 and S7) and mounted a strong humoral response with neutralizing antibodies first detectable seven days post-infection, followed by a rapid increase in neutralizing titer (fig. 3H). All animals of this group were fully

protected against a lethal CDV challenge with 10 LD_{50}, administered 35 days after the original infection and 18 days after completion of treatment.

Effect of viral resistance to ERDRP-0519 on pathogenicity

Allosteric polymerase inhibitors are compromised for antiretroviral therapy by the rapid development of resistance in chronic infections (*35*). However, morbilliviruses predominantly cause acute disease and all therapeutically dosed animals completely cleared the infection by day 28 pI, ruling out viral escape. Likewise, none of four re-isolates from the prophylactic group showed robust resistance (fig. S8). We therefore employed the resistant recombinants generated *in vitro* to assess the effect of escape from ERDP-0519 on relative viral fitness. To establish an *in vitro* competition assay (fig. 4A), we exchanged the eGFP open reading frame in CDV-5804PeH for that of far-red fluorescent mKate2 and recovered the corresponding CDV-5804P-mKate. Infection of ferrets confirmed indistinguishable pathogenicity of this recombinant and CDV-5804PeH (fig. S9). In three independent replicates each, cells were then co-infected with equal amounts of compound-sensitive CDV-5804P-mKate and one of the six confirmed resistant mutants in the CDV-5804PeH background. Viruses were passaged eight times, and the relative prevalence of standard and resistant virus quantified by fluorescence pattern.

Of the six resistance sites identified, three recombinants (751, 816, and 835) were outgrown by the parental virus, and a fourth site (398) also showed no significant improvement of relative viral fitness (fig. 4B). Two resistant variants (589 and 776), however, reproducibly outgrew the unmodified virus, evidenced by a significant overrepresentation of green fluorescence after eight passages. Sequence analysis confirmed that the presence of viral genomes encoding mutant L proteins at conclusion of the experiment. Substitutions at L positions 589 and 776 likewise

mediated escape of MeV L from this compound class (*24*), identifying them as conserved hot-spots of morbillivirus resistance to the inhibitor with potential to also emerge in the human host.

To address whether the resistance mutations affect virulence, we infected ferrets with these two recombinants, either singly or together with an equal amount of standard CDV-5804P-mKate particles. For comparison, we included CDV-5804PeH-L_{T751I}, since this substitution resulted in attenuation *in vitro* but likewise was in close proximity to the previously identified escape sites in MeV L.

All animals infected with the parental virus experienced typical disease progression characterized by potent viremia with peak viral loads ten days post-infection and death of all infected animals within a 14-day period (fig. 4C and D). Of the escape mutants, only CDV-5804PeH-L_{T776A} induced lethal disease and viremia resembling that of the standard virus. However, median survival of CDV-5804PeH-L_{T776A}-infected animals survived for up to 21 days, indicating mild attenuation. By contrast, resistant CDV-5804PeH-L_{H589Y} and CDV-5804PeH-L_{T751I} were both attenuated, manifested by lower grade viremia and recovery of most/all animals of both groups from infection (fig. 4 C and D). Coinfection of animals with equal amounts of parental and either of the different resistant viruses did not enhance disease (fig. 4E).

To assess possible spread of viral resistance, we performed contact transmission studies with CDV-5804PeH-L_{T776A}, which was the least attenuated of all resistant viruses tested *in vivo*. Source animals were infected either singly or co-infected with equal doses of standard and resistant virus, followed by co-habitation with uninfected contact animals. Ferrets infected with CDV-5804PeH-L_{T776A} alone transmitted the virus to cage contacts, but disease progression in the contact animals was delayed compared to that after transmission of the parent virus (fig. 4F and fig. S10). After co-infection of the source animals with resistant and sensitive viruses, viremia

titers of resistant CDV-5804PeH-L_{T776A} were reduced in the contact animals compared to those of the sensitive reference virus (Fig 4G). These observations indicate a lower transmission success rate of the resistant CDV-5804PeH-L_{T776A} than the standard virus, and alleviate concerns that viral escape from inhibition may increase disease severity or induce genetic drift in endemic virus populations.

Discussion

We have pioneered the development of an orally available small-molecule morbillivirus polymerase inhibitor that is capable of curing a lethal morbillivirus infection when administered at the first onset of viremia. Low cytotoxicity in cultured and primary human cells and promising PK parameters recommend this compound for further development in preparation of clinical testing for human or veterinary therapy.

The level of viremia reduction (~99%) observed after prophylactic or therapeutic dosing with the clinical candidate is groundbreaking in the CDV/ferret system. This can be attributed to the favorable pharmacological properties of the compound after repeated oral dosing. Closely overlapping ferret, rat, and human cell-based metabolic profiles of the scaffold (*26*) suggest that these favorable characteristics may equally extend to human therapy.

Several lines of evidence support a conserved inhibitory mechanism and docking pose with the viral polymerase between the MeV and CDV targets. First, the compound class specifically blocks RdRp activity of both CDV and MeV; second, the molecular basis for resistance to this class was traced to the L subunit of the CDV and MeV (*24*) polymerase complex; and, third, two hot-spots of resistance were fully conserved between the different scaffold analogs and

morbillivirus targets (*24*). These findings validate the CDV/ferret system as a relevant model for efficacy assessment.

Our study indicates that post-exposure treatment commencing at the onset of viremia primes a robust immune response through initially unimpaired replication of a non-attenuated pathogenic virus. Uncontrolled, morbillivirus replication induces lymphopenia in experimental (*2, 4*) and clinical (*1, 3*) settings; in the CDV/ferret system, adaptive immunity collapses and the host succumbs to the disease before immune control can be established. We hypothesize that under post-exposure therapy, inhibition of virus replication at the onset of viremia takes full advantage of initial immune priming. The subsequent pharmacological attenuation of the virus, however, prevents immune collapse and allows a robust induction of the innate host antiviral response. Suppressed lymphopenia and lymphocyte unresponsiveness opens a window for the generation of a robust host antiviral response, leading to viral clearance and high neutralizing antibody titers. Consistent with this reaction, all PET dosed animals were after recovery fully protected against re-challenge with a lethal CDV dose. In the absence of strong initial immune stimulation through freely replicating pathogenic virus, the drug is efficacious but insufficient to prevent host immune-collapse in a disease situation as extreme as the CDV/ferret system, despite a reduction in viremia, delayed lymphopenia, and alleviated lymphocyte unresponsiveness. This differential response to prophylactic versus PET dosing showcases a critical role of the very early phase of morbillivirus infection in immune dynamics and disease outcome, which is discussed for a variety of acute respiratory virus infections (*36*). Our results underscore that clinical benefit of therapeutic intervention will best be achieved in conjunction with a competent innate host immune response.

The CDV/ferret-based findings allow five major extrapolations to the MeV/human disease problem, given the conservation of key infection features among morbilliviruses (*4, 37*):

i) Efficacy; post-exposure treatment commencing during the prodromal phase of MeV infection has high potential for clinical success, characterized by an asymptomatic course of infection and the induction of robust, protective immunity. We have not yet monitored surviving ferrets over extended time periods, but consider it likely that the extensive immunosuppression phase following morbillivirus infection (*3, 28*) may also be alleviated or eliminated. Based on a 10 to 14-day latent and prodromal phase of MeV in humans, we anticipate that a 14-day oral treatment cycle of immunologically-naïve contacts of a confirmed index case will recapitulate the efficacy seen in the CDV/ferret surrogate. We have not observed signs of compound-induced toxicity in the PET group, and are confident that higher *in vitro* sensitivity of MeV than CDV to ERDRP-0519 will allow even lower dosing for human therapy.

ii) Immune response; it is well documented that vaccine-induced protection against MeV infection is less robust than naturally acquired immunity (*38*). All therapeutically treated ferrets were fully protected against a lethal CDV challenge dose, indicating that infection with non-attenuated MeV followed by pharmaceutical virus attenuation through ERDRP-0519 induces robust immunity. This observation outlines the potential impact of treatment on MeV eradication efforts; preventing symptomatic disease in the unvaccinated, blocking viral spread in local outbreak areas, and contributing to closing herd immunity gaps due to vaccine refusal as currently experienced in Europe.

iii) Disease management; measles is largely an immunologic disease and viral titers in infected individuals decline rapidly after the onset of symptoms (*8*). Due to faster onset of CDV disease in ferrets than measles in humans, we expect efficacy tests exploring initiation of

treatment during the prodromal phase to be problematic to interpret in the CDV/ferret system. While the full efficacy time window for therapeutic intervention should therefore be evaluated in the MeV/primate model, we would expect little impact when treatment is initiated subsequent to rash. Consequently, therapeutic effort is best directed at contacts of an index case, who are still in the prodromal or very early symptomatic phase. However, we anticipate therapy to improve management of complications involving persistent infection, such as measles inclusion body encephalitis in the immunocompromised (*39*).

iv) Prophylaxis; pre-exposure prophylaxis of ferrets must be evaluated in the context of an exceptionally severe disease phenotype. We consider it likely that proven drug efficacy in the form of substantially prolonged (up to 2-fold) survival of treated ferrets observed in our study will translate into mild, or entirely asymptomatic, presentation of the more moderate MeV disease experienced in humans. Moreover, prophylactically treated ferrets eventually initiated a neutralizing antibody response and showed a milder lymphocyte proliferation arrest. These results alleviate concerns that prophylactic treatment may predispose for severe disease as experienced with a formalin-inactivated MeV vaccine in the 1960s (*40*), since this "atypical measles" syndrome was due to failed affinity maturation, resulting in nonprotective antibodies and immune complex deposition (*41*).

v) Resistance; viral adaptation revealed that escape from ERDRP-0519 inhibition coincides with attenuation. We furthermore found no evidence for enhanced disease in the presence of wild type and resistant virus, or superior transmission rates of resistant virus. Since hot-spots of resistance are conserved between CDV and MeV, similar molecular escape profiles can be anticipated clinically. Morbilliviruses predominantly cause acute disease, followed by rapid immune-mediated viral clearance, mandating high-frequency transmission to sustain the

infection in a population (*42*). Based on the absence of secondary transmission of the attenuated measles vaccine (*8*) and preferential transmission of standard virus from co-infected animals, we propose that in the context of acute morbillivirus disease, attenuated resistant virions will likely remain clinically insignificant.

Beyond the morbillivirus system, our data provide proof-of-concept for the currently unexplored clinical potential of allosteric polymerase inhibitors for the treatment of acute viral infections. The clinical candidate is in principle suitable for veterinary and human use. However, effective suppression of symptomatic disease and the development of robust antiviral immunity after post-exposure treatment predestine the compound as a second weapon in our struggle for the endgame of global MeV eradication.

Materials and Methods

Study design

This study established the CDV/ferret model as a surrogate system to assess the efficacy and resistance package of an anti-measles virus therapeutic candidate. After mechanistic characterization of the compound against the CDV target *in vitro* and the development of an oral PK profile for the ferret host, the effect of different dosing regimens on animal survival, viremia titers, induction of innate host immune responses and immune suppression, and the development of protective immunity was determined. Resistance was induced through viral adaptation, genetically controlled resistant CDV recombinants were generated and their relative fitness, pathogenicity, and potential for transmission assessed *in vitro* and *in vivo*. Animals were assigned randomly to the different treatment groups. Specific information regarding sampling and replication of individual assays is provided in the figure legends.

Cell culture and viruses

All cell lines were maintained at 37°C and 5% CO_2 in Dulbecco's modified Eagle's medium supplemented with 7.5% fetal bovine serum. Vero (African green monkey kidney epithelial) cells (ATCC CCL-81) stably expressing human or canine signaling lymphocytic activation molecule (Vero-hSLAM cells and Vero-cSLAM cells (*43*), respectively) and baby hamster kidney (BHK-21) cells stably expressing T7 polymerase (BSR-T7/5 (BHK-T7) cells) received 500 μg/ml G-418 (Geneticin) for selection. Human peripheral blood mononuclear cells (PBMCs) were prepared and stimulated as previously described (*31*). Lipofectamine 2000 (Invitrogen) was used for transfections. Virus strains used in this study were recombinant MeV-Edmonston (recMeV) and endemic typing strains MVi/Ibadan.NIE/97/1 [B3-2], MVi/Maryland.USA/77 [C2-1], MVi/Illinois.USA/46.02 [D3], MVi/New Jersey.USA/94/1 [D6], MVi/Illinois.USA/50.99 [D7-2], and MVi/Alaska.USA/16.00 [H] (genotypes in parentheses), and neuroadapted CDV isolate Snyder Hill (*30*) and CDV-5804PeH, which is based on the CDV-5804Han89 isolate (*29*). MeV and CDV stocks were grown and titrated through $TCID_{50}$ titration on Vero-hSLAM and Vero-cSLAM cells, respectively.

Compound synthesis and formulation

Compound synthesis was carried out as described (*26*) with the modifications specified in supplements. Compound was dissolved in DMSO for cell culture studies, and formulated in PEG200/0.5% methylcellulose (10/90) for *in vivo* dosing.

In vitro efficacy testing

Cells were infected with MeV or CDV strains (MOI 0.1 $TCID_{50}$/cell) in the presence of three-fold serial compound dilutions (30 μM highest) or vehicle, and incubated with compound until vehicle controls showed 90% CPE. Cell-associated progeny particles were titered and

inhibitory concentrations calculated through four-parameter variable slope non-linear regression fitting.

Assessment of compound cytotoxicity

A CytoTox96 non-radioactive cytotoxicity assay (Promega) was used to quantify toxicity (highest concentration assessed 75 μM). Values were normalized for vehicle controls according to %-toxicity = 100-((specific$_{490nm}$)/(vehicle$_{650nm}$)*100). To calculate CC_{50} concentrations, mean values of four replicates were analyzed.

Pharmacokinetics profiling

Ferrets were dosed p.o. with ERDRP-0519, followed by blood sampling. Plasma was purified from heparinized blood and drug concentrations determined using internal standard, reversed phase isocratic HPLC method with positive ion electrospray ionization (ESI) mass spectrometry detection (LC/MS/MS) on an AB-SCIEX API 4000 MS/MS instrument (5 μl injection volume). Pharmacokinetic parameters were estimated using WinNonlin 5.3 (Pharsight).

Replicon reporter assays

Luciferase replicon reporter systems for MeV, CDV and respiratory syncytial virus (RSV) were described previously (*29, 31, 32*). Reporter activities were determined in the presence of three-fold serial dilutions of ERDRP-0519 (10 μM highest). Luciferase activities in cell lysates were measured in a Synergy H1 microplate reader (BioTek) in top-count mode. Inhibitory concentrations were calculated through four-parameter variable slope regression modeling.

In vitro virus adaptation

Vero-cSLAM cells were infected with CDV strains Snyder Hill or 5804PeH at an MOI of 0.1 $TCID_{50}$/cell and incubated in the presence of ERDRP-0519 starting at 0.5 μM. When

extensive viral CPE was detected, cell-associated viral particles were released, diluted 20-fold and used for re-infection in the presence of increased compound concentrations.

RT-PCR and sequencing of viral cDNAs

RNA was extracted using the RNeasy mini kit (Qiagen) and cDNAs created using random hexamer primers and Superscript III reverse transcriptase (Invitrogen). Modified genome regions were amplified using appropriate primers and subjected to cDNA sequencing.

Molecular biology and recovery of recombinant CDV

Candidate resistance mutations were rebuild in a pTM1-CDV-L expression plasmid (*29*) and subjected to replicon reporter assays for confirmation. The QuikChange protocol (Stratagene) was applied for all site-directed mutagenesis reactions. Confirmed escape mutations were transferred into a full-length cDNA clone of the CDV-5804PeH genome (*4*). To generate CDV-5804P-mKate, the eGFP open reading frame in p(+)CDV-5804PeH was replaced with an equivalent fragment containing mKate2 and the resulting genomic p(+)CDV-5804P-mKate plasmid corrected for the paramyxovirus rule-of-six. All recombinant CDV virions were recovered following a general strategy optimized for MeV (*24*). The presence of engineered point mutations in recovered virions was confirmed through RT-PCR and cDNA sequencing.

In vivo efficacy testing

Male and female adult European ferrets (*mustela putorious furo)* without immunity against CDV were used in this study. All animal experiments were approved by the SingHealth IACUC Committee or were carried out in compliance with the regulations of the German animal protection law. For efficacy studies, animals were infected intranasally with 1×10^5 $TCID_{50}$ of CDV-5804PeH/animal and treated with ERDRP-0519 via gastric gavage at 50 mg/kg body mass as specified. Gavage tubes were flushed with 5 ml of a high caloric fluid. Blood samples were

collected from the jugular vein and the animals were weighed on days 0, 3, 7, 10, 14, and weekly thereafter. All animals were observed daily for clinical signs.

For white blood cell counts, 10 µl of heparinized blood was diluted in 990 µl 3% acetic acid. Prior to Ficoll gradient centrifugation (GE Healthcare), plasma was collected for the quantification of drug concentrations and neutralizing antibodies. To quantify cell-associated viremia, total white blood cells were isolated and added to Vero-cSLAM cells in tenfold dilution steps. To assess proliferation activity of isolated PBMCs, cells were stimulated with 0.2 µg phytohemagglutinin (PHA, Sigma) for 24 hours, followed by addition of 10 µM 5-bromo-2'deoxyuridine (BrdU, Roche). After a 24-hour incubation period, cells were fixed and BrdU incorporation quantified using a peroxidase-linked anti-BrdU antibody in a chemiluminescence assay. Signals were detected in a microplate luminescence counter (Pherastar), and the extent of proliferation expressed as the ratio of non-stimulated to stimulated cells. Neutralizing antibodies were quantified by mixing two-fold plasma dilutions starting at 1:10 with 10^2 $TCID_{50}$ of CDV-5804PeH for 30 min before adding Vero-cSLAM cells. Neutralizing antibody titers were expressed as reciprocal values of the last dilution without syncytia formation.

mRNA induction analysis

Relative IFN α, β, and Mx1 mRNA induction levels in PBMCs were determined by semi-quantitative real-time PCR analysis as described previously (*44*). RNA was isolated from PBMCs collected on days 0, 3, and 7 post-infection, and the corresponding cDNAs subjected to real-time PCR using a QuantiTect SYBR Green PCR master mix (Qiagen). GAPDH mRNA served as an internal reference, and mRNA induction levels were normalized to day 0 values. Relative change in transcription levels was calculated using the formula [fold change = $2^{-\Delta\Delta Ct}$] (*45*).

In vitro fitness competition assay

Vero-cSLAM cells were infected with CDV-5804P-mKate and one of the resistant mutants in the CDV-5804PeH background at an MOI of 0.01 $TCID_{50}$/cell each. When CPE reached >80%, cell-associated progeny virions were harvested, diluted 5,000-fold, and used for infection of fresh Vero-cSLAM cells. Of each passage, viral titers were determined. At the specified passage numbers, Vero cells were infected at an MOI of 0.1 $TCID_{50}$/cell through spin-inoculation (30 minutes, 1,500 rpm, 4°C). Three days post-infection, eGFP and mKate2 fluorescence of individual infectious centers determined using a Zeiss Axio Observer fluorescence microscope. For each passage and independent competition infection, at least 50 distinct infectious centers were analyzed. After eight passages, RNA was extracted from infected cells and subjected to RT-PCR and cDNA sequencing.

In vivo pathogenesis

Ferrets were infected with 2×10^5 $TCID_{50}$ of CDV-5804PeH or a resistant variant in the CDV-5804PeH background. Disease progression was monitored as above. For *in vivo* fitness testing, ferrets were infected intranasally with 2×10^5 $TCID_{50}$/animal of CDV-5804P-mKate, or co-infected with 1×10^5 $TCID_{50}$/animal each of CDV-5804P-mKate and a resistant variant in the CDV-5804PeH background. Disease progression was monitored as above, and viremia titers determined independently based on eGFP and mKate2 fluorescence using a Zeiss Axio Vert.A1 fluorescence microscope.

Statistical analysis

To determine active concentrations from dose-response curves, four parameter variable slope regression modeling was performed using the Prism (GraphPad) software package. Results were expressed as 50% or 90% inhibitory concentrations with 95% asymmetrical confidence

intervals. To assess the statistical significance of differences between sample means, unpaired two-tailed t-tests were applied. Statistical significance of differences between treatment groups was assessed by analysis of variance (ANOVA) in combination with multiple comparison tests as specified in the figure legends. Survival curves were analyzed using a log-rank (Mantel-Cox) test. Experimental uncertainties are identified by error bars, representing standard deviation (SD) or standard error of the mean (SEM) as specified.

List of Supplementary Materials

Table S1. Cytotoxicity of ERDRP-0519 in immortalized cell lines and primary human PBMCs

Table S2. Oral PK profile of ERDRP-0519 in the ferret host

References:

1. R. D. de Vries, A. W. Mesman, T. B. Geijtenbeek, W. P. Duprex, R. L. de Swart, The pathogenesis of measles. *Curr Opin Virol* **2**, 248-255 (2012).
2. R. D. de Vries, S. McQuaid, G. van Amerongen, S. Yuksel, R. J. Verburgh, A. D. Osterhaus, W. P. Duprex, R. L. de Swart, Measles immune suppression: lessons from the macaque model. *PLoS Pathog* **8**, e1002885 (2012).
3. D. E. Griffin, Measles virus-induced suppression of immune responses. *Immunol Rev* **236**, 176-189 (2010).
4. V. von Messling, D. Milosevic, R. Cattaneo, Tropism illuminated: lymphocyte-based pathways blazed by lethal morbillivirus through the host immune system. *Proc Natl Acad Sci U S A* **101**, 14216-14221 (2004).
5. R. T. Perry, N. A. Halsey, The clinical significance of measles: a review. *J Infect Dis* **189 Suppl 1**, S4-16 (2004).
6. M. Ludlow, D. T. Nguyen, D. Silin, O. Lyubomska, R. D. de Vries, V. von Messling, S. McQuaid, R. L. De Swart, W. P. Duprex, Recombinant canine distemper virus strain Snyder Hill expressing green or red fluorescent proteins causes meningoencephalitis in the ferret. *J Virol* **86**, 7508-7519 (2012).
7. M. Davidson, Canine distemper, virus infection in the domestic ferret. *Compend. Contin. Educ. Pract. Vet.* **8**, 448-453 (1986).

8. W. J. Moss, D. E. Griffin, Global measles elimination. *Nat Rev Microbiol* **4**, 900-908 (2006).

9. W. J. Moss, D. E. Griffin, Measles. *Lancet* **379**, 153-164 (2012).

10. WHO. Measles. http://www.who.int/mediacentre/factsheets/fs286/en/index.html (2013).

11. E. Simons, M. Ferrari, J. Fricks, K. Wannemuehler, A. Anand, A. Burton, P. Strebel, Assessment of the 2010 global measles mortality reduction goal: results from a model of surveillance data. *Lancet* **379**, 2173-2178 (2012).

12. European Center for Disease Control and Prevention. Number of measles cases, 2011. http://ecdc.europa.eu/en/healthtopics/measles/epidemiological_data/ Pages/Number-of-measles-cases-2011.aspx. (2011).

13. S. Santibanez, A. Mankertz, [Molecular surveillance shows progress in measles elimination process]. *Bundesgesundheitsblatt Gesundheitsforschung Gesundheitsschutz* **56**, 1238-1242 (2013).

14. H. J. Larson, L. Z. Cooper, J. Eskola, S. L. Katz, S. Ratzan, Addressing the vaccine confidence gap. *Lancet* **378**, 526-535 (2011).

15. S. H. Murch, A. Anthony, D. H. Casson, M. Malik, M. Berelowitz, A. P. Dhillon, M. A. Thomson, A. Valentine, S. E. Davies, J. A. Walker-Smith, Retraction of an interpretation. *Lancet* **363**, 750 (2004).

16. J. L. Goodson, S. Y. Chu, P. A. Rota, W. J. Moss, D. A. Featherstone, M. Vijayaraghavan, K. M. Thompson, R. Martin, S. Reef, P. M. Strebel, Research priorities for global measles and rubella control and eradication. *Vaccine* **30**, 4709-4716 (2012).

17. K. F. Brown, S. J. Long, M. Ramsay, M. J. Hudson, J. Green, C. A. Vincent, J. S. Kroll, G. Fraser, N. Sevdalis, U.K. parents' decision-making about measles-mumps-rubella

(MMR) vaccine 10 years after the MMR-autism controversy: a qualitative analysis. *Vaccine* **30**, 1855-1864 (2012).

18. P. J. Smith, S. G. Humiston, E. K. Marcuse, Z. Zhao, C. G. Dorell, C. Howes, B. Hibbs, Parental delay or refusal of vaccine doses, childhood vaccination coverage at 24 months of age, and the Health Belief Model. *Public Health Rep* **126 Suppl 2**, 135-146 (2011).
19. D. S. Saint-Victor, S. B. Omer, Vaccine refusal and the endgame: walking the last mile first. *Philos Trans R Soc Lond B Biol Sci* **368**, 20120148 (2013).
20. Centers for Disease Control and Prevention, Measles - United States, 2011. *MMWR Morb Mortal Wkly Rep* **61**, 253-257 (2012).
21. W. A. Orenstein, A. R. Hinman, Measles: the burden of preventable deaths. *Lancet* **379**, 2130-2131 (2012).
22. P. Rice, Y. Young, B. Cohen, M. Ramsay, MMR immunisation after contact with measles virus. *Lancet* **363**, 569-570 (2004).
23. C. R. Ganellin, R. Jefferis, S. M. Roberts, Eds., *Introduction to biological and small molecule drug research and development : theory and case studies*, (Academic Press, Oxford, 2013), pp. 1 volume.
24. J. J. Yoon, S. A. Krumm, J. M. Ndungu, V. Hoffman, B. Bankamp, P. A. Rota, A. Sun, J. P. Snyder, R. K. Plemper, Target analysis of the experimental measles therapeutic AS-136A. *Antimicrob Agents Chemother* **53**, 3860-3870 (2009).
25. L. K. White, J. J. Yoon, J. K. Lee, A. Sun, Y. Du, H. Fu, J. P. Snyder, R. K. Plemper, Nonnucleoside inhibitor of measles virus RNA-dependent RNA polymerase complex activity. *Antimicrob Agents Chemother* **51**, 2293-2303 (2007).

26. J. M. Ndungu, S. A. Krumm, D. Yan, R. F. Arrendale, G. P. Reddy, T. Evers, R. Howard, M. G. Natchus, M. T. Saindane, D. C. Liotta, R. K. Plemper, J. P. Snyder, A. Sun, Non-nucleoside inhibitors of the measles virus RNA-dependent RNA polymerase: synthesis, structure-activity relationships, and pharmacokinetics. *J Med Chem* **55**, 4220-4230 (2012).

27. P. G. Auwaerter, P. A. Rota, W. R. Elkins, R. J. Adams, T. DeLozier, Y. Shi, W. J. Bellini, B. R. Murphy, D. E. Griffin, Measles virus infection in rhesus macaques: altered immune responses and comparison of the virulence of six different virus strains. *J Infect Dis* **180**, 950-958 (1999).

28. S. Pillet, N. Svitek, V. von Messling, Ferrets as a model for morbillivirus pathogenesis, complications, and vaccines. *Curr Top Microbiol Immunol* **330**, 73-87 (2009).

29. V. von Messling, C. Springfeld, P. Devaux, R. Cattaneo, A ferret model of canine distemper virus virulence and immunosuppression. *J Virol* **77**, 12579-12591 (2003).

30. J. H. Gillespie, C. G. Rickard, Encephalitis in dogs produced by distemper virus. *Am J Vet Res* **17**, 103-108 (1956).

31. S. A. Krumm, J. M. Ndungu, J. J. Yoon, M. Dochow, A. Sun, M. Natchus, J. P. Snyder, R. K. Plemper, Potent host-directed small-molecule inhibitors of myxovirus RNA-dependent RNA-polymerases. *PLoS One* **6**, e20069 (2011).

32. A. L. Hotard, F. Y. Shaikh, S. Lee, D. Yan, M. N. Teng, R. K. Plemper, J. E. Crowe, Jr., M. L. Moore, A stabilized respiratory syncytial virus reverse genetics system amenable to recombination-mediated mutagenesis. *Virology* **434**, 129-136 (2012).

33. A. Chattopadhyay, T. Raha, M. S. Shaila, Effect of single amino acid mutations in the conserved GDNQ motif of L protein of Rinderpest virus on RNA synthesis in vitro and in vivo. *Virus Res* **99**, 139-145 (2004).

34. N. Svitek, I. Gerhauser, C. Goncalves, E. Grabski, M. Doring, U. Kalinke, D. E. Anderson, R. Cattaneo, V. von Messling, Morbillivirus Control of the Interferon Response: Relevance of STAT2 and mda5 but not STAT1 for Canine Distemper Virus Virulence in Ferrets. *J Virol* **88**, 2941-2950 (2013).

35. E. De Clercq, Non-nucleoside reverse transcriptase inhibitors (NNRTIs): past, present, and future. *Chem Biodivers* **1**, 44-64 (2004).

36. J. R. Tisoncik, M. J. Korth, C. P. Simmons, J. Farrar, T. R. Martin, M. G. Katze, Into the eye of the cytokine storm. *Microbiology and molecular biology reviews: MMBR* **76**, 16-32 (2012).

37. K. Lemon, R. D. de Vries, A. W. Mesman, S. McQuaid, G. van Amerongen, S. Yuksel, M. Ludlow, L. J. Rennick, T. Kuiken, B. K. Rima, T. B. Geijtenbeek, A. D. Osterhaus, W. P. Duprex, R. L. de Swart, Early target cells of measles virus after aerosol infection of non-human primates. *PLoS Pathog* **7**, e1001263 (2011).

38. J. Mossong, C. J. O'Callaghan, S. Ratnam, Modelling antibody response to measles vaccine and subsequent waning of immunity in a low exposure population. *Vaccine* **19**, 523-529 (2000).

39. D. R. Hardie, C. Albertyn, J. M. Heckmann, H. E. Smuts, Molecular characterisation of virus in the brains of patients with measles inclusion body encephalitis (MIBE). *Virol J* **10**, 283 (2013).

40. C. H. Carter, T. J. Conway, D. Cornfeld, D. G. Iezzoni, C. H. Kempe, C. Moscovici, L. W. Rauh, A. J. Vignec, J. Warren, Serologic response of children to in-activated measles vaccine. *JAMA* **179**, 848-853 (1962).

41. F. P. Polack, S. J. Hoffman, G. Crujeiras, D. E. Griffin, A role for nonprotective complement-fixing antibodies with low avidity for measles virus in atypical measles. *Nature Med* **9**, 1209-1213 (2003).

42. M. J. Keeling, B. T. Grenfell, Disease extinction and community size: modeling the persistence of measles. *Science* **275**, 65-67 (1997).

43. F. Seki, N. Ono, R. Yamaguchi, Y. Yanagi, Efficient isolation of wild strains of canine distemper virus in Vero cells expressing canine SLAM (CD150) and their adaptability to marmoset B95a cells. *J Virol* **77**, 9943-9950 (2003).

44. N. Svitek, V. von Messling, Early cytokine mRNA expression profiles predict Morbillivirus disease outcome in ferrets. *Virology* **362**, 404-410 (2007).

45. T. D. Schmittgen, B. A. Zakrajsek, A. G. Mills, V. Gorn, M. J. Singer, M. W. Reed, Quantitative reverse transcription-polymerase chain reaction to study mRNA decay: comparison of endpoint and real-time methods. *Anal Biochem* **285**, 194-204 (2000).

Acknowledgments: We thank P.A.Rota for providing MeV typing strains from the collection of the CDC, M.L.Moore for RSV replicon plasmids, Y.Yanagi for Vero-hSLAM and Vero-cSLAM cell lines, and M.L.Moore and A.L.Hammond for comments on the manuscript.

Funding: E.H. received an Erasmus Scholarship. This work was supported by a Duke-NUS Signature Research Program start-up grant by the Agency for Science, Technology and Research, Ministry of Health, Singapore, funding from the German Ministry of Health (to

V.v.M.), and by Public Health Service grants AI071002 and AI057157 from the NIH/NIAID (to R.K.P.).

Author contributions: S.A.K., D.Y., E.H. and T.E. performed the experiments. A.S. and M.T.S. performed chemical synthesis. T.J.E., G.P.R. and R.F.A. performed mass-spectrometry and pharmacokinetic analyses. G.P., D.C.L., M.G.N., V.v.M. and R.K.P. provided study design. V.v.M. and R.K.P. supervised the experiments and analyzed data. R.K.P. coordinated the project and wrote the manuscript.

Competing interests: A.S. and R.K.P. are inventors on patent application PCT/US2012/030866, which includes the structure and method of use of ERDRP-0519.

Data and materials availability: Distribution of compound ERDRP-0519 for research purposes is regulated through an MTA from Emory University.

Figure Captions:

Fig. 1. Identification of a clinical candidate morbillivirus inhibitor for efficacy testing in the CDV/ferret system. **A)** Structure of the lead compound ERDRP-0519. **B)** *In vitro* efficacy testing of ERDRP-0519 against a panel of MeV isolates representing seven distinct, currently endemic genotypes (specified in parentheses). EC_{50} concentrations were calculated through four-parameter variable slope regression modeling. Values are based on at least three independent experiments for each virus, 95% asymmetrical confidence intervals are shown in parentheses. Specificity indexes (SI) correspond to CC_{50}/EC_{50}. **C)** Dose-response inhibition curves of two pathogenic CDV isolates (5804PeH and Snyder Hill). Two MeV representatives are shown for comparison. EC_{50} concentrations and SI values were determined as in (B). **D)** Single-dose oral PK study of ERDRP-0519 in ferrets. The article was dosed p.o. in a PEG-200/0.5% methylcellulose (10/90) formulation at 50 mg/kg body mass at zero hours; blood samples were taken at the specified time points post-dosing and drug plasma concentration determined by LC/MS/MS. Shown are mean concentrations (n = 3) ± SEM. Key PK parameters were calculated using the WinNonlin PK software package (C_{max}: maximum observed concentration; $t_{1/2}$: terminal elimination half-life; $AUC_{0-\infty}$: area under the curve extrapolated to infinity).

Fig. 2. Mechanism of activity and molecular target of ERDRP-0519 against CDV. **A)** Plasmid-based minigenome luciferase reporter assay to determine bioactivity of RSV, CDV, and MeV polymerase complexes. Relative luciferase units (RLUs) were normalized for values obtained in the presence of vehicle control and represent means of three independent experiments ± SD. EC_{50} concentrations and 95% asymmetric confidence

intervals were determined as in (fig. 1B). To determine the statistical significance of differences between sample means and values obtained at 0.12 μM, unpaired two-tailed *t* tests were applied (*: $p<0.05$; **: $p<0.01$; ***: $p<0.001$; NS: not significant). **B)** Summary of confirmed resistance sites identified in the CDV L polymerase subunit through nine independent adaptations of virus strains 5804PeH or Snyder Hill to growth in the presence of ERDRP-0519. Numbers correspond to CDV L amino acid positions. The insert shows the proposed GDNQ catalytic center for phosphodiesterbond formation (underlined), flanked by two resistance sites (dark grey shading). White squares specify mutations previously identified in MeV L that mediate resistance to an earlier analog of ERDRP-0519 (*24*). **C)** Dose-response inhibition curves of six genetically-controlled CDV-5804PeH recombinants each harboring a single resistance mutant candidate. Values represent mean viral titers of at least three independent experiments ± SD. Numbers in parentheses specify EC_{90} concentrations. To test the statistical significance of differences between means of mutant recombinants and standard CDV-5804PeH, unpaired two-tailed *t* tests were applied; symbols as in (A).

Fig. 3. Oral efficacy assessment of ERDRP-0519 against pathogenic CDV in ferrets. **A)** Prophylactic and PET dosing scheme of ferrets. Animals received ERDRP-0519 orally b.i.d. (black arrows) at 50 mg/kg body mass in a PEG-200/0.5% methylcellulose (10/90) formulation. Controls were dosed with vehicle only. All control animals were dosed with vehicle only following the prophylactic protocol (n=9 (vehicle); n=3 (PET); n=9 (prophylactic)). Virus (1×10^5 $TCID_{50}$ units/animal) was given intranasally at day 0 (grey arrows). **B)** Survival curves of animals after prophylactic or PET dosing. Mantel-Cox tests were applied to assess the statistical significance of differences between the vehicle

and treated survival curves. **C)** Cell-associated viremia titers after prophylactic or PET dosing. Values represent means of $TCID_{50}$ units in 10^6 isolated PBMCs ± SEM. Bonferroni multiple comparison tests were applied after ANOVA; *: $p<0.05$; **: $p<0.01$; ***: $p<0.001$; NS: not significant; black symbols: PET dosing; grey symbols: prophylactic dosing). **D)** Lymphopenia assessment after prophylactic or PET dosing. Values represent means of lymphocyte counts per mm^3 blood ± SEM. Statistical analysis and symbols as in (C). **E)** Multiple-dose drug plasma levels in animals dosed prophylactically or PET. Values represent mean ERDRP-0519 plasma concentrations determined as in (fig. 1D) ± SD. Last sampling at day 14. **F)** Unspecific PBMC proliferation capacity after prophylactic, PET, or vehicle treatment of animals. PBMCs were stimulated with PHA. Values represent mean ratios of BrdU incorporation relative to non-stimulated PBMCs ± SEM. **G)** Induction levels of type I interferon and Mx1 mRNAs in prophylactically, therapeutically, or vehicle-dosed animals at days 0, 3 and 7 post-infection, respectively. PBMCs from three animals per treatment group were analyzed, and values represent relative mRNA fold change in individual animals and means (lines), all normalized for day 0 levels. One-way ANOVA and Tukey's multiple comparison test was applied for statistical analysis. **H)** Neutralizing antibody titers in animals treated prophylactically, PET, or receiving vehicle only. Data represent mean reciprocal dilutions that fully suppressed microscopically detectable CDV cytopathicity ± SEM.

Fig. 4. Resistance package of ERDRP-0519 in the CDV/ferret system. **A)** Schematic of an *in vitro* CDV fitness assay based on co-infection of cells with CDV-5804PeH harboring eGFP or mKate as additional transcription units. Alternatives outcomes after repeat

passaging are specified. **B)** Relative *in vitro* fitness of six distinct resistant CDV-5804PeH (challenge) compared to parental CDV-5804P-mKate (standard). The relative prevalence of standard and challenge virus was determined based on fluorescence. Values represent mean distributions of three independent experiments each ± SD. After eight passages, total RNA was isolated and the prevalent residue at the resistance sites determined. Symbols depict statistical significance of deviation of passage 8 sample means from competition of unmodified CDVs, determined through *t* tests (*: $p<0.05$; ***: $p<0.001$; NS: not significant). **C)** Cell-associated viremia titers after intranasal infection with 2×10^5 $TCID_{50}$ units/animal with standard CDV-5804PeH or resistant variants CDV-5804PeH-L_{T776A}, CDV-5804PeH-L_{H589Y}, or CDV-5804PeH-L_{T751I} (n = 9 (CDV-5804PeH); n = 3 each for resistant CDVs). Values represent means of $TCID_{50}$ units in 10^6 isolated PBMCs ± SD. **D)** Survival curves of animals shown in (C). Mantel-Cox tests were applied to assess the statistical significance of differences between survival of animals infected with standard CDV-5804P-mKate and resistant CDVs. **E)** Survival curves after intranasal infection with 2×10^5 $TCID_{50}$ units/animal of standard CDV-5804PeH (n = 9), or co-infection with 1×10^5 $TCID_{50}$ units/animal each of CDV-5804P-mKate and a resistant CDV-5804PeH variant (n = 3 each). **F)** Contact transmission study. Survival curves of source animals (open symbols) infected with standard CDV-5804P-mKate, resistant CDV-5804PeH-L_{T776A}, or co-infected with both viruses, and the corresponding contact animals (filled symbols). Ferrets were housed in pairs of one source and contact animal (symbols are color matched by co-housed pair; two pairs were tested per virus inoculum). Median survival of contact animals in the CDV-5804P-mKate group was 21 days, in the CDV-5804PeH-L_{T776A} group 27.5 days. **G)**

Cell-associated viremia titers in source (open symbols) and contact (filled symbols) animals after intranasal co-infection of source animals with 1×10^5 $TCID_{50}$ units/animal each of CDV-5804P-mKate and CDV-5804PeH-L_{T776A}. Titers of each virus were determined individually based on fluorescence. Symbols are color matched by co-housed animal pairs and represent viremia titers of individual animals.

A

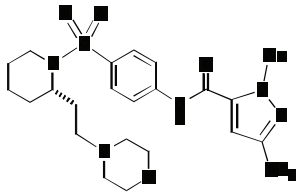

B

Virus	EC_{50} [M]	SI
MVi/Ibadan.NIE/97/1 (B3-2)	0.07 (0.04-0.12)	1071
MVi/Maryland.USA/77 (C2-1)	0.21 (0.07-0.67)	357
MVi/Illinois.USA/46.02 (D3)	0.3 (0.01-25.8)	250
MVi/New Jersey.USA/94/1 (D6)	0.11 (0.01-2.7)	682
MVi/Illinois.USA/50.99 (D7-2)	0.11 (0.09-0.13)	682
MVi/Alaska.USA/16.00 (H)	0.23 (0.01-4.4)	326

C

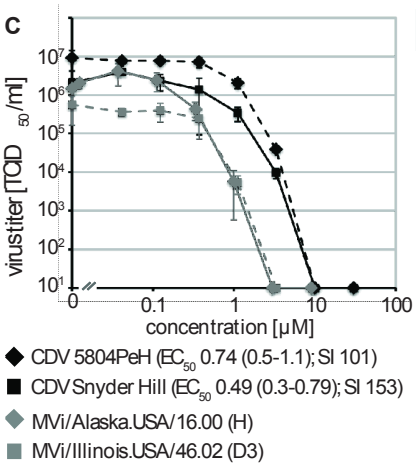

D

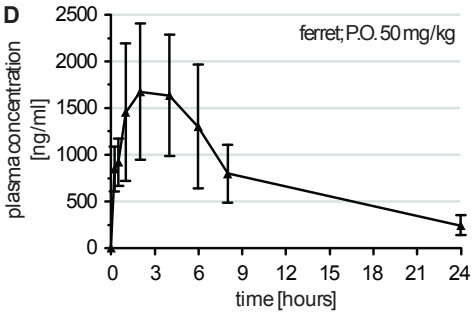

C_{max} [ng/ml]	T½ [hr]	AUC (0-∞) [hr × ng/ml]
1677	8	22063

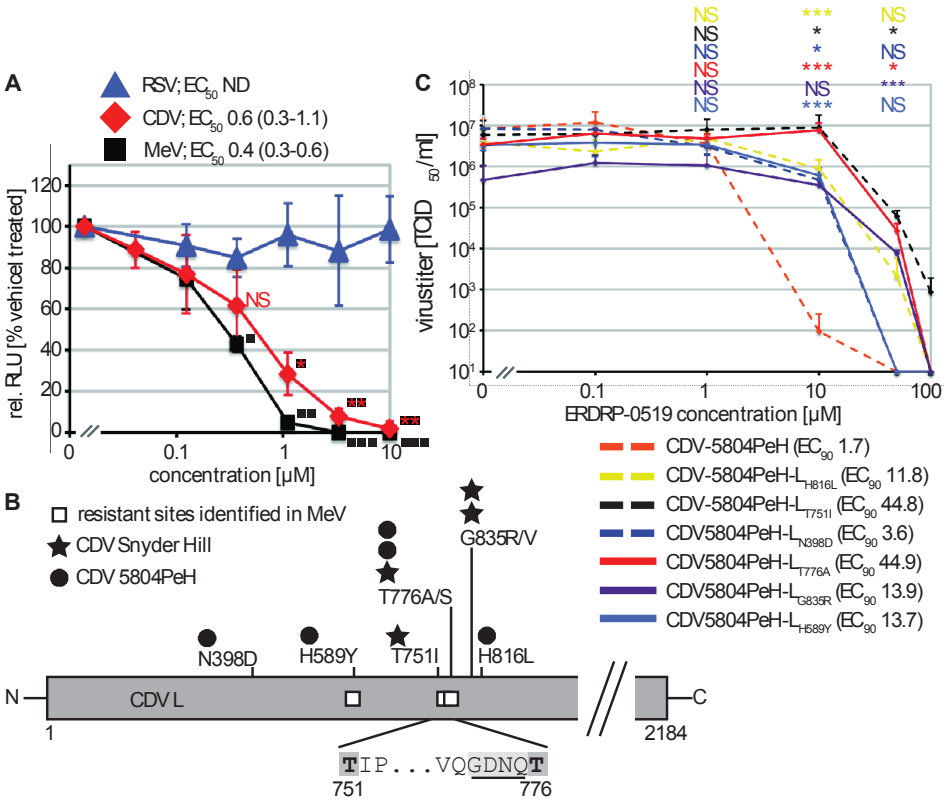
A
RSV; EC50 ND
CDV; EC50 0.6 (0.3-1.1)
MeV; EC50 0.4 (0.3-0.6)
rel. RLU [% vehicel treated]
concentration [µM]
NS
B
resistant sites identified in MeV
CDV Snyder Hill
CDV 5804PeH
G835R/V
T776A/S
N398D
H589Y
T751I
H816L
N
CDV L
C
1
2184
TIP...VQGDNQT
751
776
C
virustiter [TCID50/ml]
ERDRP-0519 concentration [µM]
CDV-5804PeH (EC90 1.7)
CDV-5804PeH-LH816L (EC90 11.8)
CDV-5804PeH-LT751I (EC90 44.8)
CDV5804PeH-LN398D (EC90 3.6)
CDV5804PeH-LT776A (EC90 44.9)
CDV5804PeH-LG835R (EC90 13.9)
CDV5804PeH-LH589Y (EC90 13.7)

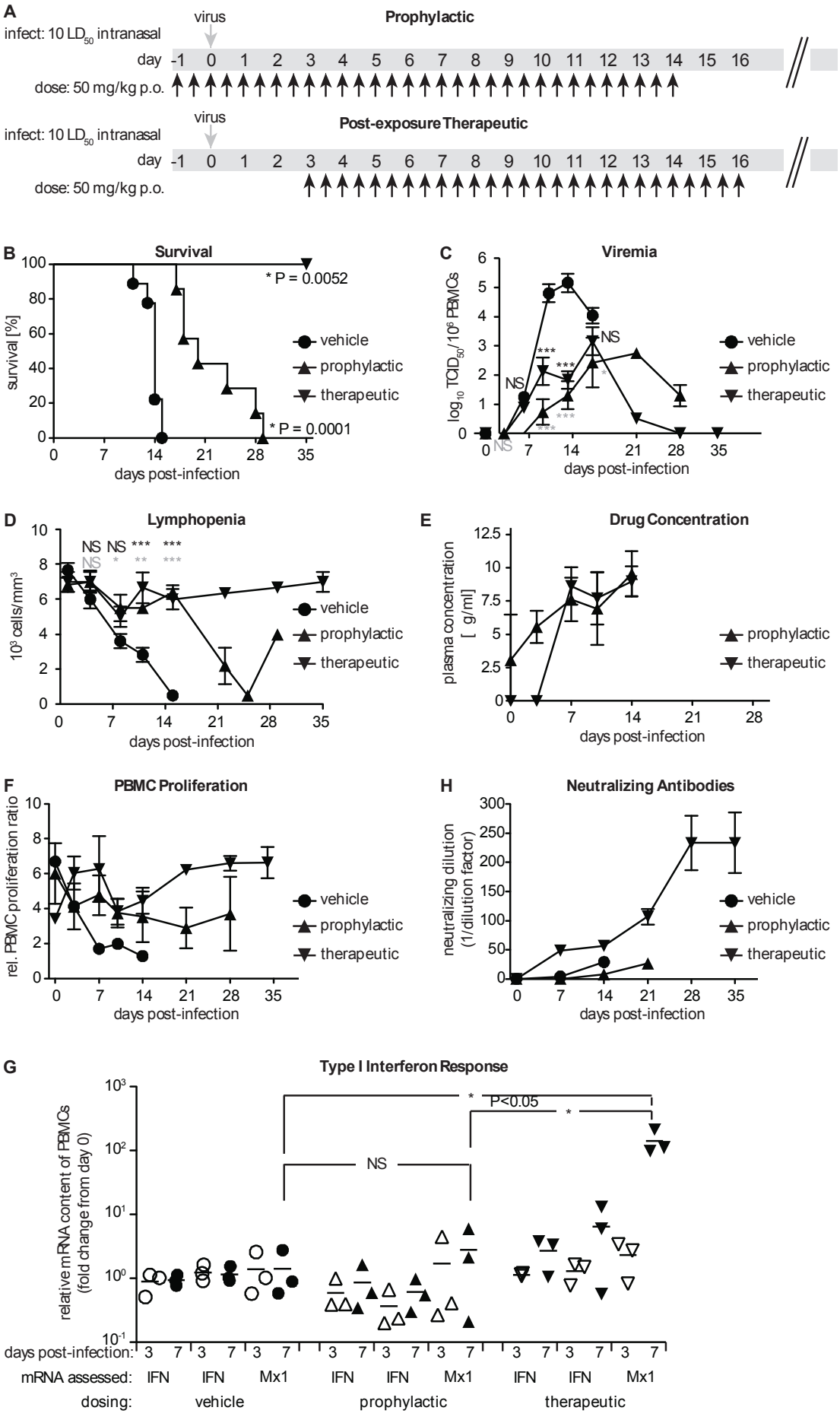
A
virus
Prophylactic
infect: 10 LD50 intranasal
day -1 0 1 2 3 4 5 6 7 8 9 10 11 12 13 14 15 16
dose: 50 mg/kg p.o.
virus
Post-exposure Therapeutic
infect: 10 LD50 intranasal
day -1 0 1 2 3 4 5 6 7 8 9 10 11 12 13 14 15 16
dose: 50 mg/kg p.o.
B
Survival
survival [%]
* P = 0.0052
* P = 0.0001
vehicle
prophylactic
therapeutic
days post-infection
C
Viremia
log10 TCID50/10^6 PBMCs
NS
***
vehicle
prophylactic
therapeutic
days post-infection
D
Lymphopenia
10^3 cells/mm^3
NS NS *** ***
NS * ** ***
vehicle
prophylactic
therapeutic
days post-infection
E
Drug Concentration
plasma concentration [g/ml]
prophylactic
therapeutic
days post-infection
F
PBMC Proliferation
rel. PBMC proliferation ratio
vehicle
prophylactic
therapeutic
days post-infection
H
Neutralizing Antibodies
neutralizing dilution (1/dilution factor)
vehicle
prophylactic
therapeutic
days post-infection
G
Type I Interferon Response
relative mRNA content of PBMCs (fold change from day 0)
* P<0.05
NS
days post-infection: 3 7 3 7 3 7 3 7 3 7 3 7 3 7 3 7 3 7
mRNA assessed: IFN IFN Mx1 IFN IFN Mx1 IFN IFN Mx1
dosing: vehicle prophylactic therapeutic

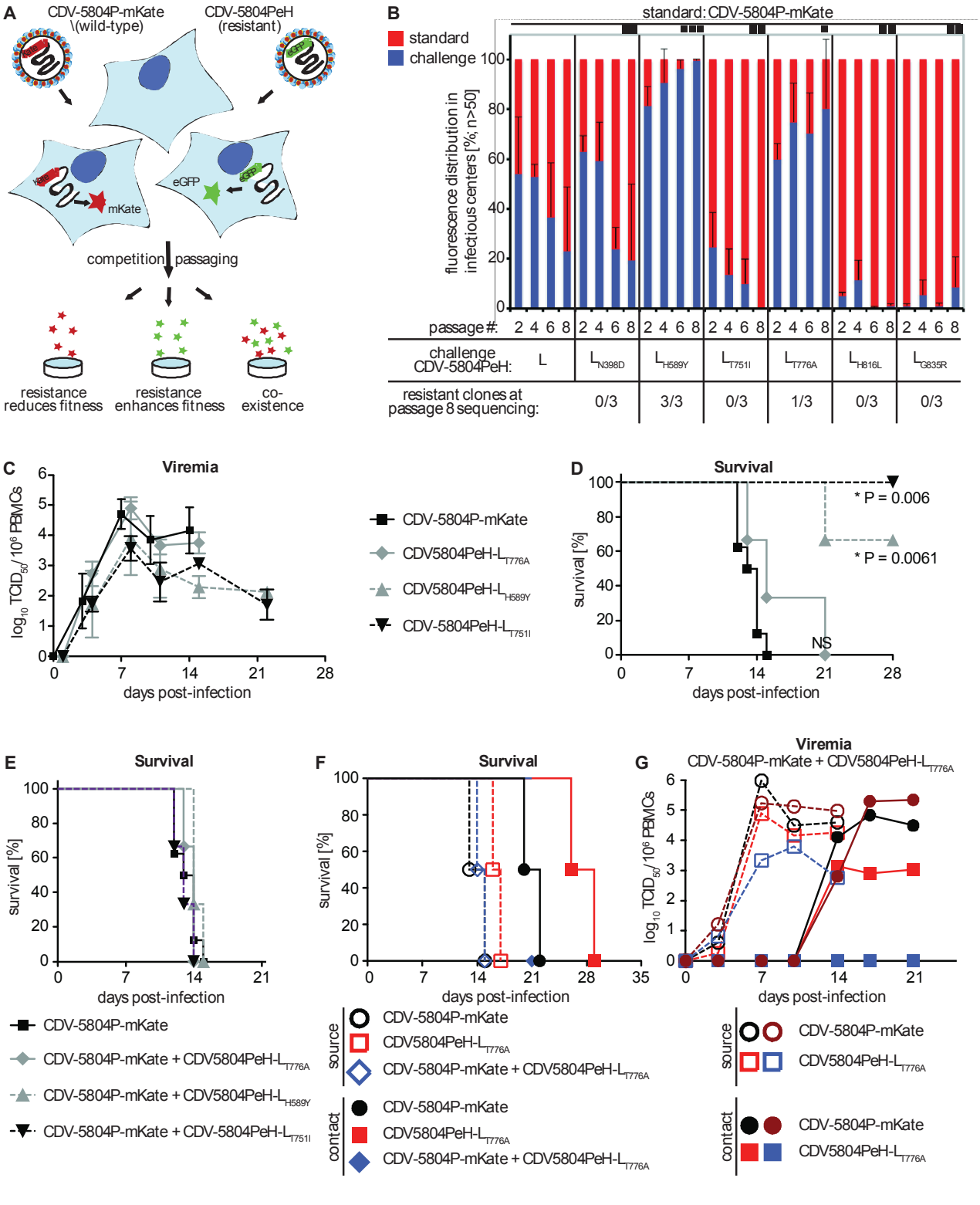
A
CDV-5804P-mKate
\(wild-type)
CDV-5804PeH
(resistant)
mKate
eGFP
competition, passaging
resistance
reduces fitness
resistance
enhances fitness
co-
existence
B
standard: CDV-5804P-mKate
standard
challenge
fluorescence distribution in
infectious centers [%; n>50]
passage #: 2 4 6 8 2 4 6 8 2 4 6 8 2 4 6 8 2 4 6 8 2 4 6 8
challenge
CDV-5804PeH:
L
L N398D
L H589Y
L T751I
L T776A
L H816L
L G835R
resistant clones at
passage 8 sequencing:
0/3
3/3
0/3
1/3
0/3
0/3
C
Viremia
log10 TCID50/10^6 PBMCs
days post-infection
CDV-5804P-mKate
CDV5804PeH-L T776A
CDV5804PeH-L H589Y
CDV-5804PeH-L T751I
D
Survival
survival [%]
* P = 0.006
* P = 0.0061
NS
days post-infection
E
Survival
survival [%]
days post-infection
CDV-5804P-mKate
CDV-5804P-mKate + CDV5804PeH-L T776A
CDV-5804P-mKate + CDV5804PeH-L H589Y
CDV-5804P-mKate + CDV-5804PeH-L T751I
F
Survival
survival [%]
days post-infection
source
CDV-5804P-mKate
CDV5804PeH-L T776A
CDV-5804P-mKate + CDV5804PeH-L T776A
contact
CDV-5804P-mKate
CDV5804PeH-L T776A
CDV-5804P-mKate + CDV5804PeH-L T776A
G
Viremia
CDV-5804P-mKate + CDV5804PeH-L T776A
log10 TCID50/10^6 PBMCs
days post-infection
source
CDV-5804P-mKate
CDV5804PeH-L T776A
contact
CDV-5804P-mKate
CDV5804PeH-L T776A

Publication 3

Stefanie A Krumm, Makoto Takeda and Richard K Plemper
“The Measles Virus Nucleocapsid Protein Tail Domain is Dispensable for Viral Polymerase Recruitment and Activity”
THE JOURNAL OF BIOLOGICAL CHEMISTRY, October 2013

JBC accepted manuscript by copyright permission of The American Society for Biochemistry and Molecular Biology, Inc

The Measles Virus Nucleocapsid Protein Tail Domain is Dispensable for Viral Polymerase Recruitment and Activity

Stefanie A Krumm[1], Makoto Takeda[2] and Richard K Plemper[1]

[1]From the Center for Inflammation, Immunity & Infection
Georgia State University, Atlanta, GA 30303

[2]Department of Virology III
National Institute of Infectious Diseases, Tokyo, Musashimurayama, Japan

*Running title: *N-tail independent MeV polymerase recruitment*

To whom correspondence should be addressed: Richard K. Plemper, Center for Inflammation, Immunity & Infection, Georgia State University, Petit Science Center/Ste 712, 100 Piedmont Av., Atlanta, GA 30303, USA, Tel.: (404) 413-3579; Fax: (404) 413-3580; E-mail: rplemper@gsu.edu

Keywords: Microbiology, virus, RNA viruses, viral replication, viral polymerase

Background: The carboxy-terminal tail domain of the paramyxovirus nucleoprotein is considered instrumental for polymerase recruitment to the template.
Results: Truncated nucleoproteins reveal that the tail domain is dispensable for viral polymerase loading and activity.
Conclusion: The viral polymerase complex is capable of productively docking directly to the nucleocapsid core.
Significance: This finding alters the current paradigm of paramyxovirus polymerase recruitment.

ABSTRACT

Paramyxovirus genomes are ribonucleoprotein (RNP) complexes consisting of nucleoprotein (N)-encapsidated viral RNA. Measles virus (MeV) N features an amino-terminal RNA-binding core and a 125-residue tail domain, of which only the last 75 residues are considered fully mobile on the nucleocapsid surface. A molecular recognition element (MoRE) domain mediates binding of the viral phosphoprotein (P). This P N-tail interaction is considered instrumental for recruiting the polymerase complex to the template. We have engineered MeV N variants with tail truncations progressively eliminating the MoRE domain and upstream tail sections. Confirming previous reports, RNPs with N truncations lacking the carboxy-terminal 43-residues harboring the MoRE domain cannot serve as polymerase template. Remarkably, further removal of all tail residues predicted to be surface exposed significantly restores RNP bioactivity. Insertion of structurally active tags into the central N-tail section reduces bioactivity, but the negative regulatory effect of exposed N-tail stems is sequence independent. Bioactive N-RNAs lacking exposed N-tail sections are unable to sustain virus replication, due to weakened interaction of the advancing polymerase complex with the template. Deletion of the N-MoRE binding domain in P abrogates polymerase recruitment to standard nucleocapsids, but polymerase activity is partially restored when N-tail truncated RNPs serve as template. Revising central elements of the current replication model, these data reveal that MeV polymerase is capable of productively docking directly to the nucleocapsid core. Dispensable for polymerase recruitment, N-MoRE binding to P-tail stabilizes the advancing polymerase-RNP complex and may rearrange unstructured central tail sections to facilitate polymerase access to the template.

The order of non-segmented negative strand RNA viruses (NNVs) comprises viral families of major clinical significance such as Ebola virus of the filovirus family, rabies virus of the *rhabdoviridae*, and MeV, mumps virus and respiratory syncytial virus (RSV) of the *paramyxoviridae*. For all NNVs, only assembled

RNPs can serve as a template for transcription and replication, which are both mediated by the viral RNA-dependent RNA-polymerase (RdRp) complex (1). Despite the health impact of these pathogens, our current understanding of central aspects of RdRp recruitment onto the template and progression along the nucleocapsid remains limited.

Paramyxovirus RdRps are hetero-oligomers composed of the polymerase (L) protein and an essential co-factor, the P protein, which is required for nucleocapsid binding. Important functional insight has come from the MeV and related Sendai virus (SeV) systems (2-5). MeV RNPs assume a helical organization characteristic for the *paramyxoviridae* and other NNVs (1). The amino-terminal 400 residues of the viral N protein form the RNA-binding N-core, which determines the spatial organization of the nucleocapsid (6). The carboxy-terminal 125-residue N-tail domain is intrinsically disordered, but considered essential for RNA transcription and replication (3,7-9). In addition, the tail domain modulates RNP structure, since EM studies have shown that tail removal decreases diameter and pitch of the nucleocapsids, resulting in a rigid, rod-like organization (1,9-11). Docking of RSV nucleoprotein-RNA crystal structures (12) into EM density maps of MeV RNPs posited the beginning of the MeV N-tail domain at the interior of the RNP helix (9). *In situ* structural analysis of viral nucleocapsids then suggested that N-tails protrude through the interstitial spaces between adjacent RNP helical turns, freely exposing only the carboxy-terminal half of the tail, approximately MeV N residues 450-525, on the surface of assembled RNPs (7). Supporting the validity of this RSV-based MeV nucleocapsid model, removal of the interstitial tail residues should result in direct contact between adjacent RNP turns, rigidifying the helical structure as observed experimentally (9).

According to the current paradigm of paramyxovirus RNP replication, these exposed N-tail sections are thought to serve as essential anchor points for recruitment of the polymerase complex (6,13,14). In the case of MeV N, the MoRE domain (amino acids 488-499), and flanking tail residues 486-502 assume an α-helical configuration when binding to the carboxy-terminal XD-domain of the P protein (6,15,16). Exposed tail residues 450-487 are thought to provide flexibility for the MoRE domain to recruit soluble polymerase complexes from the cytosol to the RNP through a casting mechanism (17) and allow close proximity of the MoRE-P-L complex with N-core (7). Once RdRp is loaded onto the template, the XD-domain interactions of tetrameric P (18) with the N-tails may allow progress of the polymerase along the nucleocapsid through iterative cycles of XD to N-tail binding and release (19-21).

Consistent with this view, previous functional studies with carboxy-terminally truncated SeV and MeV N lacking the P binding domains suggested an inability of N-tail truncated nucleocapsids to serve as template for RdRp activity (8,13). Biochemical binding studies with truncated MeV N, and functional assays combining purified, standard SeV RNPs with soluble truncated SeV N demonstrated that the N-tails are not required for the formation of proper P-L complexes itself or the interaction of P with free N (3,13). Somewhat unexpectedly, a recent study found that individual point mutations near the MeV N-MoRE domain, which measurably reduced P-XD affintiy to N-tail, did not abolish polymerase activity (22). However, this may be due to the high avidity of tetrameric P interaction with nucleocapsid, since measurable affinity of the mutated MoRE domains for P-XD was maintained in these N variants.

Building on the structural reconstructions of MeV nucleocapsids, we test in this study central elements of the current paramyxovirus replication model in the context of transient replicon systems and virus replication. Specifically, we examine the importance of the carboxy-terminal P-binding domains in the MeV N-tail for polymerase recruitment to the nucleocapsid, and explore the mechanistic contribution of the unstructured central N-tail section to RNP template function. Our results redefine the role of the exposed N-tail sections in RdRp loading onto, and movement along, the viral nucleocapsid.

EXPERIMENTAL PROCEDURES

Cell culture, transfection, and virus stocks–Baby hamster kidney cells (C-13; ATCC) stably expressing T7 polymerase (BSR-T7/5, (23)) and African green monkey kidney epithelial cells (CCL-81; ATCC) stably expressing human signaling lymphocytic activation molecule (Vero/hSLAM, (24)) were maintained at 37°C and

5% CO_2 in Dulbecco's modified Eagle's medium supplemented with 10% fetal bovine. Both cell lines were incubated in the presence of G-418 (100 µg/ml) every fifth passage. Cells were transfected using either Lipofectamine 2000 (Invitrogen) or, for virus recovery transfections, calcium phosphate precipitation (Promega). Virus stocks were prepared by infecting Vero/hSLAM cells at a multiplicity of infection (MOI) of 0.001, followed by incubation at 37°C. Cell-associated progeny particles were released through freeze/thaw and titers determined by 50% tissue culture infectious dose ($TCID_{50}$) as described (25).

Recombinant MeV–RecMeV particles were generated using a modified recovery protocol as described (26). Emerging infectious particles were transferred onto Vero/hSLAM cells for generation of virus stocks. To confirm integrity of recombinant viruses, RNA was extracted from infected cells using the RNeasy mini kit (Quiagen) and cDNAs created using random hexamer primers and Superscript II reverse transcriptase (Invitrogen). Modified genome regions were amplified using appropriate primers and sequenced.

Molecular biology–Plasmids encoding the MeV (-) replicon (27), MeV Edm N, P or L (28), or MeV IC-B N, P or MeV 9301B L (29) were previously described. For N-tail truncation screening, tandem stop codons (TAGTGA) were introduced into the N-tail ORF through site-directed mutagenesis following the QuikChange protocol (Stratagene). An N-Δ86 expression plasmid truly lacking the last 86 codons of the N ORF was generated through PCR-based shortening of the plasmid and PstI-mediated religation of the amplicon. Both the tandem stop and true deletion N-Δ86 constructs showed equal bioactivities in our assays. To randomize central N-tail sections, frame shifts were introduced through addition or deletion of one or two nucleotides by directed mutagenesis. Tetracysteine tags (SGGGFLNCCPGC CMEPGGGS) (30) were inserted into the N-tail through PCR amplification and religation of the amplicons using a SmaI restriction site engineered into the tag sequence. The (+) replicon was generated using a recombination PCR strategy based on the (-) construct that inverted the entire leader-luciferase-trailer cassette relative to the T7 promoter and the hepatitis delta virus ribozyme element. An expression plasmid encoding the amino-terminal section of P (PNT, amino acids 1-230) was generated through introduction of a Flag epitope tag followed by a tandem stop codon at P residue 230. The corresponding carboxy-terminal PCT expression construct (amino acids 231-507) was generated through PCR amplification and religation of the shortened amplicon using an engineered EcoRI restriction site located upstream of the newly inserted start codon. The P-ΔXD expression construct was generated through insertion of tandem-stop codons after p position 456 into the MeV Edm-P plasmid, abrogating expression of the XD domain starting a P position 459.

Plasmids containing cDNA copies of the MeV Edm or MeV IC-B (31) genomes were further modified by replacing the N open reading frame (ORF) with an Edm or IC-B-based N-Δ86 ORF, respectively. RecMeV N-Δ86-P-N and recMeV N-P-N were generated through doubling of the P-M intergenic junction using appropriate primers and transfer of an appropriately prepared cassette encoding standard N using the AatII restriction site in the P-M junction. All constructs generated in this study were sequence-confirmed. Sequences of oligonucleotide used in this study are available upon request.

Antibodies, SDS-PAGE and immunoblotting–BSR-T7/5 cells ($4x10^5$ per well in a 12-well plate format) transfected with 2 µg of N-encoding plasmid DNA were washed in PBS and lysed in RIPA buffer as described (32). Samples were fractionated on 8% SDS-PAGE gels, transferred to polyvinylidene difluoride (PVDF) membranes (Millipore), and subjected to enhanced chemiluminescence detection (Pierce) using specific antibodies directed against MeV N (83KKKII; Millipore), MeV P (9H4; Abcam), GAPDH (6C5; Ambion), or Flag (M2; Sigma) as specified. Immunoblots were developed using a ChemiDoc digital imaging system (Bio-Rad). The Image Lab package (Bio-Rad) was used for densitometry.

Minireplicon luciferase reporter assays– BSR-T7/5 cells ($4x10^5$ per well in a 12-well plate format) transfected with all MeV Edm or IC-B polymerase helper plasmids and the (+) or (-) reporter constructs were lysed after 40 hours (unless otherwise specified) in Glo lysis buffer (Promega). Luciferase activities in cleared lysates (20,000xg, 5 min, 4°C) were determined using

Bright-Glo firefly luciferase substrate (Promega) and an Envision Multilabel microplate reader (PerkinElmer Life Sciences) in top-count mode.

Co-immunoprecipitation–BSR-T7/5 cells ($8x10^5$ per well in a 6-well plate format) transfected with 2 µg each of plasmid DNA encoding an MeV N construct and either MeV PNT or MeV PCT were harvested and subjected to co-immunoprecipitation as described (32). Following immunoprecipitation using α-Flag or α-P antibodies, samples were fractionated on 10% SDS-PAGE gels, followed by immunoblotting and chemiluminescence detection as outlined.

Terminal RACE–Total RNA was isolated from infected Vero/hSLAM cells as outlined. For first strand synthesis, a positive polarity RNA-specific oligonucleotide primer (CAGTTATTGAGGAGAGTT) annealing in the F ORF was used to reduce contamination by polycistronic viral mRNA. The RACE System (Invitrogen) was used for cDNA end amplification with the following modifications: tailing reactions were performed in the presence of 10% DMSO, 400 µM dCTP for 1-hour at 4°C, followed by incubation at 37°C for 30 minutes. PCR and nested PCR were performed with the gene specific primers (GATTCCTCTGA TGGCTC; for standard N) or (GACGTAG CCTTCGGGCATGG; for N-Δ86). PCR product was subcloned into the TOPO 2.1 vector (Invitrogen) and individual clones amplified and sequence analyzed.

Nucleocapsid preparation–Vero/hSLAM cells ($2.2x10^6$ in 100 mm dishes) infected with recMeV N-P-N or recMeV N-Δ86-P-N (MOI 0.005 $TCID_{50}$/cell) were harvested in RNP lysis buffer (33) when maximal CPE was observed. Cleared lysates (5,000xg, 5 minutes, 4°C) were layered on CsCl density gradients (2.4ml 40% CsCl, 2.4 ml 30% CsCl, 2.4 ml 20 % CsCl, 0.8 ml 30% glycerol) in TNE buffer (25 mM Tris/Cl pH 7.4, 50 mM NaCl, 2 mM EDTA) and subjected to ultracentrifugation in an SW41 rotor (32,000 rpm, 16 hours, 12°C). Eight 1.5 ml gradient fractions were collected, samples concentrated by TCA precipitation, and fractionated through SDS-PAGE as described.

qPCR–Total RNA was isolated from BSR-T7/5 cells ($8x10^5$ per well in a 6-well format) transfected with plasmids encoding MeV RdRp components, standard N or N-Δ86, and the (+) replicon or the (+) MeV-Luc N-Δ86 genome as outlined. Contaminating DNA was removed through an on-column DNaseI digest and cDNA generated of 3 µg total RNA using oligo-dT primer. qPCR was performed in a 7500 Fast real-time PCR system (Applied Biosystems) using iTaq Fast SYBR Green Supermix with ROX (Bio-Rad) and specific primers annealing in the firefly luciferase (CGCCAAAAGCACTCTGATTGAC; CTCGGGTGTAATCAGAATAGCTG) or cellular GAPDH (CATGTTCCAGTATGACTCTACCC; GACCTTGCCCACAGCCTTGG) ORFs. ΔΔCt values were calculated using GAPDH as cellular standard, followed by calculating the ratios of relative mRNA levels obtained with each replicon construct in the presence of N-Δ86 and standard N.

Statistical analysis–To assess the statistical significance of differences between sample means, unpaired two-tailed t-tests were applied using the Prism 5 (GraphPad) or Excel 14 (Microsoft) software packages.

RESULTS

MeV RNP reconstructions posit N-tail residues 450-525 to be exposed and fully mobile on the nucleocapsid surface (7). If this is the case, we expect previously reported carboxy-terminal tail truncations removing the MoRE domain (8) to generate highly flexible 40 to 50-residue tail stems that protrude from the RNPs. We hypothesized that a negative regulatory effect of these stems, rather than the absence of MoRE domain and carboxy-terminal tail residues, may, in fact, account for the lack of template activity of RNPs with carboxy-terminal P-binding domain truncations (8,13). To test this idea experimentally, we designed a series of progressive N truncation constructs guided by the currently available structural information and bioactivity data (figure 1A). All N variants were expressed at levels comparable to unmodified MeV N and showed the anticipated mobility pattern in SDS-PAGE (figure 1B).

The N-tail MoRE domain is dispensable for RdRp activity–To assess bioactivity of these constructs, we first examined RdRp transcriptase activity in a conventional MeV minigenome reporter assay (27), which predominantly monitors primary RdRp-mediated mRNA synthesis after generation of a negative polarity RNA template by T7-polymerase (figure 1C, (-) replicon). Consistent

with previous reports (8), RdRp activity was only partially affected by deletion of box 3 in the N-tail (MeV N-Δ20), which was shown to be involved in N binding to viral matrix protein (34) and host factors such as hsp70 (35,36). Furthermore, RNPs with N-tail truncations deleting the MoRE domain and carboxy-terminal residues (MeV N-Δ43) were biologically inactive (figure 1D).

Strikingly however, even larger truncations removing part of the N-tail upstream of the MoRE domain (MeV N-Δ86) substantially restored RdRp bioactivity. Equivalent results were obtained when we assessed our panel of N truncation constructs in a positive polarity minigenome system that requires both RdRp replicase and transcriptase activity for reporter expression (figures 1C, (+) replicon, and 1D). Kinetic comparison with standard N revealed an initial delay in reporter expression in the presence of MeV N-Δ86, followed by a plateau phase of nearly reference-like activity (figure 1E).

Protein interactions between the N protein core and an amino-terminal P protein fragment (PNT), and the N protein tail and the carboxy-terminal section of P (PCT) harboring the XD domain were mapped biochemically in previous studies (3). However, none of the N protein tail modifications assessed supported RdRp activity. Since our bioactivity data for N-Δ86 were rather unexpected, we generated MeV PNT and PCT expression plasmids and re-examined the interaction profile with bioactive MeV N-Δ86 by co-immunoprecipitation. These experiments reiterated the efficient interaction of full length P and PNT with N variants containing large tail deletions (MeV N-Δ86 and N-Δ125), and confirmed that PCT interaction with the N protein requires the presence of the MoRE domain in the N-tail (figures 2A and B).

Taken together, these data demonstrate that an interaction between the N-tail MoRE domain and P-XD is not required for RdRp recruitment to, and/or movement along, the RNP template. In addition, they reveal a regulatory role in polymerase activity of the exposed central N-tail section upstream of the MoRE domain.

Regulatory effect of the unstructured, central N-tail section–To address the question of whether this effect depends on the primary sequence of the N-tail section present in MeV N-Δ43 but absent in N-Δ86 (N residues 439-482) or length of the exposed tail stem, we sequence randomized this region in the context of otherwise unchanged full length N (MeV N-(rd86-43)) and the series of N-tail truncations (figure 3A). All constructs were efficiently expressed (figure 3B) and showed slightly increased bioactivity when compared to N-Δ43, but none of the truncated N variants restored RdRp activity to the level observed for N-Δ86 (figure 3C). In contrast, randomizing the central N-tail section between residues 439 and 482 in the background of full length N resulted in slightly higher RdRp activity (approximately 135%) than that observed with standard N.

To test the effect of restricted tail flexibility on N bioactivity, we inserted structurally active tetracysteine tags (30,37) at 4 different tail positions into otherwise unchanged full length N. With the exception of an insertion at N position 446, tagged N proteins were efficiently expressed (figure 3D). However, bioactivity was reduced by approximately 60-80% in each replicon system compared to that observed in the presence of standard N (figure 3E), demonstrating that structurally-active elements are poorly tolerated in the central N-tail domain.

Taken together, these findings support that the central, unstructured N section does not engage in specific protein interactions with viral or host factors proteins. They reveal a regulatory effect of this N-tail domain on polymerase activity in the context of N truncations lacking the MoRE domain and box 3.

The central N-tail region and MoRE domain are required for virus replication–Having demonstrated that removal of the central N-tail section efficiently restores bioactivity of an MeV N variant lacking the MoRE domain and box 3, we next asked whether MeV particles can be recovered that express N-Δ86 in the place of full length N. We exchanged the N open reading frame against that of the N-Δ86 in a cDNA copy of the MeV-Edmonston (MeV-Edm) genome (31), but initial virus recovery attempts failed. This outcome could have been due to the approximately 30% reduction in RdRp activity by N-Δ86 that we observed in replicon assays or, alternatively, could indicate a fundamental role of the central N-tail region and intact MoRE domain and box 3 for virus replication. To distinguish between these possibilities, we rebuilt the N-Δ86 construct in the background of the non-attenuated MeV IC-B

isolate (31), which we had found to return approximately 10-fold higher RdRp activities in transient replicon assays than the MeV Edm-based system (figure 4A). IC-B N-Δ86 was generated by insertion of tandem stop codons at N positions 440 and 441. This construct was efficiently expressed and showed an electrophoretic mobility profile equivalent to that of Edm N-Δ86 (figure 4B). Reproducing our experience with the Edm-based replicon system, RdRp activity of an IC-B replicon containing IC-B N-Δ86 was reduced by approximately 40% compared to standard IC-B N. Importantly, however, the IC-B replicon containing N-Δ86 returned approximately 6-fold higher reporter expression levels than the unchanged, standard Edm replicon (figure 4A).

We therefore transferred IC-B N-Δ86 into the cloned IC-B genome (31). Individual infectious centers were identified after virus recovery transfection that could be passaged laterally (figure 4C), but virus spread was severely impaired for approximately 40 days post-recovery. This period was followed by a phase of rapidly improving replication. Sequencing of the N protein tail after RT-PCR at different times post-recovery transfection revealed spontaneous viral adaptation, gradually replacing both stop codons in the IC-B N-tail with regular codons, as the molecular basis for regained viral growth (figure 4D).

These data indicate that the unsuccessful recovery attempts of recMeV-Edm N-Δ86 did not reflect insufficient RdRp activity *per se* when N-Δ86 is present. Rather, they highlight a fundamental mechanistic role of the central and C-terminal sections of the N protein tail in the context of virus replication that is distinct from basic RdRp recruitment to the nucleocapsid template.

Generation of a replication competent recMeV N-Δ86 variant–To characterize the mechanistic role of N-tail in the context of virus replication, we generated a recMeV variant encoding the N-Δ86 protein in addition to standard N in a recMeV-GFP background, also harboring an eGFP open reading frame as an additional transcription unit (38). Taking advantage of the transcription gradient of paramyxovirus gene expression (39), we moved the standard N reading frame into a post-P position (figure 5A), resulting in substantially higher N-Δ86 than full length N protein levels in infected cells after virus recovery (figure 5B). Despite productive passaging of recMeV N-Δ86-P-N virions, virus growth was severely impaired as evidenced by limited lateral virus spread through cell monolayers (figure 5C) and reduced viral titers compared to standard recMeV and a recMeV N-P-N variant harboring two copies of the unchanged N reading frame (figure 5D). In contrast to recMeV N-Δ86, a recombinant virus lacking only the box 3 region of the N-tail (recMeV N-Δ20) could be recovered without additional full length N complementation, but also showed substantially lower viral titers than standard recMeV (figure 5D). These phenotypes confirm a negative regulatory effect of the N-Δ86 construct in the context of virus replication.

Binding of P-XD to the N-tail is required to stabilize RdRp-RNP interaction during virus replication–In comparison to RdRp activity in minireplicon assays, self-sustained viral genome replication adds at least two additional functional requirements to helper plasmid-driven (+) replicon reporter expression: the correct inaugural positioning of the RdRp replicase complex on the template for generation of complete antigenomic and genomic RNA copies, and sufficient stability of the RdRp-RNP complex during polymerization to ensure faithful replication of RNA sequences substantially longer than the minireplicon reporter constructs.

To test whether these RdRp functionalities are affected by the N-Δ86 truncation, we firstly assessed the molecular nature of the terminal leader sequence of viral genomes in cells infected with standard MeV (recMeV-Edm or recMeV-IC-B) or recMeV N-Δ86-P-N, using rapid amplification of cDNA ends (RACE) and sequencing of 29-40 independent subclones per virus examined. Of a combined 53 genomic sequences obtained for the standard MeV strains, 51 represented complete genome copies while two showed partial terminal truncations (figure 6A). These data closely matched those obtained for recMeV N-Δ86-P-N: 34 genomic sequences were obtained; of these, 33 represented complete genome copies and one a truncated sequence. These results indicate successful replication of the genome termini in the presence of the N-Δ86 variant.

Secondly, we purified intact RNPs from cells infected with recMeV N-P-N or recMeV N-Δ86-

P-N through flotation in cesium chloride gradients. Consistent with previous studies (3,5), RNPs containing full length or truncated N proteins accumulated predominantly in higher gradient fractions (figure 6B). P protein antigenic material was likewise concentrated in these fractions. When we adjusted the nucleocapsid-containing fraction seven for equal N signal intensity and thus overall nucleocapsid content for subsequent immunoblots, quantification of the relative P protein content revealed an approximately 4-fold lower amount of P in RNP samples derived from recMeV N-Δ86-P-N compared to recMeV N-P-N infected cells (figure 6C).

To test the implication of this phenotype on polymerase function, we generated an MeV-luciferase genomic plasmid ((+) MeV-Luc N-Δ86 genome). This construct is equivalent in organization to the (+) replicon reporter plasmid but is approximately 10-times larger in overall size. In addition, it contains an N to N-Δ86 exchange to ensure that transfected cells are void of any full length N protein material at all times (figure 6D). Upon co-transfection with the MeV RdRp helper plasmids, we noted through quantitative real-time PCR analysis that in the case of the (+) replicon, the presence of N-Δ86 reduced relative luciferase mRNA levels to approximately 40% of that observed for full length N. When the larger (+) MeV-Luc N-Δ86 genome plasmid was examined under otherwise identical experimental conditions, however, we found relative luciferase mRNA levels of only 5% that generated in the presence of full length N (figure 6E). Taken together, these data indicate that P-XD binding to the N-tail is not required for initial RdRp positioning on the RNP template, but critically stabilizes the RNP-RdRp complex as RNA polymerization proceeds.

Truncated P-ΔXD partially regains bioactivity when combined with an N-Δ86-RNP template–The P-XD assembles into an antiparallel three-helix bundle that provides the binding site for the N-MoRE domain (17). For counter-analysis of the N-Δ86 bioactivity data, we generated a carboxy-terminally truncated MeV P variant lacking the entire XD domain. Immunodetection confirmed efficient expression of the resulting P-ΔXD construct (figure 7A). When subjected to replicon assays, P-ΔXD lacked all bioactivity when combined with standard nucleocapsid templates composed of full-length N subunits (figure 7B). In the presence of N-Δ86-RNP nucleocapsids, however, we observed a significant increase in reporter expression, indicating that polymerase activity of P-ΔXD-L was partially restored in the absence of the freely flexible N-tail domains. This finding reveals that the presence of either the N-MoRE or the P-XD domain alone blocks polymerase activity in the absence of the binding partner. However, simultaneous deletion of both domains restores access of the polymerase complex to the template and bioactivity.

DISCUSSION

The current model of MeV RdRp recruitment to the RNP template for genome replication and mRNA synthesis assumes an inaugural interaction between a high-affinity MoRE domain in the N-tail and the XD-domain in the viral P protein (7,17). After polymerization is initiated, recurring release and rebinding of XD domains in tetrameric P to MoRE elements in N-RNA is thought to allow progress of the P-L polymerase along the RNP template.

Based on the insight gained in our study, we propose that central elements of this model need to be redefined (figure 7C). Specifically, we found that the recruitment of the MeV polymerase complex to the RNP template occurs independently of any interaction between the N-tail MoRE/box 3 region and P-XD. This initiation mechanism stands in stark contrast to the current paradigm that paramyxovirus P proteins must interact with the C-terminal tail region of N for RNP binding (13,15,40). The previous polymerase binding models were heavily influenced by experiments showing that progressive C-terminal truncations of the MeV N-tail, which partially or completely remove the MoRE domain and downstream residues, largely eliminate polymerase function in replicon assays (8).

Our study reproduced these earlier activity data, but revealed that a substantially larger truncation, removing the unstructured central N-tail section in addition to the MoRE domain and box 3, significantly restores polymerase activity. This finding illuminates a novel regulatory function of the central N-tail region and demonstrates that P-XD interaction with the carboxy-terminal N-tail section is dispensable for productive template binding and RNA synthesis. Supported by essentially equivalent RdRp activity

results obtained with (-) and (+)-type replicon constructs, N-tail independent polymerase loading appears not to be limited to RdRp in transcriptase configuration but also applies to the replicase complex.

We note that even larger tail truncations (i.e. N-Δ108) again abolished N-RNA bioactivity. Since these deletions remove N residues posited in the interstitial space between RNP turns (7), loss of bioactivity may likely reflect transition from native, loosely coiled MeV nucleocapsids to condensed, rigid structures (9). Sequence-randomizing the central N-tail section did not substantially alter RdRp bioactivity in the context of full length (remained active) or MoRE/box 3-truncated (remained largely inactive) N. However, introduction of structurally active tetracysteine tags into the central tail region significantly reduced polymerase activity. We conclude that the regulatory effect of the central N-tail section is unlikely based on direct binding of host co-factors to this region, which would be expected to be sensitive to sequence randomization. Rather, P-XD docking to the N-tail may rearrange and/or organize the tails, giving the polymerase complex access to productive interaction with the RNP template through a direct, previously unappreciated interaction of MeV P-L polymerase complexes with the nucleocapsid core.

Strong support for this model arises from the bioactivity profile of truncated P protein lacking the XD domain (figure 7C). The inability of P-ΔXD-L complexes to organize the N-tails through XD-MoRE domain interactions may account for the loss of bioactivity when combined with standard nucleocapsids. In contrast, Δ86N-tail truncated nucleocapsids are directly accessible by the polymerase without a need for tail reorganization, resulting in partially restored bioactivity of P-ΔXD-L polymerase complexes. Tetracysteine tags in the N-tail may likewise impede this P-XD binding-induced preparation of the RNP core for polymerase docking.

Direct binding of polymerase complexes to the ~40-residue tail stems present in N-Δ86 appears unlikely, due to the proposed position of these tail residues in the interstitial space between nucleocapsid turns (7) and our co-immunoprecipitation results. Also, a conserved box 1 located at the beginning of the tail (amino acids 401-420) was implicated in binding to a cellular N receptor (NR) of unknown molecular nature (41,42). Earlier truncation studies of SeV and MeV N reached the conclusions that N proteins with C-terminal deletions are i) capable of encapsidating RNA (3,5,13), but ii) the resulting RNPs do not support P binding (5,43); and iii) cannot serve as template for the polymerase (8,13,43). In the light of our present findings, we interpret these experiments for MeV, and possibly also SeV, to likely reflect obscured polymerase complex access to the RNP core by the remaining central tail sections in partially truncated N variants. Interestingly, a recent characterization of the related mumps virus P protein revealed that its interaction with nucleocapsid does not fully require the N-tail but can be mediated by other contact domains in P and N (14,44).

Our molecular analysis of the genome termini of over 30 independent clones each of recombinant MeVs harboring truncated or standard N demonstrated accurate replication of RNPs in both cases. Simultaneous analysis of gradient-purified nucleocapsid confirmed that RNPs of recMeV N-Δ86-P-N were predominantly composed of truncated N variants, indicating that the full-length N is not preferentially incorporated into nascent RNPs during replication of this virus. These results underscore that correct, initial positioning of the polymerase on the nucleocapsid template is independent of the P-XD and N-MoRE interaction.

The severely restricted growth phenotype of the recMeV N-Δ86-P-N dual-N recombinant virus, the unsuccessful rescue attempts of recMeV-Edm N-Δ86, and the spontaneous adaptation of recMeV-IC-B N-Δ86 prove, however, that all tail-truncated N variants are incapable of supporting virus replication. Through regulatory functions and/or interaction with the viral matrix protein (34-36), the box 3 section of the MeV N-tail facilitates efficient genome replication and incorporation into nascent particles. Conceivably, the elimination of this region 3, rather than the deletion of the N-MoRE domain, may prevent the recovery of recombinant MeV N-Δ86 virions. However, M-deleted MeV recombinants replicate in cell culture (45) and we recovered an MeV N-Δ20 recombinant, which lacks box 3 but leaves the MoRE domain intact.

Considering approximately 70% bioactivity of N-Δ86-containing RNPs in replicon assays, we

are confident that the inability of N-Δ86 to support virus replication is based on a fundamental difference between the replicon system and self-sustained replication, rather than an overall reduction in RdRp activity. The successful recovery of the MeV recombinant harboring the N-Δ20 construct, which showed a similar reduction in bioactivity in replicon assays, corroborates this interpretation. Fulfilling an auxiliary role, dynamic cycles of N-tail to P-XD docking and release may be required to stabilize the RdRp-RNP complex as the polymerase moves along the template. This view is supported by our observation that increasing RNP template length in transient replicon assays results in an overproportional decline in efficiency of successful replication in the presence of N-Δ86. Purified nucleocapsids of recMeV N-Δ86-P-N show a reduced, but appreciable, level of co-floating P compared to standard MeV RNPs. Under these conditions, the full length N subunits present in the mixed RNPs may contribute to the biochemically detectable association.

In conclusion, we propose that the tightly orchestrated N-MoRE interaction with P-XD is not required to recruit or position the polymerase complex on the RNP template, but may rather arrange the central N-tail sections to allow access for direct polymerase docking to the nucleocapsid core. As such, the interaction of N-MoRE with P-XD may help to overcome a negative-regulatory effect of central N-tail domains that limit polymerase loading on, or advancing along, the template. After successful initiation of polymerization, iterative cycles of release and rebinding between N-MoRE and P-XD are not essential for polymerase activity *per se*, but reduce the frequency of premature chain termination by dynamically stabilizing the interaction between P and the template.

REFERENCES

1. Ruigrok, R. W., Crepin, T., and Kolakofsky, D. (2011) Nucleoproteins and nucleocapsids of negative-strand RNA viruses. *Current opinion in microbiology* **14**, 504-510
2. Longhi, S. (2009) Nucleocapsid structure and function. *Current topics in microbiology and immunology* **329**, 103-128
3. Bankamp, B., Horikami, S. M., Thompson, P. D., Huber, M., Billeter, M., and Moyer, S. A. (1996) Domains of the measles virus N protein required for binding to P protein and self-assembly. *Virology* **216**, 272-277
4. Curran, J., Pelet, T., and Kolakofsky, D. (1994) An acidic activation-like domain of the Sendai virus P protein is required for RNA synthesis and encapsidation. *Virology* **202**, 875-884
5. Buchholz, C. J., Retzler, C., Homann, H. E., and Neubert, W. J. (1994) The carboxy-terminal domain of Sendai virus nucleocapsid protein is involved in complex formation between phosphoprotein and nucleocapsid-like particles. *Virology* **204**, 770-776
6. Kingston, R. L., Hamel, D. J., Gay, L. S., Dahlquist, F. W., and Matthews, B. W. (2004) Structural basis for the attachment of a paramyxoviral polymerase to its template. *Proceedings of the National Academy of Sciences of the United States of America* **101**, 8301-8306
7. Jensen, M. R., Communie, G., Ribeiro, E. A., Jr., Martinez, N., Desfosses, A., Salmon, L., Mollica, L., Gabel, F., Jamin, M., Longhi, S., Ruigrok, R. W., and Blackledge, M. (2011) Intrinsic disorder in measles virus nucleocapsids. *Proceedings of the National Academy of Sciences of the United States of America* **108**, 9839-9844
8. Zhang, X., Glendening, C., Linke, H., Parks, C. L., Brooks, C., Udem, S. A., and Oglesbee, M. (2002) Identification and characterization of a regulatory domain on the carboxyl terminus of the measles virus nucleocapsid protein. *Journal of virology* **76**, 8737-8746
9. Desfosses, A., Goret, G., Farias Estrozi, L., Ruigrok, R. W., and Gutsche, I. (2011) Nucleoprotein-RNA orientation in the measles virus nucleocapsid by three-dimensional electron microscopy. *Journal of virology* **85**, 1391-1395
10. Schoehn, G., Mavrakis, M., Albertini, A., Wade, R., Hoenger, A., and Ruigrok, R. W. (2004) The 12 A structure of trypsin-treated measles virus N-RNA. *Journal of molecular biology* **339**, 301-312

11. Bhella, D., Ralph, A., and Yeo, R. P. (2004) Conformational flexibility in recombinant measles virus nucleocapsids visualised by cryo-negative stain electron microscopy and real-space helical reconstruction. *Journal of molecular biology* **340**, 319-331
12. Tawar, R. G., Duquerroy, S., Vonrhein, C., Varela, P. F., Damier-Piolle, L., Castagne, N., MacLellan, K., Bedouelle, H., Bricogne, G., Bhella, D., Eleouet, J. F., and Rey, F. A. (2009) Crystal structure of a nucleocapsid-like nucleoprotein-RNA complex of respiratory syncytial virus. *Science* **326**, 1279-1283
13. Curran, J., Homann, H., Buchholz, C., Rochat, S., Neubert, W., and Kolakofsky, D. (1993) The hypervariable C-terminal tail of the Sendai paramyxovirus nucleocapsid protein is required for template function but not for RNA encapsidation. *Journal of virology* **67**, 4358-4364
14. Kingston, R. L., Baase, W. A., and Gay, L. S. (2004) Characterization of nucleocapsid binding by the measles virus and mumps virus phosphoproteins. *Journal of virology* **78**, 8630-8640
15. Longhi, S., Receveur-Brechot, V., Karlin, D., Johansson, K., Darbon, H., Bhella, D., Yeo, R., Finet, S., and Canard, B. (2003) The C-terminal domain of the measles virus nucleoprotein is intrinsically disordered and folds upon binding to the C-terminal moiety of the phosphoprotein. *The Journal of biological chemistry* **278**, 18638-18648
16. Bourhis, J. M., Canard, B., and Longhi, S. (2006) Structural disorder within the replicative complex of measles virus: functional implications. *Virology* **344**, 94-110
17. Longhi, S. (2012) The measles virus N(TAIL)-XD complex: an illustrative example of fuzziness. *Advances in experimental medicine and biology* **725**, 126-141
18. Communie, G., Crepin, T., Maurin, D., Jensen, M. R., Blackledge, M., and Ruigrok, R. W. (2013) Structure of the tetramerization domain of measles virus phosphoprotein. *Journal of virology* **87**, 7166-7169
19. Houben, K., Blanchard, L., Blackledge, M., and Marion, D. (2007) Intrinsic dynamics of the partly unstructured PX domain from the Sendai virus RNA polymerase cofactor P. *Biophysical journal* **93**, 2830-2844
20. Curran, J. (1998) A role for the Sendai virus P protein trimer in RNA synthesis. *Journal of virology* **72**, 4274-4280
21. Longhi, S. (2011) *Structural disorder within the measles viurs nucleoprotein and phosphoprotein: functional implications for transcription and replication.*, World Scientific, Hackensack, N.J.
22. Shu, Y., Habchi, J., Costanzo, S., Padilla, A., Brunel, J., Gerlier, D., Oglesbee, M., and Longhi, S. (2012) Plasticity in structural and functional interactions between the phosphoprotein and nucleoprotein of measles virus. *The Journal of biological chemistry* **287**, 11951-11967
23. Buchholz, U. J., Finke, S., and Conzelmann, K. K. (1999) Generation of bovine respiratory syncytial virus (BRSV) from cDNA: BRSV NS2 is not essential for virus replication in tissue culture, and the human RSV leader region acts as a functional BRSV genome promoter. *Journal of virology* **73**, 251-259
24. Ono, N., Tatsuo, H., Hidaka, Y., Aoki, T., Minagawa, H., and Yanagi, Y. (2001) Measles viruses on throat swabs from measles patients use signaling lymphocytic activation molecule (CDw150) but not CD46 as a cellular receptor. *Journal of virology* **75**, 4399-4401
25. Doyle, J., Prussia, A., White, L. K., Sun, A., Liotta, D. C., Snyder, J. P., Compans, R. W., and Plemper, R. K. (2006) Two domains that control prefusion stability and transport competence of the measles virus fusion protein. *Journal of virology* **80**, 1524-1536
26. Paal, T., Brindley, M. A., St Clair, C., Prussia, A., Gaus, D., Krumm, S. A., Snyder, J. P., and Plemper, R. K. (2009) Probing the spatial organization of measles virus fusion complexes. *Journal of virology* **83**, 10480-10493
27. Krumm, S. A., Ndungu, J. M., Yoon, J. J., Dochow, M., Sun, A., Natchus, M., Snyder, J. P., and Plemper, R. K. (2011) Potent host-directed small-molecule inhibitors of myxovirus RNA-dependent RNA-polymerases. *PloS one* **6**, e20069

28. Radecke, F., Spielhofer, P., Schneider, H., Kaelin, K., Huber, M., Dotsch, C., Christiansen, G., and Billeter, M. A. (1995) Rescue of measles viruses from cloned DNA. *The EMBO journal* **14**, 5773-5784
29. Seki, F., Yamada, K., Nakatsu, Y., Okamura, K., Yanagi, Y., Nakayama, T., Komase, K., and Takeda, M. (2011) The SI strain of measles virus derived from a patient with subacute sclerosing panencephalitis possesses typical genome alterations and unique amino acid changes that modulate receptor specificity and reduce membrane fusion activity. *Journal of virology* **85**, 11871-11882
30. Madani, F., Lind, J., Damberg, P., Adams, S. R., Tsien, R. Y., and Graslund, A. O. (2009) Hairpin structure of a biarsenical-tetracysteine motif determined by NMR spectroscopy. *Journal of the American Chemical Society* **131**, 4613-4615
31. Takeda, M., Takeuchi, K., Miyajima, N., Kobune, F., Ami, Y., Nagata, N., Suzaki, Y., Nagai, Y., and Tashiro, M. (2000) Recovery of pathogenic measles virus from cloned cDNA. *Journal of virology* **74**, 6643-6647
32. Dochow, M., Krumm, S. A., Crowe, J. E., Jr., Moore, M. L., and Plemper, R. K. (2012) Independent structural domains in the paramyxovirus polymerase protein. *The Journal of biological chemistry*
33. Buchholz, C. J., Spehner, D., Drillien, R., Neubert, W. J., and Homann, H. E. (1993) The conserved N-terminal region of Sendai virus nucleocapsid protein NP is required for nucleocapsid assembly. *Journal of virology* **67**, 5803-5812
34. Iwasaki, M., Takeda, M., Shirogane, Y., Nakatsu, Y., Nakamura, T., and Yanagi, Y. (2009) The matrix protein of measles virus regulates viral RNA synthesis and assembly by interacting with the nucleocapsid protein. *Journal of virology* **83**, 10374-10383
35. Couturier, M., Buccellato, M., Costanzo, S., Bourhis, J. M., Shu, Y., Nicaise, M., Desmadril, M., Flaudrops, C., Longhi, S., and Oglesbee, M. (2010) High affinity binding between Hsp70 and the C-terminal domain of the measles virus nucleoprotein requires an Hsp40 co-chaperone. *Journal of molecular recognition : JMR* **23**, 301-315
36. Zhang, X., Bourhis, J. M., Longhi, S., Carsillo, T., Buccellato, M., Morin, B., Canard, B., and Oglesbee, M. (2005) Hsp72 recognizes a P binding motif in the measles virus N protein C-terminus. *Virology* **337**, 162-174
37. Griffin, B. A., Adams, S. R., and Tsien, R. Y. (1998) Specific covalent labeling of recombinant protein molecules inside live cells. *Science* **281**, 269-272
38. Duprex, W. P., McQuaid, S., Hangartner, L., Billeter, M. A., and Rima, B. K. (1999) Observation of measles virus cell-to-cell spread in astrocytoma cells by using a green fluorescent protein-expressing recombinant virus. *Journal of virology* **73**, 9568-9575
39. Collins, P. L., and Wertz, G. W. (1983) cDNA cloning and transcriptional mapping of nine polyadenylylated RNAs encoded by the genome of human respiratory syncytial virus. *Proceedings of the National Academy of Sciences of the United States of America* **80**, 3208-3212
40. Houben, K., Marion, D., Tarbouriech, N., Ruigrok, R. W., and Blanchard, L. (2007) Interaction of the C-terminal domains of sendai virus N and P proteins: comparison of polymerase-nucleocapsid interactions within the paramyxovirus family. *Journal of virology* **81**, 6807-6816
41. Laine, D., Trescol-Biemont, M. C., Longhi, S., Libeau, G., Marie, J. C., Vidalain, P. O., Azocar, O., Diallo, A., Canard, B., Rabourdin-Combe, C., and Valentin, H. (2003) Measles virus (MV) nucleoprotein binds to a novel cell surface receptor distinct from FcgammaRII via its C-terminal domain: role in MV-induced immunosuppression. *Journal of virology* **77**, 11332-11346
42. Laine, D., Bourhis, J. M., Longhi, S., Flacher, M., Cassard, L., Canard, B., Sautes-Fridman, C., Rabourdin-Combe, C., and Valentin, H. (2005) Measles virus nucleoprotein induces cell-proliferation arrest and apoptosis through NTAIL-NR and NCORE-FcgammaRIIB1 interactions, respectively. *The Journal of general virology* **86**, 1771-1784

43. Cevik, B., Kaesberg, J., Smallwood, S., Feller, J. A., and Moyer, S. A. (2004) Mapping the phosphoprotein binding site on Sendai virus NP protein assembled into nucleocapsids. *Virology* **325**, 216-224
44. Cox, R., Green, T. J., Purushotham, S., Deivanayagam, C., Bedwell, G. J., Prevelige, P. E., and Luo, M. (2013) Structural and functional characterization of the mumps virus phosphoprotein. *Journal of virology* **87**, 7558-7568
45. Cathomen, T., Mrkic, B., Spehner, D., Drillien, R., Naef, R., Pavlovic, J., Aguzzi, A., Billeter, M. A., and Cattaneo, R. (1998) A matrix-less measles virus is infectious and elicits extensive cell fusion: consequences for propagation in the brain. *The EMBO journal* **17**, 3899-3908
46. Johansson, K., Bourhis, J. M., Campanacci, V., Cambillau, C., Canard, B., and Longhi, S. (2003) Crystal structure of the measles virus phosphoprotein domain responsible for the induced folding of the C-terminal domain of the nucleoprotein. *The Journal of biological chemistry* **278**, 44567-44573

Acknowledgements-We thank A. L. Hammond and B. Bankamp for discussion and comments on the manuscript.

FOOTNOTES

*This work was supported, in part, by Public Health Service grants AI071002 and AI085328 from the NIH/NIAID (to R.K.P.).

[1] The abbreviations used are: RNP: Ribonucleoprotein; N: nucleoprotein; MeV: measles virus; MoRE: molecular recognition element; P: phosphoprotein; N-RNA: nucleocapsid; NNV: non-segmented negative strand RNA virus; RSV: respiratory syncytial virus; RdRp: RNA-dependent RNA polymerase; L: polymerase; SeV: Sendai virus; XD domain: MoRE-binding domain in P protein; $TCID_{50}$: 50% tissue culture infectious dose; MeV-Edm: measles virus Edmonston strain; WCL: whole cell lysates; RLU: relative luciferase units; PNT: amino-terminal N protein section; PCT: carboxy-terminal N protein section

FIGURE LEGENDS

FIGURE 1: Progressive MeV N-tail truncations significantly restore bioactivity. A. Schematic of the N-tail organization. Conserved microdomains (box 1-3) and the MoRE domain are highlighted. Arrows mark individual truncations generated, and numbers refer to amino acids. B. Immunoblots (IB) of whole cell lysates (WCL) of cells transfected with N-encoding plasmids or vector DNA (mock). Blots were probed with specific antibodies for the MeV N protein, and reprobed with antibodies directed against cellular GAPDH. C. Schematic of the negative and positive polarity minireplicon reporter constructs used for RdRp activity assays. D. Relative luciferase reporter activity (RLU) in cells expressing the (-) or (+) minireplicon construct, L, P, and the specified N variant. Otherwise identically transfected control cells received vector DNA in place of the N expression plasmid (mock). Values were normalized for those obtained in the presence of standard N and represent averages of at least four independent experiments ± SD (***: $p<0.001$). E. Kinetics of reporter expression in the presence of N-Δ86. Cells were transfected as in (D). For each time point, values were normalized for those obtained with standard N. Averages of at least five experiments ± SD are shown.

FIGURE 2: Bioactive MeV N-Δ86 does not interact with a carboxy-terminal PCT fragment harboring the P-XD domain. Lysates of cells expressing the specified N construct and either A. the Flag epitope-tagged amino-terminal PNT fragment or B. full length P or the carboxy-terminal PCT fragment (46) were subjected to direct immunoblotting (WCL) or immunoprecipitation of PNT (α-Flag) or N (α-N). Co-precipitated (co-IP) N or P material, respectively, was detected in immunoblots using specific antibodies. Immunoblots shown are representative of three independent experiments.

FIGURE 3: The central N-tail section downregulates polymerase activity. A. Sequences of full length and truncated N constructs generated with randomized central tail sections. Areas shaded in grey denote scrambled sequence sections. B. Immunoblots of whole lysates of cells expressing the N variants shown in (A). C. Minireplicon reporter assays to assess bioactivity of tail randomized N variants. D. Immunoblot-analysis of cells expressing full-length MeV N variants with tetracysteine (4xcys) epitope tags at the indicated positions. E. Minireplicon reporter assays to determine bioactivity of tetracysteine-tagged N variants shown in (D). In (C) and (E), values and statistical analyses are relative to the minireplicon system containing standard N, and represent averages of at least four experiments ± SD (*: $p<0.05$; ***: $p<0.001$).

FIGURE 4: MeV N-Δ86 does not sustain efficient virus replication. A. Comparison of minireplicon reporter expression driven by wild type MeV (P, N: MeV IC-B; L: MeV 9301B)-derived vs. MeV Edm-derived polymerase helper proteins. All results were normalized for those obtained with the wild type MeV system and in the presence of standard IC-B N. Values represent averages of three experiments ± SD (**: $p<0.01$; ***: $p<0.001$). B. Immunoblot analysis of cells expressing MeV Edm or IC-B-derived P and N variants. C. Microphotographs of cell monolayers infected with newly recovered recMeV IC-B N-Δ86. Representative fields of view are shown at a magnification of 200x. D. Sequence analysis of recMeV IC-B N-Δ86 at the time of recovery (day 0), and after 40 and 56-days of continued incubation.

FIGURE 5: recMeV encoding both N-Δ86 and standard N are replication competent. A. Schematic of the genomes of standard recMeV GFP and newly generated recMeV N-Δ86-P-N. B. Immunoblot analysis of N protein expression in cells infected with recMeV N-Δ86-P-N or standard recMeV. For comparison, total lysates of cells transfected with N-Δ86 or standard N expression plasmids were analyzed in parallel. Control cells received infection media only (mock). C. Cytopathic effect and lateral spread of cells infected with recMeV N-Δ86-P-N or recMeV GFP, monitored by following eGFP expression in infected cells. Representative fields of view are shown at a magnification of 200x. D. Stock titers of cell-associated particles of a panel of three recombinants generated for this study in comparison with standard recMeV or recMeV lacking the M protein (recMeV ΔM). Error bars represent the titer range observed.

FIGURE 6: Presence of N-Δ86 in nucleocapsids affects the stability of P binding to RNPs. A. RACE analysis of viral genome termini present in cells infected with the specified MeV recombinants. Values represent the total number of independent genomes subcloned and analyzed (clones anal.), and the subset of these that featured complete leader sequences (cpl. leader), termini-truncated sequences (trunc. leader), and first open reading frame viral mRNA (vr. mRNA). B. Purification of viral nucleocapsids through cesium chloride gradient fractionation. Gradient fractions were loaded from top (1) to bottom (8), and immunoblots were decorated with specific antibodies directed against the MeV N or P protein, respectively. C. Fraction seven material from (B) was densitometrically adjusted for ± 10% equal amounts of nucleocapsid material by N signal intensity, subjected to SDS-PAGE, and the relative amounts of co-floating P material determined. Numbers represent averages of densitometric quantifications of three independent experiments ± SD. D. Schematic of the (+) replicon and the (+) MeV-Luc N-Δ86 genome construct, drawn to scale. E. qPCR analysis of relative luciferase mRNA levels obtained after co-transfection of cells with MeV P and L expression plasmids, the replicon constructs shown in (D), and either standard N or N-Δ86-encoding plasmids. Columns show ratios of relative mRNA levels obtained with each replicon construct in the presence of N-Δ86 and standard N. Values represent averages of at least three independent experiments, each quantified in duplicates, ± SD (*: $p<0.05$).

Figure 7: A. Immunoblots (IB) of whole lysates of cells transfected with P-encoding plasmids or vector DNA (mock). Blots were probed with specific antibodies for the MeV P protein, and reprobed with antibodies directed against cellular GAPDH. B. Luciferase reporter activity in cells expressing the (-) MeV-Edm replicon, L, truncated P-ΔXD, and the specified N variant. Otherwise identically transfected

control cells received vector DNA in place of the N expression plasmid (mock). Values represent averages of thirteen independent experiments ± SEM (***: $p<0.001$). C. Revised model of MeV polymerase recruitment. The P-L polymerase complex directly engages the nucleocapsid for N-tail-independent loading and progress. If nucleocapsids are composed of full length N (ia), the P-XD interaction with N-MoRE rearranges the central N-tail sections to facilitate polymerase binding to the core and stabilizes binding of the advancing complex to the template. In the absence of the P-XD domain (ib) or in the case of a MoRE-deleted N-Δ43 and P or P-ΔXD (iia and b), the exposed, freely mobile central tail sections prevent polymerase binding and/or progress. Absence of these mobile tail sections in N-Δ86 nucleocapsids (iiia and b) allows productive interaction of the polymerase complex with, and advancement along, the template.

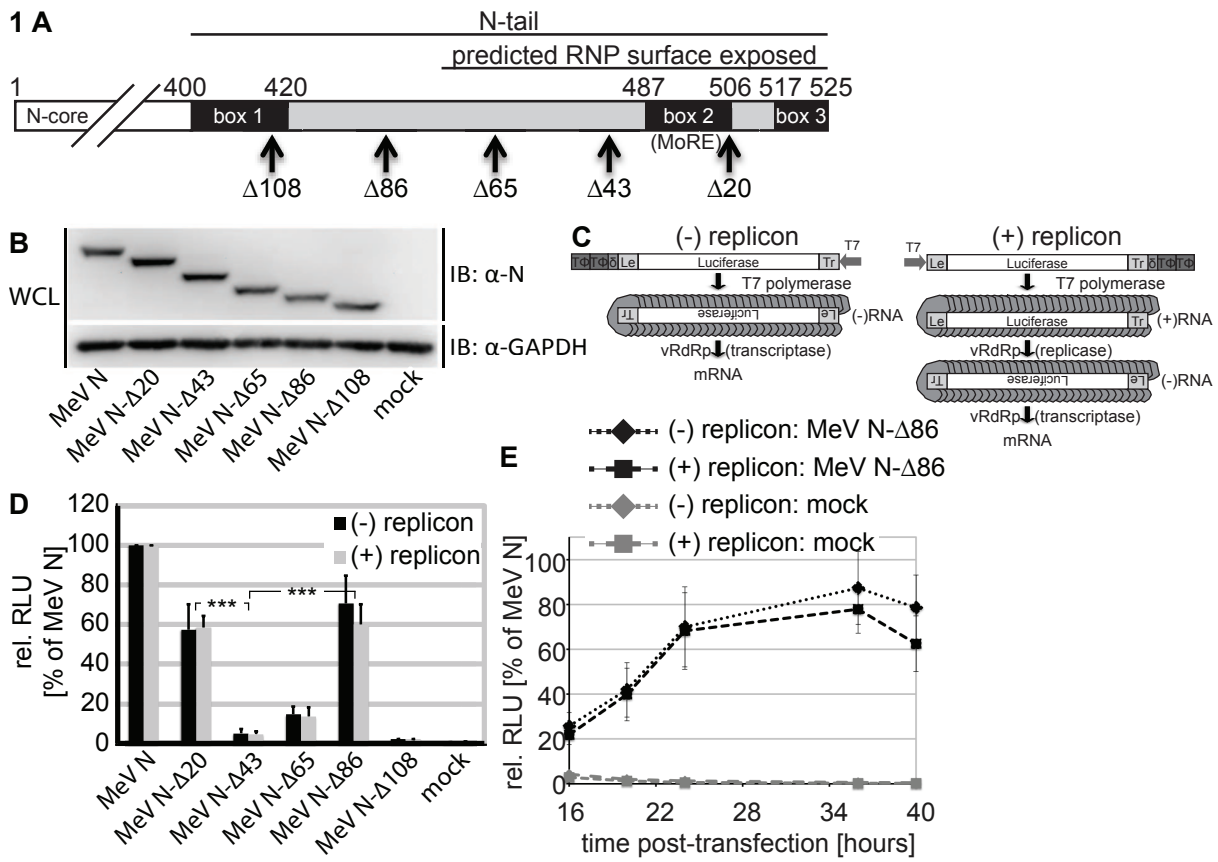
1 A
N-tail
predicted RNP surface exposed
1
400
420
487
506 517 525
N-core
box 1
box 2
box 3
(MoRE)
Δ108
Δ86
Δ65
Δ43
Δ20
B
WCL
IB: α-N
IB: α-GAPDH
MeV N
MeV N-Δ20
MeV N-Δ43
MeV N-Δ65
MeV N-Δ86
MeV N-Δ108
mock
C
(-) replicon
T7
Luciferase
T7 polymerase
(-)RNA
vRdRp (transcriptase)
mRNA
(+) replicon
(+)RNA
vRdRp (replicase)
D
(-) replicon
(+) replicon
rel. RLU [% of MeV N]
***
***
E
(-) replicon: MeV N-Δ86
(+) replicon: MeV N-Δ86
(-) replicon: mock
(+) replicon: mock
rel. RLU [% of MeV N]
time post-transfection [hours]

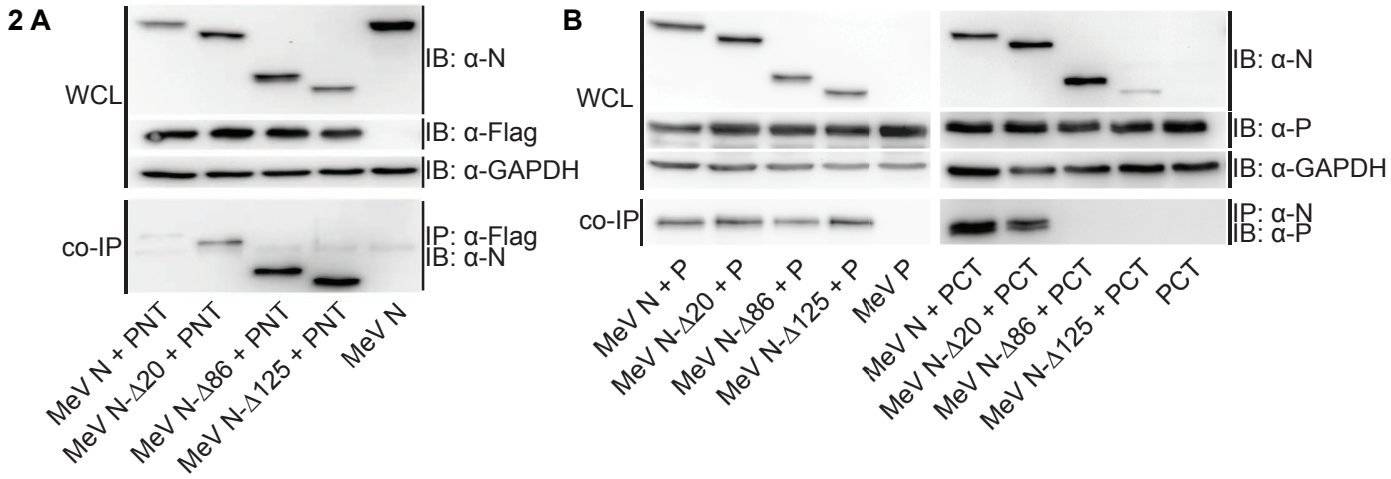
2 A
WCL
co-IP
IB: α-N
IB: α-Flag
IB: α-GAPDH
IP: α-Flag
IB: α-N
MeV N + PNT
MeV N-Δ20 + PNT
MeV N-Δ86 + PNT
MeV N-Δ125 + PNT
MeV N
B
WCL
co-IP
IB: α-N
IB: α-P
IB: α-GAPDH
IP: α-N
IB: α-P
MeV N + P
MeV N-Δ20 + P
MeV N-Δ86 + P
MeV N-Δ125 + P
MeV P
MeV N + PCT
MeV N-Δ20 + PCT
MeV N-Δ86 + PCT
MeV N-Δ125 + PCT
PCT

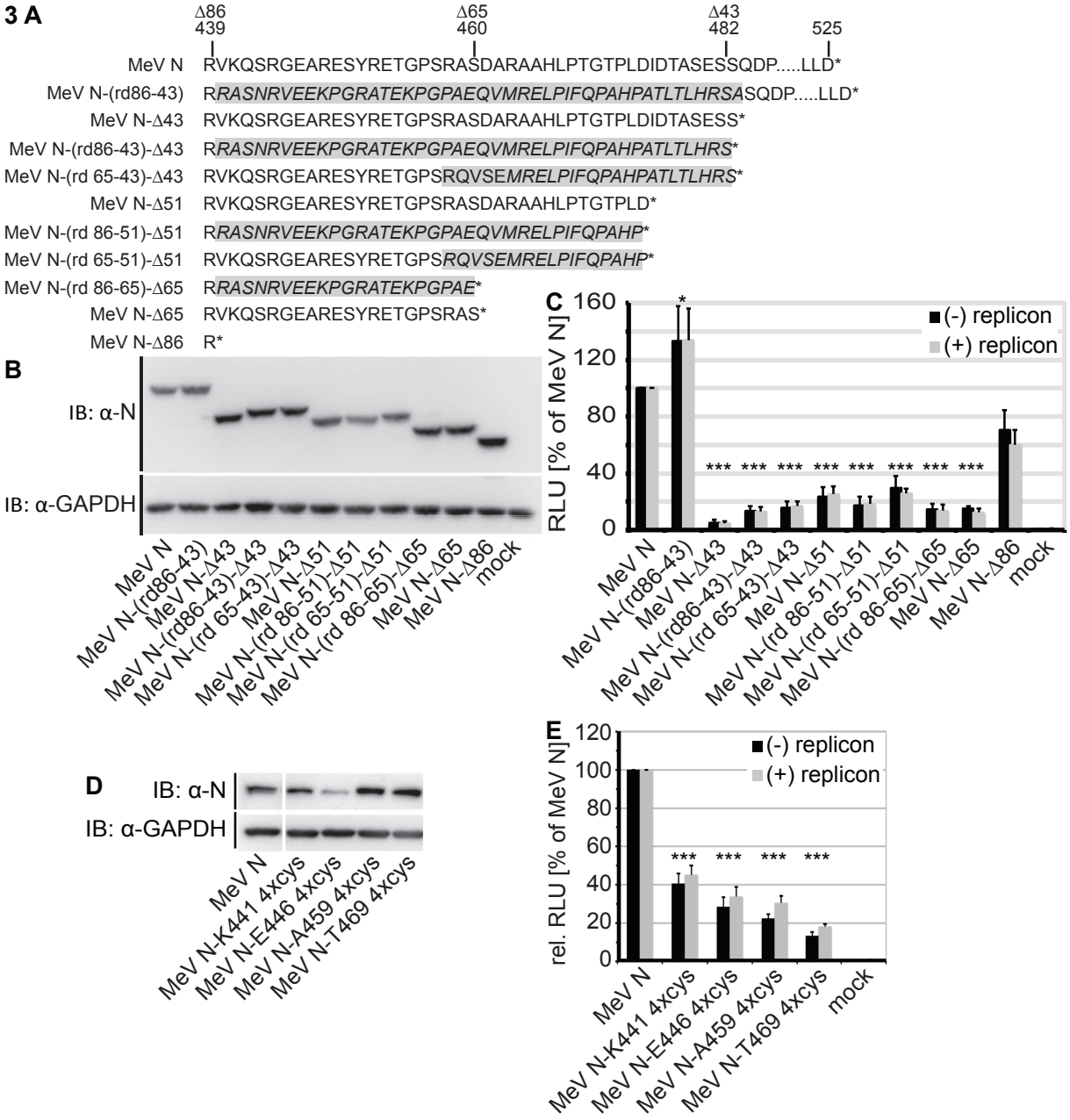
3 A
Δ86
439
Δ65
460
Δ43
482
525
MeV N RVKQSRGEARESYRETGPSRASDARAAHLPTGTPLDIDTASESSQDP.....LLD*
MeV N-(rd86-43) RRASNRVEEKPGRATEKPGPAEQVMRELPIFQPAHPATLTLHRSASQDP.....LLD*
MeV N-Δ43 RVKQSRGEARESYRETGPSRASDARAAHLPTGTPLDIDTASESS*
MeV N-(rd86-43)-Δ43 RRASNRVEEKPGRATEKPGPAEQVMRELPIFQPAHPATLTLHRS*
MeV N-(rd 65-43)-Δ43 RVKQSRGEARESYRETGPSRQVSEMRELPIFQPAHPATLTLHRS*
MeV N-Δ51 RVKQSRGEARESYRETGPSRASDARAAHLPTGTPLD*
MeV N-(rd 86-51)-Δ51 RRASNRVEEKPGRATEKPGPAEQVMRELPIFQPAHP*
MeV N-(rd 65-51)-Δ51 RVKQSRGEARESYRETGPSRQVSEMRELPIFQPAHP*
MeV N-(rd 86-65)-Δ65 RRASNRVEEKPGRATEKPGPAE*
MeV N-Δ65 RVKQSRGEARESYRETGPSRAS*
MeV N-Δ86 R*
B
IB: α-N
IB: α-GAPDH
MeV N
MeV N-(rd86-43)
MeV N-Δ43
MeV N-(rd86-43)-Δ43
MeV N-(rd 65-43)-Δ43
MeV N-Δ51
MeV N-(rd 86-51)-Δ51
MeV N-(rd 65-51)-Δ51
MeV N-(rd 86-65)-Δ65
MeV N-Δ65
MeV N-Δ86
mock
C
RLU [% of MeV N]
160
120
80
40
0
(-) replicon
(+) replicon
*
***
D
IB: α-N
IB: α-GAPDH
MeV N
MeV N-K441 4xcys
MeV N-E446 4xcys
MeV N-A459 4xcys
MeV N-T469 4xcys
E
rel. RLU [% of MeV N]
120
100
80
60
40
20
0
(-) replicon
(+) replicon
***
mock

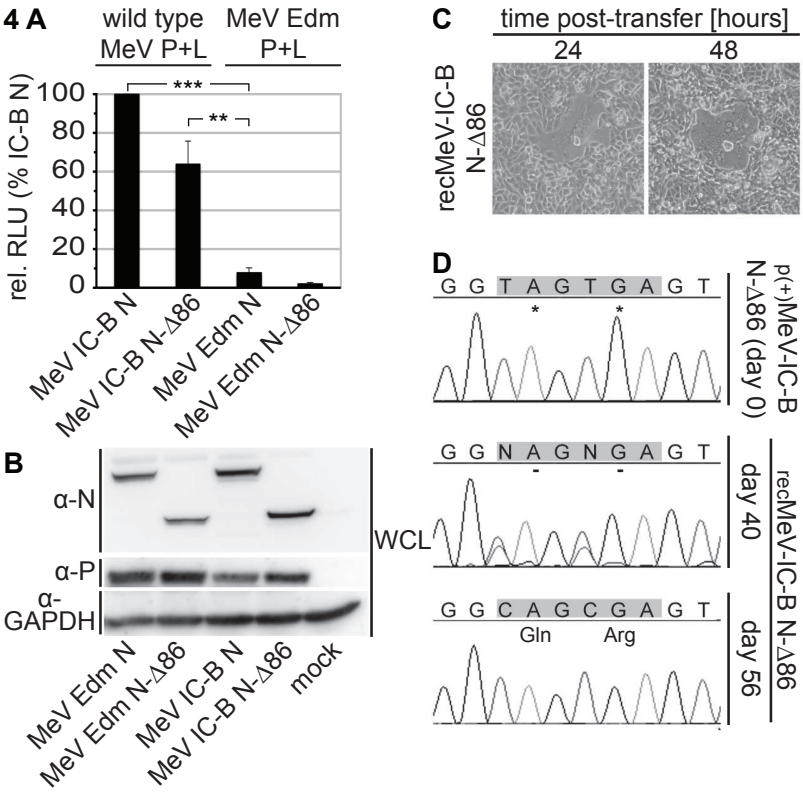
4 A
wild type MeV P+L
MeV Edm P+L
rel. RLU (% IC-B N)
100
80
60
40
20
0
***
**
MeV IC-B N
MeV IC-B N-Δ86
MeV Edm N
MeV Edm N-Δ86
B
α-N
α-P
α-GAPDH
WCL
MeV Edm N
MeV Edm N-Δ86
MeV IC-B N
MeV IC-B N-Δ86
mock
C
time post-transfer [hours]
24
48
recMeV-IC-B N-Δ86
D
G G T A G T G A G T
p(+)MeV-IC-B N-Δ86 (day 0)
G G N A G N G A G T
day 40
recMeV-IC-B N-Δ86
G G C A G C G A G T
Gln
Arg
day 56

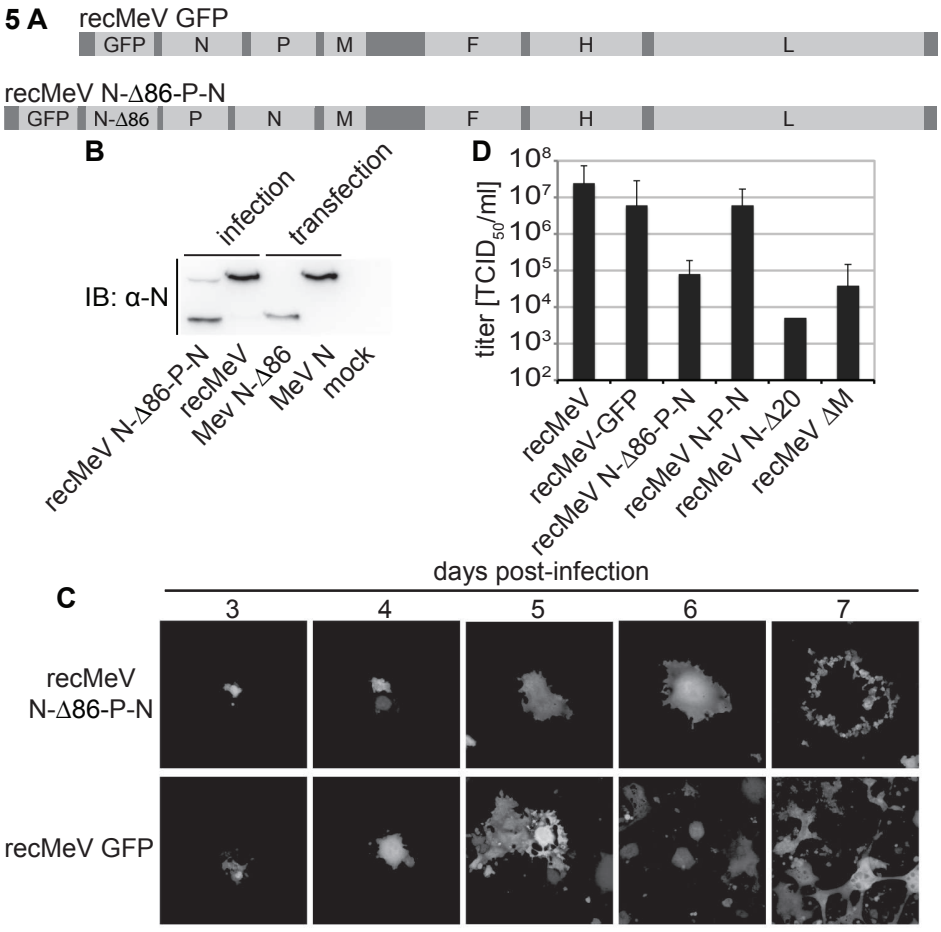
5 A
recMeV GFP
GFP
N
P
M
F
H
L
recMeV N-Δ86-P-N
GFP
N-Δ86
P
N
M
F
H
L
B
infection
transfection
IB: α-N
recMeV N-Δ86-P-N
recMeV
Mev N-Δ86
MeV N
mock
D
titer [TCID50/ml]
10^8
10^7
10^6
10^5
10^4
10^3
10^2
recMeV
recMeV-GFP
recMeV N-Δ86-P-N
recMeV N-P-N
recMeV N-Δ20
recMeV ΔM
C
days post-infection
3
4
5
6
7
recMeV
N-Δ86-P-N
recMeV GFP

6 A

virus	clones anal.	cpl. leader	trunc. leader	vr. mRNA
recMeV-Edm	36	27	-	9
recMeV-IC-B	29	24	2	3
recMeV N-Δ86-P-N	40	33	1	6

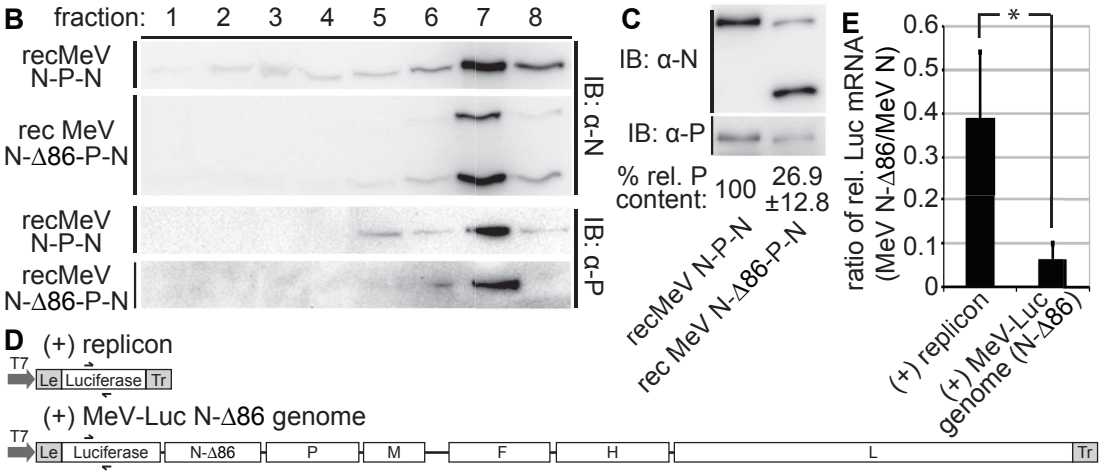

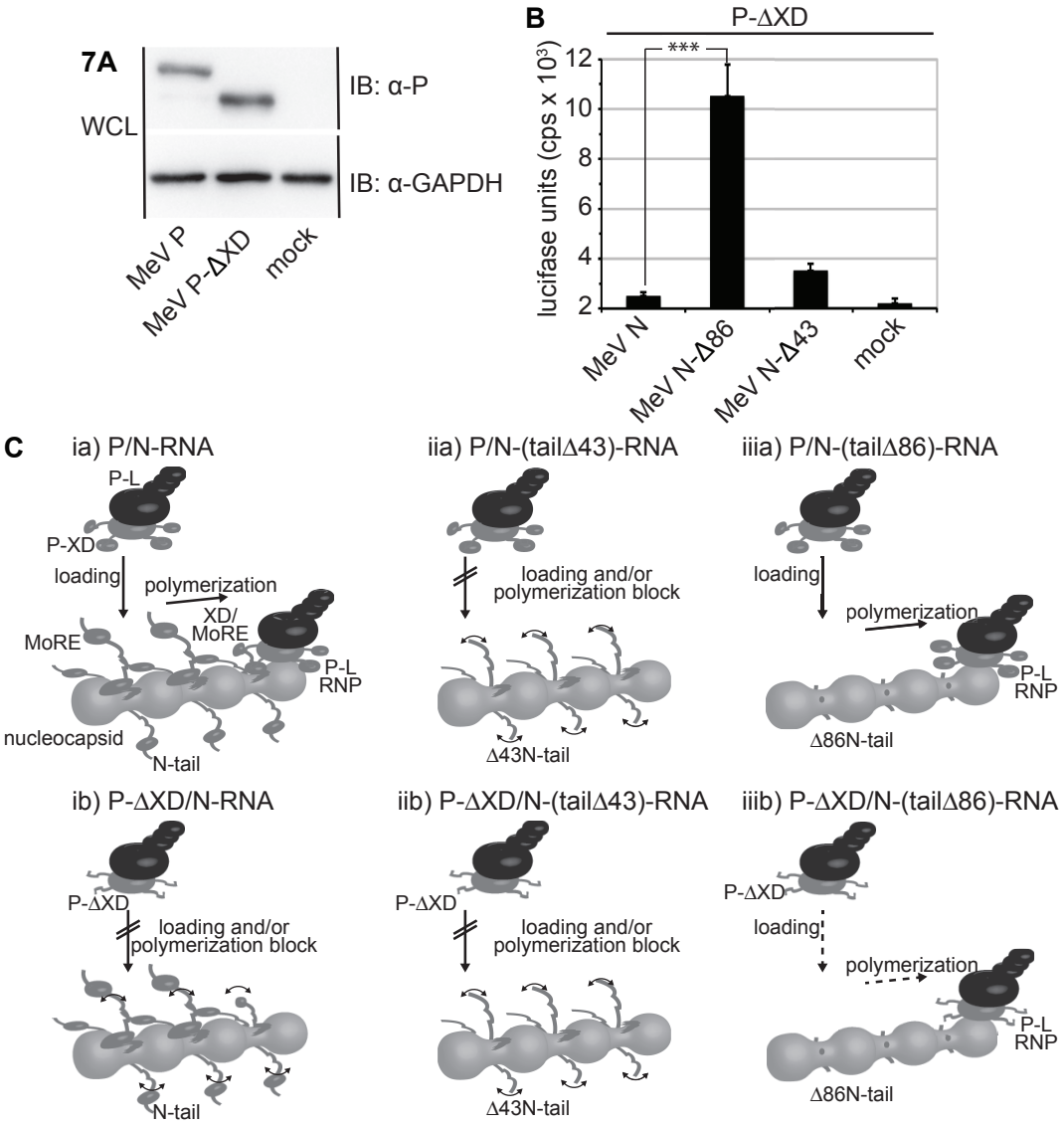
7A
WCL
IB: α-P
IB: α-GAPDH
MeV P
MeV P-ΔXD
mock
B
P-ΔXD
***
lucifase units (cps x 10³)
12
10
8
6
4
2
MeV N
MeV N-Δ86
MeV N-Δ43
mock
C
ia) P/N-RNA
P-L
P-XD
loading
polymerization
XD/
MoRE
MoRE
P-L
RNP
nucleocapsid
N-tail
iia) P/N-(tailΔ43)-RNA
loading and/or
polymerization block
Δ43N-tail
iiia) P/N-(tailΔ86)-RNA
loading
polymerization
P-L
RNP
Δ86N-tail
ib) P-ΔXD/N-RNA
P-ΔXD
loading and/or
polymerization block
N-tail
iib) P-ΔXD/N-(tailΔ43)-RNA
P-ΔXD
loading and/or
polymerization block
Δ43N-tail
iiib) P-ΔXD/N-(tailΔ86)-RNA
P-ΔXD
loading
polymerization
P-L
RNP
Δ86N-tail

Publication 4

Dan Yan, **Stefanie A Krumm**, Aiming Sun, David A Steinhauer, Mingh Luo, Martin L Moore and Richard K Plemper

“Dual Myxovirus Screen Identifies a Small-Molecule Agonist of the Host Antiviral Response”

JOURNAL OF VIROLOGY, August 2013

Reproduced from JVI by copyright permission of American Society for Microbiology

JVI
Journals.ASM.org

Dual Myxovirus Screen Identifies a Small-Molecule Agonist of the Host Antiviral Response

Dan Yan,[a] Stefanie A. Krumm,[a] Aiming Sun,[b] David A. Steinhauer,[c] Ming Luo,[d] Martin L. Moore,[e,f] Richard K. Plemper[a,e]

Center for Inflammation, Immunity & Infection, Georgia State University, Atlanta, Georgia, USA[a]; Emory Institute for Drug Development, Emory University, Atlanta, Georgia, USA[b]; Department of Microbiology & Immunology, Emory University School of Medicine, Atlanta, Georgia, USA[c]; Department of Microbiology, University of Alabama at Birmingham, Birmingham, Alabama, USA[d]; Department of Pediatrics, Emory University School of Medicine, Atlanta, Georgia, USA[e]; Children's Healthcare of Atlanta, Atlanta, Georgia, USA[f]

As we are confronted with an increasing number of emerging and reemerging viral pathogens, the identification of novel pathogen-specific and broad-spectrum antivirals has become a major developmental objective. Targeting of host factors required for virus replication presents a tangible approach toward obtaining novel hits with a broadened indication range. However, the identification of developable host-directed antiviral candidates remains challenging. We describe a novel screening protocol that interrogates the myxovirus host-pathogen interactome for broad-spectrum drug candidates and simultaneously probes for conventional, pathogen-directed hits. With resource efficiency and pan-myxovirus activity as the central developmental parameters, we explored coscreening against two distinct, independently traceable myxoviruses in a single-well setting. Having identified a pair of unrelated pathogenic myxoviruses (influenza A virus and measles virus) with comparable replication kinetics, we observed unimpaired coreplication of both viruses, generated suitable firefly and *Renilla* luciferase reporter constructs, respectively, and validated the protocol for up to a 384-well plate format. Combined with an independent counterscreen using a recombinant respiratory syncytial virus luciferase reporter, implementation of the protocol identified candidates with a broadened antimyxovirus profile, in addition to pathogen-specific hits. Mechanistic characterization revealed a newly discovered broad-spectrum lead that does not block viral entry but stimulates effector pathways of the innate cellular antiviral response. In summary, we provide proof of concept for the efficient discovery of broad-spectrum myxovirus inhibitors in parallel to para- and orthomyxovirus-specific hit candidates in a single screening campaign. The newly identified compound provides a basis for the development of a novel broad-spectrum small-molecule antiviral class.

In recent decades, small-molecule therapeutics have revolutionized the treatment of a variety of viral infections. Despite this success, the reach of licensed antivirals is frequently limited by a single pathogen indication profile and preexisting or rapidly emerging viral resistance. Furthermore, the significant resources required for clinical drug development prohibit attempts to generate individual antivirals against all clinically relevant viral pathogens or to flexibly respond to newly emerging virological threats. New antiviral leads and novel discovery strategies are therefore needed to expand the portfolio of treatable viral diseases within the realms of presently available manufacturing technologies.

Therapeutic targeting of host factors required for virus replication has emerged as a novel concept of antiviral therapy that has high promise to advance beyond some of these limitations (1–3). Different viruses, in particular those representing related viral families, frequently rely on an overlapping set of host cell factors and pathways for their replication (1, 2). As substantiated by recent evidence (4, 5), many host requirements are conserved among related viruses, increasing the possibility for broad-spectrum antiviral activity. Likewise, the host-directed approach may contribute to reducing the frequency of viral escape from inhibition (6–8), since individual viral mutations are less likely to compensate for functional loss of a host factor or pathway required for viral replication.

Recognizing that these advantages will be offset by a heightened risk of inducing drug-related side effects, viral pathogens associated predominantly with acute disease appear particularly suitable for this therapeutic approach, because treatment time, and hence host exposure to the drug, can be kept limited. Myxoviruses such as influenza viruses, in the *Orthomyxoviridae* family, and respiratory syncytial virus (RSV), human parainfluenza viruses (HPIVs), mumps virus (MuV), and measles virus (MeV), in the *Paramyxoviridae* family, are collectively responsible for major human morbidity and mortality due to acute viral respiratory disease (9–14).

Influenza virus in particular remains the leading cause of death from respiratory disease in the United States, despite the existence of vaccine prophylaxis. The licensed influenza virus neuraminidase inhibitors zanamivir and oseltamivir carboxylate are beneficial when treatment is initiated early, but this is increasingly offset by viral resistance (15–17). Despite extensive research, no vaccines are currently available for paramyxoviruses such as RSV and the HPIVs, and declining mumps vaccine uptake in several developed countries has, in conjunction with primary and secondary vaccine failures, resulted in a recent resurgence of mumps (14). Ribavirin is approved for RSV treatment, but its utility is limited due to efficacy and toxicity issues (18). RSV prophylaxis using antibody therapies (19, 20) is reserved for high-risk pediatric patients. Considering their clinical significance, unmet medical need, and pre-

Received 28 May 2013 Accepted 28 July 2013
Published ahead of print 7 August 2013
Address correspondence to Richard K. Plemper, rplemper@gsu.edu.
Copyright © 2013, American Society for Microbiology. All Rights Reserved.
doi:10.1128/JVI.01425-13

dominant association with acute disease, myxovirus family members are viable targets for novel pathogen- and host-directed antiviral campaigns.

Discovery paths toward pathogen-directed drug candidates are well established, but diverse strategies are currently used to identify druggable host targets. For influenza virus in particular, several target-driven approaches have recently been employed, originating from either knowledge-based host target selection (21–23) or systemwide genetic screens for host factors that are involved in pathogen replication (24–26). Chosen targets can then be pursued through narrow drug screens or, if available, use of existing inhibitors. Repurposing of the MEK kinase inhibitor U0126, blocking the Raf/MEK/ERK cascade (21, 27), and the CDC-like kinase 1 inhibitor TG003 (24) for influenza virus inhibition serves as a case in point. While these examples hold some promise, the limited pool of attractive knowledge-based druggable targets, the low reproducibility between comparable RNA interference (RNAi) screens (28), misjudgment of the druggability of target candidates (29), and the challenges associated with bioinformatics-driven triaging of systemwide gene data sets based on differently curated pathway databases (8) are major obstacles in the path toward developing applicable host-directed therapeutics.

In search of an alternative, compound-driven approach, we propose a resource-efficient drug discovery protocol that allows the interrogation of the full host-pathogen interactome for druggable host targets with broad-spectrum antiviral effects in parallel to the discovery of conventional, pathogen-directed hits. In this study, we examined the hypothesis that the anticipated broadened pathogen indication spectrum of host-directed antivirals itself can be employed as a viable selector for host-directed hits. Having identified representatives of the *Ortho-* and *Paramyxoviridae* with compatible replication kinetics, we examined independent virus replication after coinfection of cells with both viruses in a single-well setting. Usage of independently quantifiable luciferase reporters set the stage for a high-throughput screening (HTS) protocol design that affords the identification of paramyxovirus-specific, orthomyxovirus-specific, and broadly myxovirus-specific, likely host-directed, compounds in a single assay (visualized conceptually in Fig. 1A). Implementation of the protocol against a 10,000-entry diversity set identified, among others, a novel chemical class of broad-spectrum myxovirus inhibitors.

MATERIALS AND METHODS

Cells, viruses, and cloning. All cell lines were maintained at 37°C and 5% CO_2 in Dulbecco's modified Eagle's medium supplemented with 7.5% fetal bovine serum. Vero (African green monkey kidney epithelial) cells (ATCC CCL-81) stably expressing human signaling lymphocytic activation molecule (Vero-SLAM cells) (30) and baby hamster kidney (BHK-21) cells stably expressing T7 polymerase (BSR-T7/5 [BHK-T7] cells) (31) were incubated at every third passage in the presence of 500 μg/ml G-418 (Geneticin). Human peripheral blood mononuclear cells (PBMCs) (obtained under Emory University Institutional Review Board approval IRB00045690) were prepared and stimulated as previously described (4). Lipofectamine 2000 (Invitrogen) was used for cell transfections. The QuikChange protocol (Stratagene) was used for all standard site-directed mutagenesis assays. Virus strains used in this study were recombinant MeV-Edmonston (recMeV) (32), MuV strain F, recombinant RSV A2 (recRSV) (33), and influenza A virus strains IAV/New York/55/2004 (H3N2) (IAV-New York), IAV/Aichi/2/1968 (H3N2) (IAV-Aichi), IAV/Mexico/INDRE4489/2009 (H1N1) (IAV-Mexico), IAV/WSN/1933 (H1N1) (IAV-WSN), IAV/Brisbane/59/2007 (H1N1) (IAV-Brisbane), IAV/Pennsylvania/08/2008 (H1N1) (IAV-Pennsylvania), and IAV/Texas/15/2009 (H1N1) (IAV-Texas). MeV stocks were grown and titrated by 50% tissue culture infective dose ($TCID_{50}$) titration on Vero-SLAM cells. MuV was grown and plaque assay titrated on Vero cells. RSV was grown and immuno-plaque assay titrated on HEp-2 cells (ATCC HB-8065), as described previously (33). IAV strains were grown and plaque assay titrated on Madin-Darby canine kidney (MDCK) cells or grown on MDCK cells and titrated by TaqMan real-time PCR-based quantification of progeny genome copy numbers, as described previously (4). recMeV-ren and recRSV-ren stocks were subjected to ultracentrifugation through a 20%-60% one-step sucrose gradient (90 min, 100,000 × *g*, 4°C), with recovery of viral particles concentrated at the gradient interphase to reduce contamination with free luciferase protein synthesized during virus amplification.

Compounds. All compounds were dissolved in dimethyl sulfoxide (DMSO) and stored at −80°C. The previously characterized pan-myxovirus inhibitor JMN3-003 (4), MeV RNA-dependent RNA polymerase (RdRp) inhibitor AS-136A (34), and MeV entry inhibitor AS-48 (35) were synthesized in-house, and their purity was confirmed to be >95% by liquid chromatography-mass spectrometry (LC-MS) and nuclear magnetic resonance (NMR) analysis. The screening library (ChemDiv) was designed to cover a broad chemical space within the boundaries of drug-like physical-chemical properties, a molecular weight range of 120 to 500, and best adherence to the Lipinski rule of 5 (36). Individual hit candidates were sourced from ChemDiv, MolPort, or Ambienter.

Generation of luciferase reporter systems. The basis for the generation of recMeV-ren was a plasmid harboring a complete cDNA copy of the recMeV-eGFP genome (37), which contains the enhanced green fluorescent protein (EGFP) open reading frame in the pre-MeV N position. EGFP and *Renilla* luciferase open reading frames were exchanged using standard cloning techniques, and viral recombinants were recovered after sequence confirmation, as described previously (38). The generation and recovery of the equivalently designed recRSV-ren recombinant were described previously (33). For construction of an IAV-firefly luciferase minireplicon reporter plasmid under the control of the RNA polymerase I (Pol I) promoter, the firefly luciferase gene was amplified with appropriate primers and transferred into the pHH21 vector, restoring the noncoding flanking regions of IAV gene segment 5 as specified previously (39), with the exception of an A-to-G exchange at position 8 in the 5′-noncoding region.

Virus-driven luciferase reporter assays. Luciferase enzymatic activity was measured to quantify reporter protein expression. Unless otherwise specified, 293T cells were transfected with 1.0 μg of IAV-firefly luciferase minigenome reporter plasmid/10^5 cells and then cryopreserved at 28 h posttransfection. Thawed cells were seeded at a density of 3×10^4 cells/well in a 96-well plate and infected with tosylsulfonyl phenylalanyl chloromethyl ketone (TPCK)-treated trypsin-activated IAV strains (multiplicity of infection [MOI] = 0.1 PFU/cell), recMeV-ren (MOI = 0.2 $TCID_{50}$/cell), and/or recRSV-ren (MOI = 0.2 PFU/cell) after a 20-hour incubation, unless stated otherwise for individual experiments. Twenty-eight hours after infection with IAV strains or recMeV-ren, Bright-Glo, Renilla-Glo, or Dual-Glo substrate (all from Promega) was added as specified in the manufacturer's instructions, and bioluminescence intensities were determined using an Envision Multilabel microplate reader (PerkinElmer). For experiments involving recRSV-ren, HEp-2 cells were seeded at a density of 1.5×10^4 cells/well and bioluminescence was assessed at 40 h postinfection (hpi). Where specified, the previously characterized pan-myxovirus inhibitor JMN3-003 (4), MeV RdRp inhibitor AS-136A (34), or ERK2 inhibitor 5-iodotubercidin (40) was added as a control.

Fluorescence microscopy. Vero-SLAM cells seeded in multiwell slides were infected with recMeV-eGFP (MOI = 0.2 $TCID_{50}$/cell) and IAV-WSN (MOI = 0.1 PFU/cell), followed by a 40-hour incubation. Where indicated, 100 μM fusion inhibitory peptide (FIP) was added to the cultures at 1 h postinfection. Slides with 4% paraformaldehyde-fixed cells were blocked with bovine serum albumin (BSA), washed, and stained

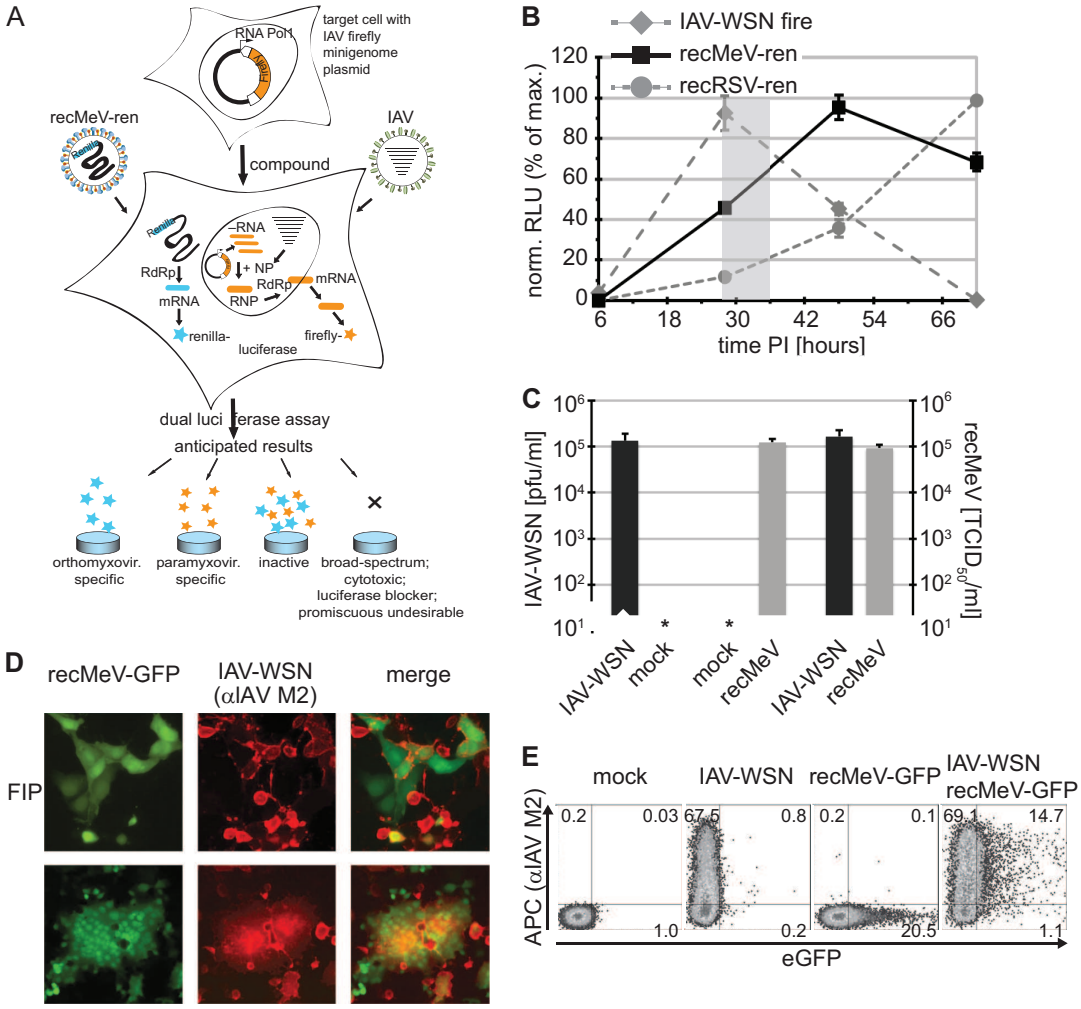

FIG 1 Coinfection assay to identify host-directed pan-myxovirus inhibitors. (A) Schematic of the dual-target antiviral screen. Anticipated outcomes are specified. (B) Expression profiles of the different luciferase reporter constructs. Vero cells were independently infected with recMeV-ren and recRSV-ren (MOI = 0.2) or transfected with the IAV-firefly luciferase reporter and superinfected with IAV-WSN (MOI = 0.1). At the indicated times postinfection (PI), relative luciferase units (RLU) were determined. The shaded area shows the experimental window (28 to 34 hpi). Values were normalized to peak activities of the respective data series and represent means ± SD for three experiments. (C) Progeny titers of released (IAV-WSN) or cell-associated (recMeV) particles after infection of Vero cells singly or in combination. Values represent means and SD for three experiments. (D) Microscopic examination of Vero cells coinfected with recMeV-GFP and IAV-WSN. Where indicated, cells were incubated in the presence of 100 μM fusion inhibitory peptide (FIP). Recording was done at a magnification of ×200. (E) Cytometric analysis of doubly infected cells as described for panel B, with cells incubated in the presence of 100 μM FIP until harvest. Cells were immunostained with specific anti-IAV M2 antibodies (with APC conjugate), and APC fluorescence and EGFP autofluorescence were determined. Numbers show % distributions of singly and doubly fluorescent cells.

with specific anti-IAV M2 protein antibodies (Thermo Scientific) and allophycocyanin (APC)-labeled anti-mouse secondary antibodies (Jackson). Images were taken on a Nikon Diaphot 200 fluorescence microscope at a magnification of ×200.

Flow cytometry. Vero cells infected with recMeV-eGFP (MOI = 0.8 $TCID_{50}$/cell) and IAV-WSN (MOI = 0.1 PFU/cell) were incubated in the presence of 100 μM FIP for 40 h, stained with anti-IAV M2 protein antibodies and APC-conjugated secondary antibodies, fixed, and subjected to cytometric analysis in a FACSCanto II instrument as previously described (38).

HTS. Cryopreserved cells transfected with the IAV-firefly luciferase minigenome plasmid were seeded as described above in white 96-well plates or, at a density of 10^4 cells/well, in 384-well plates, followed by a 20-hour incubation. Test articles dissolved in DMSO were added at a 5 μM final concentration (final DMSO concentration, <0.2%). As a control, the pan-myxovirus inhibitor JMN3-003 (final concentration, 1 μM) and vehicle (DMSO)-only wells were added to each plate in four (96-well plate format) or eight (384-well plate format) replicates each. Cells were then infected with a mixture of TPCK-trypsin-activated IAV-Texas (MOI = 0.1 PFU/cell) and recMeV-ren (MOI = 0.2 $TCID_{50}$/cell). In the time window of 28 to 32 h postinfection, Dual-Glo luciferase substrate was added, and firefly and *Renilla* luciferase activities were quantified in an Envision Multilabel or Synergy H1 (BioTek) microplate reader.

HTS data analysis and IP search. Complete plate reader raw data sets were automatically reformatted into a three-column layout by use of an in-house program, followed by import into the cellHTS2 application package (41, 42). For analysis according to the plate median method, each value was normalized to the median value for all compound wells, and normalized values were scaled to the median absolute deviation of the plate. Stronger inhibition (a reduction in signal) is represented by larger (positive) *Z* scores. For data analysis of confirmatory screens after cherry picking of hits, the normalized percent inhibition (NPI) method was applied, and relative values were calculated by subtracting each compound value from the average for the plate vehicle controls, followed by dividing

the results by the difference between the means for the plate vehicle and JMN3-003 controls. The SciFinder database package (American Chemical Society) was used to query chemical databases with hit candidate structures to evaluate known bioactivities of analogs, commercial availability, and free intellectual property (IP) space. Z' values were calculated based on the following formula: $Z' = 1 - [(3\,SD_C + 3\,SD_B)/(mean_C - mean_B)]$, where SD is the standard deviation, C is the control, and B is the background (43). The coefficient of variation (CV) was calculated as follows: $CV = SD_C/mean_C$.

Assessment of compound cytotoxicity. The CytoTox 96 nonradioactive cytotoxicity assay (Promega) was used to quantify compound toxicity. In 96-well plates, cells were exposed to candidates for 28 hours at 2-fold the screening concentration (10 μM). Substrate was then added, and color development was recorded at 490 nm (specific value) and 650 nm (reference value) in a Synergy H1 microplate reader. Values were normalized to vehicle controls according to % toxicity as follows: % toxicity = 100 − {[(specific value − reference value)/(vehicle value − reference value)] × 100}. To calculate 50% cytotoxic concentrations (CC_{50}s), the compound was added in a 3-fold serial dilution range from 30 to 0.1 μM, and mean values for three replicates were subjected to three-parameter nonlinear regression fitting.

Dose-response curves and EC_{50} calculation. Cells were infected with TPCK-trypsin-activated IAV (MOI = 0.002 PFU/cell) in the presence of 3-fold serial dilutions of compound (the highest concentration assessed was 10 μM) or vehicle. At 1 h postinfection, virus inoculum was removed and cells were incubated in the presence of compound and 3 μg/ml TPCK-trypsin for 40 to 44 h. Progeny virions in culture supernatants were quantified as described above. For all paramyxovirus inhibition curves, infected cells (MuV MOI = 0.1 PFU/cell, recMeV MOI = 0.4 $TCID_{50}$/cell, and recRSV MOI = 0.05 PFU/cell) were incubated in the presence of serial dilutions of compound as described above, for 40 (recMeV) to 72 (MuV and recRSV) hours, followed by titration of cell-associated progeny particles. Fifty percent effective concentrations (EC_{50}s) were calculated based on four-parameter variable-slope nonlinear regression fitting of mean values for three experiments.

Minireplicon reporter assay. 293T cells were transfected with plasmid DNA encoding the IAV (0.5 μg)- or MeV (1 μg) (44)-luciferase minigenome reporter and plasmids encoding the RdRp components MeV-L (1.1 μg), MeV-N (0.4 μg), and MeV-P (0.3 μg), for MeV replicon assays, or IAV-NP, -PA, -PB1, and -PB2 (0.5 μg each), for IAV replicon assays. In the case of MeV replicons, cells were infected with modified vaccinia virus Ankara expressing T7 polymerase (MVA-T7) (45) at 16 h pretransfection. Compound 09167 was added at 4 h posttransfection, and luciferase reporter activities were determined using Bright-Glo substrate as described above.

Fusion-from-without cell-to-cell fusion assay. A dual split-protein cell content mixing assay was employed to quantify MeV envelope glycoprotein-mediated membrane fusion in the presence of compound. NP2-DSP_{1-7} and NP2-DSP_{8-11} cells (46), stably transfected with EGFP-*Renilla* luciferase dual split fusion proteins DSP_{1-7} and DSP_{8-11}, respectively, were coseeded in black 96-well microtiter plates, preloaded with EnduRen luciferase substrate (Promega) at 1 h preinfection, and then spin inoculated with recMeV (1,000 × *g*, 30 min, 4°C; MOI = 10 $TCID_{50}$/ml). Plates were transferred to 37°C, and luciferase activity was recorded in an Envision Multilabel microplate reader (PerkinElmer) at the specified time points. As a control, the MeV entry inhibitor AS-48 was added to a 50 μM final concentration.

Time-of-addition variation (TOAV) assays. 293T cells were incubated in the presence of compound 09167 at a final concentration of 1.0 or 0.25 μM at 37°C for up to 6 h preinfection, followed by infection with recMeV (MOI = 0.8 $TCID_{50}$/ml) in the presence of equal compound concentrations. Where indicated, the compound was added to infected cells at the specified time points postinfection. Cell-associated progeny particles were titrated at 24 hpi. Reference samples received volume equivalents of vehicle (DMSO) only.

Quantitation of cellular mRNA levels. 293T cells (9×10^5) were incubated in the presence of compound 09167 (final concentration, 1.0 μM) or the volume equivalent of vehicle (DMSO) for 20 h at 37°C, followed by preparation of total RNA by use of a QIAcube automated extractor (Qiagen) and an RNeasy minikit (Qiagen) as described above. Quantitative TaqMan reverse transcription-PCR (RT-PCR) was performed using TaqMan Fast master mix (Applied Biosystems) combined with proprietary primer and probe sets specifically detecting spliced mRNAs, but not genomic DNA, for IL28A, IFNB1, IL3RA, IRF3, IRGM, ISG15, MDA5, RIG-I, and IFIT1. To calculate $\Delta\Delta C_T$ values, threshold cycle (C_T) values obtained for each sample were standardized to expression levels of the 60S ribosomal protein L30 (RPL30) as a reference, and then ΔC_T values of compound 09167-treated samples were normalized to the vehicle controls. Final quantification was based on three independent experiments, each conducted in duplicate.

Immunoblotting. Cells (approximately 1×10^6 per treatment condition) were lysed in RIPA buffer (1% sodium deoxycholate, 1% NP-40, 150 mM NaCl, 50 mM Tris-Cl, pH 7.2, 10 mM EDTA, 50 mM NaF, 0.05% SDS, protease inhibitors [Roche], 1 mM phenylmethylsulfonyl fluoride). Cleared lysates (20,000 × *g*, 30 min, 4°C) were mixed with urea buffer (200 mM Tris, pH 6.8, 8 M urea, 5% SDS, 0.1 mM EDTA, 0.03% bromophenol blue, 1.5% dithiothreitol) for 30 min at 50°C, fractionated by SDS-PAGE, and blotted onto polyvinylidene difluoride (PVDF) membranes. Immunoblots were decorated with anti-RIG-I (Cell Signaling), anti-IFIT1 (Pierce), and anti-glyceraldehyde-3-phosphate dehydrogenase (anti-GAPDH) (Calbiochem) monoclonal antibodies and developed using a species-specific IgG light chain conjugate and a ChemiDoc XRS digital imaging system (Bio-Rad).

RESULTS

Productive coinfection of cells in a high-throughput drug screen mandates the following: (i) the replication profiles of the selected myxovirus representatives must be compatible with each other to allow synchronized infection and analysis, and (ii) infection and protein expression from either viral genome must be unaffected by the presence of the other virus in the same cell population. Members of both the orthomyxovirus (47) and paramyxovirus (48, 49) families employ different strategies to block the cellular antiviral response, including the suppression of host cell protein expression in infected cells (47, 50). However, neither myxovirus family induces rapid host cell lysis or apoptosis, and genome transcription and replication of the *Paramyxoviridae* occur in the cytosol, while the orthomyxoviruses adhere to nuclear transcription and replication of their genetic information. We therefore hypothesized that myxovirus family members may be suitable for productive coinfection of cells.

A myxovirus reporter pair with compatible expression profiles. In search of a clinically relevant myxovirus pair meeting the above requirements, we focused on RSV, MeV, and IAV, and we first generated reporter constructs that allowed independent quantification of para- and orthomyxovirus replication. In the case of RSV and MeV, recombinant reporter viruses were generated by inserting an additional transcription unit encoding *Renilla* luciferase in the primary position into cDNA copies of the viral genomes, followed by recovery of the corresponding viral recombinants, recRSV-ren (33) and recMeV-ren, respectively. For IAV, we generated a minigenome reporter plasmid on the basis of gene segment 5 (NP) through insertion of a firefly luciferase transcription unit. Expression of the resulting IAV-firefly luciferase replicon reporter is driven through superinfection of transfected cells with IAV, which provides the required viral NP and polymerase proteins.

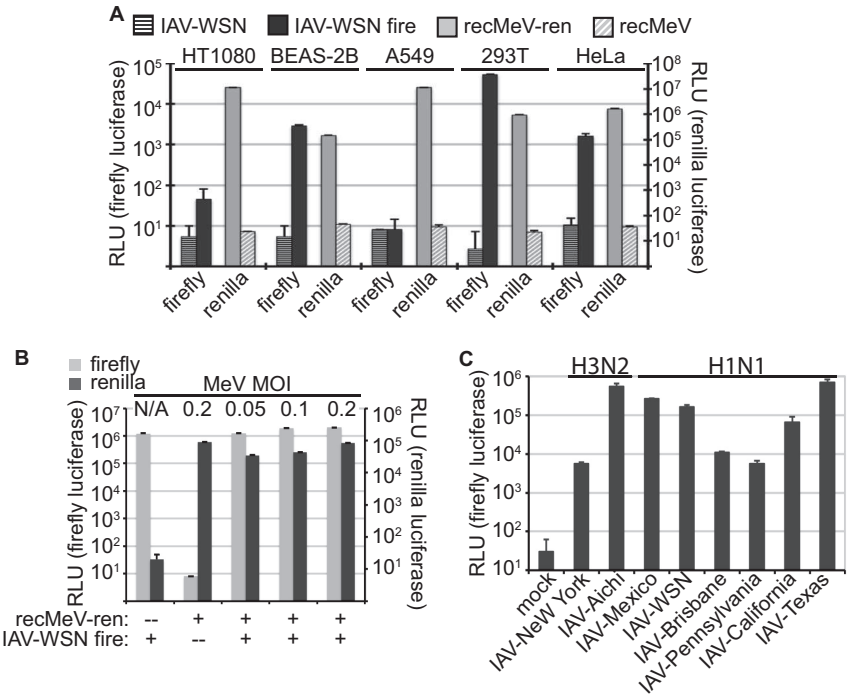

FIG 2 Assay optimization. (A) 293T cells returned the highest activity levels for both reporter constructs. Cells were infected individually with recMeV-ren or transfected with the IAV minigenome reporter and superinfected with IAV-WSN. RLU values represent means and SD for four experiments. (B) Efficient expression of both luciferase reporters in coinfected 293T cells. Cells transfected with the IAV-firefly luciferase plasmid were superinfected with IAV-WSN and increasing amounts of recMeV-ren, ranging from 0.05 to 0.2 infectious unit/cell. Relative activities of either reporter were determined at 30 hpi. Controls lacked either recMeV-ren or IAV-WSN. Values represent means and SD for three experiments. (C) The highest IAV-firefly luciferase reporter expression levels were achieved with swine-origin IAV-Texas. Cells transfected with IAV-firefly luciferase minigenome plasmid DNA were infected with different IAV strains at an MOI of 0.1 infectious unit/cell. Luciferase activities were determined at 30 hpi. Values represent means and SD for three experiments.

When we compared relative luciferase activity profiles after individual infections of cells with these reporter systems, we found a broad overlap of MeV- and IAV-driven reporter activity peaks at approximately 28 to 36 h postinfection. In contrast, substantial luciferase activity in cells infected with recRSV-ren emerged only after approximately 50 h postinfection (Fig. 1B). The highest paramyxovirus MOI assessed in this assay was 0.2 infectious unit/cell, since limited virus titers achievable in stock preparations restrict the maximal MOI that can be realized in 96- and 384-well plate formats. Based on these expression profiles, we selected recMeV-ren as the better-suited paramyxovirus representative for coinfection with IAV, and we chose a harvesting time of 28 to 32 hpi as the target window for subsequent experiments.

Myxovirus replication after coinfection. To assess the level of viral replication after coinfection, we infected cells with recMeV and IAV-WSN, either individually or in combination, and quantified yields of progeny virus. The resulting viral titers were essentially identical, regardless of whether they originated from individual or coinfections (Fig. 1C). Microscopic examination of cells infected with both viruses revealed a mixture of individually and doubly infected cells, provided that MeV glycoprotein-induced syncytium formation was chemically suppressed (Fig. 1D, top panels). Under standard conditions, however, the high cell-to-cell fusion activity of MeV resulted in the rapid formation of large, multinucleated syncytia harboring both viruses (Fig. 1D, bottom panels). Quantitative analysis of doubly infected cells by flow cytometry confirmed that the majority of cells expressing MeV proteins also stained positive for IAV-WSN antigen (Fig. 1E). Taken together, these findings indicate unrestricted coreplication of both IAV and MeV in a single-well setting.

Optimization of coinfection conditions for HTS. To prepare the single-well coinfection–luciferase reporter system for automated screening, we interrogated the assay in a 96-well plate format for host cell type, effect of MOI on reporter expression after coinfection, and IAV strain used. When a panel of human cell lines were infected individually with either virus, we found that all lines supported efficient recMeV-ren replication, returning high luciferase activity levels (Fig. 2A). However, IAV-driven IAV-firefly luciferase replicon expression was highest in 293T cells (Fig. 2A) and remained stable over a spectrum of 0.5 to 1.5 μg plasmid DNA/10^5 cells transfected. Using this robust 293T cell host system and 1.0 μg of replicon DNA/10^5 cells, we explored the effects of coinfection with increasing amounts of recMeV-ren particles on firefly and *Renilla* luciferase activities. Over a recMeV-ren MOI range of 0.05 to 0.2 infectious unit/cell, activity levels of both luciferases remained largely unchanged compared to those found in individually infected controls (Fig. 2B). Since slightly higher *Renilla* luciferase activity levels were observed after infection of cells with 0.2 infectious unit of recMeV-ren/cell, this MOI was chosen for all subsequent screens.

In search of the most competent driver of the IAV-firefly luciferase replicon, we scanned a panel of different IAV strains representing H1N1 and H3N2 genotypes. Under the experimental conditions established above, infection of minireplicon-transfected cells with swine-origin IFA/Texas/2009 (H1N1) (IAV-Texas) resulted in the highest luciferase activities overall, which were ap-

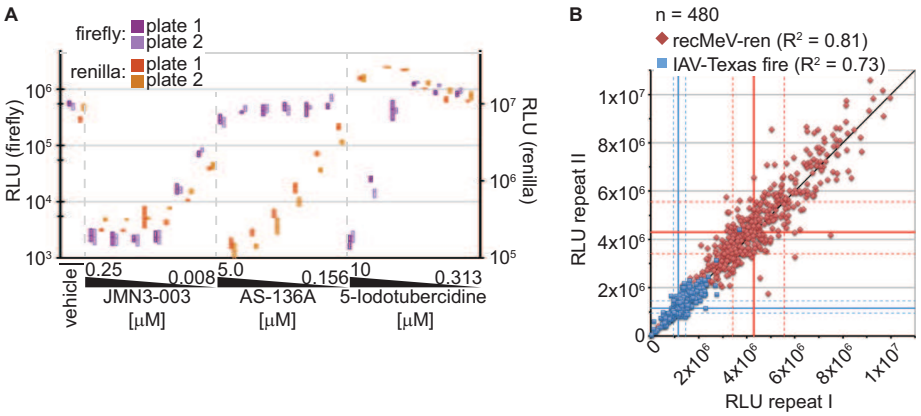

FIG 3 Assay validation for high-throughput inhibitor screening. (A) Control inhibitors with distinct antimyxovirus profiles were reproducibly identified in single-well coinfection assays. IAV-firefly luciferase-transfected cells were infected with IAV-Texas and recMeV-ren in the presence of JMN3-003 (pan-myxovirus inhibitor), AS-136A (MeV RdRp inhibitor), 5-iodotubercidin (IAV inhibitor), or vehicle control (DMSO). Relative luciferase activities in the wells were determined at 30 hpi. Each concentration was assessed in three replicates; two independent plates were prepared and analyzed. Symbols show means (lines) and minimum and maximum values (floating bars). (B) Plate-to-plate variation assessment using a random test set of 480 compounds. Cells were treated at a final concentration of 5 μM and then coinfected, and luciferase activities were determined at 30 hpi. Symbols represent values for each compound obtained from two independent replicate sets. A direct linear correlation (black line), median RLU values for each reporter data set (solid blue and red lines), and 25th and 75th percentiles (dashed blue and red lines) are shown.

proximately 4-fold higher than those observed for IAV-WSN (Fig. 2C). We therefore selected IAV-Texas as the orthomyxovirus representative of choice for subsequent validation and screening campaigns.

Assay validation and miniaturization. Having established the basic infection parameters, we first tested the robustness of the protocol in a 96-well plate format, and the assay was then miniaturized to a 384-well scale. For positive controls with distinct antiviral profiles, we chose the previously developed small-molecule compounds AS-136A, an MeV-specific RdRp inhibitor (34, 51); JMN3-003, a broadly acting pan-myxovirus inhibitor (4); and 5-iodotubercidin, a potent ERK2 inhibitor (40) that we found to block IAV, but not MeV, replication. Using the coinfection protocol, the effect of each of these control compounds was assessed in dose-response assays in independent replicate plates. This approach yielded dose-dependent paramyxovirus-specific, orthomyxovirus-specific, and pan-myxovirus antiviral profiles with little plate-to-plate variation (Fig. 3A), confirming the capacity of the assay to reliably detect representatives of each desired inhibitor class in a single screen.

Using a random test set of 480 small-molecule compounds (six plates) with unknown antiviral activity, we next quantified plate-to-plate variability for each reporter under screening conditions. Plotting of relative luciferase activities obtained for each compound in replicate experiments for both target viruses resulted in linear correlations with R^2 values of 0.73 and 0.81 (Fig. 3B). To quantitatively assess the suitability of the assay for automated screening, we selected the myxovirus inhibitor JMN3-003 as a pan-myxovirus positive control and calculated Z' values (43), signal-to-background ratios, and coefficients of variation for the 96-well and, after miniaturization, 384-well plate sizes (Table 1). For both formats, the values were within the acceptable range for automated screening (43, 52).

HTS of a 10,000-entry diversity set. To conceptually test the assay in HTS mode, we screened a 10,000-entry diversity set of drug-like small molecules following the filter strategy depicted in Fig. 4A. All compounds were tested at a concentration of 5 μM, and each plate contained vehicle controls and the pan-myxovirus reference inhibitor JMN3-003 in quadruplicate. Primary HTS data were normalized by plate to the control inhibitor, Z score scaled, and organized by increasing score values (Fig. 4B). The top-scoring candidates, with Z scores of ≥2 standard deviations above the mean for IAV-Texas (238 entries) or ≥2.5 standard deviations above the mean for MeV (246 entries), were cherry picked for further analysis. Of these, 124 showed broad antiviral activity against both myxovirus targets in the primary screen (Fig. 4C) and were thus considered pan-myxovirus inhibitor candidates.

For second-tier hit filtration, we tested the primary candidates individually against recRSV-ren, which served as an independent confirmatory paramyxovirus target. Of 360 distinct compounds examined in this assay, 13 candidates exclusively blocked IAV-Texas and RSV, a 3-fold larger contingent (39 entries) inhibited MeV and RSV—and were thus considered pan-paramyxovirus inhibitor candidates—and 51 suppressed reporter expression by all three viral targets (Fig. 4D). Since the library was not pretested

TABLE 1 Comparison of assay formats used in this study

Plate format	Target virus[a]	Z' value[b]	S/B ratio[c]	% CV
96 wells	recMeV-ren	0.74	31	8.0
	IAV-firefly luciferase IAV-Texas	0.79	109	6.7
384 wells	recMeV-ren	0.74	41	8.2
	IAV-firefly luciferase IAV-Texas	0.67	89	10.9

[a] Cryopreserved 293T cells transfected with IAV-firefly luciferase were plated and coinfected with recMeV-ren and IAV-Texas in the presence of the pan-myxovirus inhibitor JMN3-003 (final concentration, 1 μM) or an equivalent amount of vehicle (DMSO). Relative luciferase unit values were determined at 30 hpi.
[b] Z factor (43). Statistical analyses are based on means for four independent experiments.
[c] Ratio of signal to background.

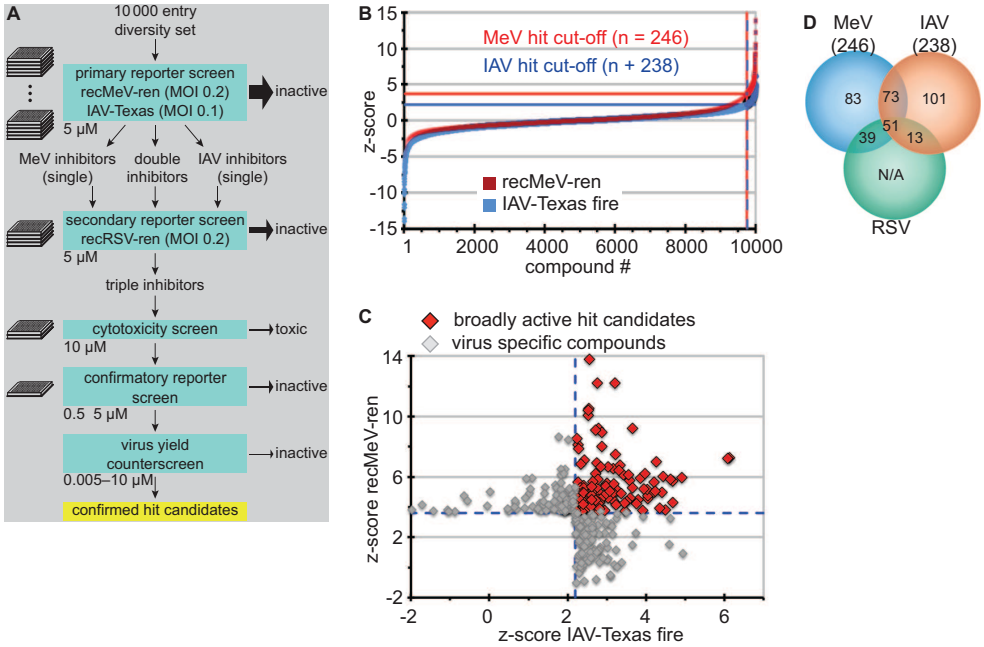

FIG 4 Dual myxovirus screen of a 10,000-entry diversity set. (A) Schematic of primary, confirmatory, and counterscreens for hit identification. (B) Normalized, scaled, and ordered screening scores (*Z* scores) obtained for each target virus. Lines mark hit selection cutoffs; selected hit candidates are shown to the right of the dashed lines. (C) Selected hit candidates plotted by the *Z* score obtained for each target virus. Dashed blue lines mark the cutoffs for MeV (approximately 2.5 SD above the mean) and IAV-Texas (approximately 2 SD above the mean). Red symbols mark compounds with activity against both myxovirus targets. (D) Venn diagram summarizing the second-tier confirmatory screen of all 360 primary hit candidates shown in panel C against recRSV-ren (hit cutoff, 2 SD above the mean).

for cytotoxic compounds, the last group was anticipated to comprise cytotoxic compounds, promiscuous hits (53, 54), and pan-myxovirus inhibitor candidates.

Hit confirmation and counterscreening. To distinguish between these alternatives and provide further insight into the inhibitory potential of individual hits, all 51 candidates that suppressed MeV, RSV, and IAV were subjected to quantitative cytotoxicity assessment at twice the screening concentration (final concentration, 10 μM) and to an independent, two-concentration (5 and 0.5 μM) third-tier confirmatory screen against MeV and IAV-Texas. For quantitative comparisons after cherry picking, we calculated toxicity and virus inhibition relative to those of vehicle-treated controls. Antiviral effects of the hit candidates with the highest *Z* scores against all targets were due to strong toxicity, defined as <75% of cellular metabolic activity remaining after 28 h of exposure (Fig. 5A). However, 15 candidates returned >85% inhibition against both MeV and IAV-Texas at 5 μM, and in the case of 4 candidates, this also extended to ≥50% inhibition of viral titers at 0.5 μM (Fig. 5A).

Visual inspection of the chemical scaffolds of all 15 candidates with confirmed bioactivity identified three compounds with undesirable properties, such as highly reactive substructures or other common features of promiscuous small-molecule screening hits (53, 54), and another five compounds represented analogs of only two distinct chemical scaffolds. Excluding these readily undesirable and structurally redundant candidates, we subjected the remaining nine compounds to counterscreening, assessing their ability to reduce yields of progeny recMeV and IAV-WSN viral particles at concentrations of 2.5 and 0.5 μM, respectively (Fig. 5B). Three candidates reduced titers of both target viruses by >90% at 2.5 μM, and one compound (09167) induced >99% inhibition at submicromolar concentrations.

The lead candidate, compound 09167 (Fig. 5C), was sourced for further characterization. Database queries with the chemical scaffold did not return close (≥90% similarity) chemical analogs with defined bioactivity, arguing against multitarget promiscuity. Virus yield-based dose-response curves furthermore confirmed nanomolar EC_{50}s of the compound against a set of three different IAV strains (Fig. 5D). Potent antiviral activity was not restricted to orthomyxovirus family members but extended equally to a group of clinically relevant paramyxoviruses, including MeV, MuV, and RSV. Based on these results, we selected the 09167 hit for initial characterization of the mechanism of action (MOA).

MOA of first-generation lead 09167. A host-directed antiviral mechanism frequently coincides with host cell species dependence of the inhibitory activity (4). When we examined the bioactivity of 09167 in a variety of cell lines of different species origins, we observed the most potent inhibition in human and canine cell lines and primary human PBMCs (Fig. 6A). IAV-WSN was more sensitive to inhibition than recMeV-Edm in both 293T and Vero cell lines in this assay. In contrast, antiviral activity was minimal or absent in cell lines of nonhuman primate and avian origins. These data exclude a direct virucidal effect of the compound and confirm a host-directed mechanism of action.

To narrow the range of possible host-pathogen interactome targets of compound 09167, we examined the effect of time-of-addition variation (TOAV) on antiviral potency. MeV served as the viral reporter in these experiments, and the compound was administered at concentrations equivalent to 1.25- and 5-fold higher than the EC_{50} at distinct time points pre- or postinfection.

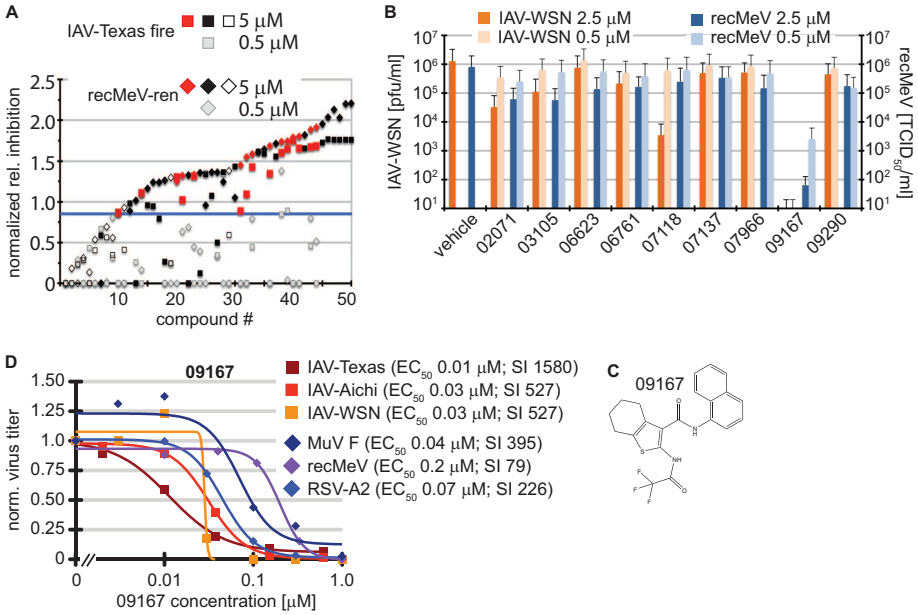

FIG 5 Identification of a nanomolar pan-myxovirus inhibitor class. (A) Two-concentration confirmatory screen of the selected 51 hit candidates. Values were normalized to those for plate controls and represent inhibition relative to that of JMN3-003. Compounds are ordered by increasing relative inhibition values. Black filled symbols mark cytotoxic compounds (reducing cell metabolic activity by >25%), open symbols represent compounds that were inactive against at least one of the target viruses at 5 μM, and red symbols highlight the remaining hit candidates. Gray symbols show the corresponding normalized scores obtained for each entry at 0.5 μM. The blue line marks the hit cutoff (0.85) relative to JMN3-003 for all candidates at 5.0 μM. (B) Virus yield-based counterscreen of nine candidates at 2.5 and 0.5 μM against IAV-WSN and recMeV. Values represent averages for two independent experiments, and error bars show data ranges. (C) Chemical scaffold of lead candidate 09167 {2,2,2-trifluoro-*N*-[3-(*N*-naphthylcarbamoyl)(4,5,6,7-tetrahydrobenzo [β]thiophen-2-yl)]acetamide}. (D) Virus yield-based dose-response assays. Virus titers were determined through plaque assay (IAV-WSN, MuV F, and RSV-A2), TaqMan genome copy number quantification (IAV-Texas and IAV-Aichi), or $TCID_{50}$ titration (recMeV) and then normalized to vehicle (DMSO) controls. Data points represent means for three experiments. EC_{50}s were calculated based on four-parameter variable-slope nonlinear regression models. Specificity indices (SI) represent CC_{50}/EC_{50}.

Virus replication was completely suppressed over a wide addition time frame at the higher concentration, indicating a fast-acting host effect of the compound. Importantly, dosing at lower levels revealed significantly increased antiviral potency when cells were pretreated with the compound prior to infection (Fig. 6B), suggesting priming of a host cell antiviral stage. Supporting the TOAV profile, we found the kinetics of virus-to-cell fusion to be unimpaired by 09167 (Fig. 6C), but we observed a dose-dependent inhibition of the viral RNA-dependent RNA polymerase activity (Fig. 6D), which would be expected if the compound stimulates cellular antiviral defense pathways (55, 56).

To test this hypothesis, we determined whether 09167 triggers traditional RNA virus pattern recognition receptor (PRR) signaling pathways, such as RIG-I/MDA5 and Toll-like receptor 3 (TLR3), resulting in activation of the type I interferon (IFN) response and IFN-β secretion. TaqMan RT-PCR revealed that IFNB1 and IRF3 mRNA levels were unaffected by the compound (Fig. 6E), and enzyme-linked immunosorbent assay (ELISA)-based quantification of IFN-β in culture supernatants showed no compound 09167-induced increase in interferon release. In contrast, expression of several IFN-stimulated downstream effector genes (ISGs), including the ISG15, RIG-I, and IFIT1 genes, was significantly increased after treatment of cells with 09167 (Fig. 6E). Immunodetection of RIG-I and IFIT1 after exposure of cells to 09167 confirmed that changes in relative mRNA contents translate into increased effector protein steady-state levels. Taken together, these results advocate that screening lead 09167 represents a novel small-molecule activator of the host cell antiviral ISG system.

DISCUSSION

Emerging and reemerging viral pathogens mandate the development of novel therapeutic strategies. Broad-spectrum antivirals have become a major goal of drug discovery campaigns, but selecting druggable host targets and identifying viable leads remain challenging.

Recent genomewide RNA interference screens have expanded our insight into the host-pathogen interactome for several viruses, including influenza virus (24–26). Genetically identified host target candidates could be pursued through repurposing known drugs or can become the objective of target-based HTS activities. However, large-scale implementation of such a strategy with an antibacterial endpoint has yielded sobering results (29), demonstrating that the genomics-based deliberate selection of fruitful drug targets remains challenging. These experiences have resulted in the realization that "following the compound" rather than the target may in fact be the more rewarding path toward drug discovery (57).

Guided by these considerations, we describe an HTS protocol that supports identification of pathogen-specific and broad-spectrum myxovirus hit candidates through parallel interrogation of possible pathogen targets and the host-pathogen interactome. Based on the approximately 30-hour (to harvest) timeline of the protocol and the nature of the readout, we anticipate such screens to reveal predominantly inhibitors of virus attachment, entry, and/or polymerase activity, while late-stage blockers of particle assembly and egress are less likely to be discovered. Simultaneous screening against two viral targets representing related but distinct

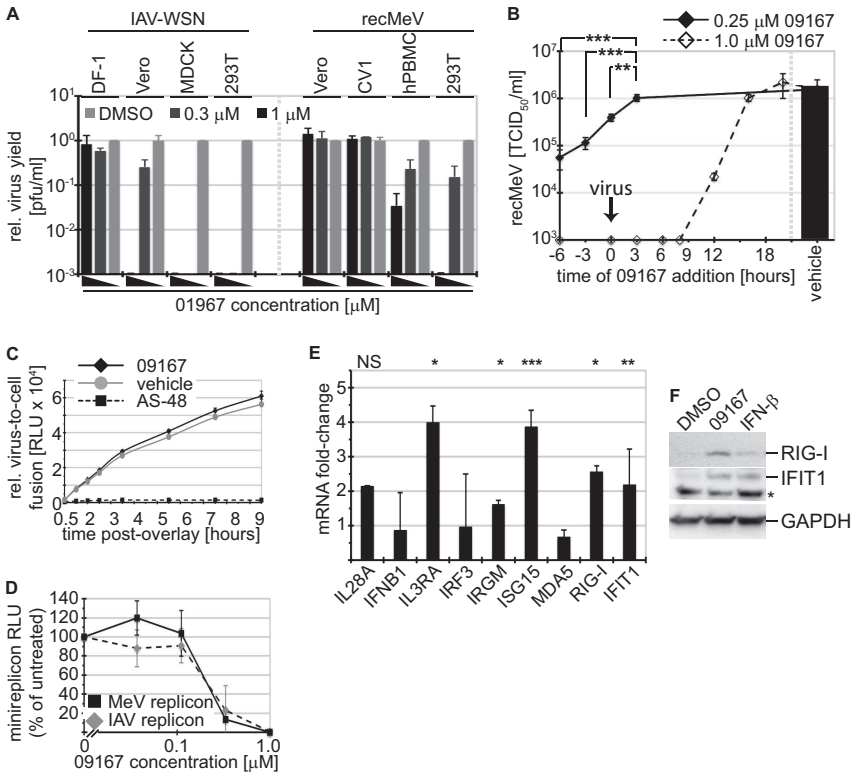

FIG 6 Lead candidate 09167 primes the host antiviral response. (A) Host cell species dependence of 09167 antiviral activity. Avian DF-1, canine MDCK, primate Vero and CV1, and human 293T cells were infected with IAV-WSN or MeV in the presence of 1.0 and 0.33 μM 09167 or vehicle control. Progeny virus yields were normalized to titers in vehicle controls. (B) Priming of target cells with 09167 enhances antiviral activity. The compound was added to cells at 0.25 and 1.0 μM at the specified time points before or after infection with MeV, and progeny virus titers were determined at 24 hpi. Values represent means ± SD for three experiments (**, $P < 0.01$; ***, $P < 0.001$). (C) Quantitative cell content mixing assay assessing MeV glycoprotein-induced virus-to-cell fusion kinetics, carried out in the presence of 1 μM 09167, vehicle (DMSO), or 75 μM fusion inhibitor AS-48 (control). At the indicated time points, reconstitution of double GFP-*Renilla* split-luciferase proteins, indicating cell content mixing, was determined. Values represent averages ± SD for five replicates/time point. (D) Plasmid-based IAV and MeV minigenome reporter assays to determine viral RdRp activity in the presence of increasing 09167 concentrations. Relative luciferase reporter activities were determined after 24 hours of exposure. Values represent means ± SD for at least three experiments. (E) Treatment of 293T cells with 09167 stimulates expression of several ISGs. Cells were exposed to 1.0 μM 09167 or vehicle (DMSO) for 20 h, followed by TaqMan RT-PCR quantitation of relative expression levels of a panel of genes associated with the host innate immune system. IL28A, interleukin-28; IFNB1, IFN-β; IL3RA, interleukin-3 receptor α; IRF3, interferon regulatory factor 3; IRGM, interferon-inducible protein 1; ISG15, interferon-induced 17-kDa protein; MDA5, melanoma differentiation-associated protein 5; RIG-I, retinoic acid-inducible gene 1; IFIT1, interferon-induced protein with tetratricopeptide repeats 1. Values represent averages and SD for three independent experiments; each sample was analyzed in duplicate. Symbols: *, $P < 0.05$; **, $P < 0.01$; ***, $P < 0.001$; NS, not significant. (F) Total lysates of cells treated as described for panel E or exposed to 50 U IFN-β were subjected to gel fractionation and immunoblotting using specific antibodies directed against RIG-I and IFIT1. As a control, blots were decorated with anti-GAPDH antibodies. *, nonspecific crossreaction.

viral families does not guarantee *per se* that broad-spectrum hits will follow a host-directed activity profile. Broadened activity could, alternatively, ensue from interference with conserved pathogen structures; for instance, inhibition of viral glycoprotein-mediated virus entry through lectins (58) in a topical application or the use of lipid-active compounds suggested to interfere with membrane function of enveloped viruses (59) serve as cases in point. A mechanistic analysis of successful small-molecule antivirals (60) reveals, however, that the majority of pathogen-targeting compounds are highly virus specific, whereas broad-spectrum hits engage predominantly host factors required for virus replication or host pathogen control.

In primary HTS assays, broad-spectrum and pathogen-specific antiviral activities can be assessed *in silico* after distinct serial screens of a single library against individual viral targets or by simultaneous probing against both viruses in a single-well format. Provided that replication of either target virus is not affected by the presence of the other, a parallel screening campaign is substantially more effective in regard to equipment, reagents and supplies, and time, resulting in significant resource advantages when larger diversity sets are assessed. In addition, this approach adds confidence to the identification of pathogen-specific inhibitor candidates, since highly divergent screening scores of a candidate compound for either viral target will argue against common cell-based HTS liabilities such as general cytotoxicity, compound promiscuity, or technical issues. Independent of serial or parallel screening strategies, however, broad-spectrum hit candidates must be considered at risk of being enriched for undesirable compounds (61).

Although coinfection with ortho- and paramyxoviruses has been observed clinically (62), downregulation of host protein expression by pathogens of either family could prevent successful coreplication in a single-well format. For instance, the influenza virus NS1 protein has been demonstrated to block correct processing of cellular mRNAs (47), while the MeV N protein has been implicated in interference with host mRNA translation through interaction with the translation initiation factor eIF3-p40 (63).

Moreover, the high cell-to-cell fusion activity associated with MeV infection (64) results in the rapid formation of very large syncytia that can comprise entire cell monolayers. One can therefore assume that both pathogens will rapidly be located in the same cellular environment after coinfection, even when originally added at lower multiplicities of infection. However, protein expression shutoff by MeV is inefficient (65), and cytosolic transcription and replication may shield paramyxovirus genomes from the nuclear functions of NS1. Our results demonstrating efficient IAV and MeV coreplication and protein expression are consistent with this view, and they identify ortho- and paramyxovirus family members as suitable target pairs for parallel drug screens.

Quantitative validation of the firefly and *Renilla* luciferase reporter-based screen returned the anticipated distinct hit profiles for positive-control compounds with defined pathogen-specific or broad antimyxovirus patterns with a high reproducibility. Application to a 10,000-entry test set demonstrated the general feasibility of the strategy for simultaneous identification of pathogen-specific and broad-spectrum hit candidates. We noted some bias toward doubly false-positive results after coinfection, but we found a nearly 2-fold higher count of MeV-IAV double inhibitor candidates than, for instance, MeV-RSV blockers after primary and confirmatory screening. The screen also confirmed that the pool of primary broad-spectrum candidates was enriched for cytotoxic, promiscuous, and/or assay-interfering compounds.

Triangular confirmatory screening of all MeV and IAV hit candidates against RSV provided an attractive avenue toward reducing the rate of assay false-positive results and potentially identifying pan-paramyxovirus blockers. Although they represent distinct paramyxovirus subfamilies, the phylogenetic proximity of RSV and MeV to each other is substantially closer than that of either to IAV. Indeed, our assay returned a 3-fold higher hit rate for MeV-RSV than IAV-RSV inhibitor candidates. While the molecular characterization of these compounds is pending, we consider it unlikely that this pattern reflects pathogen-directed inhibition of conserved paramyxovirus targets. Rather, we would expect members of different paramyxovirus subfamilies to rely on a more homogenous host factor pool than those for ortho- and paramyxovirus representatives. Follow-up testing in search of candidates with an antiparamyxovirus as opposed to pan-myxovirus profile will center on those compounds that combine the highest *Z* values against both MeV and RSV with the lowest scores against IAV as the point of entry.

Our test screen combined with virus titer-based counterscreens yielded a single pan-myxovirus inhibitor with nanomolar potency. This small hit number may well reflect the challenge of broad-spectrum inhibition and may be accentuated further by the stringent screening criteria applied. While a more relaxed screen may identify additional viable scaffolds, this potential gain must be offset against the likely discovery of undesirable promiscuous hits with essentially flat structure-activity relationships (SARs). Three lines of evidence support the hypothesis that the confirmed hit compound represents a novel class of agonists of the host innate immune response. First, compound 09167 shows host cell species dependence of the antiviral effect, supporting a host-directed mechanism of activity. Second, host cell preexposure substantially enhances the antiviral potency of the compound. This TOAV profile suggests priming of a host antiviral state as the basis for inhibitory activity. Lastly, quantitative analysis of ISG mRNA and protein levels demonstrated that the compound upregulates the expression of a subset of antiviral effector genes, including those for ISG15 and IFIT1, which recognize viral genomic and antigenomic RNAs bearing 5′-triphosphate groups (66, 67). Expression of multiple ISG products may be synergistically responsible for the potent overall antiviral effect of the compound. Current work is directed at the systematic characterization of the specific pathways triggered and the positive identification of the molecular target.

Despite the effective and well-documented stimulation of a broad antiviral state by type I IFN, small-molecule agonists of the innate immune system have not yet been exploited clinically for antiviral therapies. However, specific activation of innate immune signaling pathways for an antiviral endpoint has experienced a renaissance in recent drug screening campaigns (68–70). Several of these activities have identified fused heterocyclic compounds with DNA-binding (68) and/or DNA-intercalation activity (70, 71), which is inherently associated with high mutagenic potential (72), creating a developmental liability. Compound 09167 is structurally distinct from this set of DNA-active small molecules, but it features a thiophene substructure which is potentially reactive (61) and has appeared in low-potency hits (i.e., hits with EC_{50}s of 13 to 300 μM) in previous screening campaigns (73, 74). This chemical scaffold therefore mandates careful examination. Based on consistent activity in our orthogonal counterscreening assays and the nanomolar, approximately 1,000-fold higher potency than that found for promiscuous thiophenes, 09167 shows all the features of a viable lead suitable for advanced synthetic hit-to-lead optimization.

In toto, we have demonstrated unrestricted coreplication of ortho- and paramyxovirus representatives after coinfection, which set the stage for a novel time- and resource-efficient HTS protocol that affords the identification of broad-spectrum myxovirus inhibitors in parallel to the discovery of conventional, pathogen-specific antivirals. This approach is readily transferable to nonmyxovirus pathogen-target pairs, provided that they share comparable replication kinetics capable of unimpaired coreplication. Application to a small-molecule test set emphasized the necessity for orthogonal counterscreening, in particular for the pursuit of broad-spectrum candidates, and identified a promising novel small-molecule inhibitor with nanomolar antimyxovirus activity.

ACKNOWLEDGMENTS

We thank M. Currier for software development, N. Kondo and Z. Matsuda for split-luciferase reporter plasmids, M. A. Brindley and R. Suter for help with computer graphics, and T. W. Moore, M. A. Brindley, and A. L. Hammond for discussions and comments on the manuscript.

This work was supported in part by Public Health Service grants AI087798 and AI095227 (to M.L.M.) and by grants AI071002, AI057157, and AI085328 from the NIH/NIAID (to R.K.P.).

REFERENCES

1. **Schwegmann A, Brombacher F.** 2008. Host-directed drug targeting of factors hijacked by pathogens. Sci. Signal. **1:**re8.
2. **Tan SL, Ganji G, Paeper B, Proll S, Katze MG.** 2007. Systems biology and the host response to viral infection. Nat. Biotechnol. **25:**1383–1389.
3. **Muller B, Krausslich HG.** 2009. Antiviral strategies. Handb. Exp. Pharmacol. **2009:**1–24.
4. **Krumm SA, Ndungu JM, Yoon JJ, Dochow M, Sun A, Natchus M, Snyder JP, Plemper RK.** 2011. Potent host-directed small-molecule in-

hibitors of myxovirus RNA-dependent RNA-polymerases. PLoS One **6:**e20069. doi:10.1371/journal.pone.0020069.
5. **Hoffmann HH, Kunz A, Simon VA, Palese P, Shaw ML.** 2011. Broad-spectrum antiviral that interferes with de novo pyrimidine biosynthesis. Proc. Natl. Acad. Sci. U. S. A. **108:**5777–5782.
6. **Salerno D, Hasham MG, Marshall R, Garriga J, Tsygankov AY, Grana X.** 2007. Direct inhibition of CDK9 blocks HIV-1 replication without preventing T-cell activation in primary human peripheral blood lymphocytes. Gene **405:**65–78.
7. **Schang LM.** 2006. First demonstration of the effectiveness of inhibitors of cellular protein kinases in antiviral therapy. Expert Rev. Anti Infect. Ther. **4:**953–956.
8. **Prussia A, Thepchatri P, Snyder JP, Plemper RK.** 2011. Systematic approaches towards the development of host-directed antiviral therapeutics. Int. J. Mol. Sci. **12:**4027–4052.
9. **Thompson WW, Comanor L, Shay DK.** 2006. Epidemiology of seasonal influenza: use of surveillance data and statistical models to estimate the burden of disease. J. Infect. Dis. **194**(Suppl 2)**:**S82–S91.
10. **Thompson WW, Shay DK, Weintraub E, Brammer L, Bridges CB, Cox NJ, Fukuda K.** 2004. Influenza-associated hospitalizations in the United States. JAMA **292:**1333–1340.
11. **Johnson D.** 2009. Croup. Clin. Evid. (Online) **2009:**0321. http://www.ncbi.nlm.nih.gov/pmc/articles/PMC2907784/.
12. **Bjornson CL, Johnson DW.** 2008. Croup. Lancet **371:**329–339.
13. **World Health Organization.** 2012. World Health Statistics 2012. WHO, Geneva, Switzerland. http://www.who.int/gho/publications/world_health_statistics/en/index.html.
14. **MacDonald N, Hatchette T, Elkout L, Sarwal S.** 2011. Mumps is back: why is mumps eradication not working? Adv. Exp. Med. Biol. **697:**197–220.
15. **De Clercq E.** 2006. Antiviral agents active against influenza A viruses. Nat. Rev. **5:**1015–1025.
16. **Kiso M, Mitamura K, Sakai-Tagawa Y, Shiraishi K, Kawakami C, Kimura K, Hayden FG, Sugaya N, Kawaoka Y.** 2004. Resistant influenza A viruses in children treated with oseltamivir: descriptive study. Lancet **364:**759–765.
17. **Sugaya N, Mitamura K, Yamazaki M, Tamura D, Ichikawa M, Kimura K, Kawakami C, Kiso M, Ito M, Hatakeyama S, Kawaoka Y.** 2007. Lower clinical effectiveness of oseltamivir against influenza B contrasted with influenza A infection in children. Clin. Infect. Dis. **44:**197–202.
18. **Anderson LJ, Parker RA, Strikas RL.** 1990. Association between respiratory syncytial virus outbreaks and lower respiratory tract deaths of infants and young children. J. Infect. Dis. **161:**640–646.
19. **Groothuis JR, Simoes EA, Levin MJ, Hall CB, Long CE, Rodriguez WJ, Arrobio J, Meissner HC, Fulton DR, Welliver RC, Tristram DA, Siber GR, Prince GA, Van Raden M, Hemming VG, Respiratory Syncytial Virus Immune Globulin Study Group.** 1993. Prophylactic administration of respiratory syncytial virus immune globulin to high-risk infants and young children. N. Engl. J. Med. **329:**1524–1530.
20. **Johnson S, Oliver C, Prince GA, Hemming VG, Pfarr DS, Wang SC, Dormitzer M, O'Grady J, Koenig S, Tamura JK, Woods R, Bansal G, Couchenour D, Tsao E, Hall WC, Young JF.** 1997. Development of a humanized monoclonal antibody (MEDI-493) with potent in vitro and in vivo activity against respiratory syncytial virus. J. Infect. Dis. **176:**1215–1224.
21. **Pleschka S, Wolff T, Ehrhardt C, Hobom G, Planz O, Rapp UR, Ludwig S.** 2001. Influenza virus propagation is impaired by inhibition of the Raf/MEK/ERK signalling cascade. Nat. Cell Biol. **3:**301–305.
22. **Kujime K, Hashimoto S, Gon Y, Shimizu K, Horie T.** 2000. p38 mitogen-activated protein kinase and c-jun-NH_2-terminal kinase regulate RANTES production by influenza virus-infected human bronchial epithelial cells. J. Immunol. **164:**3222–3228.
23. **Moss RB, Hansen C, Sanders RL, Hawley S, Li T, Steigbigel RT.** 2012. A phase II study of DAS181, a novel host directed antiviral for the treatment of influenza infection. J. Infect. Dis. **206:**1844–1851.
24. **Karlas A, Machuy N, Shin Y, Pleissner KP, Artarini A, Heuer D, Becker D, Khalil H, Ogilvie LA, Hess S, Maurer AP, Muller E, Wolff T, Rudel T, Meyer TF.** 2010. Genome-wide RNAi screen identifies human host factors crucial for influenza virus replication. Nature **463:**818–822.
25. **Konig R, Stertz S, Zhou Y, Inoue A, Hoffmann HH, Bhattacharyya S, Alamares JG, Tscherne DM, Ortigoza MB, Liang Y, Gao Q, Andrews SE, Bandyopadhyay S, De Jesus P, Tu BP, Pache L, Shih C, Orth A, Bonamy G, Miraglia L, Ideker T, Garcia-Sastre A, Young JA, Palese P, Shaw ML, Chanda SK.** 2010. Human host factors required for influenza virus replication. Nature **463:**813–817.
26. **Shapira SD, Gat-Viks I, Shum BO, Dricot A, de Grace MM, Wu L, Gupta PB, Hao T, Silver SJ, Root DE, Hill DE, Regev A, Hacohen N.** 2009. A physical and regulatory map of host-influenza interactions reveals pathways in H1N1 infection. Cell **139:**1255–1267.
27. **Ludwig S.** 2009. Targeting cell signalling pathways to fight the flu: towards a paradigm change in anti-influenza therapy. J. Antimicrob. Chemother. **64:**1–4.
28. **Barrows NJ, Le Sommer C, Garcia-Blanco MA, Pearson JL.** 2010. Factors affecting reproducibility between genome-scale siRNA-based screens. J. Biomol. Screen. **15:**735–747.
29. **Payne DJ, Gwynn MN, Holmes DJ, Pompliano DL.** 2007. Drugs for bad bugs: confronting the challenges of antibacterial discovery. Nat. Rev. **6:**29–40.
30. **Ono N, Tatsuo H, Hidaka Y, Aoki T, Minagawa H, Yanagi Y.** 2001. Measles viruses on throat swabs from measles patients use signaling lymphocytic activation molecule (CDw150) but not CD46 as a cellular receptor. J. Virol. **75:**4399–4401.
31. **Buchholz UJ, Finke S, Conzelmann KK.** 1999. Generation of bovine respiratory syncytial virus (BRSV) from cDNA: BRSV NS2 is not essential for virus replication in tissue culture, and the human RSV leader region acts as a functional BRSV genome promoter. J. Virol. **73:**251–259.
32. **Radecke F, Spielhofer P, Schneider H, Kaelin K, Huber M, Dotsch C, Christiansen G, Billeter MA.** 1995. Rescue of measles viruses from cloned DNA. EMBO J. **14:**5773–5784.
33. **Hotard AL, Shaikh FY, Lee S, Yan D, Teng MN, Plemper RK, Crowe JE, Jr, Moore ML.** 2012. A stabilized respiratory syncytial virus reverse genetics system amenable to recombination-mediated mutagenesis. Virology **434:**129–136.
34. **Yoon JJ, Krumm SA, Ndungu JM, Hoffman V, Bankamp B, Rota PA, Sun A, Snyder JP, Plemper RK.** 2009. Target analysis of the experimental measles therapeutic AS-136A. Antimicrob. Agents Chemother. **53:**3860–3870.
35. **Plemper RK, Erlandson KJ, Lakdawala AS, Sun A, Prussia A, Boonsombat J, Aki-Sener E, Yalcin I, Yildiz I, Temiz-Arpaci O, Tekiner B, Liotta DC, Snyder JP, Compans RW.** 2004. A target site for template-based design of measles virus entry inhibitors. Proc. Natl. Acad. Sci. U. S. A. **101:**5628–5633.
36. **Lipinski CA, Lombardo F, Dominy BW, Feeney PJ.** 2001. Experimental and computational approaches to estimate solubility and permeability in drug discovery and development settings. Adv. Drug Deliv. Rev. **46:**3–26.
37. **Ehrengruber MU, Hennou S, Bueler H, Naim HY, Deglon N, Lundstrom K.** 2001. Gene transfer into neurons from hippocampal slices: comparison of recombinant Semliki Forest virus, adenovirus, adeno-associated virus, lentivirus, and measles virus. Mol. Cell. Neurosci. **17:**855–871.
38. **Paal T, Brindley MA, St Clair C, Prussia A, Gaus D, Krumm SA, Snyder JP, Plemper RK.** 2009. Probing the spatial organization of measles virus fusion complexes. J. Virol. **83:**10480–10493.
39. **Neumann G, Watanabe T, Kawaoka Y.** 2000. Plasmid-driven formation of influenza virus-like particles. J. Virol. **74:**547–551.
40. **Fox T, Coll JT, Xie X, Ford PJ, Germann UA, Porter MD, Pazhanisamy S, Fleming MA, Galullo V, Su MS, Wilson KP.** 1998. A single amino acid substitution makes ERK2 susceptible to pyridinyl imidazole inhibitors of p38 MAP kinase. Protein Sci. **7:**2249–2255.
41. **Boutros M, Bras LP, Huber W.** 2006. Analysis of cell-based RNAi screens. Genome Biol. **7:**R66.
42. **Pelz O, Gilsdorf M, Boutros M.** 2010. web cellHTS2: a web-application for the analysis of high-throughput screening data. BMC Bioinformatics **11:**185. doi:10.1186/1471-2105-11-185.
43. **Zhang JH, Chung TDY, Oldenburg KR.** 1999. A simple statistical parameter for use in evaluation and validation of high throughput screening assays. J. Biomol. Screen. **4:**67–73.
44. **Dochow M, Krumm SA, Crowe JE, Jr, Moore ML, Plemper RK.** 2012. Independent structural domains in paramyxovirus polymerase protein. J. Biol. Chem. **287:**6878–6891.
45. **Sutter G, Ohlmann M, Erfle V.** 1995. Non-replicating vaccinia vector efficiently expresses bacteriophage T7 RNA polymerase. FEBS Lett. **371:**9–12.
46. **Kondo N, Miyauchi K, Matsuda Z.** 2011. Monitoring viral-mediated membrane fusion using fluorescent reporter methods. Curr. Protoc. Cell Biol. Chapter 26:Unit 26.9. doi:10.1002/0471143030.cb2609s50.

47. **Garcia-Sastre A.** 2011. Induction and evasion of type I interferon responses by influenza viruses. Virus Res. **162:**12–18.
48. **Goodbourn S, Randall RE.** 2009. The regulation of type I interferon production by paramyxoviruses. J. Interferon Cytokine Res. **29:**539–547.
49. **Ramachandran A, Horvath CM.** 2009. Paramyxovirus disruption of interferon signal transduction: STATus report. J. Interferon Cytokine Res. **29:**531–537.
50. **Vreede FT, Chan AY, Sharps J, Fodor E.** 2010. Mechanisms and functional implications of the degradation of host RNA polymerase II in influenza virus infected cells. Virology **396:**125–134.
51. **White LK, Yoon JJ, Lee JK, Sun A, Du Y, Fu H, Snyder JP, Plemper RK.** 2007. Nonnucleoside inhibitor of measles virus RNA-dependent RNA polymerase complex activity. Antimicrob. Agents Chemother. **51:**2293–2303.
52. **Iversen PW, Beck B, Chen YF, Dere W, Devanarayan V, Eastwood BJ, Farmen MW, Iturria SJ, Montrose C, Moore RA, Weidner JR, Sittampalam GS.** 2004. HTS assay validation, p 1–31. *In* Sittampalam GS, Gal-Edd N, Arkin M, Auld D, Austin C, Bejcek B, Glicksman M, Inglese J, Lemmon V, Li Z, McGee J, McManus O, Minor L, Napper A, Riss T, Trask OJ, Weidner J. (ed), Assay guidance manual. Eli Lilly & Company and the National Center for Advancing Translational Sciences, Bethesda, MD.
53. **McGovern SL, Caselli E, Grigorieff N, Shoichet BK.** 2002. A common mechanism underlying promiscuous inhibitors from virtual and high-throughput screening. J. Med. Chem. **45:**1712–1722.
54. **Coan KE, Maltby DA, Burlingame AL, Shoichet BK.** 2009. Promiscuous aggregate-based inhibitors promote enzyme unfolding. J. Med. Chem. **52:**2067–2075.
55. **Sadler AJ, Williams BR.** 2008. Interferon-inducible antiviral effectors. Nat. Rev. Immunol. **8:**559–568.
56. **Borden EC, Sen GC, Uze G, Silverman RH, Ransohoff RM, Foster GR, Stark GR.** 2007. Interferons at age 50: past, current and future impact on biomedicine. Nat. Rev. **6:**975–990.
57. **Elliot RL.** 2012. Four lessons from global health drug discovery: medicine for an ailing industry? Med. Chem. Lett. **3:**688–690.
58. **Lifson J, Coutre S, Huang E, Engleman E.** 1986. Role of envelope glycoprotein carbohydrate in human immunodeficiency virus (HIV) infectivity and virus-induced cell fusion. J. Exp. Med. **164:**2101–2106.
59. **Wolf MC, Freiberg AN, Zhang T, Akyol-Ataman Z, Grock A, Hong PW, Li J, Watson NF, Fang AQ, Aguilar HC, Porotto M, Honko AN, Damoiseaux R, Miller JP, Woodson SE, Chantasirivisal S, Fontanes V, Negrete OA, Krogstad P, Dasgupta A, Moscona A, Hensley LE, Whelan SP, Faull KF, Holbrook MR, Jung ME, Lee B.** 2010. A broad-spectrum antiviral targeting entry of enveloped viruses. Proc. Natl. Acad. Sci. U. S. A. **107:**3157–3162.
60. **De Clercq E.** 2012. Human viral diseases: what is next for antiviral drug discovery? Curr. Opin. Virol. **2:**572–579.
61. **Baell JB, Holloway GA.** 2010. New substructure filters for removal of pan assay interference compounds (PAINS) from screening libraries and for their exclusion in bioassays. J. Med. Chem. **53:**2719–2740.
62. **Esper FP, Spahlinger T, Zhou L.** 2011. Rate and influence of respiratory virus co-infection on pandemic (H1N1) influenza disease. J. Infect. **63:**260–266.
63. **Sato H, Masuda M, Kanai M, Tsukiyama-Kohara K, Yoneda M, Kai C.** 2007. Measles virus N protein inhibits host translation by binding to eIF3-p40. J. Virol. **81:**11569–11576.
64. **Griffin DE.** 2007. Measles virus, p 1551–1585. *In* Knipe DM, Howley PM, Griffin DE, Lamb RA, Martin MA, Roizman B, Straus SE (ed), Fields virology, 5th ed, vol 1. Lippincott Williams & Wilkins, Philadelphia, PA.
65. **Wechsler SL, Fields BN.** 1978. Intracellular synthesis of measles virus-specified polypeptides. J. Virol. **25:**285–297.
66. **Pichlmair A, Lassnig C, Eberle CA, Gorna MW, Baumann CL, Burkard TR, Burckstummer T, Stefanovic A, Krieger S, Bennett KL, Rulicke T, Weber F, Colinge J, Muller M, Superti-Furga G.** 2011. IFIT1 is an antiviral protein that recognizes 5′-triphosphate RNA. Nat. Immunol. **12:**624–630.
67. **Abbas YM, Pichlmair A, Gorna MW, Superti-Furga G, Nagar B.** 2013. Structural basis for viral 5′-PPP-RNA recognition by human IFIT proteins. Nature **494:**60–64.
68. **Martinez-Gil L, Ayllon J, Ortigoza MB, Garcia-Sastre A, Shaw ML, Palese P.** 2012. Identification of small molecules with type I interferon inducing properties by high-throughput screening. PLoS One **7:**e49049. doi:10.1371/journal.pone.0049049.
69. **Bedard KM, Wang ML, Proll SC, Loo YM, Katze MG, Gale M, Jr, Iadonato SP.** 2012. Isoflavone agonists of IRF-3 dependent signaling have antiviral activity against RNA viruses. J. Virol. **86:**7334–7344.
70. **Patel DA, Patel AC, Nolan WC, Zhang Y, Holtzman MJ.** 2012. High throughput screening for small molecule enhancers of the interferon signaling pathway to drive next-generation antiviral drug discovery. PLoS One **7:**e36594. doi:10.1371/journal.pone.0036594.
71. **Fornari FA, Randolph JK, Yalowich JC, Ritke MK, Gewirtz DA.** 1994. Interference by doxorubicin with DNA unwinding in MCF-7 breast tumor cells. Mol. Pharmacol. **45:**649–656.
72. **Babudri N, Pani B, Tamaro M, Monti-Bragadin C, Zunino F.** 1984. Mutagenic and cytotoxic activity of doxorubicin and daunorubicin derivatives on prokaryotic and eukaryotic cells. Br. J. Cancer **50:**91–96.
73. **Broom WJ, Auwarter KE, Ni J, Russel DE, Yeh LA, Maxwell MM, Glicksman M, Kazantsev AG, Brown RH, Jr.** 2006. Two approaches to drug discovery in SOD1-mediated ALS. J. Biomol. Screen. **11:**729–735.
74. **Soelaiman S, Wei BQ, Bergson P, Lee YS, Shen Y, Mrksich M, Shoichet BK, Tang WJ.** 2003. Structure-based inhibitor discovery against adenylyl cyclase toxins from pathogenic bacteria that cause anthrax and whooping cough. J. Biol. Chem. **278:**25990–25997.

Publication 5

J. Maina Ndungu, **Stefanie A Krumm**, Dan Yan, Richard F Arrendale, Reddy G Prabhakar, Taylor Evers, Randy B Howard, Michael G Natchus, Manohar T Saindane, Dennis C Liotta, Richard K Plemper, James P Snyder, and Aiming Sun
"Non-nucleoside Inhibitors of the Measles Virus RNA-dependent RNA Polymerase: Synthesis, Structure-Activity Relationships and Pharmacokinetics"
JOURNAL OF MEDICINAL CHEMISTRY, May 2012

J Med Chem accepted manuscript and published in PubMed Central by copyright permission of American Chemical Society

Non-nucleoside Inhibitors of the Measles Virus RNA-dependent RNA Polymerase: Synthesis, Structure-Activity Relationships and Pharmacokinetics

J. Maina Ndungu,[1] Stefanie A. Krumm,[2] Dan Yan, [2] Richard F. Arrendale,[1] G. Prabhakar Reddy, [1] Taylor Evers, [1] Randy Howard,[1] Michael G. Natchus,[1] Manohar T. Saindane,[1] Dennis C. Liotta,[1,3] Richard K. Plemper, [2,4] James P. Snyder, [1,3] and Aiming Sun,*[1]

[1]*Emory Institute for Drug Discovery, Emory University, 1515 Dickey Dr. Atlanta, GA, 30322*

[2]*Department of Pediatrics, Emory University School of Medicine, 2015 Uppergate Dr. Atlanta, GA, 30322*

[3]*Department of Chemistry, Emory University, 1515 Dickey Dr. Atlanta, GA, 30322*

[4]*Children's Healthcare of Atlanta, 2015 Uppergate Dr. Atlanta, Georgia, 30322*

KEY WORDS : measles virus, RNA-dependent RNA polymerase activity inhibitor, AS-136a, ERDRP-00519, pharmacokinetics.

*Corresponding author:

Phone: 404-712-8680; e-mail: asun2@emory.edu

ABSTRACT

The measles virus (MeV), a member of the paramyxovirus family, is an important cause of pediatric morbidity and mortality worldwide. In an effort to provide therapeutic treatments for improved measles management, we previously identified a small, non-nucleoside organic inhibitor of the viral RNA-dependent RNA polymerase (RdRp) by means of high-throughput screening (HTS). Subsequent structure-activity relationship (SAR) studies around the

corresponding pyrazole carboxamide scaffold led to the discovery of **2** (AS-136a), a first generation lead with low nanomolar potency against life MeV and attractive physical properties suitable for development. However, its poor water solubility and low oral bioavailability (F) in the rat suggested that the lead could benefit from further SAR studies to improve the biophysical characteristics of the compound. Optimization of *in vitro* potency and aqueous solubility led to the discovery of **2o** (ERDRP-00519), a potent inhibitor of MeV (EC_{50} = 60 nM) with aqueous solubility of approximately 60 μg/ml. The agent shows a 10-fold exposure (AUC/Cmax) increase in the rat model relative to **2,** displays near dose proportionality in the range of 10 mg/kg to 50 mg/kg, and exhibits good oral bioavailability (F = 39%) in the rat. The significant solubility increase appears linked to the improved oral bioavailability.

INTRODUCTION

The paramyxoviruses family comprised non-segmented, negative strand RNA viruses that are primarily responsible for acute respiratory diseases. The family includes major human and animal pathogens such as measles virus (MeV), human parainfluenza virus (HPIV), mumps virus, respiratory syncytial virus (RSV) and the Newcastle disease virus. Despite the existence of an effective vaccine protecting against MeV infection, we have witnessed in the recent past an increasing number of cases particularly in the developed world.[1,2] For example, in the United States from January 1 through May 21 of 2011, 118 cases were reported across 23 states according to the CDC. Recently, in Ashland, Oregon, 25-30% of children entering kindergarten were unvaccinated.[3] This has been attributed to elected exemption from vaccination on the basis of philosophical or religious beliefs. Vaccination rates in Europe in recent years have never fully recovered from a discredited 1998 British study linking the vaccine for measles, mumps and rubella to autism. At that time, parents, particularly in the U.K. abandoned the vaccine followed

by precipitous drops in vaccination rates. For 2011, the World Health Organization reported 4,937 cases of measles between January and March in France alone, compared with 5,090 cases during all of 2010. The World Health Organization reports that as of October, there have been 26,000 measles cases, and nine deaths, in Europe since the start of 2011, rendering it the worst year for MeV activity in the Western World since 1996.[4]

Measles is not currently treatable by drug therapy. Ribavirin, a nucleoside based anti-viral agent, is the only small molecule drug approved for paramyxoviruses (RSV) therapy.[5,6] However, efficacy is limited. To improve case management of severe measles and achieve rapid control of outbreaks through post-exposure prophylaxis, the development of an effective anti-measles drug is highly desirable.[7] We previously reported the discovery of an MeV inhibitor targeting the viral RNA dependent RNA polymerase (RdRp) complex by means of a cell-based high-throughput screening (HTS).[8,9] Iterative optimization of a corresponding series of pyrazole carboxamides, exemplified by hit **1** (16677), led to the first-generation lead molecule **2** (AS-136a) (Figure 1).[10,11] The latter piperidine derivative exhibits superior *in vitro* cellular potency against MeV with nanomolar EC_{50} concentrations. It was also subjected to a number of *in vitro* toxicity and metabolism assays. There, the compound was found to be non-mutagenic in a non-GLP *in vitro* bacterial reverse mutation (Ames) assay, and it did not block hERG channels at a concentration of 10 μM or below. Compound **2** shows moderate metabolic stability in mouse and human S9 fractions after one-hour incubation with 79% and 69% parent remaining, respectively. However, poor solubility and low rat plasma concentrations of **2** might hamper its *in vivo* efficacy. In an effort to improve pharmacological properties of **2**, in particular water solubility, we initiated a structure activity relationship (SAR) study to identify a suitable solubilizing group. Earlier efforts had shown that the piperidine ring is amenable to chemical manipulation without

adversely affecting activity. However, any changes to the central ring or the pyrazole group of **2** are detrimental to activity.[11] Consequently, the present study focuses on appending a solubilizing group to the piperidine ring or replacing it with either a substituted phenyl or an alicyclic group. This led to the identification of compound **2o** (ERDRP-00519, Figure 1), which has significantly improved water solubility, while retaining high antiviral potency. The agent shows a 10-fold exposure (AUC/Cmax) increase in rat relative to **2** and displays near dose proportionality in the range of 10 mg/kg to 50 mg/kg. The significant solubility increase appears to contribute to the improvement in oral bioavailability. We describe herein the synthesis and a structure-activity relationship (SAR) strategy that led to the discovery of **2o** as well as the pharmacokinetic comparison of first and second-generation lead candidates.

Figure 1. Structures of hit and lead compounds.

CHEMISTRY

Synthesis of Substituted Piperidine Analogs. Our previous work showed that introduction of a piperidine moiety resulted in compounds that were about 10 times more active than the corresponding pyrrolidine analogs.[10] Accordingly, linkers were installed at the 2-, 3- and 4-positions of the pyrrolidine ring to explore which position could best accommodate hydrophilic substituents while maintaining potency. Reaction of different amino alcohols (**4a-c**) with 4-nitrobenzene sulfonyl chloride (**5**) followed by formation of methoxymethyl (MOM) ethers and reduction of the nitro group afforded anilines **7a-c**. Coupling of acid chloride **8**, derived from 3-trifluoromethyl pyrazole using the method of Lahm,[12] with anilines **7a-c** provided analogs **1a-c** (Scheme 1). With preliminary data showing the 2-position of the piperidine to yield more active compounds compared to the 3- or 4-position (Table 1), additional analogs of the previously

reported 2-piperidinemethanol compound **2a**[13] were prepared by a sequence similar to that depicted in Scheme 1.

Scheme 1. Exploring the optimal substitution position on the piperidine ring[a]

Further analogs were prepared by PCC oxidation of **6a** to obtain aldehyde **14**, which was subjected to reductive amination with morpholine followed by the procedures illustrated in Schemes 2 to ultimately give analog **2b**. Tosylation of **6a**, reduction of the nitro group, coupling with acid chloride **8** and displacement of the tosylate with an azide furnished **2c**. Reduction of the azide, dimethylation of the resultant amine or acylation resulted in compounds **2d-f**. Further extension of the side chain including both saturated and unsaturated derivatives could be achieved from aldehyde **14**. Horner-Wadsworth-Emmons olefination of **14** gave **12**. Union of **12** with acid chloride **8** afforded analog **2g,** which was then reduced with DIBAL-H to obtain analog **2h.** Hydrogenation of **2g** delivered the saturated analog **2i**, which was converted to **2j** by treatment with DIBAL-H (Scheme 2).

Scheme 2. Synthesis of three-carbon substituents at the piperidine C-2 position[a]

Preparation of two-carbon side chain analogs was accomplished by utilizing 2-(2-piperidinyl) ethanol **9**. Direct coupling of the latter with *p*-nitro-benzenesulfonyl chloride **5** gave low yields of the desired product due to further coupling of the product with the sulfonyl chloride. To circumvent this shortcoming, the NH- and OH- groups of **9** were protected using benzyl chloroformate[14] and *t*-butyldimethylsilyl chloride (TBSCl), respectively. De-protection of the amine, coupling with **5** and reduction of the nitro group afforded aniline **11**. Coupling of **11** with acid chloride **8** followed by cleavage of the silyl group furnished alcohol **2k** which, when

subjected to Swern oxidation and reductive amination with morpholine, gave **2n** (Scheme 3). Chiral pure enantiomer **2o** was then prepared similar to **2n** starting from (*S)*-2-piperidine ethanol.

Scheme 3. Introduction of a two-carbon tether at the piperidine C-2 position[a]

We hypothesized that attaching an ethylene glycol moiety would give compounds with better aqueous solubility. Due to the instability of **6a** under basic conditions, the synthesis of **2p** was initiated by addition of a rhodium carbenoid across the hydroxylic bond[15,16] to form an ether bond. Thus, decomposition of ethyl diazoacetate in the presence of Rh_2OAc_4 generated a carbenoid that inserted into the OH bond to give **13**. Reduction of the nitro group of **13** followed by coupling with **8** afforded analog **2p**, which on hydrolysis of the ester and BOP/$NaBH_4$[17] mediated reduction of the resultant carboxylic acid, provided **2q** (Scheme 4).

Scheme 4. Synthesis of O-alkylated analogs[a]

Synthesis of the Phenyl Series. Replacement of the piperidine ring with phenyl or substituted phenyl *via* the general route shown in Scheme 5 was also explored. Unsubstituted phenyl analog **3a** was found to be as active as lead compound **2** triggering an SAR study of the series (Table 2). Coupling of 2-methoxylthiophenol **16a** with 1-fluoro-4-nitrobenzene[18] followed by oxidation of sulfur using MCPBA gave corresponding sulfone, which went through reduction of the nitro group and followed by coupling with acid chloride **8** furnished analog **3b**. Demethylation of **3b** with BBr_3 afforded phenol analog **3c**, which on acylation gave analog **3d.** Similarly, coupling of 2-bromothiophenol **16b with** 1-fluoro-4-nitrobenzene obtained **17**. To make additional analogs of the phenyl series, we envisioned utilizing bromide **17** to append substituents. However, attempts to lithiate bromide **17** using *n*-BuLi or *t*-BuLi were unfruitful resulting in decomposition of the bromide. Stille coupling offered an alternative. When **17** was treated with

tributyl(vinyl)tin in the presence of $Pd(PPh_3)_4$, the desired coupling product **18** was obtained in 80% yield. Reduction of the nitro group followed by coupling with acid chloride **8** afforded analog **3e** (Scheme 5 and Table 2). Subjecting olefin **18** to osmium tetroxide-mediated oxidative cleavage of the double bond gave aldehyde **19**, a compound utilized in the synthesis of additional analogs. Reduction of the aldehyde, $SnCl_2$ reduction of the nitro group and protection of the alcohol as a silyl ether gave aniline **20**. Coupling of **20** with acid chloride **8** followed by cleavage of the silyl group furnished analog **3f**. Aldehyde **19** was also used for the synthesis of morpholine **3g** by means of reductive-amination, followed by reduction of the nitro group and coupling with acid chloride **8** (Scheme 5).

Scheme 5. Synthesis of the phenyl series[a]

Table 1. MeV antiviral action (CPE) of the piperidine series of analogs, (EC_{50}).

Table 2. MeV antiviral action (CPE) of the phenyl and acyclic series of analogs, (EC_{50}).

Single Dose Antiviral Activity of Analogs of 2

In order to better understand the potency profile of compound **2** analogs, the most active analogs were subjected to a measles virus yield assay at a single concentration of 1.0 μM to generate data points for comparison with **2**.

Figure 2. Evaluation of **2** and analogs against MV-Alaska. All compounds were tested at 1.0 μM. Compounds comparable in activity to **2** were further examined at a range of concentrations to generate dose-response curves.

RESULTS AND DISCUSSION

The SAR data are summarized in Tables 1 and 2 for the piperidine and phenyl series, respectively. From previous experience, we have learned the necessity of preserving the structure of the phenyl, amide and fluorinated pyrazole units of the molecule in order to maintain anti-viral potency. Modification of either the 3-trifluoromethyl-pyrazole or the central phenyl ring in most cases leads to significant loss of activity.[10,11] All analogs listed in Tables 1 and 2 incorporate only variations on the left side of lead molecule **1**. The MOM ether analogs (**1a-c**) demonstrate a trend whereby substitution at C-2 of the piperidine is favored. The 2-piperidine **1a** is 2-fold more potent than the corresponding 3-piperidine, while the 4-substituted derivatives reduce activity by almost 10-fold (**1a**, **1b** and **1c**, Table 1). For compounds with a hydroxyl group, elongation of the pendant chain from one carbon to two does not adversely affect potency as exemplified by compounds **2a** and **2k**.

Further extension to three carbons leads to a decrease in activity by 3-fold (**2j**, Table 1). Introduction of basic amines led to significant reduction or complete loss of activity (**2d** and **2f**, EC_{50} = 55.0 and >150 μM, respectively). Replacement of the amino groups with a less basic morpholine (**2b** and **2n**) restored good potency. Esters **2g** and **2i** were found to be 2-fold less active by comparison with the corresponding alcohols (**2h** and **2j**, Table 1). There is a clear superiority of *S*-chirality over *R*- as demonstrated by the 3-fold loss of activity for **2l** compared to **2m**. For the phenyl series, analog **3a** is as active as the lead compound in reducing virus-induced cytopathicity, and its activity is comparable to that of methoxy **3b** and alcohol **3f** (Table 3). However, the morpholine analog **3g** loses activity completely, which stands in significant contrast to alterations in the piperidine series (**2b** and **2n**). The previous SAR and that derived from the current three series of MeV-RdRp inhibitors suggests a highly hydrophobic environment on the target protein housing the left part of the molecules, strongly disfavoring

hydrogen bonding. To explore whether poor aqueous solubility contributes to the low oral bioavailability that was observed with the existing lead **2**, we measured the aqueous solubility for some of the more potent derivatives *via* nephylometry (buffer, pH = 7.4, Table 3). **2** and phenyl analog **3a** show equally poor solubility with values at 15 μg/ml and 22 μg/ml, respectively. The alcohol analogs **2a** and **2k** both deliver improved solubility as expected with measured values at 61 and 62 μg/ml, respectively. Importantly, the morpholine analog **2n** also furnishes similar solubility compared with the corresponding free alcohol derivative **2k**. Compounds with moderate solubility (~60 μg/ml) and good potency (< 3.0 μM) in the CPE assay were advanced to assessment of virus yield reduction. The primary alcohol derivative **2k** (EC_{50} 2.7 μM, CPE assay; solubility 62 μg/ml) delivers an EC_{50} of 100 nM in this assay (**2k**; Table 3). Optically pure analogs of compound **2k**, **2l** and **2m**, both delivered slightly decreased potency (EC_{50} 8.3 and 3.1 μM, respectively, CPE assay). Replacement of the hydroxyl group with morpholine led to racemate **2n** with an EC_{50} of 4.6 μM, while the corresponding optically pure analog **2o** provided an EC_{50} of 2.5 μM in the CPE assay, 60 nM in the virus yield reduction assay and solubility around 60 μg/ml (**2o**; Table 3).

Considering the advanced potencies of **2k** and **2o** in the virus yield reduction assay (EC_{50} = 100 and 60 nM, respectively), we selected these two compounds for comparison with **2** in a pharmacokinetic (PK) study in Sprague-Dawley rats.

PHARMACOKINETIC PROFILES

Figure 3 shows oral pharmacokinetic parameters of compounds **2k** and **2o** in comparison with the first generation lead **2**; a summary of the numerical PK analysis is provided in Table 4. Compound **2o** shows a 10-fold exposure (with respect to both AUC and Cmax) increase in the

rat model relative to **2** and displays good dose proportionality in the range of 10 mg/kg to 50 mg/kg. In contrast, the primary alcohol analog **2k** reveals a good Cmax and AUC at 50 mg/kg dosing, but it generates poor plasma concentrations in rat and non- proportionality possibly due to high first-pass metabolism of the primary alcohol. On the basis of its high *in vitro* potency, good solubility and pharmacokinetic profile, the oral bioavailability of compound **2o** was assessed. The compound was dosed at 2 mg/kg i.v. and 10 mg/kg p.o. in rat and exhibits good oral bioavailability (F = 39 %) (Figure S1 and Table S1). In the Caco-2 bi-directional permeability assay, both **2** and **2o** showed high permeability with an efflux ratio of 1.1 and 2.6, respectively, which indicates that they are probably not a substrate for p-glycoprotein in humans. (Figure S2)[19, 20] However, compound **2o** proved to be less stable in human liver S9 fractions after one hour incubation. Only 24% of the parent remains as compared with 69% for compound **2**.

Table 3. Aqueous solubility, virus yields (EC_{50}) and toxicity (CC_{50}) for selected compounds.

Figure 3. Time course of rat plasma concentration following p.o. dosing by oral gavage. Preliminary pharmacokinetic (PK) studies in the Sprague-Dawley rat compared **2** with compounds **2k** and **2o** following p.o. dosing by oral gavage at 10 mg/kg and 50 mg/kg in a PEG200/0.5% methylcellulose (10/90) vehicle (n=4/group)

Table 4. PK Profile for Compounds **2**, **2k** and **2o**

Mechanism of Action of 2o.

We previously demonstrated that compound **2** blocks MeV RdRp activity by targeting the viral polymerase (L) protein.[11] To test whether this mechanism of activity likewise extends to lead molecule **2o**, a plasmid-based mini-replicon assay[21] was employed to assess RdRp activity in the

presence of **2o** and **2**, respectively. BSR-T7/5 cells were transfected with plasmid DNA encoding MeV-L, N, P and the firefly luciferse mini-genome reporter construct, and the cell were incubated in the presence of different inhibitor concentrations or vehicle for control. Relative luciferase activities in cell lysates were assessed 36 hours post-transfection and dose-response inhibition curves generated. For both compounds, we observed a dose-dependent inhibition of viral RdRp activity with virtually identical potency (**Figure 4),** supporting comparable mechanism of antiviral activity.

Figure 4. Compounds **2o** and **2** inhibit viral RdRp activity with equal potency. Values are expressed relative to vehicle-treated samples and represent averages of three experiments± SD.

SUMMARY

Modification and replacement of the piperidine moiety in the first-generation lead **2**, derived from our MeV-RdRp inhibitor program has been investigated. An SAR study revealed that hydrophilicity in this molecular sector strongly influences antiviral activity. We identified compounds incorporating hydroxyl (**2k**) and morpholinyl (**2o**) moieties that furnish potencies within a 10-fold range of **2**, but with much improved aqueous solubility and oral bioavailability. In the series that replaces piperidine with the phenyl group, the most promising compound was found to be **3a** with antiviral activity around 90 nM in a virus yield reduction assay. Unfortunately, the solubility rates of **3a** and **2** are equally low, which stands in strong contrast to analogs **2k** and **2o**. Accordingly, the latter were advanced to pharmacokinetic studies in the Sprague-Dawley rat model. Analog **2o** displays a 10-fold exposure (AUC/Cmax) increase in this model relative to **2** and displays near dose proportionality in the range of 10 to 50 mg/kg. The Caco-2 permeability assessment demonstrated the high permeability of this class of molecule.

This significant solubility increase might be a major determinant for the overall improvement in oral bioavailability. Compound **2o** was therefore identified as a second-generation lead for further development towards a novel measles therapeutic.

EXPERIMENTAL SECTION

GENERAL. Unless otherwise noted, all materials were obtained from commercial suppliers and used without purification. Dry organic solvents (DriSolv) were purchased from EMD Chemicals and packaged under nitrogen in Sure Seal bottles. Reactions were monitored using thin-layer chromatography on 250 μm plates or using Agilent 1100 series LC/MS with UV detection at 254 nm and low resonance electrospray mode (ESI). Elemental analysis was done by Atlantic Microlab. Purification of title compounds was accomplished by liquid chromatography on a Biotage SP4 purification system with normal phase silica gel. ^{1}H NMR spectra were recorded on a Varian spectrometer (400 MHz) at ambient temperature. Chemical shifts are reported in ppm relative to $CDCl_3$ or CD_3OD and coupling constants (*J*) are reported in hertz (Hz). Solvents for NMR were deuteriochloroform ($CDCl_3$) (residual shifts: δ 7.26 for ^{1}H and δ 77.7 for ^{13}C) and deuteriomethanol (CD_3OD) (residual shift: δ 3.31 for ^{1}H). The residual shifts were taken as internal references and reported in parts per million (ppm). Purities of all compounds were ≥ 95% determined by high performance liquid chromatography (HPLC) with UV detection at two wavelengths of 220 and 254 nM. Purities of key compounds were also confirmed by elemental analysis.

Typical Procedures for the Synthesis of 1-methyl-*N*-(4-(piperidin-1-ylsulfonyl)phenyl)-3-(trifluoromethyl)-1*H*-pyrazole-5-carboxamides (1a-c)

4-Amino-sulfonamide **7a-c** (1.0 mmol) in dichloromethane (5 ml) and pyridine (0.1 ml) was treated with 1-methyl-3-trifluoromethyl-5-pyrazolecarbonyl chloride (**8**) at rt. Reaction was monitored by LC-MS till no more starting material was seen, then the mixture was poured into saturated aqueous $NaHCO_3$ (10 ml), extracted with CH_2Cl_2 (3x 10ml). The CH_2Cl_2 extracts were collected and dried over anhydrous Na_2SO_4. Products were purified by chromatography.

***N*-(4-((2-((Methoxymethoxy)methyl)piperidin-1-yl)sulfonyl)phenyl)-1-methyl-3-(trifluoromethyl)-1*H*-pyrazole-5-carboxamide (1a)**. ^{1}H NMR ($CDCl_3$, 400MHz): δ 8.17 (s, 1H), 7.74 - 7.79 (m, 2H), 7.64 - 7.69 (m, 2H), 7.06 (s, 1H), 4.51 (s, 2H), 4.19 - 4.28 (m, 4H), 3.76-3.68 (m, 1H), 3.54 - 3.65 (m, 2H), 3.27 (s, 3H), 3.03-2.94 (m, 1H), 1.76-1.70 (m, 1H), 1.42 - 1.60 (m, 4H), 1.20 - 1.37 (m, 1H). Anal. calcd for $C_{21}H_{29}F_3N_4O_5S$: C, 49.79; H, 5.77; N, 11.06. Found: C, 49.07; H, 5.06; N, 11.31.

***N*-(4-((3-((Methoxymethoxy)methyl)piperidin-1-yl)sulfonyl)phenyl)-1-methyl-3-(trifluoromethyl)-1*H*-pyrazole-5-carboxamide (1b)**. ^{1}H NMR ($CDCl_3$, 400MHz): δ 8.09 (s, 1H), 7.69 - 7.78 (m, 4H), 7.03 (s, 1H), 4.56 (s, 2H), 4.25 (s, 3H), 3.78 (d, *J* = 11.7 Hz, 2H), 3.30 - 3.38 (m, 5H), 2.27 (td, *J* = 2.3, 11.9 Hz, 2H), 1.72 - 1.83 (m, 2H), 1.50 (m, 1H), 1.29 - 1.42 (m, 2H); LC-MS (ESI) (LCT, 3 min) Rt 1.58 min; >95% purity at λ 254 and 210 nm, MS: *m/z* 491.5 [M+1].

***N*-(4-((4-((Methoxymethoxy)methyl)piperidin-1-yl)sulfonyl)phenyl)-1-methyl-3-(trifluoromethyl)-1*H*-pyrazole-5-carboxamide (1c)**. ^{1}H NMR ($CDCl_3$, 400MHz): δ 7.97 (s, 1H), 7.71 - 7.77 (m, 4H), 7.01 (s, 1H), 4.56 (s, 2H), 4.26 (s, 3H), 3.79 (d, *J* = 11.3 Hz, 2H), 3.30 - 3.38 (m, 5H), 2.27 (td, *J* = 2.5, 11.8 Hz, 2H), 1.79 (d, *J* = 10.6 Hz, 2H), 1.45 - 1.56 (m, 1H),

1.35 (m, 2H). Anal. calcd for $C_{21}H_{29}F_3N_4O_5S$: C, 49.79; H, 5.77; N, 11.06. Found: C, 49.17; H, 5.09; N, 11.21.

Synthesis of *N*-(4-((2-(hydroxymethyl)piperidin-1-yl)sulfonyl)phenyl)-1-methyl-3-(trifluoromethyl)-1*H*-pyrazole-5-carboxamide (2a); A solution of (1-((4-nitrophenyl)sulfonyl)piperidin-2-yl)methanol **6a** (90 mg, 0.3 mmol) in MeOH (10 ml) was treated with H_2 (50 Psi) for 4 h in the presence of Pd/C (32 mg, 0.03 mmol). The Pd/C residue was removed by filtration, followed by evaporation of the solvent. The crude product was purified by chromatography (Hexane/EtOAc) to obtain amine product as white solid 70 mg (Y=86%).

4-Amino-sulfonamide (70 mg, 0.25 mmol) in dichloromethane (5 ml) and pyridine (0.1 ml) was treated with 1-methyl-3-trifluoromethyl-5-pyrazolecarbonyl chloride (**8**) at rt. Reaction was monitored by LC-MS till no more starting material was seen, then the mixture was poured into saturated aqueous $NaHCO_3$ (10 ml), extracted with CH_2Cl_2 (3x 10ml). The CH_2Cl_2 extracts were collected and dried over anhydrous Na_2SO_4. Products were purified by chromatography (Hex/EtOAc) to obtain product **2a** as light yellow solid (81 mg, 73%). ^{1}H NMR (400MHz, $CDCl_3$) δ 1.23-1.62 (6H, m), 2.20 (1H, m), 3.08 (1H, t, J=13.2 Hz), 3.53-3.59 (1H, m), 3.77 (1H, d, J=14.0Hz), 3.84 (1H, t, J=10.4Hz), 4.00-4.06 (1H, m), 4.26 (3H, s), 7.11 (1H, s), 7.74-7.81 (4H, m), 8.48 (1H, s). Anal. calcd for $C_{18}H_{21}F_3N_4O_4S$: C, 48.43; H, 4.74; N, 12.55. Found: C, 48.33 ; H, 4.84 ; N, 12.23.

General Procedure for the Synthesis of Morpholinyl Analog (2b, 2n and 2o). To a solution of aldehyde (1.0 mmol) in CH_2Cl_2 (10 ml) was added morpholine (1.3 eq, 1.3 mmol) and $NaBH(OAc)_3$ (2.0 eq, 2.0 mmol) and the mixture was kept stirring at room temperature for 3h. $NaHCO_3$ (sat. aq) was added and the organic layer separated and washed with brine, dried over

Na_2SO_4, filtered and concentrated. The product was purified by column to give morpholinyl analog.

1-Methyl-*N*-(4-((2-(morpholinomethyl)piperidin-1-yl)sulfonyl)phenyl)-3-(trifluoromethyl)-1*H*-pyrazole-5-carboxamide (2b). ^{1}H NMR ($CDCl_3$, 400MHz): δ 8.03 (s, 1H), 7.83 - 7.89 (m, 2H), 7.67 - 7.72 (m, 2H), 7.02 (s, 1H), 4.26 (s, 3H), 4.21 (br. s., 1H), 3.64 (m, 5H), 2.88 - 2.97 (m, 1H), 2.38 - 2.51 (m, 6H), 1.77 (m, 1H), 1.41 - 1.58 (m, 4H), 1.31(m, 1H). Anal. calcd for $C_{22}H_{28}F_3N_5O_4S$: C, 51.25; H, 5.47; N, 13.58. Found: C, 51.05; H, 5.45; N, 13.42.

***N*-(4-((2-(Azidomethyl)piperidin-1-yl)sulfonyl)phenyl)-1-methyl-3-(trifluoromethyl)-1*H*-pyrazole-5-carboxamide (2c).** ^{1}H NMR ($CDCl_3$, 400MHz): δ 7.93 (s, 1H), 7.80 - 7.86 (m, 2H), 7.69 - 7.75 (m, 2H), 6.99 (s, 1H), 4.26 (s, 3H), 4.16 (m, 1H), 3.79 (d, *J* = 13.3 Hz, 1H), 3.51 (dd, *J* = 7.2, 12.3 Hz, 1H), 3.30 - 3.38 (m, 1H), 2.92 - 3.02 (m, 1H), 1.65 - 1.71 (m, 1H), 1.53 - 1.62 (m, 5H).

***N*-(4-((2-(Aminomethyl)piperidin-1-yl)sulfonyl)phenyl)-1-methyl-3-(trifluoromethyl)-1*H*-pyrazole-5-carboxamide (2d).** ^{1}H NMR ($CDCl_3$, 400MHz): δ 8.27 (s, 1H), 7.77 - 7.83 (m, 2H), 7.68 - 7.75 (m, 2H), 7.03 (s, 1H), 4.25 (s, 3H), 3.87 - 3.96 (m, 1H), 3.77 (d, *J* = 11.0 Hz, 1H), 2.92 - 3.06 (m, 2H), 2.64 (dd, *J* = 5.7, 13.5 Hz, 1H), 1.28 - 1.60 (m, 6H). LC-MS (ESI) (LCT, 3 min) Rt 0.54 min; >95% purity at λ 254 and 210 nm, MS: *m/z* 446.0 [M+1].

***N*-(4-((2-(Acetamidomethyl)piperidin-1-yl)sulfonyl)phenyl)-1-methyl-3-(trifluoromethyl)-1*H*-pyrazole-5-carboxamide (2e)**. ^{1}H NMR ($CDCl_3$, 400MHz): δ 9.31 (s, 1H), 7.83 - 7.90 (m, 2H), 7.76 - 7.82 (m, 2H), 7.22 (s, 1H), 6.08 (t, *J* = 5.5 Hz, 1H), 4.26 (s, 3H), 4.03 - 4.13 (m, 1H), 3.67 - 3.77 (m, 1H), 3.56 (ddd, *J* = 5.3, 10.9, 14.0 Hz, 1H), 3.20 - 3.28 (m, 1H), 3.02 - 3.11 (m,

1H), 2.0 (m, 3H), 1.38 - 1.53 (m, 4H), 1.20 - 1.34 (m, 1H). Anal. calcd for $C_{20}H_{25}F_3N_4O_4S$: C, 49.28; H, 4.96; N, 14.37. Found: C, 49.02; H, 4.98; N, 14.08.

(*E*)-Ethyl 3-(1-((4-(1-methyl-3-(trifluoromethyl)-1*H*-pyrazole-5-carboxamido)phenyl)-sulfonyl)piperidin-2-yl)acrylate (2g). ^{1}H NMR ($CDCl_3$, 400MHz): δ 8.19 (s, 1H), 7.69 - 7.78 (m, 4H), 7.03 (s, 1H), 6.75 (dd, *J* = 4.0, 16.0 Hz, 1H), 5.89 (dd, *J* = 2.0, 16.0 Hz, 1H), 4.69 (br. s., 1H), 4.25 (s, 3H), 4.15 (q, *J* = 7.0 Hz, 2H), 3.67 (d, *J* = 12.9 Hz, 1H), 2.95 - 3.05 (m, 1H), 1.63 - 1.78 (m, 2 H), 1.56 (d, *J* = 11.0 Hz, 7 H), 1.32 - 1.47 (m, 7 H), 1.25 (t, *J* = 8.0 Hz, 3H). Anal. calcd for $C_{22}H_{25}F_3N_4O_5S$: C, 51.36; H, 4.90; N, 10.89. Found: C, 51.36; H, 4.90; N, 10.89. Found: C, 51.42; H, 4.90; N, 10.79.

(*E*)-*N*-(4-((2-(3-Hydroxyprop-1-en-1-yl)piperidin-1-yl)sulfonyl)phenyl)-1-methyl-3-(trifluoromethyl)-1*H*-pyrazole-5-carboxamide (2h). ^{1}H NMR ($CDCl_3$, 400MHz): δ 8.32 (s, 1H), 7.63 - 7.77 (m, 4H), 7.05 - 7.10 (m, 1H), 5.63 - 5.72 (m, 1H), 5.52 - 5.61 (m, 1H), 4.54 (br. s., 1H), 4.24 (s, 3H), 3.95 - 4.08 (m, 2H), 3.64 (d, *J* = 12.5 Hz, 1H), 3.47 (d, *J* = 5.1 Hz, 1H), 2.91 - 3.02 (m, 1H), 1.81 (t, *J* = 5.9 Hz, 1H), 1.34 - 1.74 (m, 6H). Anal. calcd for $C_{20}H_{23}F_3N_4O_4S$: C, 50.84; H, 4.91; N, 11.86. Found: C, 50.57; H, 4.98; N, 11.63.

Ethyl 3-(1-((4-(1-methyl-3-(trifluoromethyl)-1*H*-pyrazole-5-carboxamido)phenyl)-sulfonyl)piperidin-2-yl)propanoate (2i). ^{1}H NMR ($CDCl_3$, 400MHz): δ 8.34 (s, 1H), 7.66 - 7.83 (m, 4H), 7.07 (s, 1H), 4.25 (s, 3H), 4.02 (s, 1H), 3.73 (d, *J* = 14.5 Hz, 1H), 3.63 (m, 2H), 2.93 - 3.05 (m, 1H), 2.16 (s, 3H), 1.59 - 1.81 (m, 2H), 1.28 - 1.59 (m, 6H). LC-MS (ESI) (LCT, 3 min) Rt 2.11 min; >95% purity at λ 254 and 210 nm, MS: *m/z* 517.1 [M+1].

***N*-(4-((2-(3-Hydroxypropyl)piperidin-1-yl)sulfonyl)phenyl)-1-methyl-3-(trifluoromethyl)-1*H*-pyrazole-5-carboxamide (2j)**. ^{1}H NMR (CHLOROFORM-d ,400MHz): δ 8.26 (s, 1H), 7.67 - 7.79 (m, 4H), 7.06 (s, 1H), 4.25 (s, 3H), 4.11 (q, *J* = 7.0 Hz, 2H), 3.99 - 4.07 (m, 1H), 3.74 (d, *J* = 14.5 Hz, 1H), 2.96 - 3.07 (m, 1H), 2.36 (t, *J* = 7.4 Hz, 2H), 2.00 - 2.13 (m, 1H), 1.60 - 1.72 (m, 1H), 1.30 - 1.55 (m, 5H), 1.24 (t, *J* = 7.2 Hz, 3H), 1.01 - 1.17 (m, 1H). Anal. calcd for $C_{20}H_{25}F_3N_4O_4S$: C, 50.62; H, 5.31; N, 11.81. Found: C, 50.35; H, 5.28; N, 11.62.

***N*-(4-((2-(2-Hydroxyethyl)piperidin-1-yl)sulfonyl)phenyl)-1-methyl-3-(trifluoromethyl)-1*H*-pyrazole-5-carboxamide (2k).** ^{1}H NMR ($CDCl_3$, 400MHz): δ 8.00 (s, 1H), 7.86 (d, *J* = 8.6 Hz, 2H), 7.75 (d, *J* = 8.6 Hz, 2H), 6.99 (s, 1H), 4.26 (s, 3H), 4.17 - 4.25 (m, 1H), 3.90 (d, *J* = 14.1 Hz, 1H), 3.74 - 3.83 (m, 1H), 3.67 (d, *J* = 5.1 Hz, 1H), 2.97 - 3.06 (m, 1H), 2.84 (dd, *J* = 4.9, 8.4 Hz, 1H), 1.93 - 2.02 (m, 1H), 1.40 - 1.54 (m, 5H), 1.32-1.40 (M, 1H). Anal. calcd for $C_{19}H_{23}F_3N_4O_4S$: C, 49.56; H, 5.03; N, 12.17. Found: C, 49.36; H, 5.08; N, 11.98.

(*R*)-*N*-(4-((2-(2-Hydroxyethyl)piperidin-1-yl)sulfonyl)phenyl)-1-methyl-3-(trifluoromethyl)-1*H*-pyrazole-5-carboxamide (2l); ^{1}H NMR ($CDCl_3$, 400MHz): δ 8.34 (s, 1H), 7.84 (d, *J* = 8.4 Hz, 2H), 7.78 (d, *J* = 8.4 Hz, 2H), 7.07 (s, 1H), 4.27 (s, 3H), 4.22 - 4.19 (m, 1H), 3.91 (d, *J* = 14.4 Hz, 1H), 3.80 (t, *J* = 11.2 Hz, 1H), 3.67 (br, 1H), 3.06 – 2.04 (m, 2H), 2.03-1.95 (m, 1H), 1.57 - 1.41 (m, 4H), 1.28-1.21 (m, 2H). LC-MS (ESI) (LCT, 3 min) Rt 1.09 min; >95% purity at λ 254 and 210 nm, MS: *m/z* 461.2 [M+1].

(*S*)-*N*-(4-((2-(2-Hydroxyethyl)piperidin-1-yl)sulfonyl)phenyl)-1-methyl-3-(trifluoromethyl)-1*H*-pyrazole-5-carboxamide (2m). ^{1}H NMR ($CDCl_3$, 400MHz): δ 8.12 (m, 1H), 7.86 (d, *J* = 8.6 Hz, 2H), 7.75 (d, *J* = 8.6 Hz, 2H), 7.03 (s, 1H), 4.28 (s, 3H), 4.20 - 4.23 (m, 1H), 3.91 (d, *J* = 14.1 Hz, 1H), 3.81 (t, *J* = 11.6 Hz, 1H), 3.68 (m, 1H), 3.03 (t, *J* = 12.8 Hz, 1H), 2.88 (m, 1H),

2.05 – 1.96 (m, 1H), 1.58-1.26 (m, 5H), 1.13-1.08 (m, 1H). LC-MS (ESI) (LCT, 3 min) Rt 1.09 min; >95% purity at λ 254 and 210 nm, MS: *m/z* 461.2 [M+1]. Anal. calcd for $C_{19}H_{23}F_3N_4O_4S$: C, 49.56; H, 5.03; N, 12.17. Found: C, 49.50; H, 5.05; N, 11.95.

(*S*)-1-methyl-*N*-(4-((2-(2-morpholinoethyl)piperidin-1-yl)sulfonyl)phenyl)-3-(trifluoromethyl)-1*H*-pyrazole-5-carboxamid (2o). ^{1}H NMR ($CDCl_3$, 400MHz): δ 8.18 (s, 1H), 7.74 - 7.80 (m, 2H), 7.65 - 7.72 (m, 2H), 7.05 (s, 1H), 4.25 (s, 3H), 4.04 - 4.11 (m, 1H), 3.76 (dd, *J* = 4.1, 14.3 Hz, 1H), 3.67 (t, *J* = 4.5 Hz, 1H), 2.97 - 3.08 (m, 1H), 2.23 - 2.45 (m, 6H), 1.78 - 1.90 (m, 1H), 1.55 - 1.66 (m, 1H), 1.30 - 1.53 (m, 5H). LC-MS (ESI) (LCT, 3 min) Rt 0.57 min; >95% purity at λ 254 and 210 nm, MS: *m/z* 530.2 [M+1]. Anal. calcd for $C_{23}H_{30}F_3N_5O_4S.H_2O$: C, 50.45; H, 5.89; N, 12.79. Found: C, 50.98; H, 5.72; N, 12.74.

Ethyl 2-((1-((4-(1-methyl-3-(trifluoromethyl)-1*H*-pyrazole-5-carboxamido)phenyl) sulfonyl)piperidin-2-yl)methoxy)acetate (2p). ^{1}H NMR ($CDCl_3$, 400MHz): δ 8.14 (s, 1H), 7.77 - 7.83 (m, 2H), 7.65 - 7.70 (m, 2H), 7.02 - 7.06 (m, 1H), 4.25 (s, 3H), 4.14 - 4.23 (m, 3H), 3.99 (d, *J* = 3.1 Hz, 2H), 3.73 (d, *J* = 14.1 Hz, 1H), 3.60 - 3.67 (m, 2H), 2.96 - 3.06 (m, 1H), 1.77 (d, *J* = 12.9 Hz, 1H), 1.37 - 1.56 (m, 3H), 1.26 (t, *J* = 8.0 Hz, 3H). LC-MS (ESI) (LCT, 3 min) Rt 1.71 min; >95% purity at λ 254 and 210 nm, MS: *m/z* 533.2 [M+1].

***N*-(4-((2-((2-hydroxyethoxy)methyl)piperidin-1-yl)sulfonyl)phenyl)-1-methyl-3-(trifluoromethyl)-1*H*-pyrazole-5-carboxamide (2q, JMN6-093)**; ^{1}H NMR ($CDCl_3$, 400MHz): δ 8.73 (s, 1H), 7.70 - 7.83 (m, 4H), 7.11 (s, 1H), 4.30 - 4.39 (m, 1H), 4.25 (s, 3H), 3.72 (t, *J* = 9.4 Hz, 2H), 3.58 - 3.68 (m, 2H), 3.45 - 3.54 (m, 2H), 3.40 (d, *J* = 10.6 Hz, 1H), 3.25 (br. s., 1H), 2.98 (td, *J* = 2.5, 13.2 Hz, 1H), 1.63 - 1.74 (m, 2H), 1.35 - 1.63 (m, 3H). Anal. calcd for $C_{20}H_{25}F_3N_4O_5S$: C, 48.97; H, 5.14; N, 11.42. Found: C, 48.94; H, 5.08; N, 11.26.

1-Methyl-*N*-(4-(phenylsulfonyl)phenyl)-3-(trifluoromethyl)-1*H*-pyrazole-5-carboxamide (3a). ^{1}H NMR ($CDCl_3$, 400MHz): δ 8.10 (s, 1H), 7.85 - 7.93 (m, 4H), 7.69 - 7.75 (m, 2H), 7.53 - 7.59 (m, 1H), 7.46 - 7.53 (m, 2H), 7.03 (s, 1H), 4.22 (s, 3H). Anal. calcd for $C_{18}H_{14}F_3N_3O_3S$: C, 52.81; H, 3.45; N, 10.26. Found: C, 52.31; H, 3.41; N, 9.95.

***N*-(4-((2-methoxyphenyl)sulfonyl)phenyl)-1-methyl-3-(trifluoromethyl)-1*H*-pyrazole-5-carboxamide (3b).** ^{1}H NMR ($CDCl_3$, 400MHz): δ 8.11 (dd, *J* = 1.8, 8.0 Hz, 1H), 8.04 (s, 1H), 7.90 - 7.95 (m, 2H), 7.66 - 7.71 (m, 2H), 7.51 - 7.57 (m, 1 H), 7.07 - 7.13 (m, 1 H), 7.02 (s, 1 H), 6.87 - 6.91 (m, 1 H), 4.24 (s, 3 H), 3.76 (s, 3H). LC-MS (ESI) (LCT, 3 min) Rt 1.11 min; >95% purity at λ 254 and 210 nm, MS: *m/z* 440.0 [M+1].

Synthesis of *N*-(4-((2-Hydroxyphenyl)sulfonyl)phenyl)-1-methyl-3-(trifluoromethyl)-1*H*-pyrazole-5-carboxamide (3c). To a solution of **3b** (110.0 mg, 0.250 mmol) in CH_2Cl_2 (6.0 mL), was added BBr_3 (1.0 mL, 1.0 mmol) and the mixture stirred for an overnight. The reaction was cooled to 0 ^oC and $NaHCO_3$ solution (3.0 mL) slowly added. The reaction was allowed to warm to RT and CH_2Cl_2 (9.0 mL) and MeOH (1.0 mL) added. The organic layer was separated and washed with $NaHCO_3$, brine, dried over Na_2SO_4, filtered and concentrated. The product was purified by column (CH_2Cl_2/MeOH) and dried under vacuum to give 106.0 mg of a white solid in 96% yield. ^{1}H NMR ($CDCl_3$, 400MHz): δ 7.86 - 7.92 (m, 2 H), 7.77 - 7.82 (m, 2 H), 7.65 (dd, *J* = 1.6, 8.2 Hz, 1 H), 7.37 - 7.43 (m, 1H), 7.11 (s, 1H), 6.90 - 6.96 (m, 2H), 4.20 (s, 3H). Anal. calcd for $C_{18}H_{14}F_3N_3O_4S$: C, 50.82; H, 3.32; N, 9.88. Found: C, 50.67; H, 3.29; N, 9.61.

Synthesis of 2-((4-(1-Methyl-3-(trifluoromethyl)-1*H*-pyrazole-5-carboxamido)phenyl)sulfonyl)phenylacetate (3d). To a solution of **3c** (52.0 mg, 0.122 mmol) in dimethylformamide (1.0 mL) was added K_2CO_3 (33.8 mg, 0.244 mmol) and acetic anhydride (0.023 mL, 0.244 mmol)

and the mixture allowed to stir for an overnight. DMF was removed under vacuum and the residue purified by column (hexanes/ethylacetate) to give 43.4 mg of **3d** as a white solid in 76% yield. ^{1}H NMR ($CDCl_3$, 400 MHz) δ 8.14 (dd, *J* = 1.76, 8.02 Hz, 1H), 7.87 - 7.93 (m, 3H), 7.70 - 7.76 (m, 2H), 7.58 - 7.63 (m, 1H), 7.41 (dt, *J* = 1.17, 7.83 Hz, 1H), 7.14 (dd, *J* = 0.98, 8.02 Hz, 1H), 6.96 (s, 1H), 4.24 (s, 3H), 2.32 (s, 3H). Anal. calcd for $C_{20}H_{16}F_3N_3O_5S$: C, 51.39; H, 3.45; N, 8.99. Found: C, 51.31; H, 3.32; N, 8.80.

1-Methyl-3-(trifluoromethyl)-*N*-(4-((2-vinylphenyl)sulfonyl)phenyl)-1*H*-pyrazole-5-carboxamide (3e). ^{1}H NMR ($CDCl_3$, 400 MHz) δ 8.12 - 8.17 (m, 1H), 8.08 (s, 1H), 7.76 - 7.83 (m, 2H), 7.65 - 7.71 (m, 2H), 7.51 - 7.59 (m, 2H), 7.41 - 7.50 (m, 2H), 7.02 (s, 1H), 5.52 (dd, *J* = 1.17, 17.22 Hz, 1H), 5.33 (dd, *J* = 0.78, 10.96 Hz, 1H), 4.22 (s, 3H). Anal. calcd for $C_{20}H_{16}F_3N_3O_3S$: C, 55.17; H, 3.70; N, 9.65. Found: C, 54.99; H, 3.60; N, 9.64.

***N*-(4-((2-(Hydroxymethyl)phenyl)sulfonyl)phenyl)-1-methyl-3-(trifluoromethyl)-1*H*-pyrazole-5-carboxamide (3f).** ^{1}H NMR ($CDCl_3$, 400 MHz) δ 8.10 (dd, *J* = 1.17, 7.83 Hz, 1H), 8.00 (s, 1H), 7.84 - 7.90 (m, 2H), 7.71 - 7.77 (m, 2H), 7.59 - 7.65 (m, 1H), 7.48 - 7.57 (m, 2H), 6.98 (s, 1H), 4.73 (d, *J* = 6.26 Hz, 2H), 4.23 (s, 3H). Anal. calcd for $C_{19}H_{16}F_3N_3O_4S$: C, 51.93; H, 3.67; N, 9.56. Found: C, 52.01; H, 3.53; N, 9.40.

1-Methyl-*N*-(4-((2-(morpholinomethyl)phenyl)sulfonyl)phenyl)-3-(trifluoromethyl)-1*H*-pyrazole-5-carboxamide (3g). ^{1}H NMR ($CDCl_3$, 400MHz): □ 8.16 (dd, *J* = 1.2, 7.8 Hz, 1 H), 7.99 (s, 1H), 7.83 - 7.89 (m, 2H), 7.68 - 7.74 (m, 3H), 7.54 - 7.60 (m, 1H), 7.42 - 7.48 (m, 1H), 7.01 (s, 1H), 4.24 (s, 3H), 3.77 (s, 2H), 3.50 - 3.57 (m, 4H), 2.27 (m, 4H). Anal. calcd for $C_{23}H_{23}F_3N_4O_4S$: C, 54.32; H, 4.56; N, 11.02. Found: C, 54.36; H, 4.42; N, 10.85.

BIOLOGY. Antiviral assays and toxicity measurements were performed as described previously.[22]

ACKNOWLEDGEMENTS

This work was supported, in part, by Public Health Service Grants AI071002 and AI085328 (to R. K. P.) from the NIH/NIAID and by Public Health Service Grant HG003918-02 (to J.P.S.) from the NIH. We gratefully acknowledge significant funding support from The Emory Institute for Drug Discovery. We are also grateful to Deborah Culver for solubility testing.

Supporting Information Available.

Experimental details for the preparation of compounds **7a-c**, **2b, 2c, 2d, 2e, 2f, 2g, 2h, 2i, 2j, 2o, 2p, 2q, 3b, 17-19, 3f,** and **3g; Supplementary Scheme S1** (Synthetic Scheme for the synthesis of morpholinyl analog **2o); Supplementary Figure S1 (**Mean plasma concentration following i.v. and p.o. dosing of **2o** in Sprague-Dawley rat); **Supplementary Table S1 (**Summary of **2o** Pharmacokinetic properties). This material is available free of charge via the Internet at http://pubs.acs.org.

ABBREVIATION USED

MeV, measles virus; RNA, ribonucleic acid; RdRp, RNA dependent RNA polymerase; HTS, high-throughput screening; HPIV, human parainfluenza virus; RSV, respiratory syncytial virus; EC_{50}, 50% effective concentration; CC_{50}, 50% cytotoxicity concentration; MOM, methoxymethyl; TBSCl, *t*-butyldimethylsilyl chloride; DIBALH, diisobutylaluminium hydride; MCPBA, meta-chloroperoxybenzoic acid; PK, pharmacokinetic.

Table 1. MeV antiviral action (CPE) of the piperidine series of analogs, (EC_{50}).

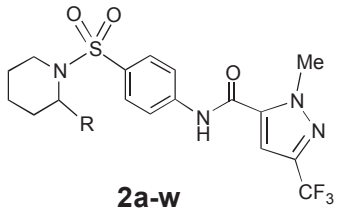

2a-w

Comp.	R	EC_{50} (μM)[a] (MV-Alaska) (CPE inhib.)	Comp.	R	EC_{50} (μM)[a] (MV-Alaska) (CPE inhib.)
2	-H	2.0	**2h**	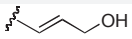	3.7
1a	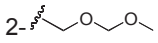	1.5	**2i**	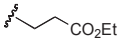	6.7
1b	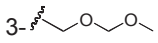	3.8	**2j**	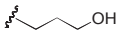	2.7
1c	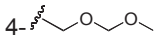	16.0	**2k**	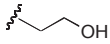	2.7
2a		2.8	**2l**	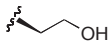	8.3
2b	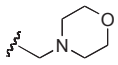	9.3	**2m**	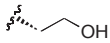	3.1
2c		1.5	**2n**	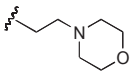	4.6
2d	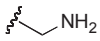	55.0	**2o**	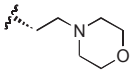	2.5
2e	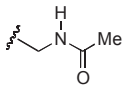	14.0	**2p**	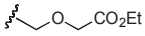	25.0
2f		>150.0	**2q**	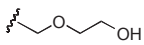	8.3
2g	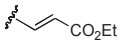	6.8			

[a]values represent averages of four experiments; highest concentration assessed 150 μM

Table 2. MeV antiviral action (CPE) of the phenyl and acyclic series of analogs, (EC_{50}).

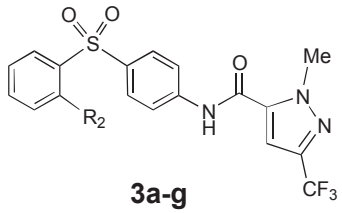

3a-g

Comp.	R_2	EC_{50} (μM)[a] (MV-Alaska) (CPE inhib.)	Comp.	R_2	EC_{50} (μM)[a] (MV-Alaska) (CPE inhib.)
3a	-H	2.8	**3e**		> 50.0
3b	-OMe	3.1	**3f**		3.5
3c	-OH	4.5	**3g**	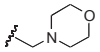	>75.0
3d	-OAc	4.5			

[a]values represent averages of four experiments; highest concentration assessed 75 μM

Table 3. Aqueous solubility, virus yields (EC_{50}) and toxicity (CC_{50}) for selected compounds.

Comp.	Solubility (μg/ml) Test[a]	EC_{50} (μM) (MV-Alaska)		CC_{50}(μM) (MTT cytotox)[d]
		CPE inhibit.[b]	virus titer reduction[c]	
2	<15	2.0	0.014	>75
2a	61	2.8	0.85	>75
2k	62	2.7	0.1	>75
2n	55	4.6	nd	>75
2o	60	2.5	0.06	>75
3a	22	2.8	0.09	>75
3b	<15	3.1	nd	>75
3c	67	4.5	nd	75
3f	46	3.5	nd	>75

[a]solubility data generated through Nephelometer using standard procedure. [b]Values represent averages of four experiments; highest concentration assessed 75 μM, lowest concentration assessed 2.0 μM. [c]Determined only when CPE inhibition-based EC50 concentration < 3.0 μM. [d]Values represent averages of at least three experiments; highest concentration assessed 75 μM.

Table 4. PK Profile for Compounds **2**, **2k** and **2o**

Comp.	oral dose (mg/kg)[a]	T_{max} (hr)	Cmax (ng/mL)[b]	T½ (hr)[b]	AUC (0-t) (hr*ng/mL)[b]	AUC (0-∞) (hr*ng/mL)[b]
2	10	2.5	26.9	12.7	132	513
2	50	2.7	72.2	3.7	308	483
2k	10	1	19.8	0.8	56.3	56.8
2k	50	0.5	184	2.7	754	973
2o	10	1.1	195	2.2	683	818
2o	50	1.5	823	6.5	3521	7860

[a]Study in Sprague-Dawley rat dosed at 10 mg/kg and 50 mg/kg as a suspension in PEG200/0.5% methylcellulose (10/90) formulation, respectively. n = 4 animals per study. [b]Estimation of PK parameters by non-compartmental analysis of these data, which was accomplished using standard PK software (WinNonlin 5.3, Pharsight®).

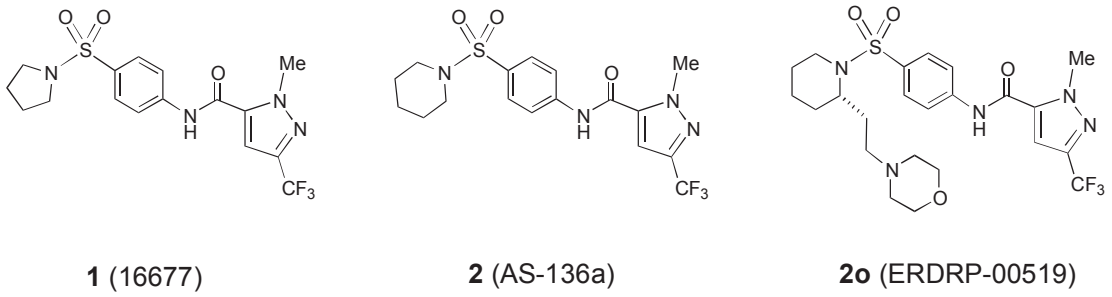

1 (16677) **2** (AS-136a) **2o** (ERDRP-00519)

Figure 1. Structures of hit and lead compounds.

Scheme 1. Exploring the optimal substitution position on the piperidine ring[a]

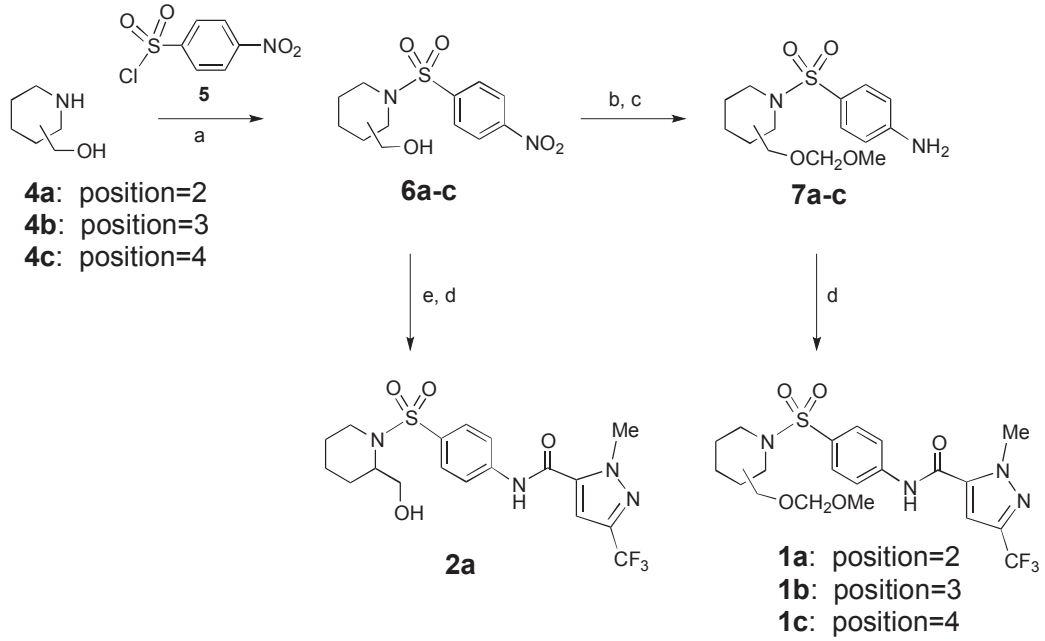

[a]Reagents and conditions: (a) Na_2CO_3, acetone; (b) MOMCl, *i*-Pr_2NEt, CH_2Cl_2; (c) $SnCl_2$. $2H_2O$, EtOAc; (d)

(**8**), Pyridine, CH_2Cl_2; (e) H2 (50 psi), Pd-C, MeOH.

Scheme 2. Synthesis of three-carbon substituents at the piperidine C-2 position[a]

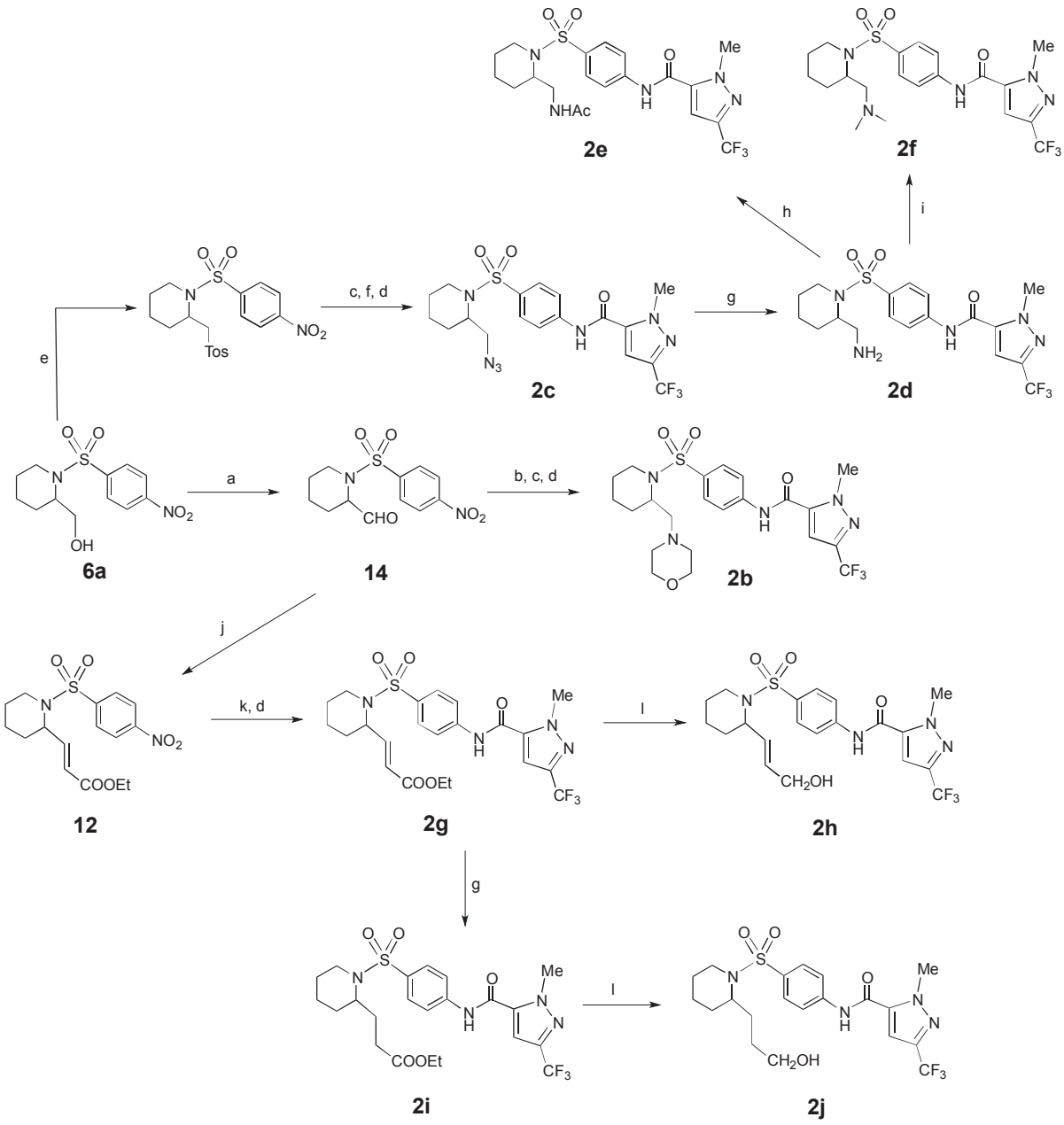

[a]Reagents and conditions: (a) PCC, CH_2Cl_2; (b) morpholine, $NaBH(OAc)_3$, CH_2Cl_2; (c)$SnCl_2.2H_2O$, CH_2Cl_2/MeOH; (d) **8**, *i*-Pr_2NEt, CH_2Cl_2; (e) 4-Toluenesulfonyl chloride, CH_2Cl_2; (f) NaN_3, DMF, 120 ^oC; (g) H_2, Pd/C, MeOH; (h) AcCl, *i*-Pr_2NEt, CH_2Cl_2; (i) CH_3I, K_2CO_3, DMF; (j)) *t*-BuOK, $Et_2P(O)CH_2COOEt$, THF/CH_2Cl_2; (k) $SnCl_2.2H_2O$, EtOAc; (l) DIBAL-H, THF;

Scheme 3. Introduction of a two-carbon tether at the piperidine C-2 position[a]

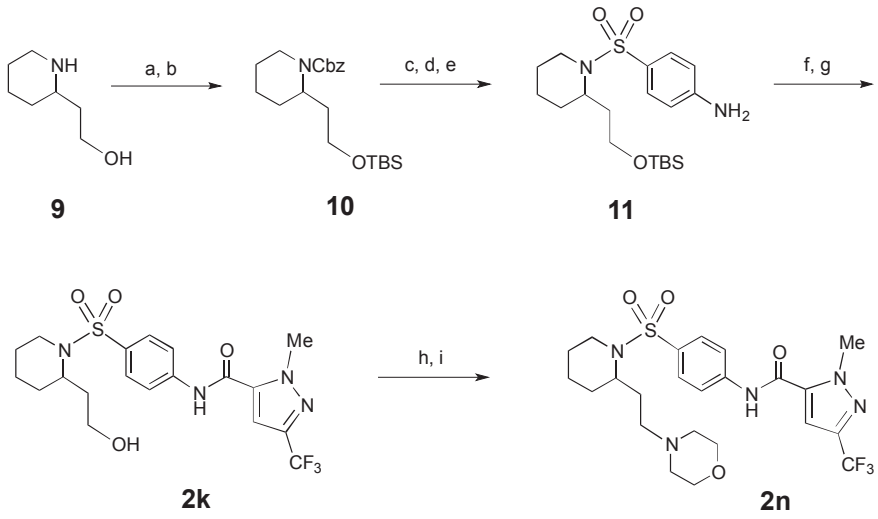

[a]Reagents and conditions: (a) Na_2CO_3, BzOCOCl, H2O/acetone; (b) TBSCl, imidazole, DMF; (c) H_2, Pd/C, ethanol; (d) **5**, *i*-Pr_2NEt, CH_2Cl_2; (e) H_2, Pd/C, ethanol, 40 psi; (f) **8**, *i*-Pr_2NEt, CH_2Cl_2; (g) TBAF, THF; (h) $(COCl)_2$, DMSO, CH_2Cl_2; (i) morpholine, $NaBH(OAc)_3$, CH_2Cl_2.

Scheme 4. Synthesis of O-alkylated analogs[a]

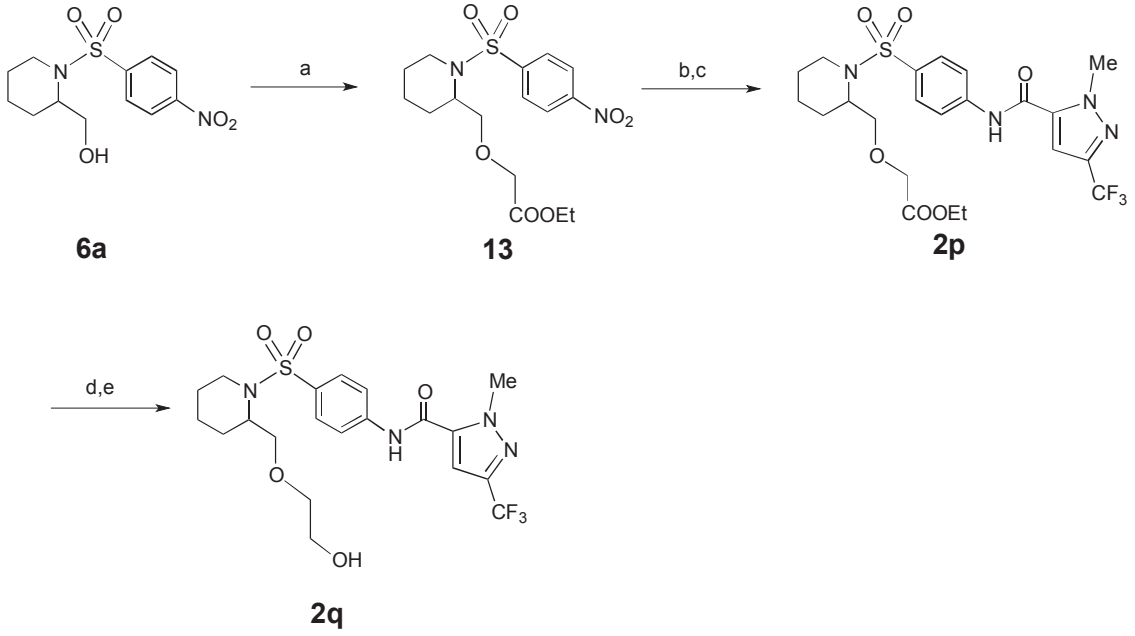

[a]Reagents and conditions: (a) ethyl diazoacetate, Rh_2OAc_4, CH_2Cl_2; (b) H_2, Pd/C, MeOH; (c) **8**, *i*-Pr_2NEt, CH_2Cl_2; (d) NaOH, THF/H_2O; (e) BOP, *i*-Pr_2NEt, THF, $NaBH_4$.

Scheme 5. Synthesis of the phenyl series[a]

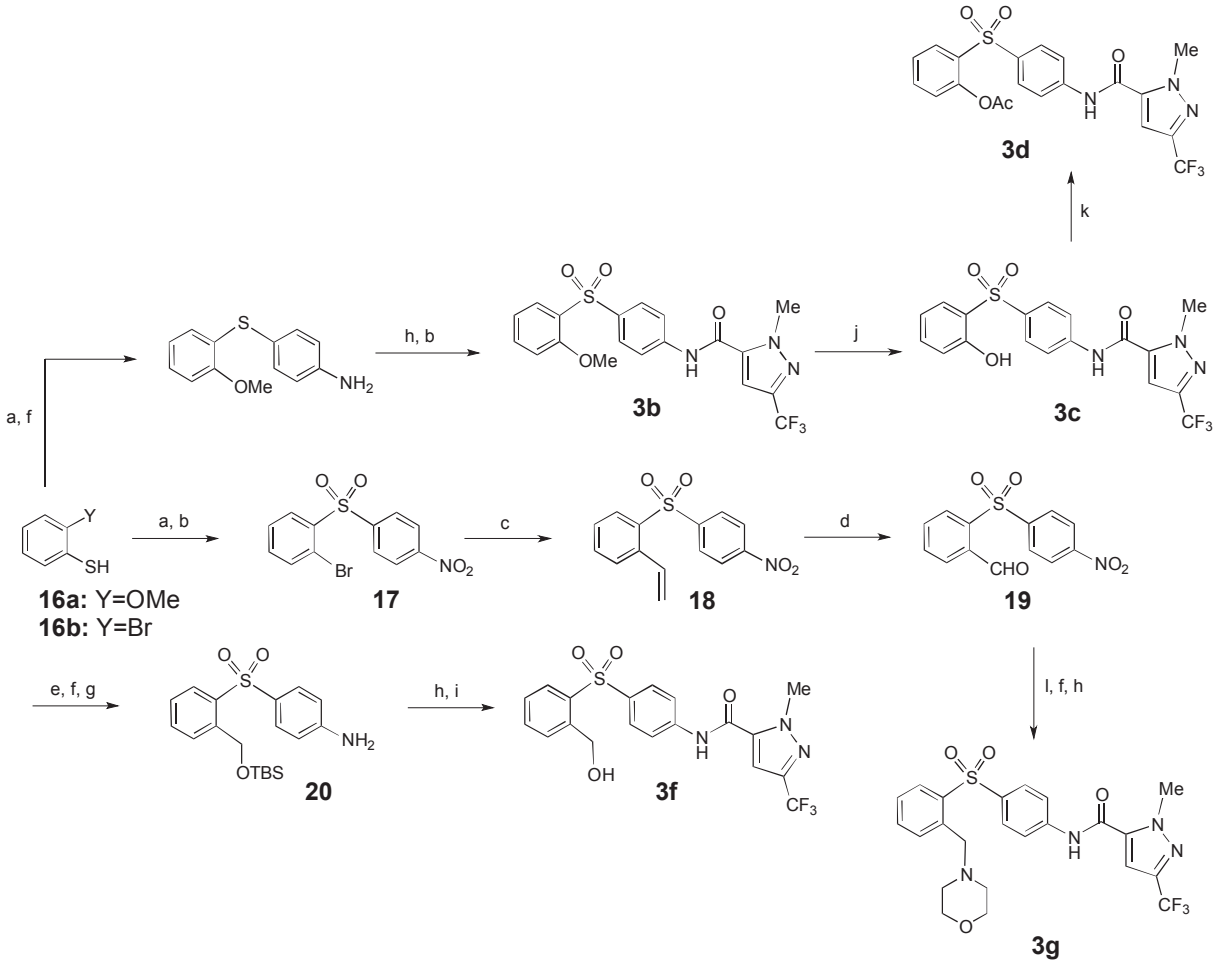

[a]Reagents and conditions: (a) 1-fluoro-4-nitrobenzene, Na_2CO_3, EtOH, 80°C; (b) *m*-CPBA, CH_2Cl_2; (c) tributyl(vinyl)tin, $Pd(PPh_3)_4$, THF, 80°C; (d)OsO_4, $NaIO_4$, THF/H_2O; (e) DIBAL-H, THF; (f) $SnCl_2.2H_2O$, CH_2Cl_2/MeOH; (g) TBSCl, imidazole, DMF; (h) **8**, *i*-Pr_2NEt, CH_2Cl_2; (i) TBAF, THF ; (j) BBr_3, CH_2Cl_2; (k) CH_3COCl, THF; (l) morpholine, $NaBH(OAc)_3$, CH_2Cl_2.

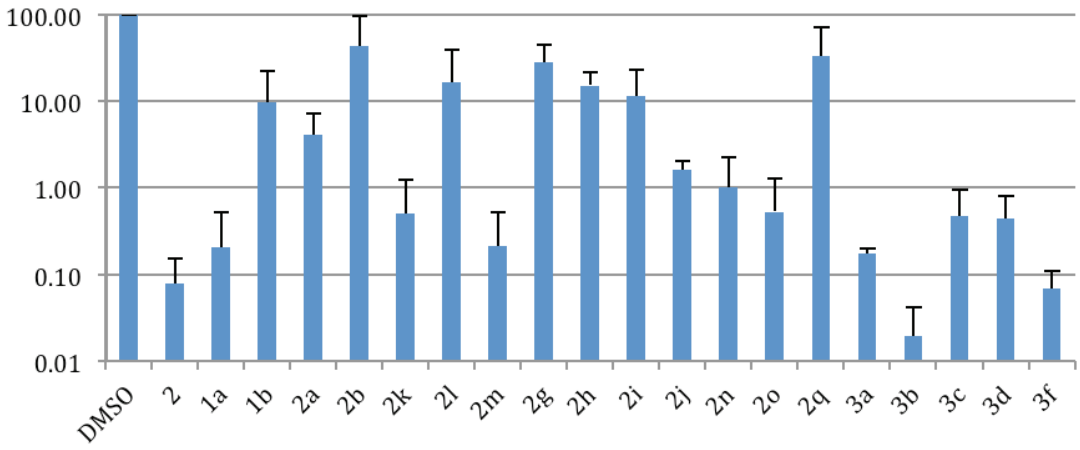

Figure 2. Evaluation of compunds **2** and analogs against MV-Alaska. All compounds were tested at 1.0 μM. Compounds comparable in activity to **2** were further examined at a range of concentrations to generate dose-response curves.

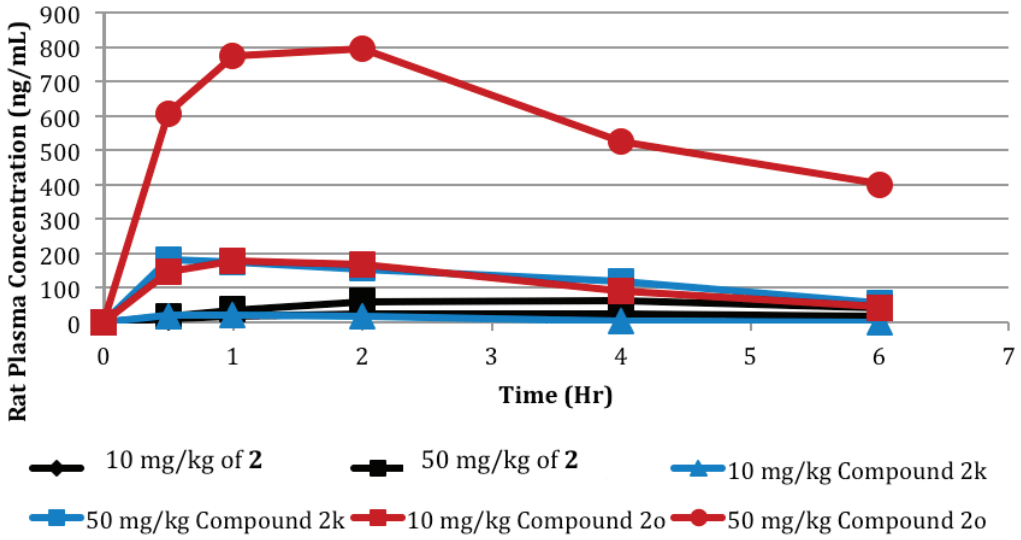

Figure 3. Time course of rat plasma concentration following p.o. dosing by oral gavage. Preliminary pharmacokinetic (PK) studies in the Sprague-Dawley rat compared **2** with compounds **2k** and **2o** following p.o. dosing by oral gavage at 10 mg/kg and 50 mg/kg in a PEG200/0.5% methylcellulose (10/90) vehicle (n=4/group)

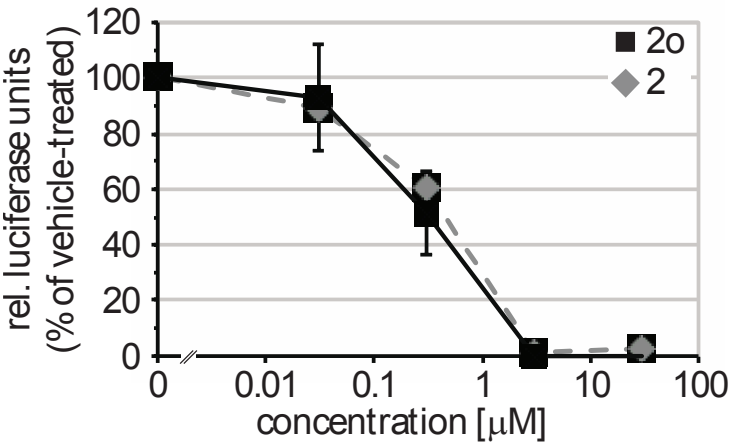

Figure 4. Compounds **2o** and **2** inhibit viral RdRp activity with equal potency. Values are expressed relative to vehicle-treated samples and represent averages of three experiments± SD.

Table of Contents Graphic

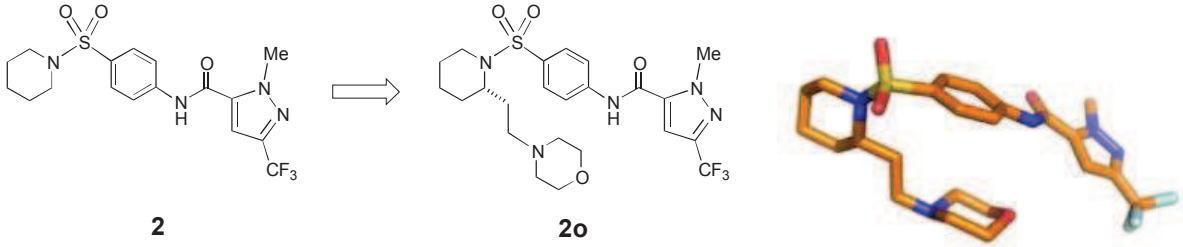

2 **2o**

EC_{50} = 14 nM
Aqueous solubility: < 15 μg/ml

EC_{50} = 60 nM
Aqueous solubility: 60 μg/ml

REFERENCES

(1) Centers for Disease Control and Prevention. Update: measles-United States, January-July 2008. *MMWR Morb. Mortal*. Wkly. Rep. **2008**, *57*, 893–896.

(2) Kremer, J. R., and C. P. Muller. Measles in Europe—there is room for improvement. *Lancet* **2009**, *373*, 356–358.

(3)http://www.oregonlive.com/opinion/index.ssf/2011/01/vaccines_halting_an_epidemic_o.html; http://www.pbs.org/wgbh/pages/frontline/vaccines/view/; last accessed 12/16/11.

(4) http://www.who.int/csr/don/2011_04_21/en/

(5) Chakrabarti, S.; Collingham, K. E.; Holder, K.; Fegan, C. D.; Osman, H.; Milligan, D. W. Pre-emptive oral ribavirin therapy of paramyxovirus infections after haematopoietic stem cell transplantation: a pilot study. *Bone Marrow Transplant*. **2001**, *21*, 759–763.

(6) Shigeta, S.; Mori, S.; Baba, M.; Ito, M.; Honzumi, K.; Nakamura, K.; Oshitani, H.; Numazaki, Y.; Matsuda, A.; T. Obara, T.; Shuto, S.; De Clercq, E. Antiviral activities of ribavirin, 5-ethynyl-1--D-ribofuranosylimidazole-4-carboxamide, and 6-(*R*)-6-*C*-methylneplanocin A against several ortho- and paramyxoviruses. *Antimicrob. Agents Chemother*. **1992***, 36*, 435–439.

(7) Plemper, R. K.; Snyder, J. P. Measles control - can measles virus inhibitors. *Current Opinion in Investigational Drugs* (BioMed Central) **2009**, 10, 811-820.

(8) White, L. K.; Yoon, J.-J.; Lee, J. K.; Sun, A.; Du, Y.; Fu, H.; Snyder, J. P.; Plemper, R. K. Non nucleoside Inhibitor of Measles Virus RNA Dependent RNA Polymerase Complex Activity. *Antimicrob. Agents Chemother.* **2007**, *51*, 2293-2303.

(9) Yoon, J.; Krumm, S. A.; Ndungu, J. M.; Hoffman, V.; Bankamp, B.; Rota, P.A.; Sun, A.; Snyder, J. P.; Plemper, R. K. Target analysis of the experimental measles therapeutic AS-136A *Antimicrob. Agents and Chemother.* **2009**, 53, 3860-3870.

(10) Sun, A.; Chandrakumar, N.; Yoon, J.-J.; Plemper, R. K.; Snyder, J. P. Non nucleoside inhibitors of the measles virus RNA-dependent RNA polymerase activity: Synthesis and in vitro evaluation. *Bioorg. Med. Chem. Lett.* **2007**, *17*, 5199–5203.

(11) Sun, A.; Yoon, J. J. Yin, Y.; Prussia, A.; Yang, Y. Min, J.; Plemper, R. K.; Snyder, J. P. Potent non-nucleoside inhibitors of the measles virus RNA-dependent RNA polymerase complex. *J. Med. Chem*. **2008**, *51*, 3731–3741.

(12) Lahm, G. P.; Selby, T. P.; Freudenberger, J. H.; Stevenson, T. M.; Myers, B. J.; Seburyamo, G.; Smith, B. K.; Flexner, L.; Clark, C. E.; Cordova, D. Insecticidal anthranilic diamides: A new class of potent ryanodine receptor activators. *Bioorg. Med. Chem. Lett*. **2005**, 15, 4898-4906.

(13) See supporting information for a detailed synthesis of **2a** and related compounds.

(14) Tanaka, M.; Nakamura, M.; Ikeda, T.; Ikeda, K.; Ando, H.; Shibutani, Y.; Yajima, S.; Kimura, K. *J. Org. Chem*. **2001**, *66*, 7008-7012.

(15) Paulissen, R.; Reimlinger, H.; Hayez, E.; Hubert, A. J.; Teyssié, P. Transition metal catalysed reaction of diazocompounds - II insertion in the hydroxylic bond. *Tetrahedron Lett*. **1973**, 2233-2236.

(16) Moody, C. J.; Miller, D. J. Synthetic applications of the O-H insertion reactions of carbenes and carbenoids derived from diazocarbonyl and related diazo compounds. *Tetrahedron*, **1995**, *51*, 10811-10843

(17) McGeary, R. P. Facile and chemoselective reduction of carboxylic acids to alcohols using BOP reagent and sodium borohydride. *Tetrahedron Lett*. **1998**, *39*, 3319.

(18) Szadkowska, A.; Makal, A.; Wozniak, K.; Kadyrov, R.; Grela, K. *Organometallics*, **2009**, *28*, 2693-2700.

(19) Sun, H.; Pang, K. S. Permeability, Transport, and Metabolism of Solutes in Caco-2 Cell Monolayers: A Theoretical Study, *Drug Metabolism and Disposition*, **2008**, 36, 102-123.

(20) Sarkadi, B; Homolya, L.; Szakacs, G.; Varadi, A. Human Multidrug Resistance ABCB and ABCG Transporters: Participation in a Chemoimmunity Defense System. *Physiol Rev.* **2006**, 86, 1179-1236.

(21) Krumm, S. A.; Ndungu, J. M.; Dochow, M.; Yoon, J.-J.; Sun, A.; Natchus, M.; Snyder, J. P.; Plemper, R. K. Host-Directed Small-Molecule Inhibitors of Myxovirus RNA-dependent RNA-polymerases. *PLoS ONE,* Epublished 16 May 2011 10.1371/journal.pone.0020069.

(22) Sun, A.; Ndungu, J. M.; Krumm, S. A.; Yoon, Jeong-J.; Thepchatri, P.; Natchus, M.; Plemper, R. K.; Snyder, J. P. Host-directed Inhibitors of Myxoviruses: Synthesis and in vitro Biochemical Evaluation, *ACS Med. Chem. Lett.* **2011**, 2, 798-803.

Publication 6

Melanie Dochow, **Stefanie A Krumm**, James E Crowe Jr, Martin L Moore and Richard K Plemper

“Independent Structural Domains in the Paramyxovirus Polymerase Protein”

THE JOURNAL OF BIOLOGICAL CHEMISTRY, February 2012

JBC accepted manuscript and published in PubMed Central by copyright permission of The American Society for Biochemistry and Molecular Biology, Inc

The Journal of Biological Chemistry
JBC ASBMB
About JBC | This Article | Submissions | Subscriptions | Contact

J Biol Chem. Feb 24, 2012; 287(9): 6878–6891.
Published online Jan 3, 2012. doi: 10.1074/jbc.M111.325258
PMCID: PMC3307299

Independent Structural Domains in *Paramyxovirus* Polymerase Protein*

Melanie Dochow,‡ Stefanie A. Krumm,‡ James E. Crowe, Jr.,§ Martin L. Moore,‡¶ and Richard K. Plemper‡¶,1

From the ‡Department of Pediatrics, Emory University School of Medicine, Atlanta, Georgia 30322,
the §Department of Pediatrics and Pathology, Vanderbilt University Medical Center, Nashville, Tennessee 37232, and
¶Children's Healthcare of Atlanta, Atlanta, Georgia 30322
1 To whom correspondence should be addressed: Dept. of Pediatrics and Children's Healthcare of Atlanta, Emory University School of Medicine, 2015 Uppergate Dr., Atlanta, GA 30322., Tel.: Phone: 404-27-1605; Fax: 404-727-9223; E-mail: rplempe@emory.edu.

Received November 17, 2011; Revised December 21, 2011

Copyright © 2012 by The American Society for Biochemistry and Molecular Biology, Inc.

Abstract

All enzymatic activities required for genomic replication and transcription of nonsegmented negative strand RNA viruses (or Mononegavirales) are believed to be concentrated in the viral polymerase (L) protein. However, our insight into the organization of these different enzymatic activities into a bioactive tertiary structure remains rudimentary. Fragments of Mononegavirales polymerases analyzed to date cannot restore bioactivity through trans-complementation, unlike the related L proteins of segmented NSVs. We investigated the domain organization of phylogenetically diverse *Paramyxovirus* L proteins derived from measles virus (MeV), Nipah virus (NiV), and respiratory syncytial virus (RSV). Through a comprehensive *in silico* and experimental analysis of domain intersections, we defined MeV L position 615 as an interdomain candidate in addition to the previously reported residue 1708. Only position 1708 of MeV and the homologous positions in NiV and RSV L also tolerated the insertion of epitope tags. Splitting of MeV L at residue 1708 created fragments that were unable to physically interact and trans-complement, but strikingly, these activities were reconstituted by the addition of dimerization tags to the fragments. Equivalently split fragments of NiV, RSV, and MeV L oligomerized with comparable efficiency in all homo- and heterotypic combinations, but only the homotypic pairs were able to trans-complement. These results demonstrate that synthesis as a single polypeptide is not required for the Mononegavirales polymerases to adopt a proper tertiary conformation. *Paramyxovirus* polymerases are composed of at least two truly independent folding domains that lack a traditional interface but require molecular compatibility for bioactivity. The functional probing of the L domain architecture through trans-complementation is anticipated to be applicable to all Mononegavirales polymerases.

Keywords: Protein Domains, RNA Polymerase, RNA Viruses, Viral Polymerase, Viral Replication

Introduction

The *Paramyxovirus* family comprises major human and animal pathogens including measles virus (MeV),[2] mumps virus, Newcastle disease virus (NDV), the recently emerged highly pathogenic Nipah virus (NiV), and respiratory syncytia virus (RSV). Collectively, members of the family are responsible for substantial morbidity and mortality worldwide. Belonging to the Mononegavirales, the Paramyxoviridae store all genetic information in a single RNA genome of negative polarity, which is encapsidated by the viral nucleocapsid (N) protein in a protein-RNA (ribonucleoprotein) complex (1). Cytosolic transcription and replication of the viral genome is mediated by the viral RNA-dependent RNA polymerase (RdRp) complex, which includes the ribonucleoprotein and viral P and ~2200-residue L proteins. Besides genome replication, the latter is responsible for viral mRNA synthesis, requiring catalysis of RNA capping, methylation, and polyadenylation in addition to phosphodiester bond formation (1).

Different catalytic activities mediated by a single polypeptide are well compatible with a multidomain architecture, in which individually folding structural domains with discrete functions are connected through linker regions with low intrinsic structure, thus ensuring local concentration of enzymatic activities in a flexible three-dimensional scaffold. Consistent with this model, analysis of purified L proteins of segmented and nonsegmented NSV proteins by electron microscopy supported a structural organization in discernible domains (2, 3). Furthermore, a systematic bioinformatics-based analysis of the L protein of Lassa virus, a distantly related segmented NSV of the *Arenavirus* family, has revealed that the protein can be split at two positions into distinct fragments that are capable of reconstituting RdRp bioactivity through trans-complementation when co-expressed (4). Thus, Lassa virus polymerase is composed of at least three distinct, independently folding-competent structural domains. Comparable trans-complementation studies with Mononegavirales-derived L proteins are limited to date to the L protein of vesicular stomatitis virus (VSV) of the Rhabdoviridae. By contrast to Lassa virus L, a recent report found N- and C-terminal VSV polymerase fragments were unable to trans-complement each other functionally (3), although these VSV L subunits tolerated separation by an enhanced

GFP moiety (5). This was interpreted to reflect that proper tertiary folding of the Mononegavirales polymerase may require synthesis of the protein as a single polypeptide (3).

Based on sequence alignments between different NNSV family representatives, six conserved regions (CR I to CR VI) of higher sequence homology have been identified in the L proteins (6, 7). Of these, the N-terminal sections harboring CR I have been implicated in L oligomerization (8–10) and/or L interaction with P (8, 9, 11–14), CR III in RNA polymerization (15, 16), and CR VI in methyltransferase activity (3, 6, 17). A conserved GXXT_nHR motif in NNSV L CR V, which was first identified in VSV L, is furthermore thought to mediate unusual capping of the viral mRNAs through transfer of 5′-monophosphate-mRNA onto GDP (18, 19). This polyribonucleotidyltransferase activity differs from that of eukaryotic mRNA capping through guanylyltransferases, which transfer guanosine monophosphate to pp-mRNA to form the cap structure (20). Surprisingly, *Paramyxovirus*, but not rhabdovirus, L proteins also may contain traditional guanylyltransferase activity. Purified polymerase of rinderpest virus, a member of the *Morbillivirus* genus within the Paramyxoviridae, reportedly formed covalent guanosine monophosphate L intermediates *in vitro* (21), and a largely conserved guanylyltransferase consensus motif required for transcriptase activity was identified near the C terminus of the human parainfluenza virus (HPIV) type 2 L protein (22).

Within the *Paramyxovirus* family, sequence alignments of different *Morbillivirus* genus polymerases suggested three large regions (LR I to LR III) separated by variable connectors (23, 24). Of these, LR I harbors CR I and II and thus the oligomerization domain, and LR II contains CR III-CR V including the predicted polymerase and polyribonucleotidyltransferase activities, whereas LR III is considered to encompass the methyltransferase and recently proposed guanylyltransferase functions. Similar to recent reports for VSV L (5), L proteins of MeV, the archetype of the *Morbillivirus* genus, and rinderpest virus furthermore tolerated insertions into the LR II/LR III but not the LR I/LR II junction (23, 25), consistent with at least a two-domain organization. However, a comprehensive analysis of the *Paramyxovirus* L domain architecture and direct assessment of whether *Paramyxovirus* L fragments located on either side of the LR II/LR III intersection remain competent for folding when expressed separately remains elusive. In analogy to the findings obtained for VSV L (3), synthesis as an intact polypeptide may constitute a generally conserved prerequisite for Mononegavirales L bioactivity.

To dissect fundamental principles that govern NNSV polymerase folding, we examined in this study three phylogenetically diverse *Paramyxovirus* L proteins. Commencing with MeV L, we employed *in silico* structure predictions combined with experimental evaluation to identify individual folding domain candidates. Guided by this screen, we generated split MeV, NiV, and RSV L pairs and explored their ability to reconstitute RdRp activity in biochemical and functional assays. Our results demonstrate that *Paramyxovirus* polymerases are composed of at least two discrete structural domains that are capable of independent folding. Neither section contains a high affinity protein-protein interface, but close physical proximity and homotypic origin from the same L protein are essential for restoring RdRp bioactivity. These findings illuminate basic principles of NNSV polymerase architecture and provide a tangible path toward characterizing the structural organization of distantly related Mononegavirales polymerases beyond the *Paramyxovirus* family. They guide the identification of meaningful NNSV substructures that may be more suitable for x-ray crystallographic analysis than full-length L proteins.

EXPERIMENTAL PROCEDURES

Cell Culture and Transfection Baby hamster kidney (BHK-21) cells stably expressing T7 polymerase (BSR-T7/5) (26) were maintained at 37 °C and 5% CO_2 in Dulbecco's modified Eagle's medium supplemented with 10% fetal bovine serum and incubated at every third passage in the presence of G-418 (Geneticin) at a concentration of 100 μg/ml. Lipofectamine 2000 (Invitrogen) was used for cell transfections.

Replicon Reporter Systems Base vectors for all MeV replicon experiments were previously reported plasmids containing the MeV-Edmonston (Edm) strain-derived L, N, or P open reading frames under the control of the T7 promoter (27). To generate an MeV luciferase replicon reporter construct, the terminal untranslated regions of the MeV genome were added to the firefly luciferase open reading frame (Promega) through recombination PCR (all oligonucleotide primers used in this study are listed in supplemental Table 1, entries #1–7) followed by replacement of the chloramphenicol (CAT) reporter cassette in the previously reported MeV-CAT replicon plasmid (27) with the sequence-confirmed recombination product. For NiV, previously described plasmids containing the NiV L, N, or P open reading frames and a NiV-CAT reporter construct were used as starting material (28). Sequence-optimized cDNA copies encoding the RSV L, N, P, or M2–1 genes based on the strain RSV A2 were synthesized *in vitro* (GeneArt; codon-optimized sequences are shown in supplemental Table 2) and cloned into the pcDNA3.1 expression vector (Invitrogen). The RSV minigenome reporter pRSVlucM5 was constructed reminiscent of a previously described RSV minigenome (29). Four overlapping oligonucleotides were annealed to form a 238-bp DNA fragment containing a terminal BamHI site, the upstream 32 nucleotide (nt) nonstructural protein 1 (NS1) nontranslated region, the 10-nt RSV NS1 gene start signal, a 44-nt RSV leader sequence, a 94-bp hammerhead ribozyme, a 47-bp T7 terminator, and a NotI compatible end (supplemental Table 1; entries #8–11). A 191-bp DNA fragment containing a terminal HindIII site, a 155-nt RSV trailer sequence, the 12-nt RSV L gene end sequence, a 12-nt nontranslated region of RSV L, and an XhoI site was synthesized *in vitro* (Integrated DNA Technologies; supplemental Table 1, entry #12). These two fragments were ligated along with a BamHI/XhoI fragment of firefly luciferase cDNA

(pGEM-luc, Promega) into the NotI and HindIII sites of pcDNA3.1 such that an antisense copy of luciferase flanked by RSV leader and trailer regulatory elements is produced by T7 polymerase transcription.

Mutagenesis and Generation of Expression Plasmids For linker insertion scanning, the MeV L expression plasmid was subjected to PCR amplification using primers that duplicate the codon at the insertion site and introduce an AfeI restriction site (supplemental Table 1, entries #13–36). Amplicons were subjected to DpnI digest to remove template material followed by digestion with AfeI and ligation. Correct insertion of the linker domain was confirmed by DNA sequencing. Analogous strategies were employed to introduce streptactin SII-triple FLAG tandem tags into MeV L or triple HA tags into MeV, NiV, and RSV L (supplemental Table 1, entries #37–40 for MeV L SII-FLAG tagging; entries # 41–44 for MeV L HA tagging; entries #45–48 for NiV L HA tagging; entries #49–52 for RSV L HA tagging).

To generate the MeV $L_{N\text{-}frag}$ expression construct, a stop codon was introduced in-frame downstream of the SII-FLAG tag in the MeV L_{FLAG} expression plasmid (supplemental Table 1, entry #53) using directed mutagenesis after the QuikChange protocol (Stratagene). Correct insertion was confirmed by sequence analysis and immunoblotting. To generate the MeV $L_{C\text{-}frag}$ construct, a SpeI site followed by an ATG start codon was introduced in MeV L_{HA} frame upstream of the HA tag (supplemental Table 1, entry #54) through PCR amplification of the C-terminal fragment. A SpeI/SalI fragment of the sequence-confirmed amplicon was then ligated into the SpeI/SalI-digested MeV L expression vector, thus replacing the L gene with the new insert.

To add a GCN4 tag to the MeV $L_{N\text{-}frag}$ construct, the BstBI site in the SII-FLAG cassette was first removed through directed mutagenesis (supplemental Table 1, entry #55). Using appropriate primers (supplemental Table 1, entries #56–57), the GCN4 tag was introduced through PCR amplification followed by DpnI digest of the template DNA and recirculation of the amplicon after BstBI digest. An equivalent strategy was employed for GCN4 tagging of the MeV $L_{C\text{-}frag}$ construct using primers annealing at the third copy of the HA tag and the ATG start codon, respectively (supplemental Table 1, entries #58–59). To generate SII-FLAG-tagged $L_{N\text{-}frag\text{-}GCN4}$ expression constructs of NiV and RSV L, the SII-FLAG-GCN4 cassette of MeV $L_{N\text{-}frag\text{-}GCN4}$ was amplified followed by joining in frame to the N termini of the L fragments through recombination PCR (supplemental Table 1, entries #60–63 for NiV; entries #66–69 for RSV). Sequence-confirmed amplicons were transferred into the NiV or RSV L expression plasmids. HA-tagged $L_{C\text{-}frag\text{-}GCN4}$ expression constructs of NiV and RSV L were generated through PCR-mediated insertion of the GCN4 sequence (supplemental Table 1, entries #64–65 for NiV L_{HA}; entries #70–71 for RSV L_{HA}). Silent BstBI (NiV L) or BlpI (RSV L) restriction sites introduced into the GCN4-encoding sequences enabled re-circularization of the amplicons after DpnI-mediated removal of the template DNA and digestion with BstBI or BlpI, respectively. All constructs were sequence confirmed before further experimentation.

Minireplicon Reporter Assays of RdRp Activity BSR-T7/5 cells (2.5×10^5 per well in a 12-well plate format) were transfected with plasmid DNAs encoding the viral RdRp components (unless otherwise specified, DNA amounts were for MeV: MeV-L (1.1 μg), MeV-N (0.4 μg), and MeV-P (0.3 μg); for NiV: NiV-L (0.2 μg), NiV-N (0.63 μg), and NiV-P (0.4 μg); for RSV, RSV-L (0.1 μg), RSV-M2 (0.15 μg), RSV-N (0.17 μg), and RSV-P (0.15 μg)), and 1 μg of the MeV or RSV luciferase replicon reporter or the NiV CAT replicon reporter plasmid. Control wells included identical amounts of reporter and helper plasmids but lacked the plasmids harboring the respective L gene or, for some experiments, L fragment subunits. In all cases vector (pUC19) DNA was added as necessary so that all transfection mixtures contained identical amounts of total DNA. Thirty-eight hours post-transfection, cells were lysed, and luciferase activities in cleared lysates were determined using Bright-Glo luciferase substrate (Promega) and an Envision Multilabel microplate reader (PerkinElmer Life Sciences), or CAT concentrations were assessed using a CAT-ELISA assay system (Roche Applied Science). Statistical significance of results was determined where indicated using Student's *t* test.

SDS-PAGE and Immunoblotting BSR-T7/5 cells (5×10^5) were transfected with 3 μg of plasmid DNA encoding MeV, NiV, or RSV L protein or L protein fragments as specified. Thirty-eight hours post-infection cells were washed in phosphate-buffered saline (PBS), lysed for 10 min at 4 °C in lysis buffer (50 mM Tris, pH 8.0, 62.5 mM EDTA, 0.4% deoxycholate, 1% Igepal (Sigma)) containing protease inhibitors (Complete mix (Roche Applied Science)) and 1 mM phenylmethylsulfonyl fluoride (PMSF), and centrifuged at 20,000 × *g* for 10 min at 4 °C. Cleared lysates were mixed with equal volumes of urea buffer (200 mM Tris-Cl, pH 6.8, 8 M urea, 5% sodium dodecyl sulfate (SDS), 0.1 mM EDTA, 0.03% bromphenol blue, 1.5% dithiothreitol) and incubated for 30 min at 50 °C. Samples were fractionated on SDS-polyacrylamide gels, blotted to polyvinylidene difluoride membranes (Millipore), and subjected to enhanced chemiluminescence detection (Amersham Biosciences) using specific antibodies directed against the FLAG (M2; Sigma) or HA (16B12; Abcam) epitopes, cellular GAPDH (Ambion), or MeV P (Chemicon) as specified. Blots were developed using a ChemiDoc XRS digital imaging system (Bio-Rad), and signals were assessed with the Image Lab software package.

Co-immunoprecipitation BSR-T7/5 cells (5×10^5/well) were transfected with plasmid DNA encoding MeV, NiV, or RSV L, different $L_{N\text{-}frag}$ or $L_{C\text{-}frag}$ subunits, or MeV P as specified in the individual experiments. At 38 h post-transfection, cells were washed 5 times with cold PBS and lysed in co-immunoprecipitation buffer (10 mM Tris, pH 7.4, 150 mM NaCl, 1% deoxycholate, 1% Triton X-100, 0.1% sodium dodecyl sulfate (SDS), protease inhibitors (Roche Applied Science), and 1 mM PMSF). Cleared lysates (20,000 × *g*; 30 min; 4 °C) were incubated with specific antibodies directed against the FLAG or HA epitopes as specified at 4 °C, followed by precipitation with immobilized protein G (Pierce) at 4 °C. Precipitates were washed 3 times each in buffer A (100 mM

Tris, pH 7.6, 500 mM lithium chloride, 0.1% Triton X-100), then buffer B (20 mM HEPES, pH 7.2, 2 mM EGTA, 10 mM magnesium chloride, 0.1% Triton X-100) followed by resuspension in urea buffer. Denatured samples were fractionated on SDS-polyacrylamide gels (4–20% gradient or 10% depending on the antigenic material assessed) followed by immunoblotting and chemiluminescence detection using specific antibodies directed against the FLAG or HA epitopes, cellular GAPDH, or MeV P as described above.

In Silico Assessment of Protein Domain Architecture For DomCut (30)-based identification of candidate linker insertion sites, *Paramyxovirus* L protein sequences were aligned using the ClustalW2 (31) and MUSCLE (32) algorithm as alternative solutions in three distinct settings representing 1) different MeV genotypes, 2) a diverse panel of morbilliviruses, or 3) members of all *Paramyxovirus* genera. For each individual input sequence, interdomain linkers were predicted, and relative DomCut propensity scores then averaged separately based on the different sequence alignments. DomCut values for all residues that lacked an L-Edm homologue were excluded. Input L sequences were derived from MeV-Edm (genotype A) (33), MeV-Gambia (genotype B2) (34), MeV-Gambia (genotype B3.2) (35), MeV-Toulon (genotype C2) (36), MeV-Illinois (genotype D3) (34), MeV-Alaska (genotype H2) (37) for (*1*), MeV-Edm, MeV-Gambia B2, MeV-Gambia B3.2, MeV-Toulon, MeV-Illinois, MeV-Alaska, rinderpest virus-KabeteO (38), rinderpest virus-RBOK (39), canine distemper virus Onderstepoort (40), canine distemper virus 5804 (41), peste des petits ruminants virus Turkey 2000 (42), dolphin *Morbillivirus* (43) for (*2*), or MeV-Edm, canine distemper virus 5804, NIV (44), HPIV type 1 C35 (45), HPIV type 3 LZ22 (46), HPIV type 2 (47), HPIV type 4 SKPIV4 (48), NDV-ISG0210 (GenBank™ JF340367), Tupaia *Paramyxovirus* (49), RSV A2 (50), human metapneumovirus Sabana (51) for (*3*). MeDor (52) was employed to independently predict disordered domains in L-Edm using the IUPred (53), GlobPlot2 (54), DisEMBL (55), FoldIndex (56), and RONN (57) algorithms. In addition, MeV L-Edm was submitted to PONDR-FIT (58) and DRIP-PRED (59) for disorder predictions. To assess the consensus of all algorithms quantitatively, GlobPlot2, FoldIndex, and DomCut average values were shifted to positive integers, and positive output scores of all algorithms were normalized for identical hit cut-off values, averaged, transformed to a 0–10 scale, and plotted as a function of L-Edm residues. MeV L-Edm secondary structure prediction was based on the StrBioLib library of the Pred2ary program (60, 61) embedded in the MeDor package.

RESULTS

In Silico Domain Analysis of Paramyxovirus L Protein Based on the concept that protein domains are the smallest autonomously folding-competent units within a protein structure (62), linker regions connecting individual domains are expected to show little structural order and comparably low sequence conservation. A variety of predictive algorithms have been developed that seek to identify intrinsically disordered proteins or disordered sections within a protein by means of specific sequence signatures of unstructured regions (63, 64). Because combining different predictors that explore discrete biophysical parameters reportedly boosts the accuracy of the prediction (52, 65, 66), we employed a panel of algorithms for a comprehensive *in silico* analysis of candidate interdomain boundaries within the *Paramyxovirus* L protein (Fig. 1, *A* and *B*).

The DomCut package predicts candidate linker regions based on a data set of domain/linker segments (30). We targeted three groups of viruses in these studies. Focusing on MeV L as the initial target for experimental assessment, we generated average DomCut interdomain propensity scores for L protein sequences representing a variety of MeV genotypes. We then examined different members of the *Morbillivirus* genus and finally members of each genus of the Paramyxovirinae and Pneumovirinae subfamilies of the Paramyxovirinae in this way. DomCut output scores then were cross-referenced quantitatively (Fig. 1*A*) and graphically (Fig. 1*B*) with the MeDor (MEtaserver of DisOrder (52)), PONDR-FIT meta-predictor (58), and DRIP-PRED (59) predictors of unstructured sections, resulting in a total application of eight algorithms. These studies highlighted 12 candidate regions in MeV L that were located between CR I and CR VI, received combined propensity scores of ≥4, and were identified by at least two of the algorithms employed. Focusing on the L core, potential interdomain regions located in the N-terminal first 408-amino acid section of MeV L, which mediates both L interaction with the viral P protein and polymerase oligomerization (8, 14), and candidates positioned downstream of the LR II/LR III junction (residues 1695–1717 (23, 24)) were not considered for experimental evaluation.

Linker Insertion Analysis of MeV Polymerase Organization To assess the quality of the *in silico* predictions, 10-residue hydrophilic linker peptides were engineered into each of the selected regions. In addition, two L variants were generated that contain HA or streptactin-FLAG epitope insertions at position 1708 in the LR II/LR III junction, guided by a previously described epitope-tagged MeV L construct (23, 25). To determine the effect of linker insertions on L bioactivity, we employed a replicon reporter system that contains a firefly luciferase reporter gene flanked by the MeV non-coding genome termini. Co-expression of this construct with MeV N, P, and L proteins generated N-encapsidated RNA of negative polarity that served as the template for luciferase mRNA synthesis by the viral RdRp complex. Variation of the molar ratio of transfected L-encoding plasmid DNA relative to N- and P-encoding plasmids revealed a steep optimum curve with peak luciferase activities measured at 0.14:0.09 and 0.06 pmol (L:N and P) of plasmid DNA transfected (Fig. 1*C*, signal:background, 320 at peak luciferase activity). Subsequent experiments were performed at this molar ratio.

When examining the different L variants with linker insertions in this assay, we found that the L-Arg-615 linker construct returned

significant luciferase activity equivalent to ~60% that of standard L, whereas all other L variants lacked appreciable bioactivity (Fig. 1*D*). Replacement of the linker domain at residue 615 with streptactin-FLAG or HA epitope tags, however, substantially reduced L bioactivity to <1% that of standard L. Consistent with previous experiments (23), insertion of these epitope tags at position 1708 in the C-terminal hypervariable region did not abolish L activity (Fig. 1*D*).

A previous molecular characterization of MeV L regions necessary for interaction with the viral P protein highlighted the N-terminal L residues 1–408 as directly required for P binding (14). To explore whether epitope insertion at L position 615 compromises the interaction with P, we examined the physical interaction of the proteins biochemically. Both bioactive L-Asn-1708-HA and inactive L-Arg-615-HA efficiently and specifically co-immunoprecipitated the P protein (Fig. 1*E*), suggesting unperturbed hetero-oligomerization of the proteins.

These results support a model in which the overall MeV L architecture comprises at least three sections that tolerate further separation through linker insertion without eliminating bioactivity. Loss of L activity after insertion of FLAG or HA epitope tags at position 615 suggests, however, that this region stands overall under tighter structural scrutiny than the LR II/LR III junction. Although P is still bound efficiently, introduction of a higher content of charged (FLAG) or aromatic/charged (HA) residues is overall not tolerated at position 615.

Independently Expressed L Fragments Assume a Physiological Conformation To assess whether L domains located up- or downstream of residue 1708 are capable of truly independent folding or require synthesis as a single polypeptide to assume their physiological conformation, we split the L gene at this position and generated separate expression plasmids for the corresponding N- and C-terminal fragments (termed $L_{N\text{-}frag}$ and $L_{C\text{-}frag}$). Streptactin-FLAG and HA epitope tags were added to the newly generated N and C termini, respectively, to facilitate the biochemical characterization of the discrete L fragments.

To test the hypothesis that the reciprocal affinity of independently expressed L domains may be low, even if folding-competent, we generated a second set of L expression plasmids in which additional GCN4 affinity tags (67) were added to the N and C termini of the L fragments (detailed in Fig. 2*A*). These tags were expected to induce intracellular dimerization of the independently synthesized constructs. All four L variants were synthesized and showed the anticipated mobility pattern when expressed individually followed by SDS-PAGE and immunodetection using antibodies directed against the different epitope tags (Fig. 2*B*).

Despite efficient fragment expression, co-transfection of plasmids encoding $L_{N\text{-}frag}$ and $L_{C\text{-}frag}$ without the GCN4 tags at equimolar DNA ratios returned essentially background luciferase activities in the replicon reporter assay. This finding was independent of the combined amount of L fragment-encoding DNA added (Fig. 2*C*). In striking contrast, the presence of the GCN4 dimerization domains at the L fragments significantly restored L bioactivity, resulting in a luciferase activity optimum curve largely mimicking that described above for standard L (Fig. 2*C*). Successful trans-complementation was dependent on GCN4-mediated oligomerization of $L_{N\text{-}frag\ GCN4}$ and $L_{C\text{-}frag\ GCN4}$, as alternative complementation attempts between $L_{N\text{-}frag}$ and $L_{C\text{-}frag\ GCN4}$ or between $L_{N\text{-}frag\ GCN4}$ and $L_{C\text{-}frag}$ did not restore bioactivity (data not shown).

Reciprocal co-immunoprecipitation of the GCN4-tagged or untagged fragments, either through precipitation with specific antibodies directed against the HA epitope followed by immunodetection with anti-FLAG antibodies or through anti-FLAG precipitation and anti-HA detection, yielded results consistent with the bioactivity data; efficient co-precipitation of the fragments was observed only in the presence of the additional GCN4 dimerization domains (Fig. 2*D*).

These data demonstrate that the MeV L sections located up- or downstream of residue 1708 have no biochemically detectable affinity for each other, arguing against the presence of a traditional protein-protein interface between the $L_{N\text{-}frag}$ and $L_{C\text{-}frag}$ subunits. Both fragments are capable, however, of folding into a physiological conformation when expressed separately, as reinstating the physical proximity of the L subunits post-translationally through added GCN4 dimerization domains restored RdRp activity.

Dominant-negative Effect of $L_{N\text{-}frag}$ and $L_{C\text{-}frag}$ Subunits on Full-length L Bioactivity To assess the full extent of functional complementation, we generated replicon-based RdRp activity curves for a set of different $L_{N\text{-}frag\ GCN4}$ and $L_{C\text{-}frag\ GCN4}$ plasmid DNA ratios ranging from 3.5:1 to 1:3.5. Bioactivity peaked when cells received equimolar amounts of L fragment-encoding plasmid DNA or a slight (1:1.75) excess of $L_{C\text{-}frag\ GCN4}$, whereas increasing the relative amount of $L_{N\text{-}frag\ GCN4}$ resulted in a significant reduction of RdRp activity (Fig. 3*A*). Co-expression of an excess of the $L_{N\text{-}frag}$ subunit with standard L confirmed a dominant-negative effect of this fragment on RdRp activity (Fig. 3*B*). Overexpression of the $L_{C\text{-}frag}$ subunit relative to standard L at a 4:1 plasmid DNA ratio did not significantly affect bioactivity of standard L. Surprisingly, we observed a reduction in activity by ~50% at a 10:1 $L_{C\text{-}frag}$:L ratio, suggesting a dominant negative effect of $L_{C\text{-}frag}$ at high relative excess.

Consistent with previous studies locating the P binding domain in the N-terminal 408-residue section of MeV L (14), we found the $L_{N\text{-}frag}$ but not the $L_{C\text{-}frag}$ subunit to be capable of efficient co-precipitation of the P protein (Fig. 3*C*). Competition for P binding between $L_{N\text{-}frag}$ and standard L thus emerges as a possible basis for the dominant-negative phenotype associated with this fragment in the RdRp activity assays. By analogy, the inhibitory effect of the $L_{C\text{-}frag}$ subunit seen at high excess could be due to direct interaction of the fragment with the corresponding C-terminal domain in standard L. To test this hypothesis, we attempted

co-immunoprecipitation of $L_{C\text{-}frag}$ and full-length L. As seen before (Fig. 3*C*) for interaction with P, however, no biochemically appreciable interaction between the $L_{C\text{-}frag}$ and standard L was detectable in this assay (Fig. 3*D*), whereas the GCN4-tagged $L_{N\text{-}frag}$ and $L_{C\text{-}frag}$ subunits added for control efficiently co-precipitated. This result was independent of whether cells were transfected with all plasmids of the minireplicon system (shown in Fig. 3*D*) or only with plasmids encoding the L variants and P protein (data not shown).

These observations re-emphasize proper folding of the $L_{N\text{-}frag}$ subunit, enabling it to compete for interaction with RdRp complex components. Unexpectedly, the data also suggest the possibility of weak interactions between the $L_{C\text{-}frag}$ subunit and full-length L or P proteins, which may be responsible for the dominant negative effect associated with the fragment at high molar excess but cannot be detected biochemically.

Epitope Tag Insertions in RSV and NiV L To explore whether the organization of MeV L into at least two independently folding functional domains constitutes a general feature of *Paramyxovirus* L proteins, we identified residues homologous to MeV L amino acid 1708 in polymerase proteins of two additional *Paramyxovirus*es in search of sites suitable for L splitting. For this proof-of-concept approach, NiV and RSV L proteins were chosen based on their diverse phylogenetic proximity to MeV; NiV, like MeV a member of the Paramyxoviridae subfamily albeit of the *Henipavirus* genus, is closely related to MeV. By contrast, RSV is a member of the *Pneumovirus* subfamily and thus a far more distantly related representative of the Paramyxoviridae (1). Separate sequence alignments of a panel of *Paramyxovirus* L proteins using ClustalW2 (31) and MUSCLE (32) as alternative algorithms posited NiV and RSV L proteins to exhibit different patterns relative to MeV polymerase (Fig. 4, *A* and *B*). In the case of RSV L in particular, residues predicted to be homologous to MeV L 1708 differed by 54 amino acids, exceeding the total length of the LR II/LR III junction in MeV L.

We, therefore, first prescreened the different predictions experimentally through HA epitope insertion in analogy to the MeV $L_{HA\text{-}(1708)}$ construct. Gel fractionation of transfected cell lysates and immunoblotting revealed expression of all tagged NiV and RSV L variants (Fig. 4*C*). However, cytosolic steady state levels varied relative to each other in the case of the NiV L constructs or were substantially reduced in the case of the RSV L_{HA} variants relative to MeV $L_{HA\text{-}(1708)}$. When analyzed in homotypic NiV and RSV replicon reporter assays, both NiV L variants nevertheless returned similar RdRp activities, ~40–60% that observed for standard NiV L, despite the difference in expression levels (Fig. 4*D*). In contrast, the two RSV L variants showed significant differences in bioactivity ranging from ~60% that of standard RSV L in the case of RSV $L_{HA\text{-}(1749)}$ to only 10% in the case RSV $L_{HA\text{-}(1695)}$ (Fig. 4*E*).

Thus, we identified at least one position for each L protein, at which significant RdRp bioactivity was retained in the reporter assays after HA epitope insertion. In the case of RSV L, ClustalW-based predictions were superior to those obtained through MUSCLE-driven alignment. Based on these results, residues 1763 in NiV L and 1749 in RSV L were chosen for L protein splitting and subsequent trans-complementation experiments.

Homo- and Heterotypic Trans-complementation of MeV, NiV, and RSV L All RSV and NiV L fragments were generated with added FLAG or HA epitope tags and terminal GCN4 dimerization domains in analogy to the MeV $L_{N\text{-}frag}$ and $L_{C\text{-}frag}$ subunits. When subjected to replicon-based quantification of RdRp activity, we observed that both the NiV and RSV L fragment pairs were capable of significant trans-complementation of bioactivity similar to our initial finding with the MeV L fragments (Fig. 5, *A–C*). In contrast, co-expressing the different L fragments in all possible heterotypic combinations did not result in the recovery of any significant L bioactivity, indicating the inability of L fragments to interact productively with each other when derived from different *Paramyxovirus*es (Fig. 5, *A–C*).

To test whether the lack of productive interaction was due to inefficient GCN4 domain-mediated L subunit dimerization under heterotypic conditions, we subjected all fragment combinations examined to co-immunoprecipitation experiments relying on the additionally added FLAG and HA epitope tags for precipitation and immunodetection. As expected, all L subunits were synthesized successfully when expressed alone or in combination with the different counterpart fragments (Fig. 5, *D* and *E*, whole cell lysate panels). Importantly, all C-terminal L fragments were also capable of efficiently co-precipitating the different N-terminal fragments regardless of their virus origin (Fig. 5, *D* and *E*, immunoprecipitation panels), confirming full functionality of the GCN4 domains under both homo- and heterotypic conditions and hence equally productive dimerization of the different L fragment combinations.

These data demonstrate that a molecular organization into at least two independent folding domains constitutes a general feature of *Paramyxovirus* polymerases, as all homotypic L fragment combinations tested returned significant bioactivity in the replicon assays. Failure of trans-complementation between the heterotypic L pairs despite efficient, GCN4-mediated fragment hetero-oligomerization reveals that molecular compatibility between the subunits is required for RdRp activity. Although a biochemically appreciable high affinity protein-protein interface is lacking between the *Paramyxovirus* L N- and C-terminal fragments, physical proximity of the subunits alone is necessary but not sufficient for RdRp bioactivity.

DISCUSSION

Reflecting their central position in the life cycle of all RNA viruses, RNA-dependent RNA polymerases are determinants for viral pathogenesis and constitute attractive targets for antiviral therapeutics (68, 69). Crystal structures, either free or complexed with nucleic acid substrates, are available for RdRps derived from a variety of different viral families (70–72). These structures revealed a conserved fundamental organization of the proteins into a geometry resembling a "right-hand" shape in which the "fingers," "palm," and "thumb" domains are thought to ensure the correct positioning of substrates and metal ion cofactors (71, 73). Although it has been proposed that this basic shape may be conserved in all nucleotide polymerases (74), our basic understanding of Mononegavirales L protein structure and organization remains in its infancy.

Examining different L proteins derived from representatives of the Paramyxovirinae and Pneumovirinae subfamily, our study illuminates three principles of *Paramyxovirus* polymerase folding. First, the proteins are composed of a set of at least two truly independent structural units that are competent of proper folding. Second, assuming an enzymatically active tertiary conformation does not require synthesis of the protein as a single polypeptide and, consequently, does not adhere to an integrated folding concept. Third, molecular compatibility between the discrete subunits is essential for functionality, but the subunits lack a high affinity protein-protein interface. Several lines of evidence support these conclusions.

Our bioinformatics analysis has highlighted multiple candidate regions in the *Paramyxovirus* L protein that may represent domain boundaries. The identification of the MeV L LR II/LR III intersection as a candidate zone by several of the algorithms used supports the validity of the *in silico* predictions, as successful expansion of this region was reported previously for *Morbillivirus* L proteins (23, 25). Our subsequent linker insertion scan confirmed these data and, by extending successful epitope insertion to distantly related L proteins, illuminated a conserved *Paramyxovirus* polymerase organization into at least two distinct sections. In addition, we identified an N-terminal position in MeV L, residue 615 located downstream of the N-terminal L-P and L-L oligomerization domain (8, 14), that likewise tolerates enlargement without eliminating L bioactivity. This finding did not extend, however, to acceptance of FLAG or HA epitope tags, which contain a high density of charged or bulky aromatic amino acids (75, 76) and are thus expected to be structurally more active than the 10-residue linker used in the primary scan. Interestingly, L proteins of the *Arenavirus* family reportedly comprise at least three independent folding domains (4).

Based on our data, we conclude with confidence that at least two defined structural domains are present in *Paramyxovirus* polymerases. The N-terminal fragment harbors P binding, polymerase and polyribonucleotidyltransferase activities, whereas the C-terminal section contains methyltransferase and guanylyltransferase motifs and thus contributes predominantly to the generation of proper mRNA cap structures. Although comparative evaluations of different algorithms have demonstrated that a combination of discrete predictors has the highest prospect to maximize the overall accuracy of the prediction (52, 65, 66), our study also highlights the limitations of currently available *in silico* tools when applied to very large polypeptides such as Mononegavirales L proteins. Therefore, additional domain intersections may well exist in the *Paramyxovirus* L protein that were not detected by our *in silico* analysis and experimental evaluation.

We have shown that the addition of GCN4 dimerization domains to independently expressed *Paramyxovirus* L N- and C-terminal fragments results in significant trans-complementation of RdRp bioactivity. These data demonstrate that post-translational interaction of individually synthesized polypeptides is sufficient for the formation of a catalytically active tertiary structure. Because the replicon reporter system used in our study first generates T7-polymerase-driven RNA molecules of negative polarity, luciferase reporter activity confirms full transcriptase functionality, comprising RNA polymerization, polyadenylation, and capping and methylation of the non-covalently linked N- and C-terminal L fragments. Differently composed NNSV polymerase oligomers are thought to carry out replicase and transcriptase activities. Although replicase activity is mediated by an L-P-N core complex, the transcriptase comprises cellular proteins in addition to L and P (77–79). Although in all cases statistically significant, luciferase activity levels representing reconstituted complexes did not reach the level of those obtained with standard L. This finding does not necessarily reflect, however, that non-covalently linked complexes are inherently less bioactive. A major contributing factor to lower activity may be that GCN4 mediated interactions are not intrinsically geared toward mediating enzymatically productive $L_{N\text{-}frag}/L_{C\text{-}frag}$ dimerization events but will most likely drive the formation of $L_{N\text{-}frag}$ and $L_{C\text{-}frag}$ homodimers with equal affinity. Our observation that a 3.5-fold molar excess of either fragment is sufficient to reduce RdRp activity substantially in the replicon trans-complementation assay supports this notion.

Last, the co-precipitation experiments and functional RdRp assays performed in the absence of additional GCN4 tags demonstrate that the L fragments, albeit competent for folding, have no biochemically appreciable inherent affinity for each other. The previously reported lack of VSV L trans-complementation (3) suggests that this may, in fact, constitute a general theme of Mononegavirales L domain interaction, which stands in stark contrast to the strong inherent domain affinities observed for L proteins of segmented negative strand RNA viruses of the *Arenavirus* family (4). Successful splitting of all three *Paramyxovirus* polymerase proteins analyzed in our study at homologous positions and the presence of comparable catalytic motifs in methyltransferase in CR VI (6, 17, 81, 82) and guanolyl-transferase near the C terminus (21, 22) in the MeV, NiV, and RSV $L_{C\text{-}frag}$ subunits support that the different L C-terminal fragments harbor equivalent enzymatic activities. Clearly, bringing the *Paramyxovirus* L N- and C-terminal fragments into close physical proximity is a prerequisite for reconstituting RdRp activity. If proximity alone were sufficient for complementation, however, heterotypic trans-complementation between L fragments derived

from different *Paramyxovirus* family members and brought into proximity through GCN4-mediated dimerization should have been successful. Because heterotypic complementation did not restore functionality despite efficient biochemical interaction of the various fragments, our data suggest an architectural model of Mononegavirales L proteins in which independently folding subdomains do not share a traditional protein-protein interface but require low affinity molecular compatibility to achieve functionality.

Mammalian cells are not capable of RNA-dependent RNA polymerization, rendering the viral RdRp complexes attractive targets for antiviral therapies. Novel nucleoside and allosteric inhibitors of hepatitis C virus polymerase, for instance, are at different stages of clinical evaluation and show strong drug potential (83–85). Experimentally tested allosteric blockers of *Paramyxovirus* polymerase likewise combine high potency with minimal cytotoxicity, opening a desirably large therapeutic window (86, 87). High resolution information about the Mononegavirales polymerase core structure would pave the path for structure-guided *de novo* drug design efforts, the informed optimization of existing inhibitor scaffolds, and the proactive design of inhibitor protected against rapid viral escape from inhibition. At present, high resolution structures of L have not been solved for any of the NNSV family members. Identifying structurally meaningful fragments that assume a physiological conformation when expressed independently emerges as a valid strategy toward obtaining structural insight. Confirming proper folding of candidate *Paramyxovirus* L fragments through successful trans-complementation after the addition of GCN4 dimerization tags provides a novel approach toward achieving this goal, which is most likely transferable to the analysis of Mononegavirales L proteins that do not originate from members of the *Paramyxovirus* family.

Supplementary Material

Supplemental Data:

Acknowledgments

We thank A. L. Hammond for critical reading of the manuscript, P. A. Rota for expression plasmids encoding NIV N, P, and L and the NIV replicon reporter construct, and J. P. Snyder and A. Prussia for helpful discussions concerning implementation of the DomCut algorithm.

*This work was supported, in whole or in part, by National Institutes of Health Grants AI071002 and AI085328 (NIAID to R. K. P.).

S This article contains supplemental Tables 1 and 2.

2 The abbreviations used are:

MeV measles virus
NiV Nipah virus
L polymerase protein
N nucleocapsid protein
NNSV nonsegmented negative-strand RNA virus
RSV respiratory syncytial virus
VSV vesicular stomatitis virus
RdRp RNA-dependent RNA polymerase, CR, conserved region
LR large region
HPIV human parainfluenza virus
Edm MeV-Edmonston
CAT chloramphenicol
nt nucleotide
P phosphoprotein.

REFERENCES

1. Lamb R. A., Parks G. D. (2007) in Fields Virology (Knipe D. M., Howley P. M., editors. , eds) pp. 1449–1496, 5 Ed., Wolters Kluwer/Lippincott Williams & Wilkins, Philadelphia

2. Kranzusch P. J., Schenk A. D., Rahmeh A. A., Radoshitzky S. R., Bavari S., Walz T., Whelan S. P. (2010) Assembly of a functional Machupo virus polymerase complex. Proc. Natl. Acad. Sci. U.S.A. 107, 20069–20074 [PMCID: PMC2993349] [PubMed: 20978208]

3. Rahmeh A. A., Schenk A. D., Danek E. I., Kranzusch P. J., Liang B., Walz T., Whelan S. P. (2010) Molecular architecture of the vesicular stomatitis virus RNA polymerase. Proc. Natl. Acad. Sci. U.S.A. 107, 20075–20080 [PMCID: PMC2993402] [PubMed: 21041632]

4. Brunotte L., Lelke M., Hass M., Kleinsteuber K., Becker-Ziaja B., Günther S. (2011) Domain structure of Lassa virus L protein. J. Virol. 85, 324–333 [PMCID: PMC3014181] [PubMed: 20980514]

5. Ruedas J. B., Perrault J. (2009) Insertion of enhanced green fluorescent protein in a hinge region of vesicular stomatitis virus L polymerase protein creates a temperature-sensitive virus that displays no virion-associated polymerase activity *in vitro*. J. Virol. 83, 12241–12252 [PMCID: PMC2786726] [PubMed: 19793815]

6. Poch O., Blumberg B. M., Bougueleret L., Tordo N. (1990) J. Gen. Virol. 71, 1153–1162 [PubMed: 2161049]

7. Sidhu M. S., Menonna J. P., Cook S. D., Dowling P. C., Udem S. A. (1993) Canine distemper virus L gene. Sequence and comparison with related viruses. Virology 193, 50–65 [PubMed: 8438585]

8. Cevik B., Holmes D. E., Vrotsos E., Feller J. A., Smallwood S., Moyer S. A. (2004) The phosphoprotein (P) and L binding sites reside in the N terminus of the L subunit of the measles virus RNA polymerase. Virology 327, 297–306 [PubMed: 15351217]

9. Cevik B., Smallwood S., Moyer S. A. (2003) The L-L oligomerization domain resides at the very N terminus of the sendai virus L RNA polymerase protein. Virology 313, 525–536 [PubMed: 12954219]

10. Smallwood S., Moyer S. A. (2004) The L polymerase protein of parainfluenza virus 3 forms an oligomer and can interact with the heterologous Sendai virus L, P, and C proteins. Virology 318, 439–450 [PubMed: 14972569]

11. Holmes D. E., Moyer S. A. (2002) The phosphoprotein (P) binding site resides in the N terminus of the L polymerase subunit of sendai virus. J. Virol. 76, 3078–3083 [PMCID: PMC135992] [PubMed: 11861877]

12. Chattopadhyay A., Shaila M. S. (2004) Rinderpest virus RNA polymerase subunits. Mapping of mutual interacting domains on the large protein L and phosphoprotein p. Virus Genes 28, 169–178 [PubMed: 14976416]

13. Chandrika R., Horikami S. M., Smallwood S., Moyer S. A. (1995) Mutations in conserved domain I of the Sendai virus L polymerase protein uncouple transcription and replication. Virology 213, 352–363 [PubMed: 7491760]

14. Horikami S. M., Smallwood S., Bankamp B., Moyer S. A. (1994) An amino-proximal domain of the L protein binds to the P protein in the measles virus RNA polymerase complex. Virology 205, 540–545 [PubMed: 7975255]

15. Malur A. G., Gupta N. K., De Bishnu P., Banerjee A. K. (2002) Analysis of the mutations in the active site of the RNA-dependent RNA polymerase of human parainfluenza virus type 3 (HPIV3) Gene Expr. 10, 93–100 [PubMed: 12064576]

16. Sleat D. E., Banerjee A. K. (1993) Transcriptional activity and mutational analysis of recombinant vesicular stomatitis virus RNA polymerase. J. Virol. 67, 1334–1339 [PMCID: PMC237502] [PubMed: 8382299]

17. Ferron F., Longhi S., Henrissat B., Canard B. (2002) Viral RNA polymerases. A predicted 2′-O-ribose methyltransferase domain shared by all Mononegavirales. Trends Biochem. Sci. 27, 222–224 [PubMed: 12076527]

18. Li J., Rahmeh A., Morelli M., Whelan S. P. (2008) A conserved motif in region v of the large polymerase proteins of nonsegmented negative-sense RNA viruses that is essential for mRNA capping. J. Virol. 82, 775–784 [PMCID: PMC2224588] [PubMed: 18003731]

19. Ogino T., Banerjee A. K. (2007) Unconventional mechanism of mRNA capping by the RNA-dependent RNA polymerase of vesicular stomatitis virus. Mol. Cell 25, 85–97 [PubMed: 17218273]

20. Shuman S., Lima C. D. (2004) The polynucleotide ligase and RNA capping enzyme superfamily of covalent nucleotidyltransferases. Curr. Opin. Struct. Biol. 14, 757–764 [PubMed: 15582400]

21. Gopinath M., Shaila M. S. (2009) RNA triphosphatase and guanylyl transferase activities are associated with the RNA polymerase protein L of rinderpest virus. J. Gen. Virol. 90, 1748–1756 [PubMed: 19297608]

22. Nishio M., Tsurudome M., Garcin D., Komada H., Ito M., Le Mercier P., Nosaka T., Kolakofsky D. (2011) Human parainfluenza virus type 2 L protein regions required for interaction with other viral proteins and mRNA capping. J. Virol. 85, 725–732 [PMCID: PMC3020016] [PubMed: 21068245]

23. Duprex W. P., Collins F. M., Rima B. K. (2002) Modulating the function of the measles virus RNA-dependent RNA polymerase by insertion of green fluorescent protein into the open reading frame. J. Virol. 76, 7322–7328 [PMCID: PMC136336] [PubMed: 12072530]

24. McIlhatton M. A., Curran M. D., Rima B. K. (1997) Nucleotide sequence analysis of the large (L) genes of phocine distemper virus and canine distemper virus (corrected sequence). J. Gen. Virol. 78, 571–576 [PubMed: 9049407]

25. Brown D. D., Rima B. K., Allen I. V., Baron M. D., Banyard A. C., Barrett T., Duprex W. P. (2005) Rational attenuation of a *Morbillivirus* by modulating the activity of the RNA-dependent RNA polymerase. J. Virol. 79, 14330–14338

[PMCID: PMC1280234] [PubMed: 16254367]

26. Buchholz U. J., Finke S., Conzelmann K. K. (1999) Generation of bovine respiratory syncytial virus (BRSV) from cDNA. BRSV NS2 is not essential for virus replication in tissue culture, and the human RSV leader region acts as a functional BRSV genome promoter. J. Virol. 73, 251–259 [PMCID: PMC103829] [PubMed: 9847328]

27. Sidhu M. S., Chan J., Kaelin K., Spielhofer P., Radecke F., Schneider H., Masurekar M., Dowling P. C., Billeter M. A., Udem S. A. (1995) Rescue of synthetic measles virus minireplicons. Measles genomic termini direct efficient expression and propagation of a reporter gene. Virology 208, 800–807 [PubMed: 7747454]

28. Halpin K., Bankamp B., Harcourt B. H., Bellini W. J., Rota P. A. (2004) Nipah virus conforms to the rule of six in a minigenome replication assay. J Gen Virol 85, 701–707 [PubMed: 14993656]

29. Grosfeld H., Hill M. G., Collins P. L. (1995) RNA replication by respiratory syncytial virus (RSV) is directed by the N, P, and L proteins. Transcription also occurs under these conditions but requires RSV superinfection for efficient synthesis of full-length mRNA. J. Virol. 69, 5677–5686 [PMCID: PMC189426] [PubMed: 7637014]

30. Suyama M., Ohara O. (2003) DomCut. Prediction of interdomain linker regions in amino acid sequences. Bioinformatics 19, 673–674 [PubMed: 12651735]

31. Larkin M. A., Blackshields G., Brown N. P., Chenna R., McGettigan P. A., McWilliam H., Valentin F., Wallace I. M., Wilm A., Lopez R., Thompson J. D., Gibson T. J., Higgins D. G. (2007) ClustalW and ClustalX version 2.0. Bioinformatics 23, 2947–2948 [PubMed: 17846036]

32. Edgar R. C. (2004) MUSCLE. Multiple sequence alignment with high accuracy and high throughput. Nucleic Acids Res. 32, 1792–1797 [PMCID: PMC390337] [PubMed: 15034147]

33. Parks C. L., Lerch R. A., Walpita P., Wang H. P., Sidhu M. S., Udem S. A. (2001) Comparison of predicted amino acid sequences of measles virus strains in the Edmonston vaccine lineage. J. Virol. 75, 910–920 [PMCID: PMC113987] [PubMed: 11134304]

34. Bankamp B., Bellini W. J., Rota P. A. (1999) Comparison of L proteins of vaccine and wild-type measles viruses. J. Gen. Virol. 80, 1617–1625 [PubMed: 10423129]

35. Druelle J., Sellin C. I., Waku-Kouomou D., Horvat B., Wild F. T. (2008) Wild type measles virus attenuation independent of type I IFN. Virol. J. 5, 22. [PMCID: PMC2275253] [PubMed: 18241351]

36. Moulin E., Beal V., Jeantet D., Horvat B., Wild T. F., Waku-Kouomou D. (2011) Molecular characterization of measles virus strains causing subactute sclerosing panencephalitis in France in 1977 and 2007. J. Med. Virol. 83, 1614–1623 [PubMed: 21739453]

37. Plemper R. K., Doyle J., Sun A., Prussia A., Cheng L. T., Rota P. A., Liotta D. C., Snyder J. P., Compans R. W. (2005) Design of a small molecule entry inhibitor with activity against primary measles virus strains. Antimicrob. Agents Chemother. 49, 3755–3761 [PMCID: PMC1195431] [PubMed: 16127050]

38. Baron M. D., Kamata Y., Barras V., Goatley L., Barrett T. (1996) The genome sequence of the virulent Kabete O strain of rinderpest virus. Comparison with the derived vaccine. J. Gen. Virol. 77, 3041–3046 [PubMed: 9000095]

39. Baron M. D., Barrett T. (1995) Sequencing and analysis of the nucleocapsid (N) and polymerase (L) genes and the terminal extragenic domains of the vaccine strain of rinderpest virus. J. Gen. Virol. 76, 593–602 [PubMed: 7897350]

40. Gassen U., Collins F. M., Duprex W. P., Rima B. K. (2000) Establishment of a rescue system for canine distemper virus. J. Virol. 74, 10737–10744 [PMCID: PMC110948] [PubMed: 11044118]

41. von Messling V., Springfeld C., Devaux P., Cattaneo R. (2003) A ferret model of canine distemper virus virulence and immunosuppression. J. Virol. 77, 12579–12591 [PMCID: PMC262577] [PubMed: 14610181]

42. Bailey D., Banyard A., Dash P., Ozkul A., Barrett T. (2005) Full genome sequence of peste des petits ruminants virus, a member of the *Morbillivirus* genus. Virus Res. 110, 119–124 [PubMed: 15845262]

43. Rima B. K., Collin A. M., Earle J. A. (2005) Completion of the sequence of a cetacean *Morbillivirus* and comparative analysis of the complete genome sequences of four morbilliviruses. Virus Genes 30, 113–119 [PubMed: 15744569]

44. Chua K. B., Bellini W. J., Rota P. A., Harcourt B. H., Tamin A., Lam S. K., Ksiazek T. G., Rollin P. E., Zaki S. R., Shieh W., Goldsmith C. S., Gubler D. J., Roehrig J. T., Eaton B., Gould A. R., Olson J., Field H., Daniels P., Ling A. E., Peters C. J., Anderson L. J., Mahy B. W. (2000) Nipah virus. A recently emergent deadly *Paramyxovirus*. Science 288, 1432–1435 [PubMed: 10827955]

45. Takimoto T., Bousse T., Portner A. (2000) Molecular cloning and expression of human parainfluenza virus type 1 L gene. Virus Res. 70, 45–53 [PubMed: 11074124]

46. Yang H. T., Jiang Q., Zhou X., Bai M. Q., Si H. L., Wang X. J., Lu Y., Zhao H., He H. B., He C. Q. (2011) Identification of a natural human serotype 3 parainfluenza virus. Virol. J. 8, 58. [PMCID: PMC3045893] [PubMed: 21306605]

47. Nishio M., Tsurudome M., Ito M., Garcin D., Kolakofsky D., Ito Y. (2005) Identification of *Paramyxovirus* V protein residues essential for STAT protein degradation and promotion of virus replication. J. Virol. 79, 8591–8601 [PMCID: PMC1143765] [PubMed: 15956600]

48. Yea C., Cheung R., Collins C., Adachi D., Nishikawa J., Tellier R. (2009) The complete sequence of a human parainfluenza virus 4 genome. Viruses 1, 26–41 [PMCID: PMC3185463] [PubMed: 21994536]

49. Tidona C. A., Kurz H. W., Gelderblom H. R., Darai G. (1999) Isolation and molecular characterization of a novel cytopathogenic *Paramyxovirus* from tree shrews. Virology 258, 425–434 [PubMed: 10366580]

50. Whitehead S. S., Juhasz K., Firestone C. Y., Collins P. L., Murphy B. R. (1998) Recombinant respiratory syncytial virus (RSV) bearing a set of mutations from cold-passaged RSV is attenuated in chimpanzees. J. Virol. 72, 4467–4471 [PMCID: PMC109683] [PubMed: 9557743]

51. Palacios G., Lowenstine L. J., Cranfield M. R., Gilardi K. V., Spelman L., Lukasik-Braum M., Kinani J. F., Mudakikwa A., Nyirakaragire E., Bussetti A. V., Savji N., Hutchison S., Egholm M., Lipkin W. I. (2011) Human metapneumovirus infection in wild mountain gorillas, Rwanda. Emerg. Infect. Dis. 17, 711–713 [PMCID: PMC3377396] [PubMed: 21470468]

52. Lieutaud P., Canard B., Longhi S. (2008) BMC Genomics 9, S25. [PMCID: PMC2559890] [PubMed: 18831791]

53. Dosztányi Z., Csizmok V., Tompa P., Simon I. (2005) IUPred. Web server for the prediction of intrinsically unstructured regions of proteins based on estimated energy content. Bioinformatics 21, 3433–3434 [PubMed: 15955779]

54. Linding R., Russell R. B., Neduva V., Gibson T. J. (2003) GlobPlot. Exploring protein sequences for globularity and disorder. Nucleic Acids Res. 31, 3701–3708 [PMCID: PMC169197] [PubMed: 12824398]

55. Linding R., Jensen L. J., Diella F., Bork P., Gibson T. J., Russell R. B. (2003) Protein disorder prediction. Implications for structural proteomics. Structure 11, 1453–1459 [PubMed: 14604535]

56. Prilusky J., Felder C. E., Zeev-Ben-Mordehai T., Rydberg E. H., Man O., Beckmann J. S., Silman I., Sussman J. L. (2005) FoldIndex. A simple tool to predict whether a given protein sequence is intrinsically unfolded. Bioinformatics 21, 3435–3438 [PubMed: 15955783]

57. Yang Z. R., Thomson R., McNeil P., Esnouf R. M. (2005) RONN. The bio-basis function neural network technique applied to the detection of natively disordered regions in proteins. Bioinformatics 21, 3369–3376 [PubMed: 15947016]

58. Xue B., Dunbrack R. L., Williams R. W., Dunker A. K., Uversky V. N. (2010) PONDR-FIT. A meta-predictor of intrinsically disordered amino acids. Biochim. Biophys. Acta 1804, 996–1010 [PMCID: PMC2882806] [PubMed: 20100603]

59. Deleted in proof.

60. Chandonia J. M., Karplus M. (1999) New methods for accurate prediction of protein secondary structure. Proteins 35, 293–306 [PubMed: 10328264]

61. Chandonia J. M. (2007) StrBioLib. A Java library for development of custom computational structural biology applications. Bioinformatics 23, 2018–2020 [PubMed: 17537750]

62. Schaeffer R. D., Daggett V. (2011) Protein folds and protein folding. Protein Eng. Des. Sel. 24, 11–19 [PMCID: PMC3003448] [PubMed: 21051320]

63. Oldfield C. J., Cheng Y., Cortese M. S., Brown C. J., Uversky V. N., Dunker A. K. (2005) Comparing and combining predictors of mostly disordered proteins. Biochemistry 44, 1989–2000 [PubMed: 15697224]

64. Uversky V. N., Radivojac P., Iakoucheva L. M., Obradovic Z., Dunker A. K. (2007) Prediction of intrinsic disorder and its use in functional proteomics. Methods Mol. Biol. 408, 69–92 [PubMed: 18314578]

65. Ferron F., Longhi S., Canard B., Karlin D. (2006) A practical overview of protein disorder prediction methods. Proteins 65, 1–14 [PubMed: 16856179]

66. Ferron F., Rancurel C., Longhi S., Cambillau C., Henrissat B., Canard B. (2005) VaZyMolO. A tool to define and classify modularity in viral proteins. J. Gen. Virol. 86, 743–749 [PubMed: 15722535]

67. Harbury P. B., Zhang T., Kim P. S., Alber T. (1993) A switch between two-, three-, and four-stranded coiled coils in GCN4

leucine zipper mutants. Science 262, 1401–1407 [PubMed: 8248779]

68. De Clercq E. (2004) Antivirals and antiviral strategies. Nat. Rev. Microbiol. 2, 704–720 [PubMed: 15372081]

69. Ferrer-Orta C., Agudo R., Domingo E., Verdaguer N. (2009) Structural insights into replication initiation and elongation processes by the FMDV RNA-dependent RNA polymerase. Curr. Opin. Struct. Biol. 19, 752–758 [PubMed: 19914060]

70. Ng K. K., Arnold J. J., Cameron C. E. (2008) Structure-function relationships among RNA-dependent RNA polymerases. Curr. Top. Microbiol. Immunol. 320, 137–156 [PMCID: PMC2441838] [PubMed: 18268843]

71. Ferrer-Orta C., Arias A., Escarmís C., Verdaguer N. (2006) A comparison of viral RNA-dependent RNA polymerases. Curr. Opin. Struct. Biol. 16, 27–34 [PubMed: 16364629]

72. Tao Y. J., Ye Q. (2010) RNA virus replication complexes. PLoS Pathog. 6, e1000943. [PMCID: PMC2908549] [PubMed: 20661480]

73. Brautigam C. A., Steitz T. A. (1998) Structural and functional insights provided by crystal structures of DNA polymerases and their substrate complexes. Curr. Opin. Struct. Biol. 8, 54–63 [PubMed: 9519297]

74. Cheetham G. M., Steitz T. A. (2000) Insights into transcription. Structure and function of single-subunit DNA-dependent RNA polymerases. Curr. Opin. Struct. Biol. 10, 117–123 [PubMed: 10679468]

75. Hopp T. P., Gallis B., Prickett K. S. (1988) A short polypeptide marker sequence useful for recombinant protein identification and purification. Bio/Technology 6, 1204–1210

76. Field J., Nikawa J., Broek D., MacDonald B., Rodgers L., Wilson I. A., Lerner R. A., Wigler M. (1988) Purification of a RAS-responsive adenylyl cyclase complex from *Saccharomyces cerevisiae* by use of an epitope addition method. Mol. Cell. Biol. 8, 2159–2165 [PMCID: PMC363397] [PubMed: 2455217]

77. Horikami S. M., Curran J., Kolakofsky D., Moyer S. A. (1992) Complexes of Sendai virus NP-P and P-L proteins are required for defective interfering particle genome replication *in vitro*. J. Virol. 66, 4901–4908 [PMCID: PMC241329] [PubMed: 1321276]

78. Qanungo K. R., Shaji D., Mathur M., Banerjee A. K. (2004) Two RNA polymerase complexes from vesicular stomatitis virus-infected cells that carry out transcription and replication of genome RNA. Proc. Natl. Acad. Sci. U. S. A. 101, 5952–5957 [PMCID: PMC395904] [PubMed: 15069200]

79. Tawar R. G., Duquerroy S., Vonrhein C., Varela P. F., Damier-Piolle L., Castagné N., MacLellan K., Bedouelle H., Bricogne G., Bhella D., Eléouët J. F., Rey F. A. (2009) Crystal structure of a nucleocapsid-like nucleoprotein-RNA complex of respiratory syncytial virus. Science 326, 1279–1283 [PubMed: 19965480]

80. Kusumaningtyas E., Tan W. S., Zamrod Z., Eshaghi M., Yusoff K. (2004) Existence of two forms of L protein of Newcastle disease virus isolates due to a compensatory mutation in Domain V. Arch. Virol. 149, 1859–1865 [PubMed: 15593426]

81. Grdzelishvili V. Z., Smallwood S., Tower D., Hall R. L., Hunt D. M., Moyer S. A. (2005) A single amino acid change in the L-polymerase protein of vesicular stomatitis virus completely abolishes viral mRNA cap methylation. J. Virol. 79, 7327–7337 [PMCID: PMC1143665] [PubMed: 15919887]

82. Ogino T., Kobayashi M., Iwama M., Mizumoto K. (2005) Sendai virus RNA-dependent RNA polymerase L protein catalyzes cap methylation of virus-specific mRNA. J. Biol. Chem. 280, 4429–4435 [PubMed: 15574411]

83. Deore R. R., Chern J. W. (2010) NS5B RNA dependent RNA polymerase inhibitors. The promising approach to treat hepatitis C virus infections. Curr. Med. Chem. 17, 3806–3826 [PubMed: 20858218]

84. Koch U., Narjes F. (2007) Recent progress in the development of inhibitors of the hepatitis C virus RNA-dependent RNA polymerase. Curr. Top. Med. Chem. 7, 1302–1329 [PubMed: 17627559]

85. Vermehren J., Sarrazin C. (2011) New HCV therapies on the horizon. Clin. Microbiol. Infect. 17, 122–134 [PubMed: 21087349]

86. White L. K., Yoon J. J., Lee J. K., Sun A., Du Y., Fu H., Snyder J. P., Plemper R. K. (2007) Nonnucleoside inhibitor of measles virus RNA-dependent RNA polymerase complex activity. Antimicrob. Agents Chemother. 51, 2293–2303 [PMCID: PMC1913224] [PubMed: 17470652]

87. Yoon J. J., Krumm S. A., Ndungu J. M., Hoffman V., Bankamp B., Rota P. A., Sun A., Snyder J. P., Plemper R. K. (2009) Target analysis of the experimental measles therapeutic AS-136A. Antimicrob. Agents Chemother. 53, 3860–3870 [PMCID: PMC2737882] [PubMed: 19528268]

88. Harcourt B. H., Tamin A., Halpin K., Ksiazek T. G., Rollin P. E., Bellini W. J., Rota P. A. (2001) Molecular characterization of

the polymerase gene and genomic termini of Nipah virus. Virology 287, 192–201 [PubMed: 11504554]

89. Ohgimoto S., Bando H., Kawano M., Okamoto K., Kondo K., Tsurudome M., Nishio M., Ito Y. (1990) Sequence analysis of P gene of human parainfluenza type 2 virus. P and cysteine-rich proteins are translated by two mRNAs that differ by two nontemplated G residues. Virology 177, 116–123 [PubMed: 2162103]

90. Okazaki K., Tanabayashi K., Takeuchi K., Hishiyama M., Okazaki K., Yamada A. (1992) Molecular cloning and sequence analysis of the mumps virus gene encoding the L protein and the trailer sequence. Virology 188, 926–930 [PubMed: 1585659]

91. Roth J. P., Li J. K., Smee D. F., Morrey J. D., Barnard D. L. (2009) A recombinant, infectious human parainfluenza virus type 3 expressing the enhanced green fluorescent protein for use in high-throughput antiviral assays. Antiviral Res. 82, 12–21 [PMCID: PMC2701465] [PubMed: 19189850]

Figures and Tables

FIGURE 1.

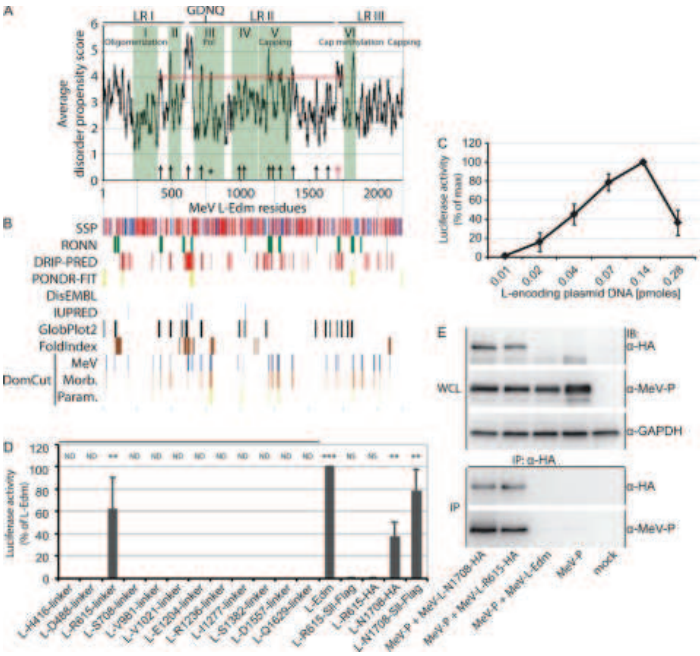

Identification of MeV L folding domains through linker insertion analysis. *A*, average disorder propensity scores obtained through a combination of eight algorithms (listed in *B*) are plotted as a function of MeV L. Conserved regions I-VI (*green shading*; annotations according to predicted activities are detailed in the Introduction), the postulated catalytic center for RNA polymerization (GDNQ), and the area and score cut-off for experimental testing (*red line*) are *highlighted. Black arrows* mark residues that were chosen for subsequent linker insertion analysis, the *red arrow* identifies the position in the LR II/LR III section that was previously demonstrated to tolerate epitope tag insertions (23), and the *black asterisk* marks a hit candidate that was not tested due to its immediate proximity to the GDNQ catalytic motif. *Pol*, polymerase domain. *B*, shown is a graphic representation of individual predictions. To identify candidate disordered domains in MeV L, the MeDor (encompassing RONN, DisEMBL REM465, IUPRED, GLOBPLOT2, and FoldIndex) meta-analysis tool, PONDR-FIT, DRIP-PRED, and DomCut algorithms were used. Secondary structure predictions (*SSP*) are based on the Pred2ary program embedded in MeDor and show postulated α-helical (*red*) or β-sheet (*blue*) regions. Graphic predictions were aligned with the propensity score averages shown in *A*. *C*, plasmid titration to determine activity maxima of a firefly luciferase MeV RdRp reporter system is shown. Peak luciferase activities were observed at a molar ratio of 1:0.6 and 0.4 (L-encoding plasmid DNA:N- and P-encoding plasmid DNA). Total amounts of DNA transfected/well were kept constant, and values represent averages of four independent experiments ± S.D. *D*, linker insertion analysis to map MeV L domain intersections is shown. Twelve 10-residue linkers of the specified sequence were inserted at the indicated positions (corresponding to the *black arrows in A*). In addition, HA and tandem SII-FLAG epitope tags were inserted after L residues 615 and 1708. Results are expressed relative to luciferase activity observed after transfection of standard L-Edm and represent averages of three independent experiments ± S.D. Statistical analysis probes activity deviation relative to control transfections that received vector DNA in place of the L expression plasmid (**, $p < 0.01$; ***, $p < 0.001$; *NS*, not significant; *ND*, not determined). *E*, inactive MeV $L_{615\text{-HA}}$ and bioactive $L_{1708\text{-HA}}$ efficiently interact with MeV P. Whole cell lysates (*WCL*) of BSR-T7/5 cells co-expressing MeV P and the different L constructs as indicated were subjected to gel fractionation and immunoblotting (*IB*) or to reciprocal immunoprecipitation (*IP*) using specific antibodies directed against the HA epitopes followed by anti-P immunostaining. GAPDH was detected as internal standard. Control samples expressed untagged standard MeV L-Edm or MeV P alone.

FIGURE 2.

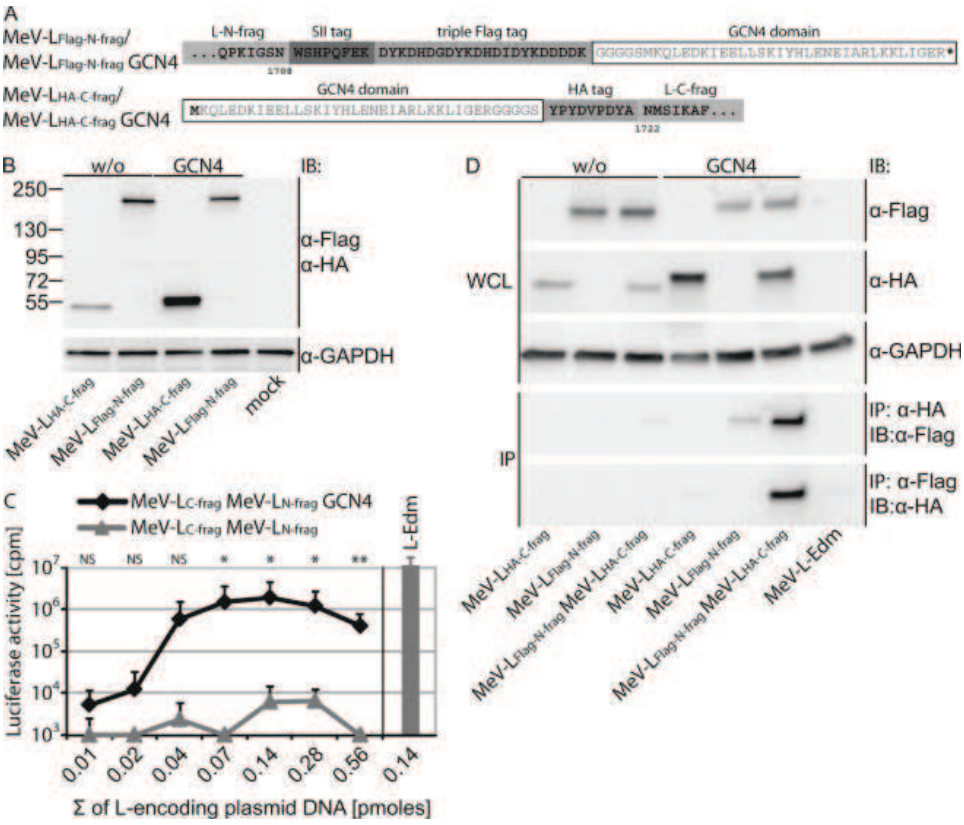

Trans-complementation of bioactivity of MeV L N- and C-terminal fragments. *A*, shown are schematic and amino acid sequences of MeV-$L_{FLAG\text{-}N\text{-}frag}$ and MeV-$L_{HA\text{-}C\text{-}frag}$ constructs. Each L fragment was generated with or without a terminal GCN4 dimerization domain (*white boxes*). *B*, expression analysis of the different MeV L fragments is outlined in *A*. Whole cell lysates of BSR-T7/5 cells transfected with L fragment-encoding plasmids as indicated were gel-fractionated followed by immunoblotting (*IB*) using specific antibodies directed against the FLAG and HA epitope tags. *Numbers* represent the migration pattern of a protein standard (in kDa). Cellular GAPDH was analyzed in identical samples as internal standard. *C*, MeV L fragment trans-complementation in the replicon reporter assay is shown. BSR-T7/5 cells were co-transfected with all replicon components and equimolar amounts of expression plasmids encoding the MeV L N- and C-terminal fragments with or without terminal GCN4 domains. *x* axis values represent the sum of L fragment-encoding plasmid DNA (in pmol). Controls received standard MeV L-Edm (*L-Edm*) or vector in place of L fragment-encoding plasmids. Total amounts of DNA transfected/well were kept constant. Values represent relative luciferase activity units and represent the averages of three independent experiments ± S.D. Statistical analysis assesses the significance of activity deviation of GCN4-tagged L fragments from those lacking the dimerization domains (*, $p < 0.05$; **, $p < 0.001$; *NS*, not significant). *D*, efficient co-immunoprecipitation of MeV L fragments requires the presence of the GCN4 domains. Whole cell lysates (*WCL*) of BSR-T7/5 cells expressing different combinations of the MeV L fragments with or without additional GCN4 domains were gel-fractionated and immunoblotted (*IB*) or subjected to reciprocal immunoprecipitation (*IP*) using specific antibodies directed against the HA or FLAG epitopes followed by anti-FLAG or anti-HA immunostaining, respectively. GAPDH was detected as the internal standard. Control samples expressed untagged standard MeV L-Edm.

FIGURE 3.

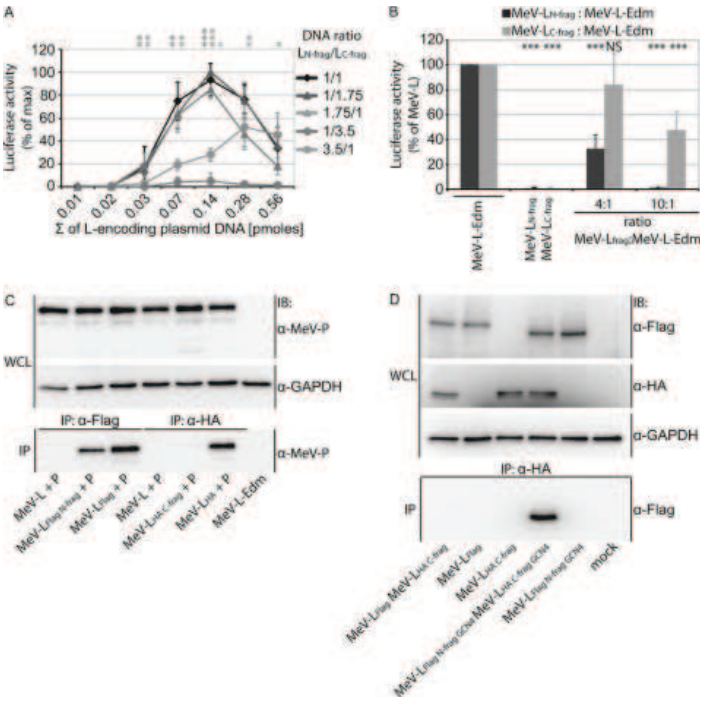

Dominant negative effect of overexpressed L fragments on RdRp activity. *A*, L trans-complementation efficiency peaks in the presence of a slight excess of the C-terminal L fragment. Trans-complementation MeV replicon activity assays were carried out as outlined for Fig. 2*C* but after transfection of different molar ratios of the $L_{N\text{-}frag}$ and $L_{C\text{-}frag}$ expression plasmids as indicated. Values are expressed relative to the L fragment combination that returned the overall highest luciferase activities (molar ratio of $L_{N\text{-}frag}$ to $L_{C\text{-}frag}$ plasmid DNA 1:1.75, total amount of L fragment-encoding plasmid DNA 0.14 pmol) and represent averages of at least three independent experiments ± S.D. Statistical analysis determines the significance of activity deviation relative to the optimum curve (molar ratio of $L_{N\text{-}frag}$ to $L_{C\text{-}frag}$ plasmid DNA 1:1.75; *, $p < 0.05$; **, $p < 0.01$; ***, $p < 0.001$). *B*, co-transfection of BSR-T7/5 cells with replicon helper components, MeV L N- or C-fragment expression constructs, and plasmids encoding full-length MeV L-Edm in either 4:1 or 10:1 molar ratios. Values are expressed relative to MeV L-Edm samples and represent the averages of four independent experiments ± S.D. Statistically significant deviation of luciferase activity was calculated relative to standard MeV L-Edm controls (***, $p < 0.001$; *NS*, not significant). In *A* and *B*, total amounts of DNA transfected/well were kept constant. *C*, MeV $L_{N\text{-}frag}$ but not $L_{C\text{-}frag}$, interacts with MeV P. Co-immunoprecipitation after transfection of cells with MeV L fragment and MeV P expression plasmids as indicated was carried out as described for Fig. 1*E*. *WCL*, whole cell lysates. *D*, MeV $L_{C\text{-}frag}$ does not efficiently co-precipitate standard MeV-L. Immunoprecipitations (*IP*) were carried out using HA epitope-specific antibodies followed by immunostaining (*IB*) with anti-FLAG antibodies. As controls, FLAG and HA epitope-containing material and cellular GAPDH were immunostained in cellular lysates (*WCL*). Mock-transfected cells received empty vector in place of L-encoding plasmid.

FIGURE 4.

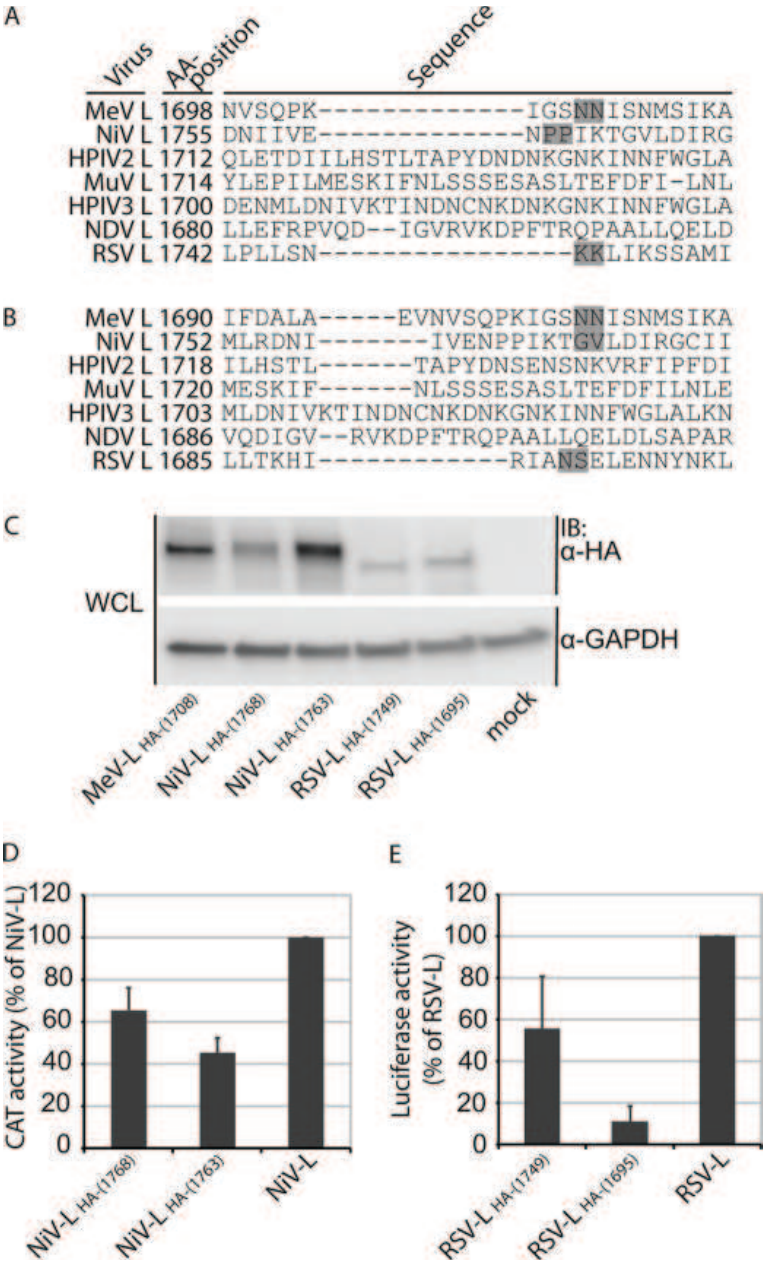

Identification of HA epitope tag insertion sites in NiV and RSV L. *A* and *B*, sequence alignments of L proteins derived from MeV-Edm, NiV (88), HPIV2 (89), MuV-Miyahara (90), HPIV3–14702 (91), NDV-AF2240 (80), and RSV-A2 using the ClustalW2 (*A*) and MUSCLE (*B*) algorithms are shown. Regions corresponding to part of the LR II/LR III intersection in MeV L are shown, and *numbers* reflect amino acid positions. *Gray boxes* mark the insertion sites of the epitope tags. *C*, shown is expression analysis of the newly generated NiV and RSV L variants. Whole cell lysates (*WCL*) of BSR-T7/5 cells transfected with the different L expression plasmids were gel fractionated and immunostained (*IB*) using specific antibodies directed against the HA epitope or cellular GAPDH. Control cells (mock) received empty vector in place of L-encoding plasmid. *D* and *E*, shown is activity testing of the HA-tagged NiV and RSV L variants using specific replicon reporter systems for NiV (*D*, CAT reporter) and RSV (*E*, firefly luciferase reporter). Values are expressed relative to activities of standard NiV or RSV L and reflect the averages of four independent experiments ± S.D.

FIGURE 5.

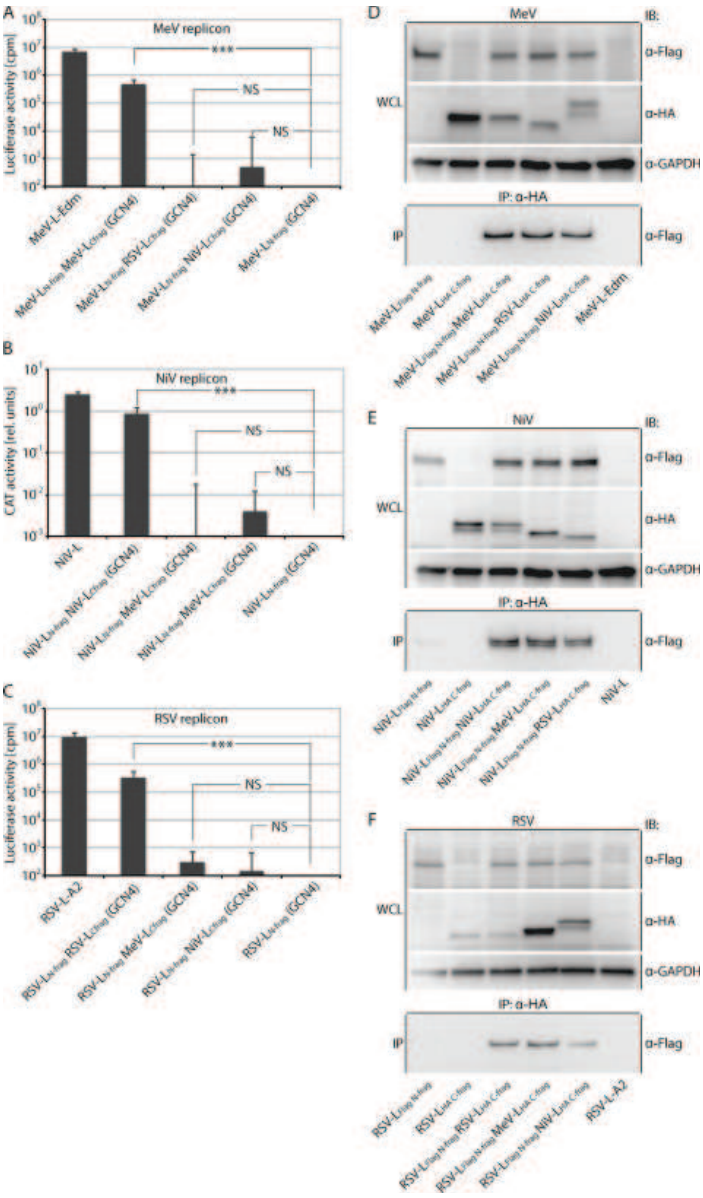

Functional trans-complementation mandates homotypic L fragment combinations. *A–C*, shown are homo- and hetero-complementation assays after co-transfection of plasmids encoding GCN4 domain-tagged MeV, NiV, or RSV L N- and C-terminal fragments in all combinations in the context of the MeV (*A*), NiV (*B*), or RSV (*C*) replicon reporter systems. Values show relative luciferase or CAT activities and represent the averages of at least three independent experiments ± S.D. Control cells received the respective $L_{N\text{-}frag}$ expression plasmid-only instead of the homotypic standard L or co-transfection of $L_{N\text{-}frag}$ and $L_{C\text{-}frag}$ encoding plasmids. Statistical analysis assesses the significance of deviation of the different L fragment combinations from the controls (***, $p < 0.001$; *NS*, not significant). *D–F*, all homo- and heterotypic L N- and C-fragment combinations analyzed in *A–C* efficiently co-immunoprecipitate. Whole cell lysates (*WCL*) of BSR-T7/5 cells expressing the GCN4-tagged homo- and heterotypic L fragment pairs as specified were subjected to immunoprecipitation (*IP*) with anti-HA antibodies followed by gel fractionation and immunoblotting (*IB*) using anti-FLAG antibodies. In parallel, lysates were directly analyzed using HA-, FLAG-, or cellular GAPDH-specific antibodies. Controls received expression plasmids encoding standard, untagged L in place of the epitope-tagged L variants.

Articles from The Journal of Biological Chemistry are provided here courtesy of **American Society for Biochemistry and Molecular Biology**

Publication 7

Aiming Sun, J. Maina Ndungu, **Stefanie A Krumm**, Jeong-Joong Yoon, Pahk Thepchatri, Michael G Natchus, Richard K Plemper, and James P Snyder
“Host-Directed Inhibitors of Myxoviruses: Synthesis and in Vitro Biochemical Evaluation”
ACS MEDICINAL CHEMISTRY LETTERS, August 2011

ACS Med Chem Lett accepted manuscript and published in PubMed Central by copyright permission of American Chemical Society

Host-directed Inhibitors of Myxoviruses: Synthesis and in vitro Biochemical Evaluation

Journal:	*ACS Medicinal Chemistry Letters*
Manuscript ID:	ml-2011-00125r.R2
Manuscript Type:	Letter
Date Submitted by the Author:	22-Aug-2011

Complete List of Authors:	Sun, Aiming; Emory Institute for Drug Discovery, Chemistry Department Ndungu, J.; Emory Institute for Drug Discovery, Chemistry Department Krumm, Stefanie; Emory University School of Medicine, Department of Pediatrics Yoon, Jeong-Joong; Emory University School of Medicine, Department of Pediatrics Thepchatri, Pahk; Emory Institute for Drug Discovery, Chemistry Department Natchus, Michael; Emory University, Chemistry Plemper, Richard; Emory University, Department of Pediatrics Snyder, James; Emory University, Department of Chemistry

SCHOLARONE™
Manuscripts

Host-directed Inhibitors of Myxoviruses: Synthesis and in vitro Biochemical Evaluation

Aiming Sun, [*,†] J. Maina Ndungu,[†] Stefanie A Krumm, [§,μ] Jeong-Joong Yoon, [§,μ] Pahk Thepchatri, [†] Michael Natchus, [†] Richard K Plemper, [§,μ,v] and James P. Snyder[†,τ]

[†]Emory Institute for Drug Discovery, Emory University, Atlanta, GA 30322

[§]Department of Pediatrics, Emory University School of Medicine, Atlanta, GA 30322

[μ] Children's Healthcare of Atlanta, Atlanta, GA 30322

[v] Department of Microbiology & Immunology, Emory University School of Medicine, Atlanta, GA, 30322

[τ] Department of Chemistry, Emory University, Atlanta, GA 30322

**Corresponding author: Phone: 404-712-8680; Fax: 404-727-6689; e-mail: asun2@emory.edu*

Abstract—Drugs targeted to viral proteins are highly vulnerable to the development of viral resistance. One little explored approach to the treatment of viral diseases is the development of agents that target host factors required for virus replication. Myxoviruses are predominantly associated with acute disease and, thus, ideally suited for this approach since the necessary treatment time is anticipated to be limited. High-throughput screening previously identified benzimidazole 22407448 with broad anti-viral activity against different influenza virus and paramyxovirus strains. Hit to lead chemistry has generated **6p** (JMN3-003) with potent antiviral activity against a panel of myxovirus family members exhibiting EC_{50} values in the low nanomolar range.

Keywords: Host-directed, non-nucleoside, small molecule inhibitor, influenza virus, myxovirus, benzimidazole

Myxoviruses are responsible for the majority of human morbidity and mortality cases due to viral respiratory illness globally.[1] Influenza virus is the leading cause of these events in North America, although vaccine prophylaxis is widely available. Despite extensive research, no vaccines currently exist for several major pathogens of the paramyxovirus family such as respiratory syncytial virus (RSV) or different human parainfluenzaviruses (HPIVs). Ribavirin (RBV) is a synthetic nucleoside analog with broad-spectrum antiviral activity. Although RBV is approved for the treatment of hepatitis C virus, RSV and Lassa fever virus infections, its efficacy is limited and the drug is compromised by several side effects.[2] Previously, we utilized high-throughput screening (HTS) to identify small molecule inhibitors against MeV RNA dependent RNA polymerase (RdRp) activity.[3] However, viral adaptation has demonstrated that robust resistance to inhibition by these compounds can originate from single point mutations in the targeted viral protein.[4,5] In an attempt to counteract viral escape from inhibition, we have explored targeting host factors required for viral replication rather than viral proteins directly. Anticipated advantages of this strategy include a decreased frequency of viral escape from inhibition and a broadened pathogen target spectrum. High-throughput screening in combination with counter-screening for a broadened viral target spectrum that extends to other pathogens of the myxovirus families, has identified several antiviral hits that likely target host cells.[6] This approach yielded several benzimidazoles of the same class (22407448 (BM-1),[7] 22404943 and 22407466) as well-behaved inhibitors of measles virus (MeV).

Potencies (EC_{50}) against MeV are 0.2, 0.7 and 2.1 μM, respectively. (**Figure 1**) Hit BM-1 in particular is unusual since it shows broad-spectrum antiviral action against various paramyxoviruses in the low micromolar to nanomolar range.[6]

Figure 1: Anti-MeV hits identified by high-throughput screening.

In order to confirm the activity, BM-1 was re-synthesized and re-assayed. For hit confirmation, dose-response curves were generated. Synthesized BM-1 revealed behavior identical to the original library member against CDV, HPIV3 and MeV. In parallel, MTT assays were employed to determine compound-induced cytotoxicity in the absence of viral infection. Synthesis was initiated by coupling of 1-fluoro-2-nitrobenzene **1** with *p*-anisidine **2** in the presence of potassium carbonate to provide N-(4-methoxyphenyl)-2-nitroaniline **3**. Reduction of **3** gave diamine **4**, which was treated with 1,1-thiocarbonyldiimidazole in dichloromethane to afford 1-(4-methoxyphenyl)-1H- benzimidazole-2-thiol **5**. The 2-thio-imidazole **5** was transformed to its potassium salt and coupled with 2-bromo-*N*-(3,5-dichloropyridin-2-yl)propanamide to give BM-1. The approach has been used for the synthesis of a set of BM-1 derivatives, which are described below (**Scheme 1**).

Scheme 1: Synthesis of screening hit BM-1[a]

A structure-activity profile has begun to emerge by examination of the three molecular fragments circumscribed in **Figure 2**; namely the benzimidazole (A), the α-thio-amide linker (B) and the substituted pyridine ring (C).

Figure 2. (a) Structure-activity modification strategy for hit compound BM-1;
(b) modification of A and C sectors of BM-1.

The first stage of hit optimization focused on introducing a variety of aromatic rings as pyridine replacements, since modification of the C sector is achieved in a straight forward fashion by employing the same synthesis methodology utilized for the synthesis of BM-1 (**Scheme 1**). A small and compact library of 30-50 analogs was obtained by utilizing different α-halide amides for the final coupling step. Substituted pyridines, pyrazoles, triazines, thiazoles and other functionalities were used instead of **7**. A second group of analogs was prepared by employing alternative anilines in sector A. The *para*-methoxy group was replaced by hydrogen, ethoxy, fluoro and hydroxyl, among others. Sector C analogs with chloro, methyl and trifluoromethyl substituents show activities very similar to BM-1 (**6a** and **6d,** Table 1). The corresponding ethoxy analog delivers slightly better activity (entry **6c**), while pyrazole and isoxazole replacements furnish 2-fold reduced potency (entries **6j** and **6n**). The fluoro-analog is virtually equipotent to BM-1 (entry **6b**). The thiazole functionality reduces activity by 10-fold (entry **6m**), while triazines are significantly weaker still (entries **6i** and **6k**). However, most of the active compounds listed in Table 1 were toxic in the Trypan blue exclusion assay with CC_{50} values of 1-10 μM. The *p*-ethoxy analog is the exception with reduced toxicity at 20 μM (entry **6c**). Encouragingly, **6p** (JMN3-003) with a substituted phenyl in sector C demonstrated strong antiviral activity (EC_{50} = 170 nM) against MeV and cell cytotoxicity over 75 μM (entry **6p**, Table 1). As outlined in the context of the recently reported detailed molecular characterization of JMN3-003, antiviral activities were evaluated using actively dividing cells, while CC_{50} values were determined for confluent cell populations, thus reflecting acute toxicity. Independent assessment of cell proliferation revealed a

cytostatic effect of JMN3-003. This was found, however, not to be the basis for the antiviral effect.[8] In order to understand the relationship between chirality and potency, R- and S- isomers of **6p** were isolated by chiral HPLC. Both isomers were subjected to the MeV inhibition assay. Potency of the S-isomer was essentially identical to the racemic mixture **6p**, while the antiviral capacity of the R-isomer was slightly reduced (Table 1). A newly developed methodology for the asymmetric synthesis of both isomers will be reported elsewhere.

Table 1. Antiviral activity and cytotoxicity of various substituted anilides, **6**.

For part A of hit modification, we initially tried to replace the fused benzene of the benzoimidazole with pyridine and functionalize the benzene moiety by substitution with Me, Br, or COOEt. Unfortunately, most of the analogs experienced either significant reduction or complete loss of activity. Thus, we didn't pursue this series further.

For replacement of the 2-thioacetamide linker, five different variations of the central tether with an equivalent number of chain atoms were prepared. Compound designations **11-15** (**Scheme 2, 3 & 4**) and the corresponding activities are recorded in **Table 2**, illustrating a significant reduction or loss of activity relative to BM-1. Systematic structural modification revealed that substitution of benzyl for phenyl at the benzimidazole *N1* position delivers analogs with similar anti-MeV viral activity. (**Figure 2**, sector A). Benzyl derivatives **20** and **21** deliver fairly good potency with EC_{50} at 0.5 μM and 0.4 μM, respectively (Table 2). Thus, both derivatives **11** and **13** bear a benzyl group instead of the *p*-methoxy phenyl group as shown in Table 2. Compound **11,** incorporating NH in the central linker, introduces additional hydrogen-

bond capacity and a new pKa center, while **12, 13, 14** and **15** (CH_2, O, SO and SO_2, respectively) sustain somewhat different linker geometries by comparison with the sulfur-containing tether of BM-1. The importance of sulfur versus other atoms was also observed during discovery of the HIV reverse transcriptase inhibitor RDEA-806,[9, 10] which shares the central 2-thio-acetamide linker with BM-1 and has achieved success in clinical trials. **(Figure 3)** Obviously, a sulfur atom in the linker is essential. However, its precise role at the binding site remains to be fully defined. Comparative conformational searches for otherwise identical analogs with O, NH and CH_2 replacements for S suggest that sulfur is possibly unique in providing an energetically accessible bioactive conformation.[11]

Figure 3. Structural comparison of RDEA-806 and BM-1.

Analog **11** was prepared as outlined in **Scheme 2**. 2-Chloro-benzimidazole was treated with *p*-methoxybenzyl bromide in the presence of potassium carbonate to provide chloro-benzimidazole **8.** The latter was coupled with racemic alanine methyl ester in the microwave at 165^{o}C for 1 h to afford 2-aminoimidazole derivative **9**, which was hydrolyzed to the corresponding acid **10**. The latter was treated with oxalyl chloride followed by coupling with 2-chloro-4-methylaniline to furnish the final product **11** (**Scheme 2**).

Scheme 2: Synthesis of 2-aminobenzimidazole[a]

The synthesis of carbon analog **12** proceeded from reaction of diamine **4** with succinic anhydride to give the benzimidazole **16**. Hydrolysis of **16** under basic conditions with lithium hydroxide (LiOH) in a mixture of THF and water delivered acid

17, which was further coupled with 2-chloro-4-methylaniline in the presence of isopropyl chloroformate and 4-methylmorpholine to afford **12** (**Scheme 3**).

Scheme 3: Synthesis of the carbon analog of **6p**[a]

The synthesis of the oxygen analog **13** commenced with the protection of benzyl-L-lactate as a silyl ether, which on hydrogenolysis furnished acid **18**. BOP-mediated coupling of **18** with 2-chloro-4-methylaniline followed by cleavage of the silyl group furnished alcohol **19**. Treatment of **19** with NaH facilitated coupling with 1-benzyl-2-chloro-1H-benzimidazole to afford **13** (**Scheme 4**).

Scheme 4: Synthesis of the oxygen analog of **6p**[a]

Sulfoxide analog **14** and sulfone analog **15** can be easily obtained by oxidation of **6p** with 1.0 eq and 2.0 eq of 3-chloroperoxybenzoic acid (MCPBA), respectively.

Table 2. Anti-MeV IC_{50} values for S-atom replacements

6p(JMN3-003) is a broadly active anti-myxovirus agent

Benzene analog **6p** has surfaced as the most promising candidate of this compound series with superb antiviral potency and low cytotoxicity. The compound shows potent activity against MeV and a selection of clinically significant members of the para- and orthomyxovirus families. We also compared the anti-myxovirus activity of **6p** with the previously reported MeV RdRp inhibitor AS-136a. The latter shows high selectivity against MeV, while **6p** exhibits a broad range of anti-myxovirus activities with EC_{50} values ranging from 10 to 70 nM in virus yield reduction assays depending on the target virus. Detailed biological evaluation and target examination have been reported elsewhere.[8]

In summary, high-throughput screening has identified several hits in the benzimidazole class with potent anti-MeV activities. Follow-up counter-screening assays uncovered BM-1 as a well-behaved inhibitor with the ability to block replication of a broad range of myxovirus family members. By optimization of BM-1, we have developed preliminary SAR within the three pharmacophoric sectors highlighted in **Figure 2**. A variety of structural modifications essentially abolishes antiviral activity or results in high cytotoxicity. Particularly influential for the SAR of these agents are the structural constitutions of the amide substituents and the sulfur atom of the central tether. The most potent analog **6p**, was generated by replacing the pyridine ring in BM-1 with a substituted phenyl ring. The compound shows activity against MeV at 170 nM (viral CPE-reduction assay) and 30 nM (virus yield reduction assay) and does not display any detectable acute cytotoxicity. **6p** was also evaluated for its antiviral activity against a selection of clinical-relevant paramyxovirus (RSV, MuV, and HPIV3) and orthomyxovirus (influenza) family members. The compound exhibits superb inhibitory activity against all the viruses tested with EC_{50} values ranging from 10 to 70 nM in virus yield reduction assays.[8] These results demonstrate that **6p** has great potential as a lead for development of host-directed antiviral drugs. Pharmacokinetics evaluation, *in vivo* efficacy and expansion of **6p** library are currently in progress.

Acknowledgments.

We are grateful to Dr. Dennis Liotta for generous financial support and scientific discussions.This work was supported, in part, by Public Health Service Grants AI071002 and AI085328 (to R. K. P.) from the NIH/NIAID and by Public Health

Service Grant HG003918-02 (to J.P.S.) from the NIH.

Supporting Information. Experimental details for the synthesis and characterization of **3-11, 12, 13**, **15, 20 and 21**. Experimental details for biology asays. This material is available free of charge via the Internet at http://pubs.acs.org.

Table of Contents Graphic (TOC)

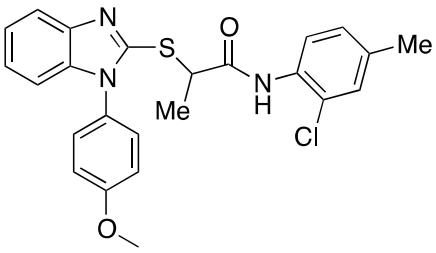

6p (JMN3-003), EC_{50} = 10-70 nM against a variety of myxoviruses; Vero Cell toxicity (CC_{50}) > 75 μM

Lay Summary

Drugs targeted to viral proteins are highly vulnerable to the development of viral resistance. High-throughput screening previously identified benzimidazole 22407448 with broad anti-viral activity against different influenza virus and paramyxovirus strains. Hit to lead chemistry has generated JMN3-003 with potent antiviral activity against a panel of myxovirus family members including influenza and measles.

Table 1. Antiviral activity and cytotoxicity of various substituted anilides **6**.

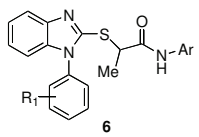

6

Entry	Comp.	R_1	Ar	EC_{50} ± SEM (μM)[a] (MeV-Alaska) CPE inhibition	CC_{50} (μM)[b] (Vero cells)
hit	BM-1	*p*-OMe	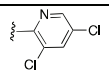	0.35±0.03	>75
6a	AS92	*p*-OMe	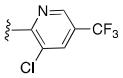	0.4±0.05	9.2-9.8
6b	AS93	*p*-F	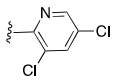	0.1±0.00	5.9-6.2
6c	AS94	*p*-OEt	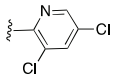	0.1±0.01	18.5-22.2
6d	AS102	*p*-OMe	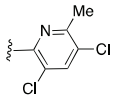	0.2±0.01	7.25-7.8
6e	AS80b	*p*-OMe	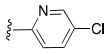	>75	ND[c]
6f	AS103b	*p*-OMe	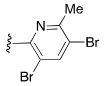	0.5±0.05	9.7-11.9
6g	AS103a	*p*-OMe	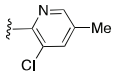	0.05±0.00	0.88-0.92
6h	AS109	*p*-OEt		1.2±0.22	ND[c]
6i	AS112	*p*-F	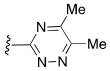	17.4±6.11	ND[c]
6j	AS114	*p*-OMe	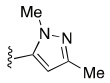	0.5±0.09	75
6k	AS115a	*p*-OMe	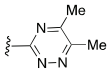	9.3±2.65	ND[c]
6l	AS120	*p*-OMe		>75	ND[c]
6m	JMN2-173	*p*-OMe	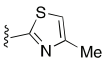	2.8±0.17	ND[c]
6n	JMN2-183	*p*-OMe	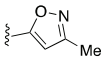	0.4±0.01	>75
6o	AS86	*p*-OMe		1.4±0.11	ND[c]
6p	JMN3-003	*p*-OMe	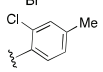	0.2±0.00	>75
(S)-6p	(s)-JMN3-003	*p*-OMe	—	0.3±0.07	>75
(R)-6p	(r)-JMN3-003	*p*-OMe	—	0.2±0.03	>75

a: 50% inhibitory concentration were calculated using the variable slope (four parameters) non-linear regression-fitting algorithm embedded in the Prism 5 software package (GraphPad Software). Values represent averages of four experiments ± SEM (standard error of the mean); highest concentration assessed, 75 μM.

b: CC_{50} values represent range of two experiments; highest concentration assessed 75 μM.

c: CC_{50} not determined (ND) when EC_{50} > 1.0 μM

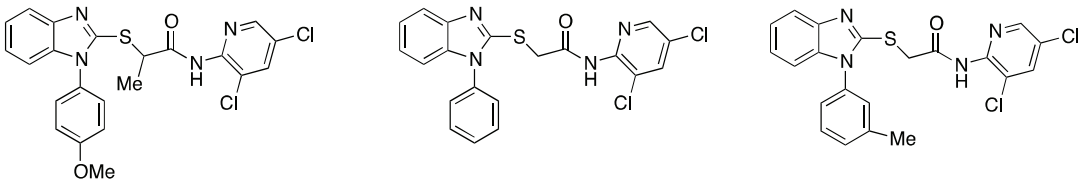

Figure 1. Anti-MeV hits identified by high-throughput screening.

Scheme 1: Synthesis of screening hit BM-1.[a]

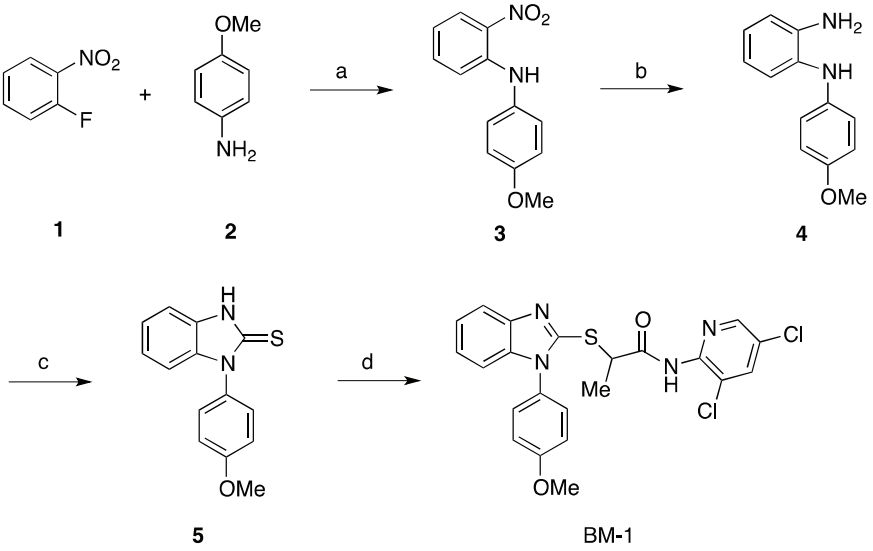

[a] Reagents: (a) K_2CO_3, 160°C, 5h; (b) Pd/C (10%), H_2 (50 psi), MeOH, 2 h; (c) 1,1-thiocarbonyldiimidazole, CH_2Cl_2, rt, 4h; (d) KOH, EtOH, reflux, 2h, then 2-bromo-*N*-(3,5-dichloropyridin-2-yl)propanamide (**7**)

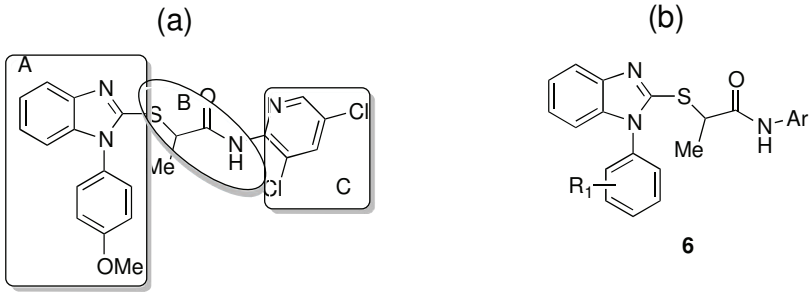

Figure 2. (a) Structure-activity modification strategy for hit compound BM-1; (b) modification of A and C sectors of BM-1.

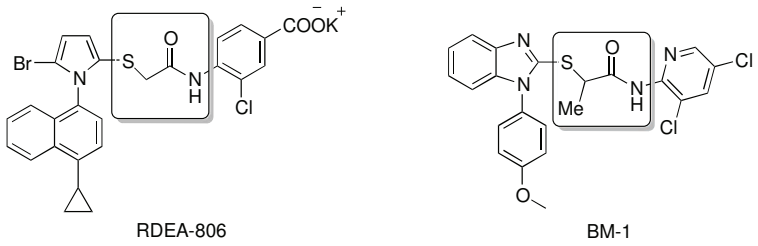

Figure 3. Structural comparison of RDEA-806 and BM-1.

Scheme 2: Synthesis of 2-aminobenzimidazole[a]

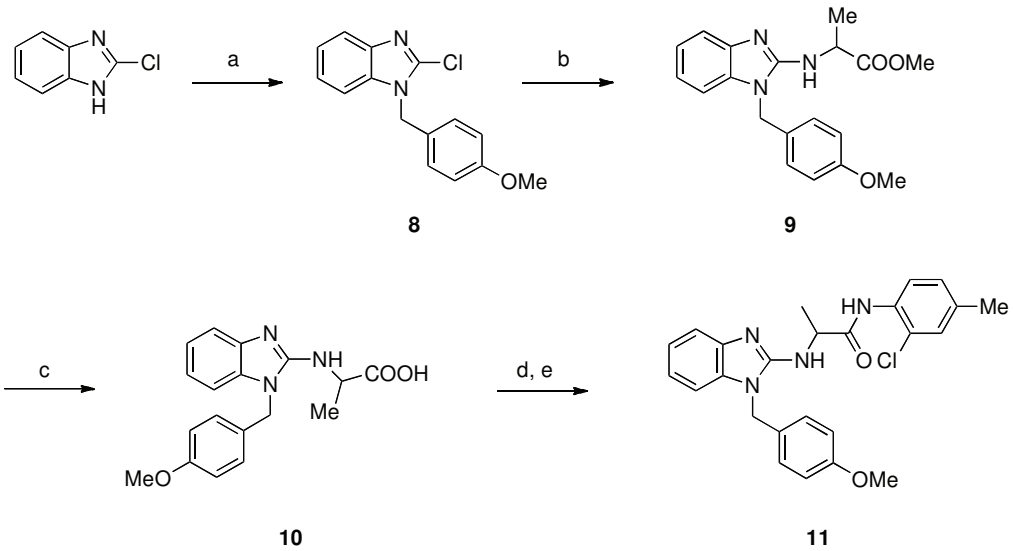

[a]Reagents and conditions: (a) *p*-Methoxybenzyl bromide, K_2CO_3, CH_3CN, reflux; (b) DL-alanine methyl ester, K_2CO_3, CH_3CN, 165°C, Microwave, 1h; (c) HCl (con.)/H_2O, reflux, 2h; (d) oxalyl chloride (2.0 eq. 2.0 M in CH_2Cl_2), CH_2Cl_2, DMF (cat.); (e) 2-chloro-4-methylaniline, 4-(dimethylamino)pyridine, (DMAP) (cat.), pyridine.

Scheme 3: Synthesis of the carbon analog of **6p**[a]

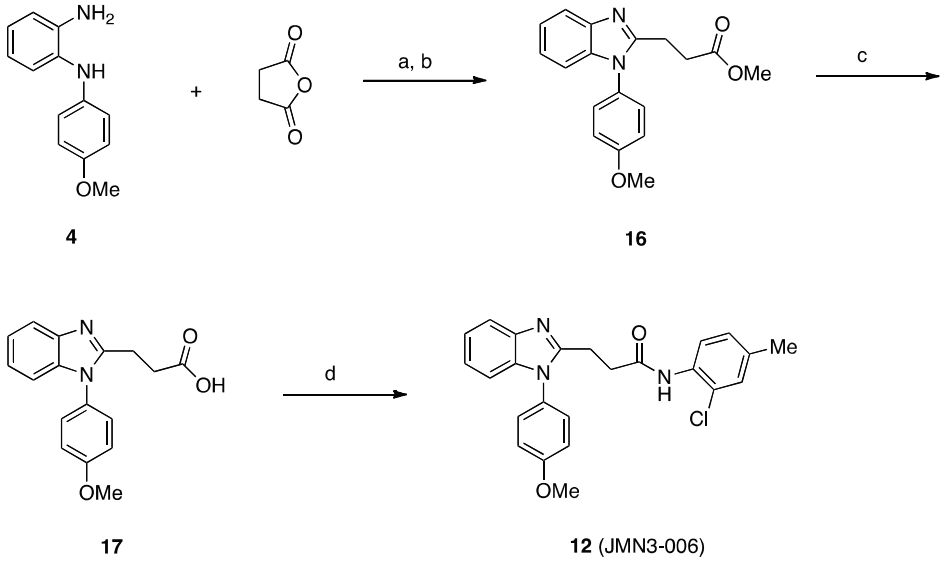

[a]Reagents and conditions: (a) CH_2Cl_2, 40°C; (b) HCl (4N), MeOH, 100°C; (c) LiOH, THF/H_2O; (d) ^{i}PrOCOCl, 4-methylmorpholine, 2-chloro-4-methylaniline, CH_2Cl_2/DMF.

Scheme 4: Synthesis of the oxygen analog of **6p**[a]

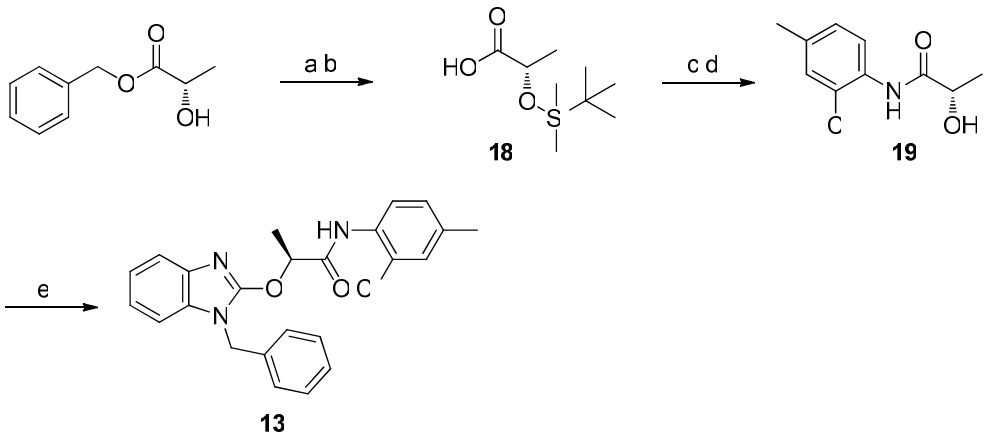

[a]Reagents and conditions: (a) tert-Butyldimethylsilyl chloride, imidazole, DMF; (b) H_2, Pd/C, MeOH; (c) benzotriazole-1-yl-oxy-tris-(dimethylamino)-phosphonium hexafluorophosphate (BOP), *i*-Pr_2NEt, 2-chloro-4-methylaniline, CH_2Cl_2 ; (d) tetrabutylammonium fluoride (TBAF), THF; (e) NaH, 1-benzyl-2-chloro-1H-benzimidazole, DMF, 100°C.

Table 2. Anti-MeV EC_{50} values for S-atom replacements

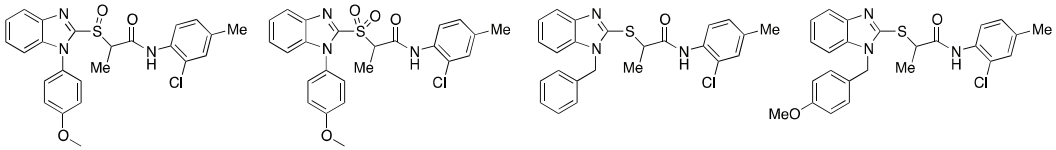

14 (JMN3-004) **15** (JMN3-005) **20** **21**

ID	Comp.	EC_{50} (μM)[a] (MeV-Alaska)	CC_{50} (μM)[b] (Vero cells)
11	AS-228	> 150	ND[c]
12	JMN3-006	>150	ND
13	JMN8-096	>150	ND
14	JMN3-004	1.3±0.06	>75
15	JMN3-005	>150	ND
20	JMN5-010	0.4±0.06	>75
21	JMN4-023	0.7±0.04	>75

a: 50% inhibitory concentration were were calculated using the variable slope (four parameters) non-linear regression-fitting algorithm embedded in the Prism 5 software package (GraphPad Software). Values represent averages of four experiments± SEM (standard error of the mean); highest concentration assessed, 75 μM.

b: values represent averages of two experiments; highest concentration assessed 75 μM

c: CC_{50} not determined (ND) when EC_{50} >150 μM

References

(1) König, R.; Stertz, S.; Zhou, Y.; Inoue, A.; Hoffmann, H-H.; Bhattacharyya, S.; Alamares, J. G.; Tscherne, D. M.; Ortigoza, M. B.; Liang, Y.; Gao, Q.; Andrews, S. E.; Bandyopadhyay, S.; Jesus, P. D.; Tu, B. P.; Pache, L.; Shih, C.; Orth, A.; Bonamy, G.; Miraglia, L.; Ideker, T.; García-Sastre, A.; Young, J. A. T.; Palese, P.; Shaw, M.

L.; Chanda, S. K. Human host factors required for influenza virus replication. *Nature* **2010**, 463, 813-817.

(2) (a) Martin, P.; Jensen, D.M. Ribavirin in the treatment of chronic hepatitis C. *J. Gastroenterol Hepatol* **2008**, 23, 844–855. (b) Dixit, N. M.; Perelson, A.S. The metabolism, pharmacokinetics and mechanisms of antiviral activity of ribavirin against hepatitis C virus. *Cell Mol Life Sci.* **2006**, 63, 832–842. (c) Buckwold, V.E.; Wei, J.; Wenzel-Mathers, M.; Russell, J. Synergistic in vitro interactions between alpha interferon and ribavirin against bovine viral diarrhea virus and yellow fever virus as surrogate models of hepatitis C virus replication. *Antimicrob Agents Chemother* **2003**, 47, 2293–2298. (d) Willis, R.C.; Carson, D.A.; Seegmiller, J.E. Adenosine kinase initiates the major route of ribavirin activation in a cultured human cell line. *Proc. Natl. Acad. Sci. USA***, 1978***,* 75, 3042–3044.

(3) (a) Sun, A.; Chandrakumar, N.; Yoon, J.-J.; Plemper, R. K.; Snyder, J. P. Nonnucleoside inhibitors of the measles virus RNA-Dependent RNA polymerase activity: Synthesis and in vitro evaluation. *Bioorg. Med. Chem. Lett.* **2007**, *17*, 5199-5203. (b) Sun, A., Yoon, J. J.; Yin, Y. Prussia, A.; Yang, Y.; Min, J.; Plemper, R. K.; Snyder. J. P. Potent non-nucleoside inhibitors of the measles virus RNA-dependent RNA polymerase complex. *J. Med. Chem*. **2008**, *51*, 3731–33741. (c) White, L. K.; Yoon, J-J.; Lee, J. K.; Sun, A.; Du, Y.; Fu, H.; Synder, J. P.; Plemper, R. K. Nonnuceloside inhibitor of measles virus RNA-dependent RNA polymerase complex activity. *Antimicrob. Agents Chemother.* **2007**, 51, 2293-2303.

(4) Yoon, J-J.; Krumm, S. A.; Ndungu, J. M.; Hoffman, V.; Bankamp, B.; Rota, P. A.; Sun, A.; Snyder, J. P.; Plemper, R. K. Target Analysis of the experimental measles therapeutic AS-136a. *Antimicrob. Agents Chemother.* **2009**, 53, 3860-3870.

(5) Doyle, J.; Prussia, A.; White, L. K.; Sun, A.; Liotta, D. C.; Snyder, J. P.; Compans, R. W.; Plemper, R. K. Two domains that control prefusion stability and transport competence of the measles virus fusion protein *J. Virology* **2006**, 80, 1524-1536.

(6) Yoon, J-J.; Chawla, D.; Paal, T.; Ndungu, M.; Du, Y.; Kurtkaya, S.; Sun, A.; Snyder, J. P.; Plemper, R. K. High-throughput screening Based Identification of Paramyxovirus Inhibitors. *J. Biomol Screen* **2008**, 13, 591.

(7) 22407448 is called BM-1 through the following parts of the paper for simplicity.

(8) Krumm, S. A.; Ndungu, J. M.; Dochow, M.; Yoon, J.-J.; Sun, A.; Natchus, M.; Snyder, J. P.; Plemper, R. K. Host-Directed Small-Molecule Inhibitors of Myxovirus RNA-dependent RNA-polymerases. *PLoS ONE,* Epublished 16 May 2011 10.1371/journal.pone.0020069.

(9) Moyle, G.; Boffito, M.; Shen, Z.; Manhard, K.; Sheedy, B.; Hingorani, V.; Nguyen, M.; Nguyen, T.; Quart, B.; Yeh, L.; Ong, V. RDEA806, a novel HIV non-nucleoside reverse transcriptase inhibitor, shows positive outcome in treatment of näive HIV patients. 48 Annual ICAAC/IDSA 46th Annual Meeting. Washington D.C. 2008.

(10) Rosa, M. De La; Kim, H. W.; Gunic, E.; Jenket, C.; Boyle, U.; Koh, Y.; Korboukh, I.; Allan, M.; Zhang, W.; Chen, H.; Xu, W.; Nilar, S.; Yao, N.; Hamatake, R.; Lang, S. A.; Hong, Z.; Zhang, Z.; Girardet, Jean-L. Z. Tri-substituted triazoles as

potent non-nucleoside inhibitors of the HIV-1 reverse transcriptase. *Bioorg. Med.Chem. Lett.* **2006**, 16, 4444-4449.

(11) Conformational searches of the S, O, NH and CH_2 analogs were performed with the OPLS-2005 force field, and a putative binding model was compared with the global minimum in each case.

Publication 8

Stefanie A Krumm, J. Maina Ndungu, Jeong-Joong Yoon, Melanie Dochow, Aiming Sun, Michael G Natchus, James P Snyder and Richard K Plemper

“Potent Host-Directed Small-Molecule Inhibitors of Myxovirus RNA-dependent RNA-polymerases”

PLoS ONE, 6 (5): e20069, May 2011

Reproduced from PLoS ONE

OPEN ACCESS Freely available online

PLoS one

Potent Host-Directed Small-Molecule Inhibitors of Myxovirus RNA-Dependent RNA-Polymerases

Stefanie A. Krumm[1,2], J. Maina Ndungu[3], Jeong-Joong Yoon[1,2], Melanie Dochow[1,2], Aiming Sun[3], Michael Natchus[3], James P. Snyder[3,4], Richard K. Plemper[1,2,5]*

1 Department of Pediatrics, Emory University School of Medicine, Atlanta, Georgia, United States of America, **2** Children's Healthcare of Atlanta, Atlanta, Georgia, United States of America, **3** Emory Institute for Drug Discovery, Emory University, Atlanta, Georgia, United States of America, **4** Department of Chemistry, Emory University, Atlanta, Georgia, United States of America, **5** Department of Microbiology & Immunology, Emory University School of Medicine, Atlanta, Georgia, United States of America

Abstract

Therapeutic targeting of host cell factors required for virus replication rather than of pathogen components opens new perspectives to counteract virus infections. Anticipated advantages of this approach include a heightened barrier against the development of viral resistance and a broadened pathogen target spectrum. Myxoviruses are predominantly associated with acute disease and thus are particularly attractive for this approach since treatment time can be kept limited. To identify inhibitor candidates, we have analyzed hit compounds that emerged from a large-scale high-throughput screen for their ability to block replication of members of both the orthomyxovirus and paramyxovirus families. This has returned a compound class with broad anti-viral activity including potent inhibition of different influenza virus and paramyxovirus strains. After hit-to-lead chemistry, inhibitory concentrations are in the nanomolar range in the context of immortalized cell lines and human PBMCs. The compound shows high metabolic stability when exposed to human S-9 hepatocyte subcellular fractions. Antiviral activity is host-cell species specific and most pronounced in cells of higher mammalian origin, supporting a host-cell target. While the compound induces a temporary cell cycle arrest, host mRNA and protein biosynthesis are largely unaffected and treated cells maintain full metabolic activity. Viral replication is blocked at a post-entry step and resembles the inhibition profile of a known inhibitor of viral RNA-dependent RNA-polymerase (RdRp) activity. Direct assessment of RdRp activity in the presence of the reagent reveals strong inhibition both in the context of viral infection and in reporter-based minireplicon assays. *In toto*, we have identified a compound class with broad viral target range that blocks host factors required for viral RdRp activity. Viral adaptation attempts did not induce resistance after prolonged exposure, in contrast to rapid adaptation to a pathogen-directed inhibitor of RdRp activity.

Citation: Krumm SA, Ndungu JM, Yoon J-J, Dochow M, Sun A, et al. (2011) Potent Host-Directed Small-Molecule Inhibitors of Myxovirus RNA-Dependent RNA-Polymerases. PLoS ONE 6(5): e20069. doi:10.1371/journal.pone.0020069

Editor: Man-Seong Park, College of Medicine, Hallym University, Republic of Korea

Received January 17, 2011; **Accepted** April 15, 2011; **Published** May 16, 2011

Copyright: © 2011 Krumm et al. This is an open-access article distributed under the terms of the Creative Commons Attribution License, which permits unrestricted use, distribution, and reproduction in any medium, provided the original author and source are credited.

Funding: This work was supported, in part, by Public Health Service Grants AI071002 and AI085328 (to R.K.P.) from the NIH/NIAID. The funders had no role in study design, data collection and analysis, decision to publish, or preparation of the manuscript. No additional external funding was received for this study.

Competing Interests: The authors have declared that no competing interests exist.

* E-mail: rplempe@emory.edu

Introduction

Myxoviruses are enveloped, negative-strand RNA viruses that are transmitted through the respiratory route. The orthomyxovirus family comprises five different genera of which the influenza viruses are clinically most relevant. Of the paramyxoviridae, respiratory syncytial virus (RSV), measles virus (MeV), mumps virus (MuV), human parainfluenzaviruses (HPIV) and the recently emerged, highly pathogenic zoonotic henipaviruses constitute major human pathogens [1]. Although clinical complications associated with some myxoviruses involve persistent infections, the viruses predominantly induce acute respiratory or systemic disease.

Collectively, myxoviruses are responsible for the majority of human morbidity and mortality due to viral respiratory illness globally [2,3]. In particular, influenza virus is the leading cause of morbidity and mortality from respiratory disease in North America despite the existence of vaccine prophylaxis. This is due to the fact that the vaccines currently in use reduce illness in approximately 70% of healthy adults when homologous to the prevalent circulating virus, but protection in the elderly reaches only approximately 40%. Vaccine efficacy is reduced substantially when the circulating strains differ from those constituting the vaccine [2].

Despite extensive research and in contrast to, for instance, MeV and MuV, no vaccines are currently available against several major pathogens of the paramyxovirus family such as RSV or different HPIVs. Infection with RSV is the leading cause of pneumonia and bronchiolitis in infants, both associated with significant mortality, while HPIV types 1 and 2 are the primary cause of croup syndrome and can likewise result in serious lower respiratory diseases such as pneumonia and bronchiolitis [4,5].

The availability of effective antiviral therapy for most clinically significant myxovirus infections is limited. Licensed neuraminidase inhibitors for influenza therapy, Zanamivir and Oseltamivir, show efficacy when administered within a 48-hour window after the onset of symptoms, but are increasingly compromised by pre-existing or emerging viral resistance [6,7,8]. Ribavirin, although approved for RSV treatment, shows limited utility due to efficacy and toxicity issues [9]. The polyclonal immunoglobulin RSV-IVIG [10] and the humanized monoclonal antibody Synagis [11] provide RSV prophylaxis, but use is limited to high-risk pediatric patients. Considering the high mutation rates seen in particular

with RNA viruses [12,13], the development of novel types of myxovirus inhibitors that circumvent the rapid development of resistance is highly desirable.

Of the strategies conceivable towards this goal, targeting host factors required for completion of the viral life cycle rather than pathogen-encoded factors directly has received heightened interest in recent years [14,15]. This approach is expected to establish a significant barrier against spontaneous viral escape from inhibition, since individual viral mutations are less likely to compensate for the loss of an essential host cofactor than to prevent high-affinity binding of a conventional, pathogen-directed antiviral. Given some degree of overlap of host cell pathways required for successful replication of related viral pathogens, host-directed antiviral approaches also have the potential to move beyond the one-bug one-drug paradigm by broadening the pathogen target range of a chemical scaffold.

Naturally, targeting host factors for antiviral therapy bears an inherently higher potential for undesirable drug-induced side effects than conventional pathogen-directed strategies. While the approach is nevertheless under investigation for the treatment of chronic viral infections such as HSV-1 and HIV-1 [16,17], an application to the inhibition of infections by pathogens predominantly associated with severe acute disease, such as most members of the myxovirus families, is anticipated to render drug-related side effects tolerable to some extent, since the necessary treatment time and concomitant host exposure to the drug remain limited. In the case of influenza infections, for instance, typical neuraminidase inhibitor regimens consist of twice daily administration for a five-day period for treatment, or a 10-day period for prophylaxis [18].

Relying on a broadened anti-myxovirus target spectrum as the main selection criterion in secondary screening assays, we have mined results of a recently completed high throughput chemical library screen [19] to identify hit candidates with a possible host-directed mechanism of action. This has yielded a compound class with broad anti-viral activity, which was subjected to synthetic scaffold optimization, quantification of active concentrations for a select group of clinically relevant ortho- and paramyxovirus family members, testing against a panel of exposed host cells of different species origin, and characterization of the compound-induced point-of-arrest in viral life cycle progression. Viral adaptation to growth in the presence of inhibitor has been employed to compare escape rates from inhibition by this new compound class with those from a well-characterized, pathogen-directed antiviral.

Results

To identify small-molecule hit candidates that block the myxovirus life cycle through a host-directed mechanism, we analyzed the results of a high-throughput cell-based anti-MeV screen of a 137,500-entry library of the NIH diversity set that we recently reported [19]. The primary screening agent, serving as the myxovirus representative, was the wild type MeV isolate MVi/Alaska.USA/16.00 (MeV-Alaska). It was chosen based on its ease of growth and readily quantifiable cytopathic effect in the automated system [19,20]. In search of candidates with a host-directed antiviral profile, we anticipated three distinct features of desirable compounds: a) potent inhibition of virus replication at the screening concentration (3.3 μM); b) a primary screening score, representative of the selectivity index (CC_{50}/EC_{50}), close to the cut-off value for hit candidates due to some anticipated host-cell interference (= 1.9); and c) a broadened viral target spectrum in counterscreening assays that extends to other pathogens of the myxovirus families.

Identification of a chemical scaffold with broad anti-viral activity

When inhibition of paramyxovirus family members was assessed, six compounds efficiently blocked the closely related canine distemper virus (CDV) and the more distantly related human parainfluenzavirus type 3 (HPIV3) in addition to MeV-Alaska, while leaving cell metabolic activity essentially unaffected [19]. Of these independent hits, three share a common molecular scaffold ([19] and figure 1A). Since HTS scores of these analogs best matched the target criteria and antiviral activity was highest in this group [19], we subjected them to further characterization and developmental efforts. Synthetic optimization and structural confirmation of the scaffold returned a lead analog JMN3-003 (figures 1B and S1), which showed potent activity against MeV, a selection of clinically significant members of the para- and orthomyxovirus families, and, albeit to a lesser degree, representatives of positive strand RNA virus (sindbis virus of the *Alphaviridae*) and DNA virus (vaccinia virus of the *Poxviridae*) families (figure 1C, inhibitory concentrations for a larger panel of myxovirus family members are summarized in table 1). As observed for the primary hit compound, metabolic activity of different established cell lines exposed to JMN3-003 was unchanged at 75 μM, the highest assessable concentration based on solubility of the substance in growth media (figure 1D and table 1). Of different primary human cells examined, metabolic activity was unaffected (PBMCs, smooth muscle cells) or only slightly affected (bronchial epithelial cells) by the compound (figure 1E). These data support potent anti-myxovirus activity of the compound with active concentrations ranging from 10 to 80 nM depending on the target virus.

Antiviral activity of lead compound JMN3-003 is host cell-specific

To further explore whether JMN3-003 meets the profile of a host-directed antiviral, we examined whether the extent of inhibition is determined by the species origin of the host cell used for virus propagation. Based on its broad host cell range, inhibition of influenza A/WSN replication was monitored. In addition to higher mammalian (HT1080 (ATCC CCL-121), HeLa (ATCC CCL-2), MDCK (ATCC CCL-34)) cell lines, cells of rodent (NIH-3T3 (ATCC CRL-1658), MEL B16 (ATCC CRL-6322), BHK-21 (ATCC CCL-10), CHO (ATCC CCL-61)) and avian (DF-1 (ATCC CRL-12203)) origin were tested, which are all permissive for influenza A/WSN infection (table 2). While inhibitory concentrations obtained for all higher mammalian cell lines examined were similar, A/WSN inhibition by JMN3-003 was found inactive on some rodent cell lines and when virus was propagated on murine or avian cells (table 2). However, inhibitory activity extended fully to primary human PBMCs (figure 2). For the latter, inhibition of MeV-Alaska was monitored due to efficient growth of MeV isolates on PBMCs [21]. The host cell species effect of antiviral activity of JMN3-003 is consistent with specific targeting of cellular factors by the compound, while arguing against docking to conserved viral factors or an undesirable promiscuous, unspecific mode of activity.

JMN3-003 shows high metabolic stability *in vitro*

The central 2-thio-connector found in the chemical scaffold of JMN3-003 may render the compound susceptible to rapid phase I oxidation *in vivo* [22], thus possibly compromising its developmental potential. To test metabolic stability of the substance early in development, we exposed JMN3-003 to human S-9 hepatocyte subcellular fractions as an *in vitro* indicator for phase I metabolism.

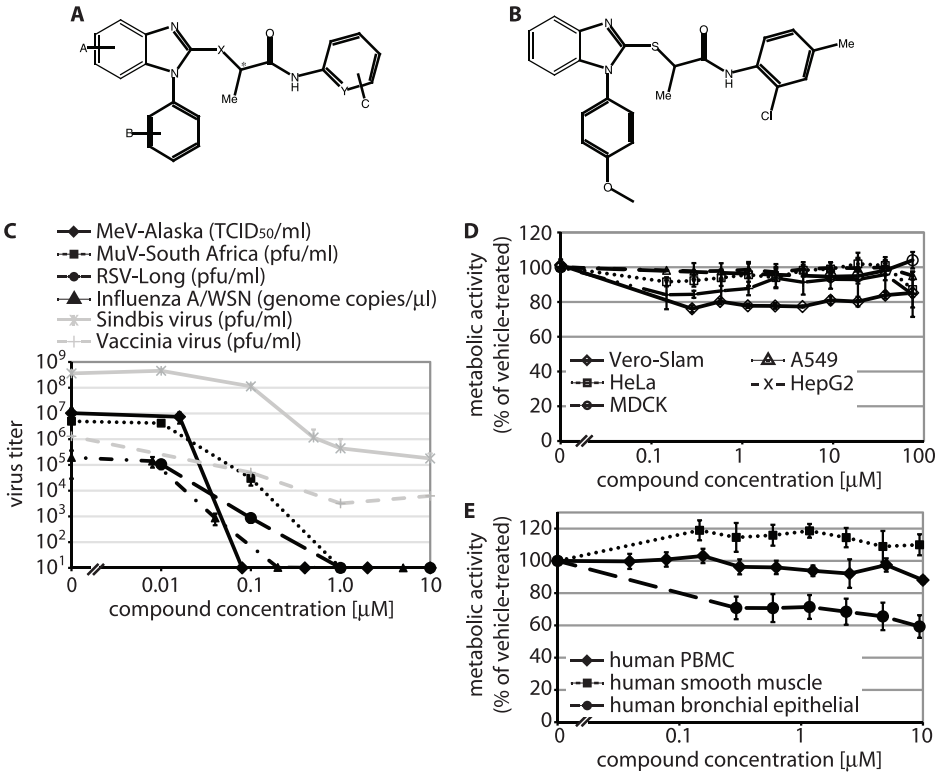

Figure 1. Identification of a chemical scaffold with broad anti-myxovirus activity. Chemical structures of the identified scaffold (**A**) and the current lead analog JMN3-003 (**B**). **C**) Dose-response curves for JMN3-003 and MeV-Alaska, MuV-South Africa, RSV Long, influenza A/WSN (H1N1), sindbis virus and vaccinia virus. Titers of cell-associated progeny viruses were determined by $TCID_{50}$ titration (MeV) or plaque assay (MuV, RSV, sindbis virus, vaccinia virus). For influenza virus, genome copy numbers of released progeny particles were quantified through TaqMan RT-PCR. Titers of released sindbis virus particles were determined by plaque assay. Values reflect averages of at least three experiments ± SD, vaccinia virus titers were determined in duplicate. **D and E**) Assessment of metabolic activity of cells after incubation of different established cell lines (D) or primary human cells (E) in the presence of JMN3-003 for 24 hours. Results for human (HeLa, A549, HepG2), primate (Vero-Slam), and canine (MDCK) cell lines and primary human cells (PBMC, smooth muscle, bronchial epithelial) are shown. Values reflect averages of four replicates ± SD.
doi:10.1371/journal.pone.0020069.g001

After a 60-minute exposure, approximately 80% of the input material remained intact, corresponding to an extrapolated half-life of approximately 200 minutes (figure 3A). Unstable analogs of JMN3-003, JMN5-165 and JMN5-166 (figure S1), returned half lives of 38 and 5 minutes in this assay, respectively, confirming metabolic competency of the S9 fractions used.

Assessment of JMN3-003 stability in human plasma in comparison with unstable Procaine and stable Procainamide

Table 1. Active (EC_{50}) and toxic (CC_{50}, determined on Vero-Slam cells) concentrations of JMN3-003 against a selection of clinically relevant para- and orthomyxovirus family members in comparison with active concentrations of AS-136A, a previously characterized, MeV-specific inhibitor of the viral RdRp complex [20,36].

Compound	Orthomyxoviridae[a]				Paramyxoviridae				Toxicity
	Influenza A/WSN	Influenza A/PR/8/34	SOI Influenza A/Texas	SOI Influenza A/Mexico	RSV[b] (Long)	MuV[b] (S. Africa)	HPIV3[b]	MeV[c] (Alaska)	Metabolic activity
	EC_{50} [µM]								CC_{50} [µM][d]
JMN3-003	0.01±0.008	0.01±0.001	0.04±0.01	0.01±0.003	0.07±0.01	0.033±0.031	0.08±0.01	0.03±0.02	>75
AS-136A	none detected	ND	ND	ND	none detected	none detected	none detected	0.03[e] (0.01–0.05)	>75

[a]For influenza virus titration, genome copy numbers of released progeny particles were quantified by TaqMan RT-PCR.
[b]Titered through plaque assaying.
[c]Titered by $TCID_{50}$ titration.
[d]Highest concentration assessed 75 µM.
[e]95% confidence interval.
ND: not determined.
doi:10.1371/journal.pone.0020069.t001

Table 2. Antiviral activity of JMN3-003 is host cell species-specific.

Host Cell		Starting Titer[a]	EC_{50}[b]	CC_{50}[c]
		Influenza A/WSN yields in controls	Inhibition of Influenza A/WSN	Metabolic Activity
Cell Line	Origin	[pfu/ml]	[μM]	[μM]
HT1080	Human	1.5×10^6	0.06±0.002	>75
HeLa	Human	1.6×10^3	0.02±0.01	>75
MDCK	Canine-dog	3.0×10^7	0.01±0.08	>75
NIH-3T3	Rodent-mouse	8.4×10^5	>10	>75
MEL B16	Rodent-mouse	5.3×10^5	>10	>75
BHK-21	Rodent-Syrian hamster	1.7×10^7	0.08±0.01	>75
CHO	Rodent-Chinese hamster	1.5×10^5	0.07±0.01	>75
DF-1	Avian-chicken	1.3×10^6	>10	>75

[a]titers of progeny virus grown on the different cell lines in the presence of vehicle (DMSO) only were determined through plaque assays on MDCK cells.
[b]EC_{50} concentrations were determined based on four parameter non-linear regression models generated for individual dose-response curves.
[c]Highest concentration assessed 75 μM.
Active concentrations (EC_{50}) of JMN3-003 against influenza A/WSN propagated on a variety of different host cell lines.
doi:10.1371/journal.pone.0020069.t002

[23] corroborated these results, since JMN3-003 integrity was virtually unaffected after a 120-minute incubation period (figure 3B). Taken together, these findings suggest desirable metabolic stability for the JMN3-003 scaffold, recommending it for further mechanistic characterization. The data are corroborated by the good metabolic stability reported for the structurally similar compound RDEA-806 (figure S2), a non-nucleoside inhibitor of HIV reverse transcriptase and clinical precedent [24], which shares the 2-thio-connector of JMN3-003 but lacks MeV inhibitory activity in our assays (data not shown).

Temporary arrest in cell cycle progression

Since direct cytotoxicity of JMN3-003 was low for all cell lines examined, we next tested the effect of the substance on cell cycle progression. Analysis of the DNA content of cells continuously treated with JMN3-003 for 36 hours by flow cytometry revealed accumulation of cells in a single population with 2N DNA content, which closely resembled the profile of a reference cell population exposed to hydroxyurea but markedly differed from the 4N DNA content of nocodazole-treated cells (figure 4A). Nocodazole interferes with microtubule polymerization [25], resulting in a G_2/M arrest, whereas hydroxyurea is thought to lead to an arrest in the G_1/S-phase through depletion of cellular dNTP pools [26,27]. To further explore the effect of JMN3-003 on cell cycle progression, we monitored the phosphorylation status of the cdc2-cyclin B kinase after exposure of cells to either the compound, hydroxyurea, nocodazole, or alsterpaullone, a nanomolar small molecule inhibitor of cyclin-dependent kinases that reportedly induces a potent G_1/S-phase cell cycle arrest [28]. Pivotal in regulating the G_2/M transition, cdc2-cyclin B kinase is inactivated through phosphorylation during the G_2-phase. Accumulation in its phosphorylated form thus indicates a G_1 arrest. As in hydroxyurea- and alsterpaullone-treated controls, exposure of cells to JMN3-003 resulted in increased steady state levels of phosphorylated cdc2-cyclin B kinase, supporting a G_1-phase arrest (figure 4B).

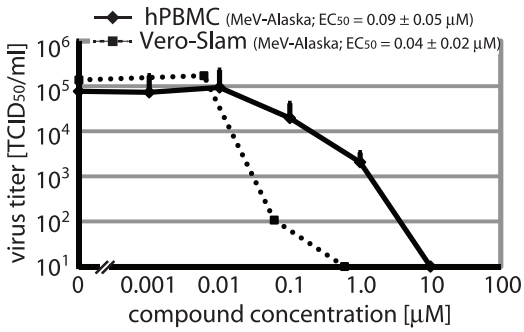

Figure 2. The cellular target range of JMN3-003 extends to primary human cells. Dose-response curves for MeV-Alaska grown in the presence of JMN3-003 on human PBMCs originating from a mixed pool of healthy donors. Vero-Slam cell-based inhibition curves are shown for comparison. Values reflect averages of three replicates. EC_{50} concentrations ± SD are derived from four-parameter non-linear regression modeling.
doi:10.1371/journal.pone.0020069.g002

To test whether this JMN3-003-induced arrest is permanent or temporary, we next incubated cells in the presence of compound or vehicle alone for 30 hours, followed by removal of the substance and reseeding of cells at identical densities. Monitoring cell growth over an additional 72-hour incubation period in the absence of JMN3-003 revealed that proliferation rates resumed those of untreated control cells after removal of the compound (figure 4C), indicating reversibility of the growth arrest.

In contrast to members of the orthomyxovirus family, paramyxovirus replication takes place in the cytosol and, thus, is considered not to be immediately dependent on active cell proliferation [1]. In fact, MeV itself has been shown to induce a G_1/S arrest in infected T lymphoyctes [29,30], confirming that cell cycle progression is not required for virus replication. To directly test whether the JMN3-003-mediated growth arrest *per se* is causal for the antiviral effect of the compound, we generated MeV-Alaska inhibition curves of JMN3-003 in comparison with the cyclin-dependent kinase inhibitor alsterpaullone. Even at the highest concentration assessed (50 μM), alsterpaullone caused only a marginal reduction in MeV yields (figure 4D). These findings indicate that the antiviral effect of JMN3-003 is based on an upstream effect of the compound rather than being a consequence of the cell cycle arrest itself.

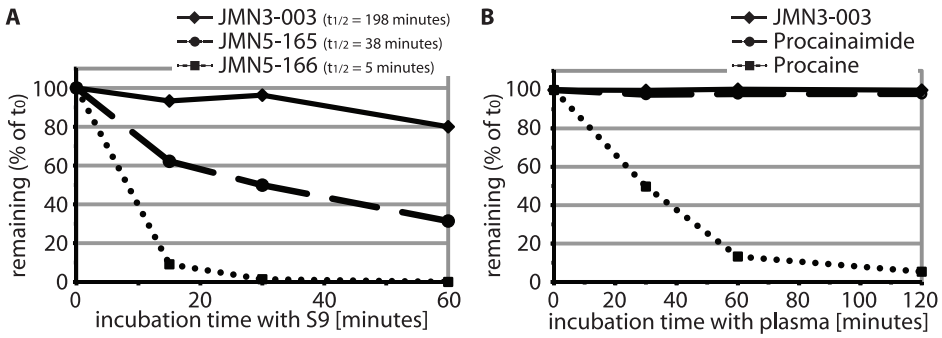

Figure 3. The JMN3-003 scaffold is metabolically stable *in vitro*. **A**) Incubation of the article with human liver S9 fractions for up to 60 minutes, followed by LC-MS/MS analysis of the material remaining. Two analogs of JMN3-003, JMN5-165 and JMN5-166 (figure S1), showed little stability and are included for comparison. Values represent averages of 2 replicates, calculated half-lives ($t_{1/2}$) are given in the figure captures. **B**) Incubation of JMN3-003 for up to 120 minutes with human plasma derived from mixed, healthy donors, followed by LC-MS/MS quantification of the material remaining. Unstable procaine and stable procainamide were examined equally for comparison. Values represent averages of three experiments ± SD.
doi:10.1371/journal.pone.0020069.g003

Cellular mRNA production and protein biosynthesis are unperturbed by JMN3-003

To explore whether growth arrest of treated cells coincides with reduced host cell RNA synthesis or overall cell protein biosynthesis, we next assessed the effect of JMN3-003 on host mRNA and protein production. Relative levels of three signature host mRNAs with short half lives, MCL1, ASB7 and MKP1 [31,32], were determined by real time PCR after incubation of cells in the presence of different JMN3-003 concentrations ranging from 0.01 to 10 μM. In all cases, mRNA levels of JMN3-003-exposed cells were similar to those of the vehicle-treated references, while exposure to Actinomycin D, which blocks RNA synthesis through arrest of the transcription initiation complex [33], resulted in a major reduction in relative mRNA levels (figure 5A).

Immunodetection of cellular GAPDH and plasmid-encoded MeV F protein under the control of the CMV promoter demonstrated that productive transcription in the presence of the compound furthermore coincides with uninterrupted translation and, in the case of F, co-translational insertion into the host secretory system (figure 5B). Furthermore, equivalent levels of proteolytically processed F_1 material in JMN3-003 and vehicle-exposed cells indicated that intracellular vesicular transport remains intact in the presence of JMN3-003, since cleavage is mediated by the cellular protease furin in a late-Golgi compartment [1]. In contrast to host-encoded or transiently expressed proteins, expression of virus-encoded proteins in the context of paramyxovirus or orthomyxovirus infection was fully blocked by 100 nM JMN3-003 (figures 5C and D). Thus, these observations demonstrate that the compound efficiently suppresses the expression of virus-encoded proteins, but that this is not due to general interference of the inhibitor with cellular mRNA synthesis or translation. This phenotype suggests possible interference of JMN3-003 with early steps of the viral life cycle, such as entry or viral RdRp activity, as the basis for antiviral activity.

Inhibition of a post-entry step of the viral life cycle

To differentiate between those alternatives and identify the point of arrest in the viral life cycle induced by JMN3-003, we first examined whether the compound blocks membrane fusion and thus viral entry. Expression of plasmid-encoded paramyxovirus envelope glycoproteins in receptor-positive cells typically results in extensive cell-to-cell fusion, the hallmark cytopathic effect associated with most paramyxovirus infections *in vitro* [1]. Transient membrane fusion assays allow a quantitative assessment of whether an inhibitor blocks viral entry or post-entry steps of the viral life cycle [20,34]. When we examined MeV glycoprotein-mediated cell-to-cell fusion microscopically (figure 6A) and in a luciferase reporter-based quantitative cell-to-cell fusion assay (figure 6B) in the presence of JMN3-003, we observed extensive membrane fusion indistinguishable from that seen in vehicle-treated controls, indicating that the compound does not act as an entry inhibitor.

To determine whether JMN3-003 predisposes host cells against viral infection by inducing an antiviral state, we pre-treated cells with the compound, followed by wash-out of the substance and virus infection after different time periods. Independent of incubation time after removal of the compound, we could not detect any substantial inhibitory effect in this set-up (figure 6C), arguing against priming of the innate antiviral response by JMN3-003. Likewise, preincubation of viral particles with JMN3-003 prior to removal of the article and infection lacked any appreciable antiviral effect (figure 6D), excluding direct virucidal activity of the substance.

When added in a time-of-addition experiment at distinct time points post-infection in comparison with two previously characterized, pathogen-targeted antivirals, the inhibition profile of JMN3-003 was distinct from that of the entry inhibitor AS-48 [34] but very closely resembled the profile of the AS-136A RdRp blocker class ([20], figure 6E). Thus, these data point towards inhibition of the viral RdRp activity by JMN3-003 as one possible underlying mechanism for antiviral activity of the compound.

Host-directed inhibitor of viral RdRp activity

For myxovirus infection, the viral RdRp complex mediates both genome transcription and replication to express viral proteins and generate progeny genomes, respectively. Replication occurs through generation of an antigenome of positive polarity, which then serves as template for negative strand genome synthesis [1]. To directly test whether JMN3-003 affects viral RdRp activity in the context of virus infection, we determined the copy numbers of MeV-Alaska mRNA and antigenome in infected, compound-treated cells relative to vehicle-treated controls by quantitative RT-PCR. Presence of JMN3-003 caused a dose-dependent reduction in viral RNA levels (figure 7A). At a concentration of 100 nM, for instance, we observed a >100-fold reduction of viral

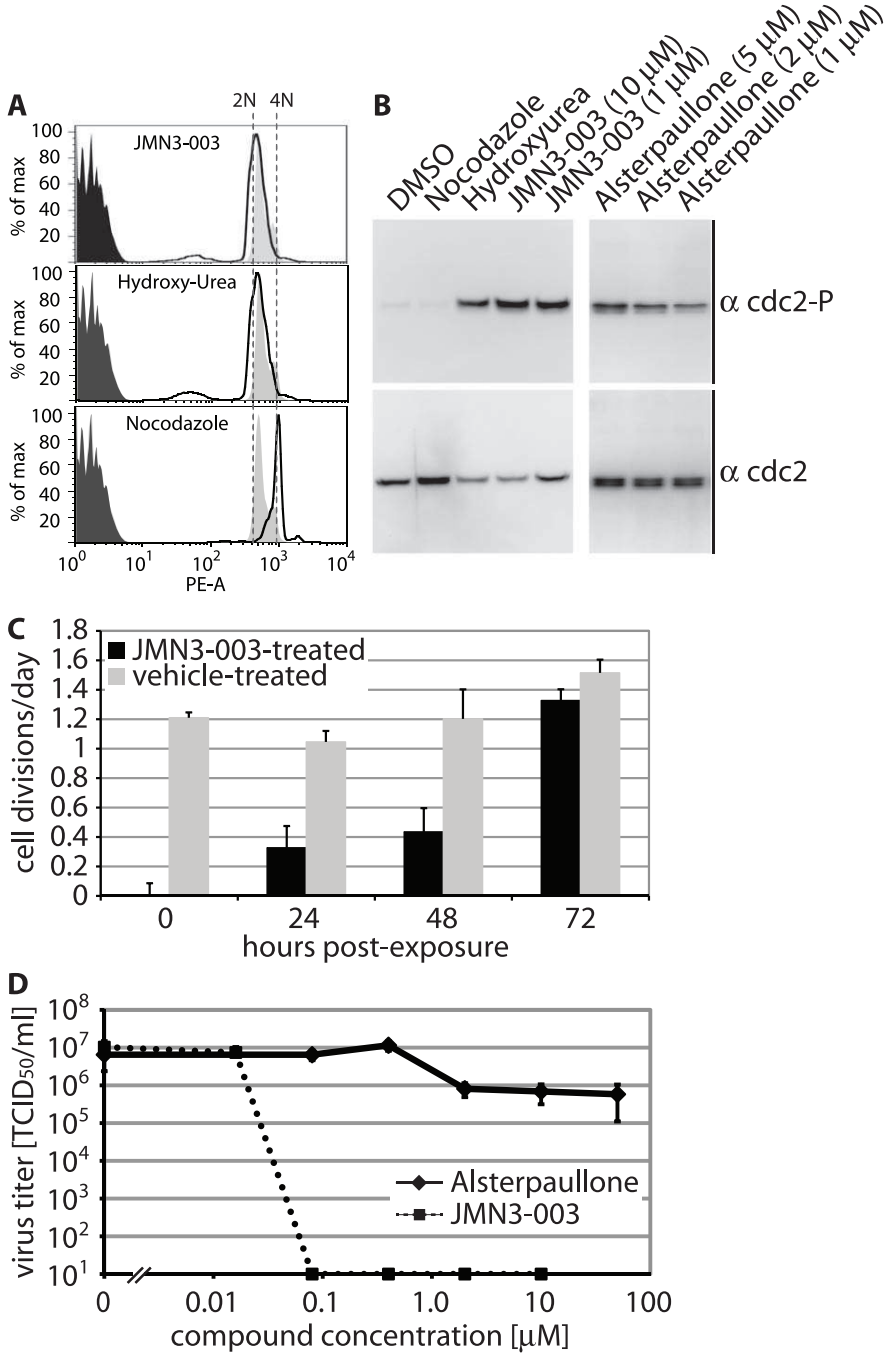

Figure 4. Cell exposure to compound JMN3-003 induces a temporary G_1/S phase cell cycle arrest. A) FACS analysis of acridine orange-stained HeLa cells incubated in the presence of JMN3-003 or hydroxyurea for 36 hours, or nocodazole for 16 hours. Dark grey shaded areas show unstained cells, light grey areas correspond to vehicle-treated control cells, and areas under open black curves represent treated cell populations. Dashed vertical lines indicate 2 N (G_1/S) and 4N (G_2/M) DNA contents. Data shown are representative of three experiments and reflect 10,000 events/condition of treatment. **B**) Analysis of the phosphorylation status of cdc2-cyclin B kinase after cell exposure to JMN3-003 through immunoblotting using specific antisera directed against phospho-cdc2 (Tyr15; α cdc2-P) or total cdc2 (α cdc2) for comparison. For control, cells were treated with nocodazole, hydroxyurea, or alsterpaullone (right panel). Results shown are representative of multiple experiments. **C**) Wash-out of JMN3-003 restores cell proliferation. Growth rates of Vero cells were determined after 30-hour exposure of cells to JMN3-003 or vehicle only, followed by wash-out of the substance. Values reflect cell divisions per day and are based on averages of six independent replicate experiments ± SEM. **D**) G_1/S phase cell cycle arrest does not affect MeV proliferation *per se*. Dose-response curves for alsterpaullone, a nanomolar CDK1/cyclin B kinase inhibitor, and MeV-Alaska grown on Vero-Slam cell. Titers of cell-associated viral particles were determined 36 hours post-infection through $TCID_{50}$ titration. JMN3-003 was examined in parallel for comparison. Values reflect averages of three replicates ± SD.
doi:10.1371/journal.pone.0020069.g004

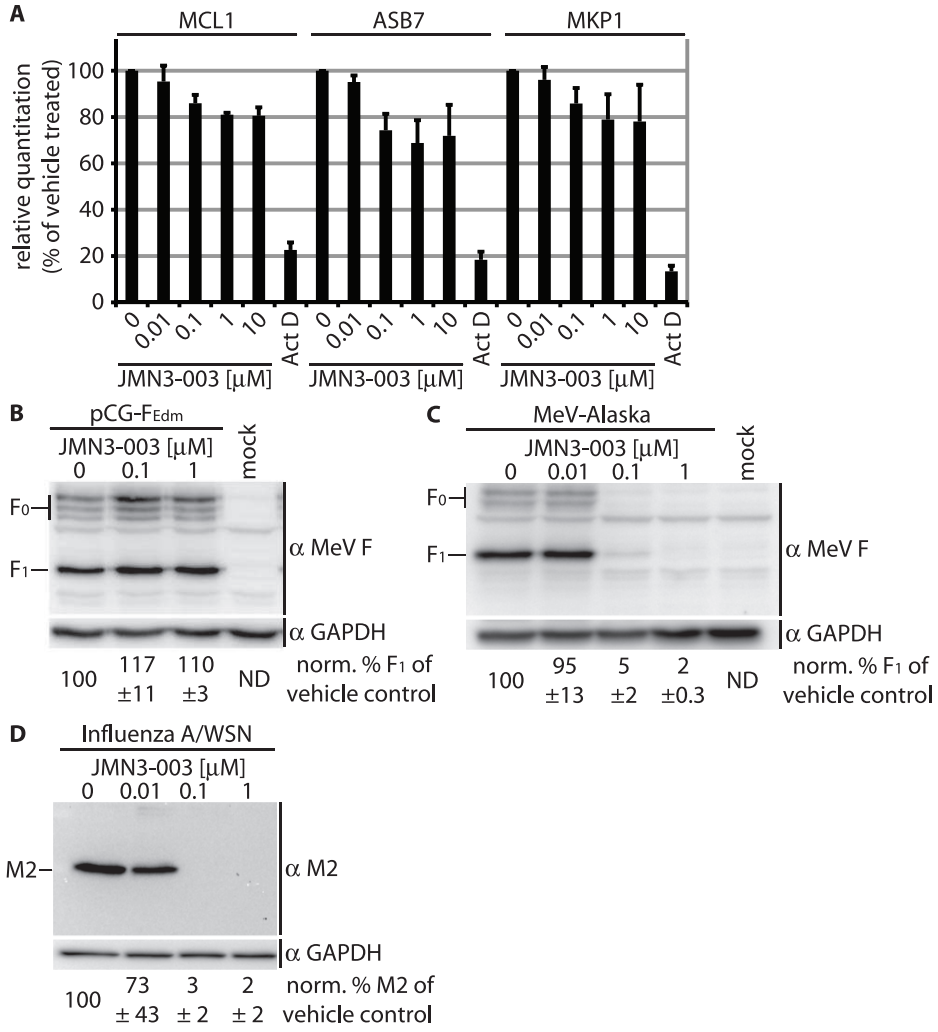

Figure 5. Host cell mRNA synthesis and translation are unaffected by compound JMN3-003. A) Relative TaqMan RT-PCR-based quantitation of three unstable cellular mRNAs (MCL1, ASB7, MKP-1) after exposure of cells to JMN3-003 for six hours. Controls were treated with Actinomycine D (Act D) for comparison. C_T values are expressed relative to vehicle-treated samples and reflect averages of three independent experiments, each analyzed in triplicate, ± SD. **B–D**) Expression of virus-encoded but not host cell or plasmid-encoded viral proteins is blocked by JMN3-003. Immunodetection of transiently expressed MeV-F (**B**), virus-encoded MeV-F (**C**), and virus-encoded influenza A/WSN M2 (**D**) in cell lysates after incubation of cells in the presence of compound or vehicle only (DMSO) for 30 hours. As internal cellular standard, membranes were probed for GAPDH in parallel. Numbers correspond to average densitometric quantitations ± SD of three experiments, representative immunoblots are shown. (ND: not determined).
doi:10.1371/journal.pone.0020069.g005

mRNA and antigenome copy numbers relative to vehicle-treated samples, indicating potent inhibition of viral replication. For comparison, a concentration of 25 μM of the RdRp inhibitor AS-136A, a nanomolar blocker of MeV replication [35], was required to achieve comparable mRNA and antigenome reduction levels (figure 7A).

When this assay was applied to orthomyxovirus infection, we likewise observed a dose-dependent inhibition of influenza A/WSN antigenome levels relative to vehicle treated controls (figure 7B). Parallel quantification of genome copy numbers of released progeny virus demonstrated that an approximate >100-fold drop in relative viral antigenome levels correlates to a >10,000-fold reduction in genome copies of released progeny virions (figure 7B).

Assessment of viral RdRp activity in a plasmid-based mini-replicon reporter system confirmed dose-dependent inhibition of RdRp by JMN3-003 also in a sub-infection setting, since luciferase reporter expression was fully blocked at compound concentrations of approximately 100 nM (figure 7C). Taken together, these data suggest indirect inhibition of the viral polymerase complex through interaction of the compound with a cellular cofactor required for RdRp activity as the basis for the antiviral effect of JMN3-003.

JMN3-003 does not induce rapid emergence of viral resistance

It has been suggested for different viral pathogens that a host-directed antiviral approach has the potential to reduce the frequency of viral escape from inhibition compared to direct targeting of pathogen components [14,15]. To explore whether resistance to JMN3-003 could be induced experimentally, we attempted stepwise viral adaptation to growth in the presence of

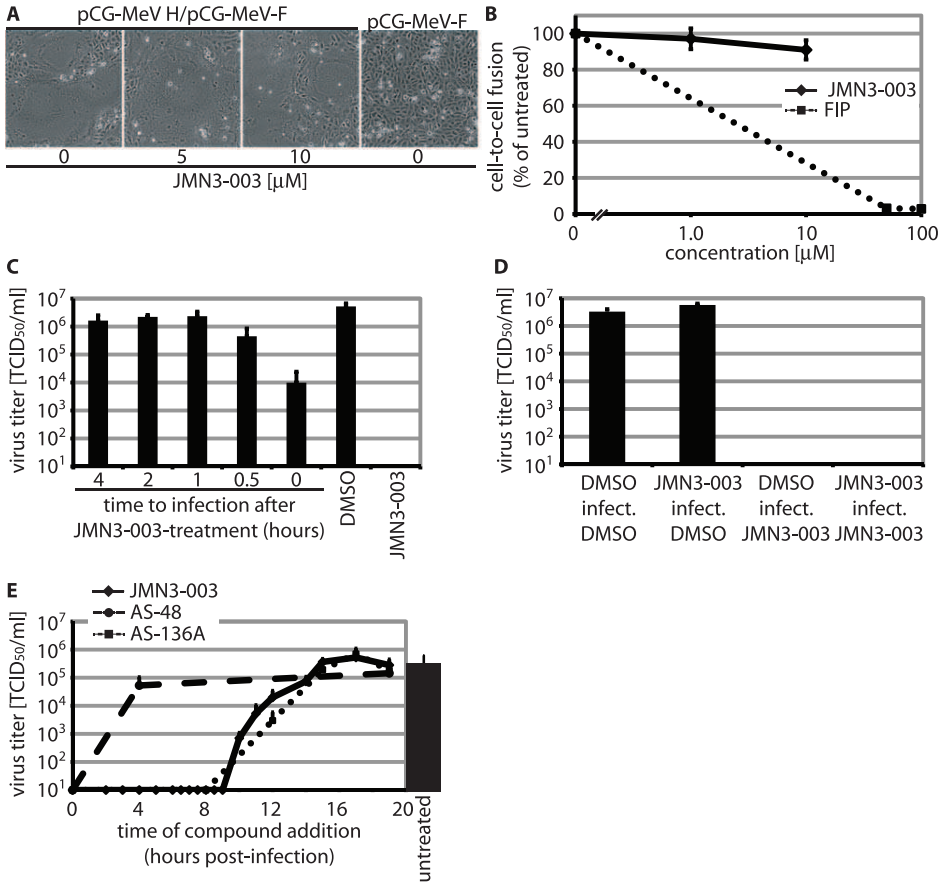

Figure 6. In time-of-addition assays, JMN3-003 shows the inhibition profile of an RdRp blocker. A–B) Cell-to-cell fusion is unaffected by the compound. Microphotographs of MeV-H and F expressing Vero-Slam cells (**A**) and quantitative cell-to-cell fusion assays (**B**) show membrane fusion activities in the presence of JMN3-003 similar to those observed for vehicle (DMSO)-treated controls. The effect of fusion inhibitory peptide (FIP) is shown in (B) for comparison. **C**) JMN3-003 antiviral activity is reversible and not based on cell priming. Vero-Slam cells were pre-treated with 1.0 μM JMN3-003 for 60 minutes, followed by compound wash-out and incubation for the indicated time periods; at t_0, cells were infected with MeV-Alaska. **D**) JMN3-003 lacks virucidal activity. MeV-Alaska particles were incubated with 1.0 μM JMN3-003 for 60 minutes, followed by dilution of compound to 1.0 nM and infection of cells at an MOI of 0.033 in the presence of vehicle (JMN3-003/infect./DMSO). Equally treated controls received vehicle only (DMSO/infect./DMSO), compound only after infection (DMSO/infect./JMN3-003), or compound for the duration of the experiment (JMN3-003/infect./JMN3-003). **E**) Addition of JMN3-003 (1.0 μM final concentration) at the indicated times post-infection of cells with MeV-Alaska. For comparison, inhibition profiles of the MeV entry inhibitor AS-48 (75 μM) and RdRp blocker AS-136A (25 μM) are shown. Controls received vehicle only (DMSO) at the time of infection. For (C–E), values show titers of cell associated viral particles ($TCID_{50}$/ml) and represent averages of at least three experiments ± SD.
doi:10.1371/journal.pone.0020069.g006

the compound in comparison with the pathogen-specific MeV RdRp inhibitor AS-136A [36]. Following an escalating dose scheme, inhibitor concentrations were doubled when virus-induced cytopathicity became detectable microscopically. While robust resistance to the pathogen-targeted AS-136A control emerged rapidly in an approximate 15 to 20-day time window (tolerated dose at the end of adaptation was ≥30 μM, equivalent to ≥100-fold resistance), only marginal increases in the tolerated dose could be detected for JMN3-003 after 90 days of continued viral incubation in the presence of the substance (figure 8). These results are consistent with a host-directed mechanism of action of JMN3-003 and suggest the existence of a systemic barrier that prevents rapid viral escape from inhibition by the article.

Discussion

In recent years, host cell-directed antivirals have experienced growing recognition as a new concept for the development of advanced generation antivirals with the potential to counteract the challenge of preexisting or rapidly emerging viral resistance [14,15]. Novel automated genomics and proteomics analyses have greatly advanced our insight into host-pathogen interactions [37,38,39,40,41,42,43,44]. These studies have underscored the notion that several cellular pathways are exploited for virus replication [45,46], supporting the hypothesis that a host-directed antiviral may enjoy an expanded viral target range, rendering it effective for the treatment of several related viral diseases.

Technologies applied for host-directed drug discovery include cDNA and siRNA-based microarray analyses combined with pathway-guided data mining [47,48,49,50,51], loss-of-function screens using aptamers or small oligonucleotides [52,53,54, 55,56,57,58], protein array analyses [59] and chemical library screening [60,61]. By combining automated library screening [19] with counter screens against a variety of related viral pathogens of the myxovirus families, we have identified a candidate scaffold that, after moderate hit-to-lead chemistry, adheres to the profile of

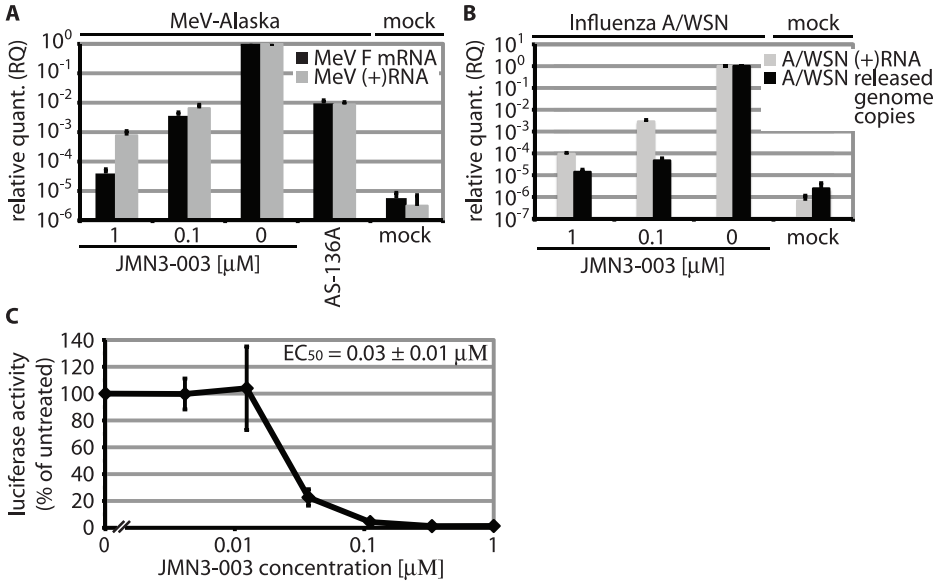

Figure 7. Compound JMN3-003 inhibits viral RNA synthesis. A) Relative quantitations of MeV F mRNA and antigenome (+RNA) levels after incubation of infected cells in the presence of compound for 40 hours. Samples were normalized for vehicle only (DMSO)-treated cells and $\Delta\Delta C_T$ values calculated using cellular GAPDH as reference. Mock samples remained uninfected. Averages of three independent experiments, assessed in triplicate each, ± SD are shown. **B**) Quantitation of influenza A/WSN segment seven antigenome (+RNA) and of released progeny genomic RNA (genome copies) after incubation of infected MDCK cells in the presence of compound for 24 hours. For +RNA quantitation, samples were normalized and $\Delta\Delta C_T$ values calculated as outlined in (A). Released genome copies were quantified by TaqMan RT-PCR relative to an external standard, then normalized for vehicle-treated controls. Averages of four experiments, assessed in triplicate each, ± SD are shown. **C**) Luciferase reporter-based assessment of viral RdRp activity in the presence of JMN3-003. BHK-T7 cells transfected with plasmids encoding the MeV minireplicon reporter system were incubated in the presence of JMN3-003 or vehicle only for 36 hours. Values were normalized for luciferase activities found in vehicle (DMSO)-treated controls and represent averages of three experiments assessed in duplicate each ± SD.
doi:10.1371/journal.pone.0020069.g007

a host-directed antiviral based on several lines of evidence: I) antiviral activity is host cell species-dependent, indicating specific interaction with a distinct host factor rather than a viral component. Host cell-specific activity is incompatible with compound docking to conserved viral factors. For example, carbohydrate structures exposed on viral envelope glycoproteins that are targeted by antiviral lectins such as pradimicin A [62]. Furthermore, it is incompatible with an undesirable unspecific, promiscuous mode of action of the compound [63]; II) affinities against a panel of human pathogens of the paramyxovirus family as well as laboratory adapted and wild type influenza virus isolates were very similar throughout (average EC_{50} concentrations are

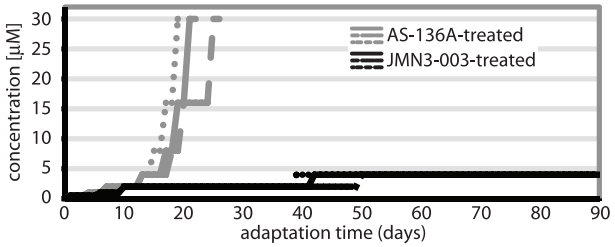

Figure 8. JMN3-003 prohibits rapid emergence of viral resistance *in vitro*. MeV-Alaska remains sensitive to the compound after continued adaptation events for a 90-day period, while resistance (extensive viral CPE detectable in the presence of 30 μM compound) to pathogen-directed AS-136A emerges in step-wise adaptations after 15–25 days. Three independent adaptations (represented by solid, dotted and dashed lines, respectively) were pursued for each compound.
doi:10.1371/journal.pone.0020069.g008

~40 nM). Equivalent active concentrations argue against compound docking to distinct viral components and suggest that inhibition of distinct myxovirus families follows the same mechanism of action; III) *in vitro* adaptation attempts to induce viral resistance were unsuccessful even after extended exposure times to the drug. A full assessment of the frequency of viral escape from inhibition by JMN3-003 will certainly need to include *in vivo* virus adaptation attempts in suitable animal models, since the rate of resistance build-up may vary between tissue culture and *in vivo* settings. We nevertheless reliably induced resistance in less than 30 days to a pathogen-directed MeV RdRp inhibitor that was analyzed in parallel, which is fully consistent with our previous experience [36] and provides confidence for the validity of our overall experimental design for viral adaptation.

Mechanistic analysis of the bioactivity of the JMN3-003 compound class through characterization of exposed cells and time-of-addition experiments revealed two distinct phenotypes, a temporary cell cycle arrest in the G_1/S phase and an arrest in the myxovirus life cycle at a post-entry step. Current libraries of chemical analogs of JMN3-003 do not yet permit a definitive conclusion as to whether both activities adhere to discrete structure-activity relationships or are causally linked, but a bulk of experimental data demonstrate that host cell cycle arrest *per se* has no inhibitory effect on replication of paramyxoviruses such as MeV. Not only does the virus itself induce a G_1/S-phase arrest in infected T lymphocytes [29,30], we also found that exposure of infected cells to alsterpaullone, a potent blocker of G_1/S-phase cell cycle progression through nanomolar inhibition of cellular cyclin-dependent kinases [28], did not affect the extent of virus replication even at concentrations exceeding reported alsterpaullone EC_{50} values by more than 1,000-fold. Likewise consistent

with the notion that the antiviral activity of JMN3-003 is not based on cell cycle arrest itself, virus inhibition was not restricted to the context of immortalized, rapidly dividing tissue culture cell lines but extended with equal potency to primary human PBMCs.

Reversible cell cycle arrest and block of virus replication indicate non-covalent docking of JMN3-003 to its target structures, which is corroborated by the compound's stability, low chemical reactivity profile and the complete absence of virucidal activity in pre-incubation settings. An inhibition profile of JMN3-003 closely mimicking that of AS-136A, the pathogen-directed blocker of MeV RdRp targeting the viral L polymerase protein [36], and the block in viral RdRp activity in the context of viral infection and minireplicon reporter assays by JMN3-003 consistently point towards interaction of the compound with a host cofactor essential for RdRp function as the basis for its antiviral activity. While viral RdRp depends on a variety of host cell components [1], unperturbed cellular mRNA synthesis and, thus, uninterrupted host RNA polymerase function in the presence of compound exclude interference of JMN3-003 with essential transcription initiation factors.

Recently, accumulating evidence has implicated host cell kinases as regulators of the activity of RdRp complexes of different negative-strand RNA viruses [64]: host cell kinases of the PI3K-Akt pathway manipulate paramyxovirus RdRp activity through Akt-mediated phosphorylation of the viral phosphoprotein, an essential component of the RdRp complex. Furthermore, Akt activity itself is upregulated through activation of PI3K during influenza A infection via direct interaction of the viral NS1 protein with PI3K [65,66]. In the case of MeV, however, published data [67,68] and our own observations (Krumm and Plemper, unpublished) demonstrate that Akt inhibition causes a moderate reduction in virus release, whereas titers of cell-associated progeny particles remain unchanged. While this rules out the PI3K-Akt pathway as a direct target for JMN3-003, it illuminates the intricate regulatory interactions between pathogen and host, which provide a wealth of possible points of entry for antiviral intervention. Future identification of the molecular target of JMN3-003 carries high potential to further our understanding of these interactions and may conceivably provide a basis for pharmacophore extraction and structure-driven scaffold optimization.

We note that the central sulfur in the JMN3-003 chemical scaffold could potentially render the molecule vulnerable to rapid phase I oxidation and thus compromise both metabolic stability and bioavailability. For instance, it has been reported that flavin-containing monooxygenases [69], dioxygenases [70] and cytochrome P-450 enzymes [71] catalyze oxidation of alkylaryl sulfides to sulfoxides ($R_2S=O$). However, the high stability of JMN3-003 in the presence of human hepatocyte subcellular fractions and human plasma argues against an undesirable short *in vivo* half-life of the substance. This is corroborated by good metabolic stability of the structurally similar HIV reverse transcriptase inhibitor RDEA-806 [72,73], which shares the central 2-thio-acetamide connector with JMN3-003 and has achieved success in clinical trials: the compound was well tolerated in both Phase 1 and 2a studies after single or multiple oral doses and showed no drug-related CNS toxicity [72,73], creating a clinical precedence for the applicability of the broader scaffold. Although RDEA-806 follows a different mechanism of action than JMN3-003 and lacks any anti-paramyxovirus activity, the structural similarities provide sufficient confidence for the overall developmental potential of the JMN3-003 class to recommend it as a promising candidate for advanced synthetic optimization towards preclinical validation and development.

In toto, we have identified a novel chemical class of viral inhibitors that block viral RdRp activity with a host factor-mediated profile. A complete activity workup after synthetic identification of a clinical lead analog will be required to fully appreciate the range of the different viral families inhibited by the substance. However, we consider human pathogens of the myxovirus families that are primarily associated with acute disease among the most suitable for host-directed antiviral efforts due to anticipated short treatment regimens. While we cannot exclude that resistance to JMN3-003 may eventually emerge in *in vivo* settings, our *in vitro* adaptation efforts support the hypothesis that the mechanism of action of this compound class establishes a strong barrier against rapid viral escape from inhibition.

Materials and Methods

Cells and viruses

All cell lines were maintained at 37°C and 5% CO_2 in Dulbecco's modified Eagle's medium supplemented with 10% fetal bovine serum. Vero (African green monkey kidney epithelial) cells (ATCC CCL-81) stably expressing human signaling lymphocytic activation molecule (CD150w/SLAM), called in this study Vero-SLAM cells [74], and baby hamster kidney (BHK-21) cells stably expressing T7 polymerase (BSR-T7/5 (BHK-T7) cells [75]) were incubated at every third passage in the presence of G-418 (Geneticin) at a concentration of 100 μg/ml. Lipofectamine 2000 (Invitrogen) was used for cell transfections. Peripheral blood mononuclear cells (PBMCs) were prepared through overlay of whole blood samples from mixed, healthy human donors (Emory University Institutional Review Board approval IRB00045690, Phlebotomy of Healthy Adults for Research in Infectious Diseases and Immunology) on Ficoll Hypaque solution, followed by centrifugation at 240×g for 30 minutes at room temperature and removal of the interphase material. Red blood cells were lysed with RBC lysis solution (Sigma), followed by repeated washing of extracted PBMCs with phosphate buffered saline and transfer to tissue culture plates pre-coated with poly-L-lysine (Sigma). Other primary human cell lines were obtained from PromoCell, Germany. Virus strains used in this study were MeV isolate MVi/Alaska.USA/16.00, genotype H2 (MeV-Alaska) [76], HPIV3, MuV strain South Africa, RSV strain Long, laboratory adapted influenza A strains WSN (H1N1) and PR8/34 (H1N1), swine-origin influenza virus isolates S-OIV Texas and Mexico, vaccinia virus and sindbis virus. To prepare virus stocks, cells permissive for the virus to be amplified (Vero-Slam, Vero, HepG2 (ATCC HB-8065), and Madin-Darby canine kidney (MDCK)) were infected and incubated at 37°C. Cell-associated paramyxovirus and vaccinia virus particles were harvested by scraping cells in OPTIMEM (Invitrogen), followed by release of virus through two consecutive freeze-thaw cycles. Influenza virus and sindbis virus particles were harvested from cell culture supernatants. Titers of MeV and MuV were determined through 50% tissue culture infective dose ($TCID_{50}$) titration according to the Spearman-Karber method [77] as described [78], titer of all other viruses were determined by plaque assay on permissive cells.

Influenza A titration by TaqMan RT-PCR

To determine genome copy numbers of released progeny influenza A particles (strains WSN, PR8/34, S-OIV Texas and Mexico), culture supernatants of infected MDCK cells (4×10^5 cells/well in a 12-well plate format) were harvested and total RNA prepared using a QIAcube automated extractor and the QIAamp viral RNA mini kit reagent. Purified RNA was then subjected to quantitative real time (qRT) PCR analysis using an Applied

Biosystems 7500 Fast real-time PCR system and the qRT-PCR TaqMan Fast Virus 1-Step Master Mix (Applied Biosystems). Primers and probe are based on recent reports [79] and universally reactive with all influenza A strains including the recent S-OIV (H1N1) isolates. To generate a qRT-PCR standard, genome segment seven of influenza A/WSN was subcloned into pCR2.1-TOPO vector (Invitrogen) and copy numbers of the resulting standard calculated using Promega's BioMath Calculator tools (http://www.promega.com/ biomath/). For each TaqMan reaction, 10-fold serial dilutions of the linearized plasmid ranging from 10^7 to 10^1 were amplified in parallel.

Compound synthesis

Chemical synthesis of compounds AS-48, AS-136A and RDEA-806 was achieved as previously described [24,34,36]. Synthesis of JMN3-003, N-(4-methoxyphenyl)-2-nitroaniline (substance (3) in figure S1), and analogs JMN5-165 and JMN5-166 was achieved as outlined schematically in figure S1. To prepare inhibitor stocks, compounds were dissolved at 75 mM in DMSO.

Viral CPE-reduction assay

Vero-SLAM cells were infected with MeV-Alaska at an MOI of 0.4 pfu/cell in the presence of the inhibitor analyzed ranging from 75 μM to 293 nM in two-fold dilutions. At 96 hours post-infection, cell monolayers were subjected to crystal violet staining (0.1% crystal violet in 20% ethanol), and the absorbance of dried plates at 560 nm determined. Virus-induced cytopathicity was then calculated according to the formula [% rel. CPE = 100−(experimental-minimum)/(maximum-minimum)*100], with minimum referring to infected, vehicle-treated wells and maximum to mock-infected wells.

Virus yield reduction assay

Cells were infected with the specified myxovirus at an MOI = 0.1 pfu/cell (all paramyxoviruses assessed), 0.05 pfu/cells (influenza viruses), 1.0 (vaccinia virus), or 10 sindbis virus) in the presence of a range of compound concentrations or equivalent volumes of solvent (DMSO) only, and incubated in the presence of compound at 37°C. When vehicle treated controls approached the end of the logarithmical growth phase, progeny viral particles were harvested and titered by $TCID_{50}$ titration, plaque assay or TaqMan real-time PCR, respectively, as described above. Plotting virus titers as a function of compound concentration allowed quantitative assessment of resistance. Where applicable, 50% inhibitory concentrations were calculated using the variable slope (four parameters) non-linear regression-fitting algorithm embedded in the Prism 5 software package (GraphPad Software).

Quantification of compound cytotoxicity

A non-radioactive cytotoxicity assay (CytoTox 96 Non-Radioactive Cytotoxicity Assay, Promega) was employed to determine the metabolic activity of cell after exposure to the compound. In a 96-well plate format, 10,000 cells per well were incubated at 37°C for 24 hours in four replicates per concentration tested in the presence of compound in two-fold dilutions starting at 75 μM. Substrate was then added and color development measured at 490 nm using a BioRad plate reader. Values were calculated according to the formula [% toxicity = 100−((experimental-background)/(maximum(vehicle treated)-background)*100)]. Values were plotted in dose-response curves and, if applicable, CC_{50} concentrations calculated.

In vitro assessment of metabolic and plasma stability

JMN3-003 was mixed with liver S9 fractions (protein concentration 2.5 mg/ml) from pooled mixed gender humans (Xeno-Tech) at a final concentration of 1 μM and reactions initiated by the addition of cofactors (1.14 mM NADPH, 1.43 mM glucose-6-phosphate, 1.43 mM uridine 5′-diphosphoglucuronic acid, 9.42 mM potassium chloride, 2.28 mM magnesium chloride) in 100 mM potassium phosphate buffer, pH 7.4. Samples were incubated at 37°C with mixing, aliquots removed after 0, 15, 30 and 60 minutes and subjected to reversed-phase LC-MS/MS (Applied Biosystems API 4000 QTRAP with heated nebulizer; Turbo IonSpray for JMN5-166) analysis. Peak areas were measured to calculate half life and percent of input compound remaining according to the formulas $t_{1/2}$ = (−0.693/slope of linear regression analysis of log transformed peak area versus) and % input remaining = (peak area of test compound at t_x/peak area of test compound at t_0)*100. Positive controls to assess the metabolic competency of the liver S9 fractions were 7-Ethoxycoumarin, Propranolol, and Verapamil (Sigma), which were analyzed in parallel to the article. To determine compound plasma stability, articles were mixed with freshly prepared human plasma at a final concentration of 0.5 mM and incubated at 37°C for up to 120 minutes. Aliquots were removed at distinct time points as indicated and analyzed by LC-MS/MS with detection of the compound at 254 nm. Values are expressed as percent of compound remaining at each time relative to the amount of that compound present at the starting time point.

Flow-cytometric analysis of cell cycle progression

Actively proliferating HeLa cells were exposed to JMN3-003 (10 μM), hydroxyurea (4 mM), or nocodazole (200 ng/ml) for 36 hours, followed by resuspension in buffer I (20 mM citrate/PO, pH 3.0, 0.1 mM EDTA, 0.2 M Sucrose, 0.1% Triton X-100) and staining in buffer II (10 mM Citrate/PO, pH 3.8, 0.1 M sodium chloride, 20 μg/ml acridine orange) as described [80]. Green fluorescence at 525 nm resulting from DNA intercalating acridine orange was then measured using a BD LSRII flow cytometer and FlowJo software (Tree Star) for data analysis. For comparison, unstained and stained, solvent-only exposed cells were examined in parallel.

SDS-PAGE and immunoblotting

Cells were lysed with RIPA buffer (50 mM Tris/CL, pH 7.2, 1% deoxycholate, 0.15% sodium dodecylsulfate, 150 mM sodium chloride, 50 mM sodium fluoride, 10 mM EDTA, 1% NP-40, 1 mM PMSF, protease inhibitors). Aliquots with equal total concentrations of cleared lysates (20,000×g; 10 min; 4°C) were mixed with 2x-urea buffer (200 mM Tris, pH 6.8; 8 M urea; 5% sodium dodecyl sulfate (SDS); 0.1 mM EDTA; 0.03% bromphenol blue; 1.5% dithiothreitol) and denatured for 25 min at 50°C. Samples were then fractionated on 10% SDS-polyacrylamide gels, blotted to polyvinylidene difluoride (PVDF) membranes (Millipore) and subjected to enhanced chemiluminescence detection (Pierce) using specific antisera directed against phosphorylated or non-phosphorylated cdc2-cyclin B kinase (Cell Signaling Technology), GAPDH (Abcam), the cytosolic tail of the MeV F protein [81], or influenza A/WSN virus M2 (Thermo Scientific). Immunostained PVDF membranes were developed using a ChemiDoc XRS digital imaging system (Bio-Rad) and horseradish peroxidase conjugated anti-species IgG (mouse or rabbit) antibodies. For densitometry, signals were quantified using the QuantityOne software package (Bio-Rad).

Assessment of cell growth rates

Vero cells were seeded at a density of 6×10^5 cells and incubated in the presence of 10 μM JMN3-003 or vehicle only for 30 hours at 37°C. Cells were then washed extensively and reseeded at a

density of 1×10^5 cells per well, followed by continued incubation at 37°C and assessment of life/dead cell numbers every 24 hours using a Countess automated cell counter (Invitrogen). Cells were reseeded as before when fastest growing cultures approached confluency. Growth rates were calculated for each 24-hour time interval using the Prism software package (GraphPad Software Inc.) based on the formula $Y = Y_0*\exp(K*X)$ with Y equaling life cell numbers, Y_0 the Y value at the starting time (t_0), and K the growth constant equaling ln(2)/doubling-time.

Quantification of cellular and viral mRNA levels

Cells were infected with either recombinant MeV Edmonston (recMeV-Edm) [82] (Vero cells, MOI = 1.0) or influenza A/WSN (MDCK cells, MOI = 0.05), followed by removal of inocula one hour post-infection and addition of JMN3-003 in growth media at 0.1 μM or 1 μM. All MeV infected wells received in addition fusion inhibitory peptide (FIP, Bachem) at 100 μM to prevent premature breakdown of the monolayer through viral CPE in the vehicle control wells prior to RNA extraction. Twenty-four (influenza A/WSN) or forty (recMeV-Edm) hours post-infection, total RNA was prepared from all wells using the QIAcube automated extractor and the RNeasy Mini Kit (Qiagen), and subjected to reverse transcription using Superscript II Reverse Transcriptase (Invitrogen). For RNA samples originating from recMeV-Edm infected cells, antigenome-specific primer 5-GGCTCCCTCTGGTTGT or oligo-dT primer (viral mRNA and GAPDH quantification) were used for cDNA priming. In the case of samples originating from influenza A/WSN infected cells, primers for cDNA synthesis were 5-AGTAGAAA-CAAGGTAGTTT (antigenome) or oligo-dT (mRNA and canine GAPDH). Real-time reactions were carried out using an Applied Biosystems 7500 Fast real-time PCR *system and iQ* Fast SYBR Green Supermix with ROX (Bio-Rad). Probes were a fragment at the N/P junction (MeV antigenomic RNA, 5-AACCAGGTCCACACAG and 5-GTTG TCTGATATTTCTGAC), a fragment of MeV F mRNA (5-GTCCACCATGGGTCTCAAGGTGAACGTCTC and 5-CAGTTATTGAGGAGAGTT), a fragment of human GAPDH (SABiosciences proprietary primers), a fragment of influenza A/WSN segment seven (influenza A/WSN antigenomic RNA, 5-tagctccagtgctggtct and 5-AAGGCCCTCCTTTCAGTCC), and a fragment of canine GAPDH (Qiagen proprietary primer). Melting curves were generated at the end of each reaction to verify amplification of a single product. To calculate $\Delta\Delta C_T$ values, CT values obtained for each sample were normalized for GAPDH as reference and then ΔC_T values of JMN3-003-treated samples normalized for the FIP-treated controls. Final quantification was based on three independent experiments in which each treatment condition and RT primer setting were assessed in triplicate. To assess the relative quantities of cellular mRNA, 9×10^5 HeLa cells were incubated in the presence of JMN3-003 (0.01, 0.1, 1.0, 10.0 μM final concentration), AS-136A (25 μM), Actinomycine D (5 μg/μl), or vehicle only for six hours at 37°C, followed by preparation of total RNA as described above. Quantitative TaqMan RT-PCR was again achieved using the TaqMan Fast Master Mix (Applied Biosystems) combined with proprietary primer and probe sets specific for Induced myeloid leukemia cell differentiation protein 1- (MCL1), MAPK phosphatase 1 (MKP1), and ankyrin repeat and SOCS box-containing protein 7- (ASB7) encoding mRNAs (Applied Biosystems). Samples were standardized for GAPDH as before and normalized values expressed relative to the equally analyzed vehicle-treated controls.

Quantitative cell-to-cell fusion assays

An effector cell population (3×10^5 cells/well) was cotransfected with 2 μg each of MeV H and F expression plasmids. To inhibit fusion until the cell overlay, the effector cells are incubated in the presence of 100 μM fusion inhibitory peptide (Bachem). Single transfections of plasmids encoding MeV F served as controls. Target cells (6×10^5 cells/well) were transfected with 4 μg of the reporter plasmid encoding firefly luciferase under the control of the T7 promoter. Two hours post-transfection, modified vaccinia virus Ankara expressing T7 polymerase at an MOI of 1.0 PFU/cell was added to the effector cells. Following incubation for 16 h at 37°C, target cells were detached and overlaid on washed effector cells at a 1:1 ratio and incubated at 37°C in the presence of different JMN3-003 concentrations as indicated. Four hours post-overlay, cells were lysed using Bright Glo lysis buffer (Promega), and the luciferase activity determined in a luminescence counter (PerkinElmer) after addition of Britelite substrate (PerkinElmer). The instrument's arbitrary values were analyzed by subtracting the relative background provided by values of the controls, and these values were normalized against the reference constructs indicated in the figure legends. On average, background values were $<1\%$ of the values obtained for reference constructs. For qualitative assessment, transfected Vero-SLAM cells were photographed 18 hours post-transfection at a magnification of ×200.

Time of compound addition analysis

For virus pre-incubation assays, 10^7 infectious MeV-Alaska particles were incubated for 60 minutes at 37°C in the presence of JMN3-003 (1.0 μM final concentration) or vehicle only, followed by 1,000-fold dilution in growth media and transferred to 3×10^5 Vero-Slam cells/well (corresponding to final compound concentrations after pre-incubation of 1 nM and an MOI = 0.033). Reference wells were kept at 1.0 μM JMN3-003 for the duration of the experiment. Cell-associated viral particles were harvested 24 hours post-infection and infectious titers determined by $TCID_{50}$ titration. To assess cell priming, Vero-Slam cells (3×10^5/well) were incubated in the presence of JMN3-003 at 1.0 μM for one hour at 37°C at the indicated time points pre-infection, followed by washing and further incubation in growth media. Immediately before infection, cells were reseeded at a density of 2.5×10^5 per well and infected with MeV-Alaska at an MOI = 0.2 pfu/cell. Inocula were replaced with growth media four hours post-infection and cells incubated for approximately 20 hours. Cell-associated viral particles were then harvested and infectious titers determined by $TCID_{50}$ titration. For post-infection time-of-addition studies, 3×10^5 Vero-Slam cells/well were infected with MeV-Alaska as before, followed by addition of JMN3-003 (1.0 μM final concentration), entry inhibitor AS-48 (75 μM), or RdRp inhibitor AS-136A (25 μM). Controls received vehicle only. All wells were harvested 19 hours post-infection and titers of cell-associated progeny virus determined by $TCID_{50}$ titration.

Minireplicon assays

BSR T7/5 cells (5×10^5/well) were transfected with plasmid DNAs encoding MeV-L (0.24 μg), MeV-N (0.94 μg) or MeV-P (0.29 μg) and 2 μg of the MeV luciferase minigenome reporter plasmid [83]. Control wells included identical amounts of reporter and helper plasmids but lacked the L-encoding plasmid. At the time of transfection, JMN3-003 was added as specified, while control wells received vehicle only for comparison. Thirty-six hours post-transfection, cells were lysed with Bright GLO lysis buffer and relative luciferase activities determined using the Britelite substrate and a luminescence counter as outlined above.

In vitro virus adaptation

Adaptations were carried out essentially as we have previously described [36]. Briefly, Vero-SLAM cells were infected with MeV-

Alaska at an MOI of 0.1 pfu/ml and incubated in the presence of gradually increasing JMN3-003 concentrations starting at 0.5 μM. Equally infected cells treated with the virus polymerase targeted RdRp inhibitor AS-136A were examined in parallel. When cultures became over confluent, cells were reseeded for continued incubation in the presence of the same compound concentration as before. At detection of extensive cell-to-cell fusion, cell-associated viral particles were harvested, diluted 10-fold and used for parallel infections of fresh cell monolayers in the presence of compound at unchanged and doubled concentrations. Cultures treated with the highest compound concentrations in which virus-induced cytopathicity became detectable were used for further adaptation. The approach was terminated after 90 days of continued incubation or when virus-induced cytopathicity was readily detectable in the presence of 30 μM compound in accordance with previous results [36].

Supporting Information

Figure S1 Synthesis of JMN3-003, JMN5-165 and JMN5-166.
(PDF)

Figure S2 Structure of RDEA-806.
(DOCX)

Acknowledgments

We are grateful to D. C. Liotta and R. W. Arrendale (Emory University and Emory Institute for Drug Development) for support and LC-MS/MS analysis of compound samples, and A. L. Hammond for critical reading of the manuscript. MuV strain South Africa, sindbis virus, and SO-influenza isolates Texas and Mexico were kind gifts of P. A. Rota (Centers for Disease Control and Prevention), W. J. Bellini (Centers for Disease Control and Prevention) and D. A. Steinhauer (Emory University), respectively. We also thank Scynexis Inc. for assistance with experimentation involving human S9 hepatocytes.

Author Contributions

Conceived and designed the experiments: SAK MN JPS RKP. Performed the experiments: SAK JMN J-JY MD AS RKP. Analyzed the data: SAK JMN JPS RKP. Contributed reagents/materials/analysis tools: AS MN. Wrote the paper: SAK JMN RKP.

References

1. Lamb RA, Parks GD (2007) Paramyxoviridae: The viruses and their replication. In: Knipe DM, Howley PM, eds. Fields Virology. 5 ed. Philadelphia: Wolters Kluwer/Lippincott Williams & Wilkins. pp 1449–1496.
2. Stiver G (2003) The treatment of influenza with antiviral drugs. Cmaj 168: 49–56.
3. WHO (2004) http://www.who.int/whr/2004/en/09_annexes_en.pdf.
4. Leung AK, Kellner JD, Johnson DW (2004) Viral croup: a current perspective. J Pediatr Health Care 18: 297–301.
5. Fry AM, Curns AT, Harbour K, Hutwagner L, Holman RC, et al. (2006) Seasonal trends of human parainfluenza viral infections: United States, 1990–2004. Clin Infect Dis 43: 1016–1022.
6. De Clercq E (2006) Antiviral agents active against influenza A viruses. Nat Rev Drug Discov 5: 1015–1025.
7. Kiso M, Mitamura K, Sakai-Tagawa Y, Shiraishi K, Kawakami C, et al. (2004) Resistant influenza A viruses in children treated with oseltamivir: descriptive study. Lancet 364: 759–765.
8. Sugaya N, Mitamura K, Yamazaki M, Tamura D, Ichikawa M, et al. (2007) Lower clinical effectiveness of oseltamivir against influenza B contrasted with influenza A infection in children. Clin Infect Dis 44: 197–202.
9. Anderson LJ, Parker RA, Strikas RL (1990) Association between respiratory syncytial virus outbreaks and lower respiratory tract deaths of infants and young children. J Infect Dis 161: 640–646.
10. Groothuis JR, Simoes EA, Levin MJ, Hall CB, Long CE, et al. (1993) Prophylactic administration of respiratory syncytial virus immune globulin to high-risk infants and young children. The Respiratory Syncytial Virus Immune Globulin Study Group. N Engl J Med 329: 1524–1530.
11. Johnson S, Oliver C, Prince GA, Hemming VG, Pfarr DS, et al. (1997) Development of a humanized monoclonal antibody (MEDI-493) with potent in vitro and in vivo activity against respiratory syncytial virus. J Infect Dis 176: 1215–1224.
12. Drake JW (1993) Rates of spontaneous mutation among RNA viruses. Proc Natl Acad Sci U S A 90: 4171–4175.
13. Duffy S, Shackelton LA, Holmes EC (2008) Rates of evolutionary change in viruses: patterns and determinants. Nat Rev Genet 9: 267–276.
14. Schwegmann A, Brombacher F (2008) Host-directed drug targeting of factors hijacked by pathogens. Sci Signal 1: re8.
15. Tan SL, Ganji G, Paeper B, Proll S, Katze MG (2007) Systems biology and the host response to viral infection. Nat Biotechnol 25: 1383–1389.
16. Salerno D, Hasham MG, Marshall R, Garriga J, Tsygankov AY, et al. (2007) Direct inhibition of CDK9 blocks HIV-1 replication without preventing T-cell activation in primary human peripheral blood lymphocytes. Gene 405: 65–78.
17. Schang LM (2006) First demonstration of the effectiveness of inhibitors of cellular protein kinases in antiviral therapy. Expert Rev Anti Infect Ther 4: 953–956.
18. RxList (2011) RxList (2010) http://www.rxlist.com/tamiflu-drug.htm, last accessed January 2011.
19. Yoon JJ, Chawla D, Paal T, Ndungu M, Du Y, et al. (2008) High-throughput screening-based identification of paramyxovirus inhibitors. J Biomol Screen 13: 591–608.
20. White LK, Yoon JJ, Lee JK, Sun A, Du Y, et al. (2007) Nonnucleoside inhibitor of measles virus RNA-dependent RNA polymerase complex activity. Antimicrob Agents Chemother 51: 2293–2303.
21. Garcia M, Yu XF, Griffin DE, Moss WJ (2005) In vitro suppression of human immunodeficiency virus type 1 replication by measles virus. J Virol 79: 9197–9205.
22. Grant DM (1991) Detoxification pathways in the liver. J Inherit Metab Dis 14: 421–430.
23. Koch-Weser J (1974) Clinical application of the pharmacokinetics of procaine amide. Cardiovasc Clin 6: 63–75.
24. Moyle G, Boffito M, Stoehr A, Rieger A, Shen Z, et al. (2010) Phase 2a randomized controlled trial of short-term activity, safety, and pharmacokinetics of a novel nonnucleoside reverse transcriptase inhibitor, RDEA806, in HIV-1-positive, antiretroviral-naive subjects. Antimicrob Agents Chemother 54: 3170–3178.
25. Zieve GW, Turnbull D, Mullins JM, McIntosh JR (1980) Production of large numbers of mitotic mammalian cells by use of the reversible microtubule inhibitor nocodazole. Nocodazole accumulated mitotic cells. Exp Cell Res 126: 397–405.
26. Gao WY, Cara A, Gallo RC, Lori F (1993) Low levels of deoxynucleotides in peripheral blood lymphocytes: a strategy to inhibit human immunodeficiency virus type 1 replication. Proc Natl Acad Sci U S A 90: 8925–8928.
27. Lori F, Malykh A, Cara A, Sun D, Weinstein JN, et al. (1994) Hydroxyurea as an inhibitor of human immunodeficiency virus-type 1 replication. Science 266: 801–805.
28. Lahusen T, De Siervi A, Kunick C, Senderowicz AM (2003) Alsterpaullone, a novel cyclin-dependent kinase inhibitor, induces apoptosis by activation of caspase-9 due to perturbation in mitochondrial membrane potential. Mol Carcinog 36: 183–194.
29. Engelking O, Fedorov LM, Lilischkis R, ter Meulen V, Schneider-Schaulies S (1999) Measles virus-induced immunosuppression in vitro is associated with deregulation of G1 cell cycle control proteins. J Gen Virol 80(Pt 7): 1599–1608.
30. Garcia M, Yu XF, Griffin DE, Moss WJ (2008) Measles virus inhibits human immunodeficiency virus type 1 reverse transcription and replication by blocking cell-cycle progression of CD4+ T lymphocytes. J Gen Virol 89: 984–993.
31. Kuwano Y, Kim HH, Abdelmohsen K, Pullmann R, Jr., Martindale JL, et al. (2008) MKP-1 mRNA stabilization and translational control by RNA-binding proteins HuR and NF90. Mol Cell Biol 28: 4562–4575.
32. Friedel CC, Dolken L, Ruzsics Z, Koszinowski UH, Zimmer R (2009) Conserved principles of mammalian transcriptional regulation revealed by RNA half-life. Nucleic Acids Res 37: e115.
33. Sobell HM (1985) Actinomycin and DNA transcription. Proc Natl Acad Sci U S A 82: 5328–5331.
34. Plemper RK, Erlandson KJ, Lakdawala AS, Sun A, Prussia A, et al. (2004) A target site for template-based design of measles virus entry inhibitors. Proc Natl Acad Sci U S A 101: 5628–5633.
35. Sun A, Yoon JJ, Yin Y, Prussia A, Yang Y, et al. (2008) Potent non-nucleoside inhibitors of the measles virus RNA-dependent RNA polymerase complex. J Med Chem 51: 3731–3741.
36. Yoon JJ, Krumm SA, Ndungu JM, Hoffman V, Bankamp B, et al. (2009) Target analysis of the experimental measles therapeutic AS-136A. Antimicrob Agents Chemother 53: 3860–3870.
37. Boucrot E, Henry T, Borg JP, Gorvel JP, Meresse S (2005) The intracellular fate of Salmonella depends on the recruitment of kinesin. Science 308: 1174–1178.

38. Cameron JE, Yin Q, Fewell C, Lacey M, McBride J, et al. (2008) Epstein-Barr virus latent membrane protein 1 induces cellular MicroRNA miR-146a, a modulator of lymphocyte signaling pathways. J Virol 82: 1946–1958.
39. Coiras M, Camafeita E, Lopez-Huertas MR, Calvo E, Lopez JA, et al. (2008) Application of proteomics technology for analyzing the interactions between host cells and intracellular infectious agents. Proteomics 8: 852–873.
40. Hilpert K, Hancock RE (2007) Use of luminescent bacteria for rapid screening and characterization of short cationic antimicrobial peptides synthesized on cellulose using peptide array technology. Nat Protoc 2: 1652–1660.
41. Honda A (2008) Role of host protein Ebp1 in influenza virus growth: intracellular localization of Ebp1 in virus-infected and uninfected cells. J Biotechnol 133: 208–212.
42. Honda A, Okamoto T, Ishihama A (2007) Host factor Ebp1: selective inhibitor of influenza virus transcriptase. Genes Cells 12: 133–142.
43. O'Connell RM, Rao DS, Chaudhuri AA, Boldin MP, Taganov KD, et al. (2008) Sustained expression of microRNA-155 in hematopoietic stem cells causes a myeloproliferative disorder. J Exp Med 205: 585–594.
44. Taganov KD, Boldin MP, Baltimore D (2007) MicroRNAs and immunity: tiny players in a big field. Immunity 26: 133–137.
45. Konig R, Stertz S, Zhou Y, Inoue A, Hoffmann HH, et al. (2010) Human host factors required for influenza virus replication. Nature 463: 813–817.
46. Karlas A, Machuy N, Shin Y, Pleissner KP, Artarini A, et al. (2010) Genome-wide RNAi screen identifies human host factors crucial for influenza virus replication. Nature 463: 818–822.
47. Alvesalo J, Greco D, Leinonen M, Raitila T, Vuorela P, et al. (2008) Microarray analysis of a Chlamydia pneumoniae-infected human epithelial cell line by use of gene ontology hierarchy. J Infect Dis 197: 156–162.
48. Reghunathan R, Jayapal M, Hsu LY, Chng HH, Tai D, et al. (2005) Expression profile of immune response genes in patients with Severe Acute Respiratory Syndrome. BMC Immunol 6: 2.
49. Taganov KD, Boldin MP, Chang KJ, Baltimore D (2006) NF-kappaB-dependent induction of microRNA miR-146, an inhibitor targeted to signaling proteins of innate immune responses. Proc Natl Acad Sci U S A 103: 12481–12486.
50. O'Connell RM, Taganov KD, Boldin MP, Cheng G, Baltimore D (2007) MicroRNA-155 is induced during the macrophage inflammatory response. Proc Natl Acad Sci U S A 104: 1604–1609.
51. Ding XR, Yang J, Sun DC, Lou SK, Wang SQ (2008) Whole genome expression profiling of hepatitis B virus-transfected cell line reveals the potential targets of anti-HBV drugs. Pharmacogenomics J 8: 61–70.
52. Kaur G, Roy I (2008) Therapeutic applications of aptamers. Expert Opin Investig Drugs 17: 43–60.
53. Mairal T, Ozalp VC, Lozano Sanchez P, Mir M, Katakis I, et al. (2008) Aptamers: molecular tools for analytical applications. Anal Bioanal Chem 390: 989–1007.
54. Borghouts C, Kunz C, Groner B (2008) Peptide aptamer libraries. Comb Chem High Throughput Screen 11: 135–145.
55. Grimm D, Kay MA (2007) Therapeutic application of RNAi: is mRNA targeting finally ready for prime time? J Clin Invest 117: 3633–3641.
56. Wu L, Belasco JG (2008) Let me count the ways: mechanisms of gene regulation by miRNAs and siRNAs. Mol Cell 29: 1–7.
57. Fewell GD, Schmitt K (2006) Vector-based RNAi approaches for stable, inducible and genome-wide screens. Drug Discov Today 11: 975–982.
58. Filipowicz W, Bhattacharyya SN, Sonenberg N (2008) Mechanisms of post-transcriptional regulation by microRNAs: are the answers in sight? Nat Rev Genet 9: 102–114.
59. Tao SC, Chen CS, Zhu H (2007) Applications of protein microarray technology. Comb Chem High Throughput Screen 10: 706–718.
60. Fink J, Gu F, Ling L, Tolfvenstam T, Olfat F, et al. (2007) Host gene expression profiling of dengue virus infection in cell lines and patients. PLoS Negl Trop Dis 1: e86.
61. Dorr P, Westby M, Dobbs S, Griffin P, Irvine B, et al. (2005) Maraviroc (UK-427,857), a potent, orally bioavailable, and selective small-molecule inhibitor of chemokine receptor CCR5 with broad-spectrum anti-human immunodeficiency virus type 1 activity. Antimicrob Agents Chemother 49: 4721–4732.
62. Balzarini J (2007) Carbohydrate-binding agents: a potential future cornerstone for the chemotherapy of enveloped viruses? Antivir Chem Chemother 18: 1–11.
63. McGovern SL, Caselli E, Grigorieff N, Shoichet BK (2002) A common mechanism underlying promiscuous inhibitors from virtual and high-throughput screening. J Med Chem 45: 1712–1722.
64. Sun M, Fuentes SM, Timani K, Sun D, Murphy C, et al. (2008) Akt plays a critical role in replication of nonsegmented negative-stranded RNA viruses. J Virol 82: 105–114.
65. Ehrhardt C, Ludwig S (2009) A new player in a deadly game: influenza viruses and the PI3K/Akt signalling pathway. Cell Microbiol 11: 863–871.
66. Ehrhardt C, Wolff T, Pleschka S, Planz O, Beermann W, et al. (2007) Influenza A virus NS1 protein activates the PI3K/Akt pathway to mediate antiapoptotic signaling responses. J Virol 81: 3058–3067.
67. Luthra P, Sun D, Wolfgang M, He B (2008) AKT1-dependent activation of NF-kappaB by the L protein of parainfluenza virus 5. J Virol 82: 10887–10895.
68. Carsillo M, Kim D, Niewiesk S (2010) Role of AKT kinase in measles virus replication. J Virol 84: 2180–2183.
69. Fisher MB, Rettie AE (1997) Prochiral sufides probes for the active-site topography of rabbit flaving containing monooxygenase 2 (FMO2). Tetrahedron 8: 613–618.
70. Boyd DR, Sharma ND, Byrne BE, Haughey SA, Kennedy MA, et al. (2004) Dioxygenase-catalysed oxidation of alkylaryl sulfides: sulfoxidation versus cis-dihydrodiol formation. Org Biomol Chem 2: 2530–2537.
71. Kagan HB (2000) Asymmetric Oxidation of Sulfides. In: Catalytic Asymmetric Synthesis Ojima I, ed. New York: Wiley-VCH. pp 327–356.
72. Moyle G, Boffito M, Shen Z, Manhard K, Sheedy B, et al. (2008) RDEA806, a novel HIV non-nucleoside reverse transcriptase inhibitor, shows positive outcome in treatment of näive HIV patients. 48 Annual ICAAC/IDSA 46th Annual Meeting. Washington D.C.
73. Girardet J-L, Koh Y-H, de la Rosa M, Gunic E, Hong Z, et al. (2006) Preparation of S-triazolyl a-mercaptoacetanilides as inhibitors of HIV reverse transcriptase. In: Appl. PI, ed.
74. Ono N, Tatsuo H, Hidaka Y, Aoki T, Minagawa H, et al. (2001) Measles viruses on throat swabs from measles patients use signaling lymphocytic activation molecule (CDw150) but not CD46 as a cellular receptor. J Virol 75: 4399–4401.
75. Buchholz UJ, Finke S, Conzelmann KK (1999) Generation of bovine respiratory syncytial virus (BRSV) from cDNA: BRSV NS2 is not essential for virus replication in tissue culture, and the human RSV leader region acts as a functional BRSV genome promoter. J Virol 73: 251–259.
76. Plemper RK, Doyle J, Sun A, Prussia A, Cheng LT, et al. (2005) Design of a small-molecule entry inhibitor with activity against primary measles virus strains. Antimicrob Agents Chemother 49: 3755–3761.
77. Spearman C (1908) The method of right and wrong cases (constant stimuli) without Gauss's formula. Br J Phsychol 2: 227–242.
78. Plemper RK, Hammond AL, Gerlier D, Fielding AK, Cattaneo R (2002) Strength of envelope protein interaction modulates cytopathicity of measles virus. J Virol 76: 5051–5061.
79. Organization WH (2009) CDC protocol of realtime RTPCR for influenza A (H1N1). AtantaGA, , USA: The WHO Collaborating Centre for influenza at CDC Atlanta, United States of America. pp 1–7.
80. Darzynkiewicz Z (1990) Differential staining of DNA and RNA in intact cells and isolated cell nuclei with acridine orange. Methods in Cell Biology 33: 285–298.
81. Lee JK, Prussia A, Snyder JP, Plemper RK (2007) Reversible inhibition of the fusion activity of measles virus F protein by an engineered intersubunit disulfide bridge. J Virol 81: 8821–8826.
82. Radecke F, Spielhofer P, Schneider H, Kaelin K, Huber M, et al. (1995) Rescue of measles viruses from cloned DNA. Embo J 14: 5773–5784.
83. Sidhu MS, Chan J, Kaelin K, Spielhofer P, Radecke F, et al. (1995) Rescue of synthetic measles virus minireplicons: measles genomic termini direct efficient expression and propagation of a reporter gene. Virology 208: 800–807.